Anders Wormsen

A Fatigue Assessment Methodology for Notched Components Containing Defects

Thesis for the degree philosophiae doctor

Trondheim, October 2007

Norwegian University of Science and Technology
Faculty of Engineering Science and Technology
Department of Engineering Design and Materials

NTNU

NTNU
Norwegian University of Science and Technology

Thesis for the degree philosophiae doctor

Faculty of Engineering Science and Technology
Department of Engineering Design and Materials

ISBN 978-82-471-4946-1 (printed version)
ISBN 978-82-471-4963-8 (electronic version)
ISSN 1503-8181

Doctoral theses at NTNU, 2007:224

Printed by NTNU-trykk

Acknowledgment

The work presented in this PhD thesis has been carried out at the *Department of Engineering Design and Materials*, *Norwegian University of Science and Technology* (NTNU), Trondheim, Norway, between September 2003 and August 2007.

This work has been fully funded by General Electric (GE) Energy (Norway) AS. The financial support is greatly acknowledged. In particular Steinar Faanes (former GE), Sebastian Videhult, Bjarne Børresen, Trond Moltubakk and Herbjørn Stenberg are gratefully acknowledged for valuable technical discussions.

I would like to express my sincere gratitude to my supervisor, Professor Gunnar Härkegård, for giving excellent guidance, valuable ideas and suggestions, constant support and encouragement during these years. His encouragement was a major reason for me to start this work. I have learned a lot! Special thanks go to Arne Fjeldstad for being an excellent colleague, co-author and friend. Without our collaboration, I would probably never have been able to finish this thesis. Thanks a lot Arne!

Furthermore, I thank my other two former colleagues at NTNU: Torsten Mann and Hans-Jörg Huth for their discussions and for making life as a PhD candidate less lonesome. Björn Sjödin* is gratefully acknowledged for giving me the opportunity to work with his Weibull code.

*Siemens Industrial Turbomachinery AB, Sweden

Abstract

A probabilistic fatigue assessment tool, P•FAT, directly applicable to the results from a standard finite element stress analysis has been developed. The fatigue assessment tool consist of two deterministic fatigue assessment methods:

- '*Local stress approach*' – Life prediction based on the equivalence between the most highly stressed point of a component and a standard smooth fatigue specimen under the same stress.
- '*Single defect approach*' – Life prediction based on the growth of a single 'worst-case' crack-like defect at the location of maximum stress.

And of two probabilistic fatigue assessment methods:

- '*Weakest-link approach*' – Assumes the probability of survival of a component to be the product of the probabilities of survival of the (small) elements into which the component has been divided for the purpose of analysis. The probability of survival of an element is a function of the stress cycle, fatigue strength and the size of the element.
- '*Random defect approach*' – The model is based on a finite element stress analysis and assumptions on the defect distribution as well as a theory for the growth of short cracks. Each finite element is associated with one or more defects by 'drawing' from a Poisson distribution. The initial posistion of a defect is obtained from a uniform distribtuion while its size is obtained from an extreme value distribution. The defects are considered to be crack-like, and the number of cycles required for each defect to become critical is determined. By carrying out a large number of such simulations, the fatigue life distribution of the component is obtained.

This thesis presents the theory behind the above fatigue assessment methods. In addition, asymptotic K and J solutions for a crack emanating from the root of a notch have been presented.

List of papers

This dissertation consists of an introduction and eight appended papers:

1. A. Wormsen, B. Sjödin, G. Härkegård and A. Fjeldstad: Non-local stress approach for fatigue assessment based on weakest-link theory and statistics of extremes. Accepted for publication in *Fatigue & Fracture of Engineering Materials & Structures*, August 2007.

2. A. Wormsen, G. Härkegård and H. J. Huth: Probabilistic fatigue assessment of a hydro-turbine blade model. Proceedings of the *International Fatigue Congress*, Atlanta, USA, 2006.

3. A. Wormsen, A. Fjeldstad and G. Härkegård: A post-processor for fatigue crack growth analysis based on a finite element stress field. Accepted for publication in *Computer Methods in Applied Mechanics and Engineering*, September 2007.

4. A. Fjeldstad, A. Wormsen and G. Härkegård: Simulation of fatigue crack growth in components with random defects. Accepted for publication in *Engineering Fracture Mechanics*, March 2007.

5. A. Fjeldstad, A. Wormsen and G. Härkegård: Reanalysis of Frost's classical fatigue tests on self-arresting cracks at notches. Department of Engineering Design and Materials, Norwegian Univeristy of Science and Technology, 2007.

6. A. Wormsen, A. Fjeldstad and G. Härkegård: The application of asymptotic solutions to a semi-elliptical crack at the root of a notch. *Engineering Fracture Mechanics*, Vol. 73, 2006, pp. 1899-1912.

7. A. Fjeldstad, A. Wormsen and G. Härkegård: Approximate stress intensity factors for cracked V-notched specimens based on asymptotic solutions with application to T-joints. Accepted for publication in *Engineering Fracture Mechanics*, March 2007.

8. G. Härkegård and A. Wormsen: Non-linear analysis of shallow cracks in smooth and notched plates. Part 1: analytical evaluation. *Journal of Strain Analysis for Engineering Design*, Vol. 40, 2005, pp. 237-244.

In addition, [1–7] have been published but are not included in the thesis.

Contents

CHAPTER 1

Introduction

1.1 Objective

The primary objective of this work has been to develop, implement and verify robust and physically consistent fatigue assessment methods for the prediction of the fatigue life and the fatigue strength of notched components containing defects.

This shall be achieved by:

- Establishing the theoretical basis for robust fatigue assessment methods that are fully compatible with the result from a standard finite element stress analysis and permit direct post-processing for obtaining the probability of fatigue failure.
- Develop, implement and verify a short-crack growth model.
- Create a stand-alone finite-element post-processor.
- Establish simple approximate methods for estimating the stress intensity factor K and the J integral for surface cracks at stress concentrations.
- Compare fatigue life predictions with experimental test data of some selected specimen types.

1.2 Motivation

Fatigue failure is one of the most common failure mode of mechanical components and is caused by the growth of cracks. A crack generally starts to grow from the first load cycle while final failure can occur after thousands (low-cycle fatigue) or millions of load cycles (high-cycle fatigue). Example of structures that are

loaded in the high-cycle fatigue range are hydraulic turbine runners, aircraft wings, marine structures, railway shafts and suspension arms in a car. Example of structure that are loaded in the low-cycle fatigue range are blades, rotors, and casings in jet engines, gas and steam turbines, as well as other high-temperature components in thermal power plant and process plant.

A component fatigue assessment evaluation is a prerequisite for obtaining a sufficiently high inherent reliability with respect to fatigue, i.e., the component can perform its intended function under given operating conditions for a given time interval. For instance, a turbine runner must be designed against fatigue due to start-stop-cycles and flow-induced vibrations. There exist empirical methods to take the stress field and the size of the component into account, but these methods are generally not compatible with finite element stress analysis. For instance, the methods due to Neuber [8] and Peterson [9] for handling notch effects require a nominal stress, which is generally unavailable from a finite element stress analysis. This thesis therefore focus on robust fatigue assessment methods that can be used directly with results from a standard finite element stress analysis to predict the fatigue life of notched components containing defects.

1.3 Short summary of the thesis

In Paper 1, a non-local stress approach for fatigue assessment based on weakest-link theory and statistics of extremes is presented. The statistical distribution of fatigue strength data from smooth standard specimens serves as a starting point for the computation of the probability of component fatigue failure. It is a non-local stress approach in the sense that it takes the complete stress field into account rather than just the highest local stress. The non-local stress approach can be linked to the probability of finding a fatigue critical defect in the most highly stressed volume of the component. The weakest-link approach has been used for predicting the fatigue limit and the fatigue life of several specimen types and predictions have been compared with test results in Papers 1 and 2.

In Paper 3, the algorithm needed for performing a crack growth analysis of a three-dimensional component by post-processing results from a standard finite element stress analysis is given. The prediction is based on the fatigue properties of the material and their scatter, and on the operating stresses from a finite element analysis of the component. The post-processing of the stresses includes residual stresses, which may be imported directly from casting or welding simulations. By 'drawing' the number, size and posistion of crack-like defects from distribution functions and repating this process for a large number of nominally equal components ('Monte Carlo' simulation), the fatigue life distribution of the component can be obtained by means of fatigue crack growth calculations. Important features of the crack growth approach, such as (i) the determination of the life-controlling defect, (ii) growth of short and long cracks, (iii) fatigue strength and fatigue life distribution and (iv) probability of component fatigue failure, have been presented in Paper 4. The crack growth analysis is carried out by using a short crack growth model. In Paper 4, the short crack growth model has been used to collapse $\mathrm{d}a/\mathrm{d}n$-data for short and long crack measurements of a low-alloy

steel [10] and an aluminium alloy [11]. In Paper 5, the short crack growth model has been used for predicting the conditions under which crack initiation, crack arrest and failure are expected to occur. These predictions have been compared with the results from the classical fatigue tests by Frost [12].

To be able to perform a fatigue crack growth calculation, the stress intensity factor K must be determined for the considered cracked configuration. The finite-element post-processor uses weight functions [13–15] together with the stress field of the associated crack-free component to obtain the stress intensity factor. Asymptotic solutions for a crack emanating from the root of a notch have been presented in Papers 6 and 7. The asymptotic solutions provides an easy-to-use tool for verification of more advanced numerically based stress intensity factor solutions. Fatigue life predictions based on the asymptotic solutions have been compared with lifetime predictions from the finite-element post-processor in Paper 4.

When the strains in the critical regions of a specimen are elastic-plastic, the crack growth rate must be characterised in terms of the cyclic J integral, ΔJ, rather than in terms of the linear elastic stress intensity range, ΔK. Simple solutions for estimating the J integral have been presented in Paper 8.

CHAPTER 2

Defects

A steel melt usually contains insoluble components in form of particles which appear as inclusions in the solid material. The main part of these particles (oxides, sulphides and nitrides) are created by reactions of elements resolved in the steel (endogenous inclusions) or by contaminations from the refractory material (exogenous inclusions). These are the so-called non-metallic inclusions [16, 17]. Fig. 2.1 shows scanning electron microscopy (SEM) images of cracked globular calcium inclusions in a AISI 8620 carburising steel. Non-metallic inclusions can behave as cracks or act as crack initiation sites. They can therefore have a large effect on the fatigue properties.

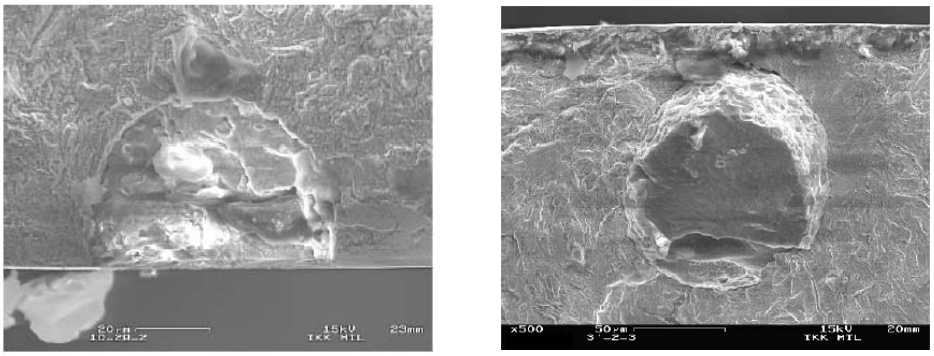

a) b)

Figure 2.1: SEM images of a globular calcium aluminate inclusion located (a) at a free surface and (b) close to a free surface in an AISI 8620 carburising steel [18].

The defect size distribution is related to the manufacturing process. Typical volume defects are non-metallic inclusions, pores and shrinkage cavities. The list of surface defects includes machining marks (surface roughness), corrosion pits welding defects and non-metallic inclusions or pores located close to or at the surface.

2.1 Inspection methods

Several inspection methods have been used for the characterisation of defects in metallic materials, e.g., conventional non-destructive testing, optical microscopy, inclusion concentration method, chemical analysis, fracture methods, oxygen determination and spark emission. A broad review of these methods have been presented in [19]. When using optical microscopy, the size and number of defects are determined by inspecting small polished control regions.

There are two different methods based on the statistics of extremes for estimating the size of the largest defect in a large volume of material. The first approach, called the *block maximum* method, uses the generalised extreme value distribution [20]. In this method, the largest defect in each of the k control regions is measured. In the second approach, all defects with sizes above a certain high threshold a_{th} are considered. The difference between the defect size and the threshold, i.e., $a - a_{\text{th}}$, are fitted to a generalised Pareto distribution [20]. This approach is therefore often called the *peak over threshold* method.

2.2 Block maximum method

When using the block maximum method, a polished cross-section is divided into k equally sized areas of size A_0 which are inspected for defects. The observation set consists then of k measurements of maximum defect sizes, $a_{\text{max}1}, \ldots, a_{\text{max}k}$. The generalised extreme value distribution is fitted to these data, see Papers 1, 3 and 4.

2.3 Peak over threshold method

For the block maximum method, all defects above the detection limit of the inspection method needs to be measured to decide which is the largest in each of the k control-regions. Defects smaller than the largest defect is discarded. Hence, valuable data are set aside. In contrast, the peak over threshold method uses all defects with sizes above a statistically determined threshold size. The peak over threshold method was applied to defects in clean steels for the first time by Shi et al. [21, 22].

When the peak over threshold method is used, all defects larger than a high threshold a_{th} are measured either from a single inspection region or from k subregions. The observation set then consists of i measurements, $a_1, \ldots, a_i$. A generalised Pareto distribution is fitted to these values, see Papers 3 and 4.

2.4 Short crack growth model

The fatigue test by Kitagawa and Takahashi [23] clearly show that the fatigue limit of a cracked solid can be determined by means of the threshold of the stress intensity range for long cracks only. For short cracks, however, the fatigue limit asymptotically approaches the ordinary fatigue limit as determined by means of

a smooth specimen. Both the long and the short crack fatigue limits are satisfied by an equation initially given by El Haddad et al. [24] for $F_0 = 1$, and generalised by Härkegård [25] to an arbitrary geometry factor, F_0, viz.

$$\Delta\sigma = \frac{\Delta K_{\mathrm{th}}}{F_0\sqrt{\pi(a+a')}} = \frac{\Delta\sigma_{\mathrm{A}}}{\sqrt{1+a/a'}}. \tag{2.1}$$

The characteristic crack length, a', which signifies the transition between short cracks, $a < a'$, and long cracks, $a > a'$, is defined by

$$a' = \frac{1}{\pi}\left(\frac{\Delta K_{\mathrm{th}}}{F_0\Delta\sigma_{\mathrm{A}}}\right)^2. \tag{2.2}$$

One may interpret a' as an 'intrinsic' crack length, which should be added to the length of the real crack to yield an 'effective' crack length. Fig. 2.2 shows a Kitagawa-Takahashi diagram together with experimental data for both ferrous and nonferrous alloys gathered by Tanaka et al. [26] and by Hertzberg [27]. When

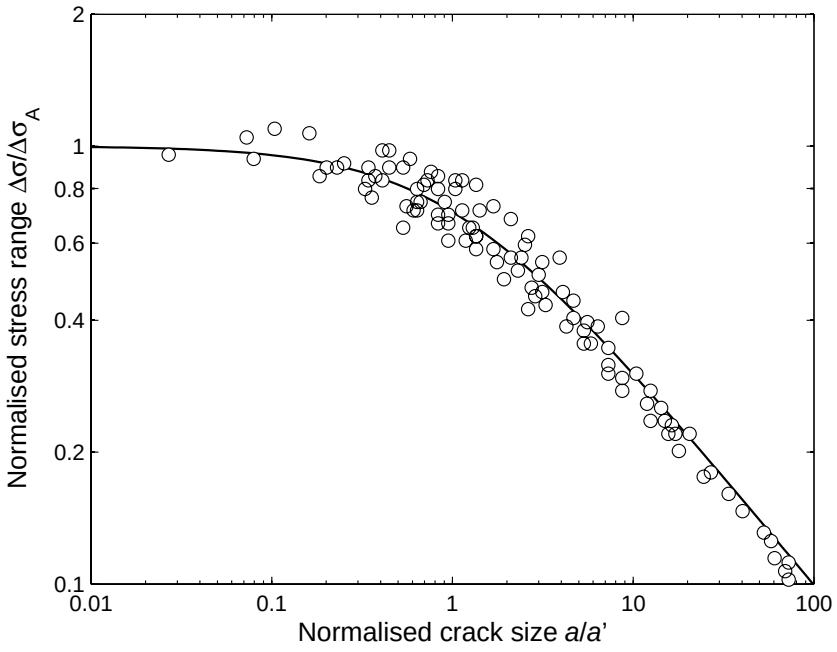

Figure 2.2: Normalised stress range, $\Delta\sigma/\Delta\sigma_{\mathrm{A}}$, versus normalised crack size a/a'. The figure is taken from Paper 4.

crack growth behaviour is controlled by linear elastic fracture mechanics, i.e., $a \gg a'$, $\Delta\sigma$ varies as $1/\sqrt{a}$. At the other extreme where $a \ll a'$, the fatigue limit asymptotically approaches the (intrinsic) fatigue limit range, of a smooth, polished fatigue specimen without major defects.

Rewriting equation (2.1) in terms of the stress intensity range yields

$$\Delta K = \frac{\Delta K_{\mathrm{th}}}{\sqrt{1+a'/a}}. \tag{2.3}$$

In Fig. 2.3, equation (2.3) is shown as a solid line together with data presented in [26,27]. For long cracks, ΔK asymptotically approaches the threshold stress intensity range ΔK_{th}. For short cracks, however, the stress intensity range required for a crack to grow varies as $\sqrt{a}$.

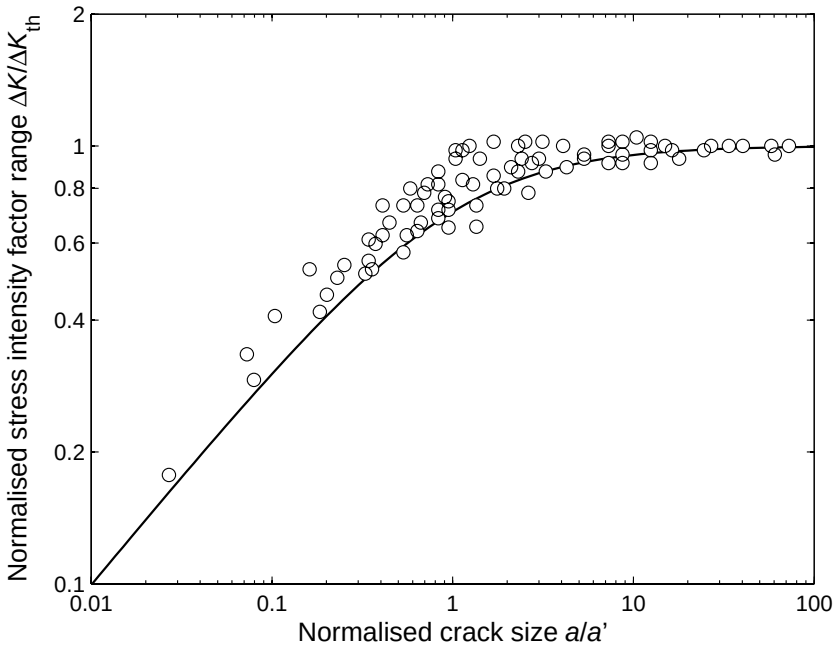

Figure 2.3: Normalised stress intensity factor range, $\Delta K/\Delta K_{\mathrm{th}}$, versus normalised crack size a/a'. The figure is taken from Paper 4.

The preceding equations explicitly depend on the intrinsic crack length, a', which, in its turn, depends on the geometry factor, F_0. The latter will not be constant, if the crack shape changes, or the finite dimensions of the solid must be considered. This inconvenience can be avoided by eliminating the crack length, a, between equations (2.1) and (2.3). Thus, one obtains

$$\left(\frac{\Delta K}{\Delta K_{\mathrm{th}}}\right)^2 + \left(\frac{\Delta \sigma}{\Delta \sigma_{\mathrm{A}}}\right)^2 = 1. \tag{2.4}$$

This equation was originally used by Härkegård et al. [28] to correlate the stress range, $\Delta\sigma$, and the stress intensity range, ΔK, below which short cracks did not propagate in two ferritic steels. In Fig. 2.4 the data points in Figs. 2.2 and 2.3 have been replotted in a diagram with $\Delta\sigma/\Delta\sigma_{\mathrm{A}}$ as the abscissa and $\Delta K/\Delta K_{\mathrm{th}}$ as the ordinate. The seemingly large scatter in Fig. 2.4 compared with that in Figs. 2.2 and 2.3 can be explained by the change to linear scales from logarithmic scales.

By using the characteristic crack length in conjunction with the fatigue crack growth law by Klesnil and Lukáš [29], one obtains the following crack growth law

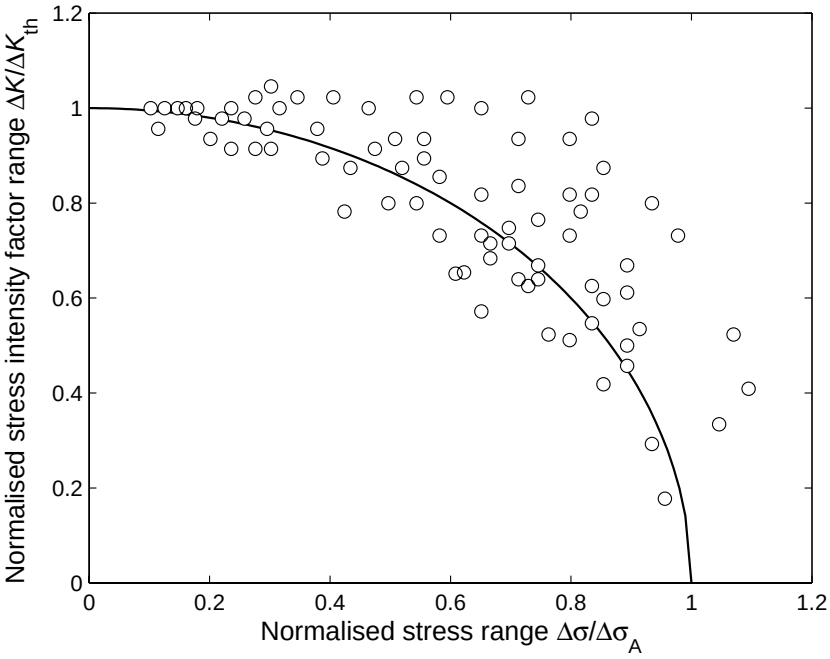

Figure 2.4: Relation between stress range and stress intensity range required to propagate a crack. The figure is taken from Paper 4.

that accounts for the growth of a short crack [Papers 4 and 5]

$$\frac{\mathrm{d}a}{\mathrm{d}n} = C\Delta K_{\mathrm{th}}^{m}\left[\left\{\left(\frac{\Delta K}{\Delta K_{\mathrm{th}}}\right)^{2}+\left(\frac{\Delta\bar{\sigma}}{\Delta\sigma_{\mathrm{A}}}\right)^{2}\right\}^{m/2}-1\right]. \tag{2.5}$$

To determine the 'effective' stress range, $\Delta\bar{\sigma}$, for a surface crack at the root of a notch (Fig. 2.5, left), the same surface crack in a semi-infinite body is considered (Fig. 2.5, right). $\Delta\bar{\sigma}$ is now defined as the remote stress range that yields the same ΔK as for the crack at the root of a notch. Hence,

$$\Delta\bar{\sigma} = \frac{\Delta K}{F_0\sqrt{\pi a}}, \tag{2.6}$$

where F_0 is the geometry factor for the current crack in a semi-infinite plate. For an edge through-crack, $F_0 = 1.122$ [30], and for an elliptic surface crack with aspect raio $a/c = 1$, $F_0 = 0.663$ [31] at the deepest point of the crack front.

In Paper 4, the short crack growth model has been used to collapse $\mathrm{d}a/\mathrm{d}n$-data for short and long crack measurements of a low-alloy steel [10] and an aluminium alloy [11]. In Paper 5, equation (2.5) has been used for predicting the conditions under which crack initiation, crack arrest and failure is expected to occur. These predictions have been compared with the results from the classical fatigue tests by Frost [12].

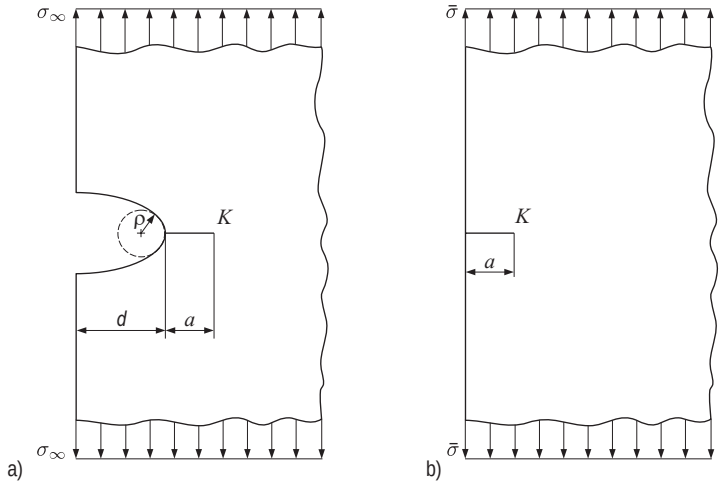

Figure 2.5: When subjected to the effective stress, $\bar{\sigma}$, the edge-crack of the smooth plate (b) has the same stress intensity factor, K, as that of the crack of the notched plate (a) subjected to the remote stress σ_∞. The figure is taken from Paper 5.

CHAPTER 3

Finite-element post-processor

At a time when the industry is continuously challenged to come up with better and less costly products, and this in ever shorter cycles, all product development processes must be improved, including fatigue design. To comply with this need, a probabilistic fatigue assessment tool, P•FAT, has been developed that is capable of predicting the fatigue life of a notched component containing defects. The prediction is based on the fatigue properties of the material and their scatter, and on the operating stresses from a finite element analysis of the component. The post-processing of the stresses includes residual stresses, which may be imported directely from casting or welding simulations.

Fatigue design is based on standard $S-N$ data or on the explicit calculation of the number of load cycles required for a crack to grow from an initial size, a_{i}, to a final size, a_{f}. Since $S-N$ data refer to the number of cycles required for a macroscopic crack to develop in a smooth test bar, the $S-N$ approach to fatigue design may be considered as an 'implicit' analysis of crack growth. Table 3.1 shows the four types of fatigue assessment methods that have been implemented in the finite-element post-processor, P•FAT. The implicit approaches, i.e., local

Table 3.1: Different approaches to fatigue analysis, all related to fatigue crack growth.

Approaches to fatigue analysis	Deterministic	Probabilistic
Implicit	Local Stress	Weakest-Link
Explicit	Single Defect	Random Defect

stress and weakest-link, use conventional $S-N$-data as a starting point, and the fatigue life, N, is usually defined as the number of load cycles required for a macroscopic crack to develop. The explicit approaches consider the actual growth of a crack from an initial (defect) size a_{i} to a final size a_{f}.

Standard methods for fatigue life predictions are deterministic by nature, i.e., material properties including defect size are considered as predetermined quantities. Two of the most widespread deterministic fatigue assessment methods are:

- '*Local stress approach*' – Life prediction based on the equivalence between the most highly stress point of a component and a standard smooth fatigue specimen under the same stress.

- '*Single defect approach*' – Life prediction based on the growth of a single 'worst-case' crack-like defect at the location of highest local stress.

The probabilistic approaches, assume material properties to be randomly distributed:

- '*Weakest-link approach*' – Assumes the probability of survival of a component to be the products of the probabilities of survival of the (small) elements into which the component has been divided for purposes of analysis. The probability of survival of an element is a function of the stress cycle, the fatigue strength and the size of the element.

- '*Random defect approach*' – The model is based on a finite element stress analysis and assumptions on the defect distribution as well as a theory for the growth of short cracks. Each finite element is associated with one or more defects by 'drawing' from a Poisson distribution. The initial posistion of a defect is obtained from a uniform distribution while its size is obtained from an extreme value distribution. The defects are considered to be crack-like, and the number of cycles required for each defect to become critical is determined. By carrying out a large number of such simulations, the fatigue life distribution of the component is obtained.

Numerical recipes for the weakest-link approach are given in Paper 1. The weakest-link approach has been used for predicting the fatigue limit and the fatigue life of several specimen types and predictions have been compared with test results in Papers 1 and 2.

The reader is referred to Paper 3 for the numerical aspects of the single defect approach and the random defect approach. Important features such as (i) the determination of the life-controlling defect, (ii) growth of short and long cracks, (iii) fatigue strength and fatigue life distribution and (iv) probability of component fatigue failure have been treated and discussed in Paper 4.

CHAPTER 4

Implicit Fatigue Assessment Methods

4.1 Local stress approach

The local stress approach tacitly assumes the fatigue life at a 'point' to agree with that of a standard test specimen subject to the same stress cycle. The local stress approach has been used for predicting the fatigue limit of several specimen types and predictions have been compared with test results in Paper 1. In Paper 2, the local stress approach is used for predicting the fatigue life of the hydro-turbine blade model shown in Fig. 4.1(a). The blade model simulates the leading-edge transition between blade and crown/band of a Francis turbine runner, see Fig. 4.1.

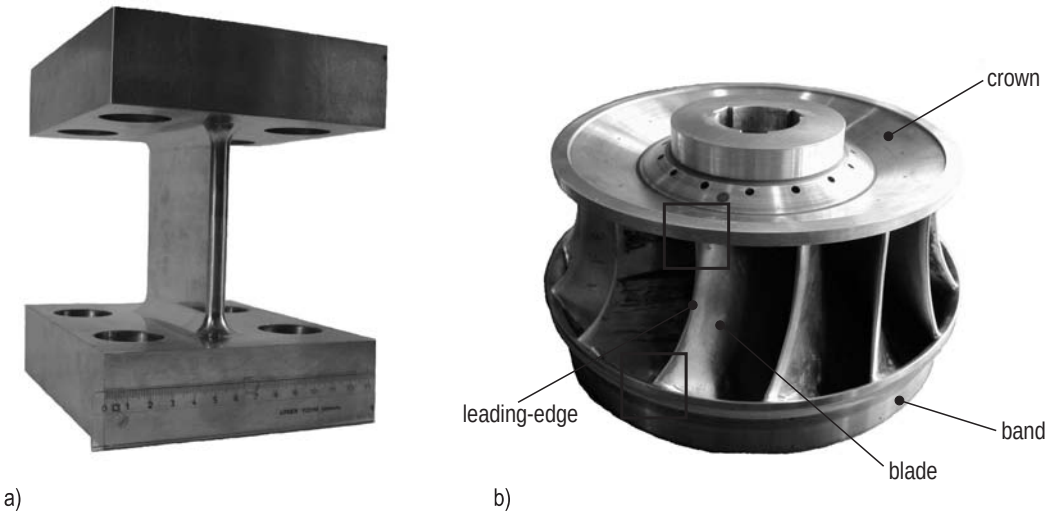

Figure 4.1: (a) Fatigue test specimen simulating the leading-edge transition zones of (b) the blade of a Francis turbine runner (leading-edge zones are indicated by squares). The figure is taken from Paper 2.

Four hydro-turbine blade models were produced from a G-X5CrNi 13-4 casting, and were experimentally tested by Huth [32]. The predicted (n_{pred}) versus the measured fatigue lives (n_{meas}) are shown in Fig. 4.2. Huth's specimens have been denoted by R in this figure The local stress approach yields conservative

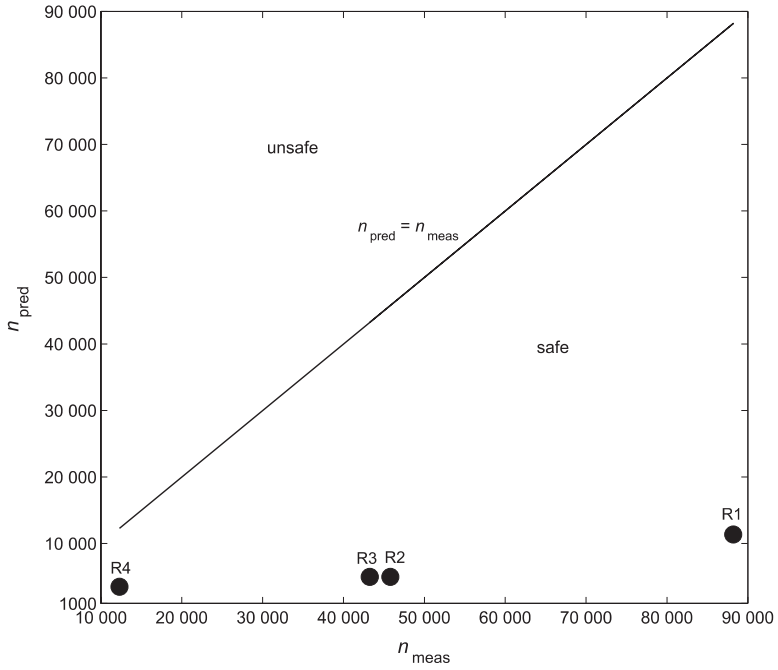

Figure 4.2: Local stress based fatigue life predictions of the hydro-turbine blade shown in Fig. 4.1(a). The figure is taken from Paper 2.

lifetime predictions deviating from the observed number of cycles by nearly a factor of 10.

4.2 Weakest-link approach

Fatigue life predictions by the local stress approach are indifferent to the *stress field* as well as to the *size* of the component, which are known to affect the fatigue strength of a mechanical component [33]. There exist empirical methods to take the stress field and the size of the component into account, but these methods are generally not compatible with finite element stress analysis. For instance, the methods due to Neuber [8] and Peterson [9] for handling notch effects require a nominal stress, which is generally unavailable from a finite element stress analysis. These shortcomings may be eliminated by means of the weakest-link theory and the statistics of extremes, which may be applied directly to the results from a finite element stress analysis. The weakest-link theory has the added advantage of predicting the probability of fatigue failure of the analysed component.

The probability of fatigue failure, P_{f}, can according to the weakest-link theory

be expressed as [Paper 1]

$$P_{\mathrm{f},V} = 1 - \exp\left[-\int_V z_1(\sigma_\mathrm{a}, R, n)\mathrm{d}V\right]. \tag{4.1}$$

The critical defect density, $z_1(\sigma_\mathrm{a}, R, n)$, is defined as the expected number of defects per unit volume V of the material that yields a fatigue strength (random variable) $\sigma_\mathrm{A} \leq \sigma_\mathrm{a}$ at a stress ratio R and fatigue life n.

By using a power-law relationship between the critical defect size and the applied stress and by assuming that the maximum defect size follows a two-parameter Fréchet distribution, the probability of component fatigue failure can be expressed as

$$P_{\mathrm{f},V} = 1 - \exp\left[-\int_V \left(\frac{\sigma_\mathrm{a}}{\sigma^*_{\mathrm{A}0}(R,n)}\right)^{b_\sigma} \frac{\mathrm{d}V}{V_0}\right], \tag{4.2}$$

This equation corresponds to a two-parameter Weibull distribution [34, 35]. b_σ and $\sigma^*_{\mathrm{A}0}$ are referred to as the Weibull (stress) exponent and the characteristic fatigue strength, respectively. b_σ is given in [1] for several different forged steels, cast steel and aluminum alloys. The Weibull exponent, b_σ, is a measure of the fatigue limit scatter, and, indirectly, a measure of the scatter of the defect size distribution. A large b_σ implies that the scatter is small.

The probability of fatigue failure of a reference specimen of volume V_0 is equal to that of an arbitrary component, if the homogeneous stress amplitude $\bar{\sigma}_\mathrm{a}$, which may be referred to as the effective stress amplitude, is defined as

$$\bar{\sigma}_\mathrm{a} = \left(\frac{1}{V_0}\int_V \sigma_\mathrm{a}^{b_\sigma}\,\mathrm{d}V\right)^{1/b_\sigma}. \tag{4.3}$$

Introducing this equation into equation (4.2) yields

$$P_{\mathrm{f},V} = 1 - \exp\left[-\left(\frac{\bar{\sigma}_\mathrm{a}}{\sigma^*_{\mathrm{A}0}(R,n)}\right)^{b_\sigma}\right]. \tag{4.4}$$

In Paper 1, it is shown that equation (4.4) can be transformed into a fatigue life distribution by means of Basquin's equation:

$$P_{\mathrm{f},V}(n, R, \bar{\sigma}_\mathrm{a}) = 1 - \exp\left[-\left(\frac{n}{N^*_0(R,\bar{\sigma}_\mathrm{a})}\right)^{b_n}\right]. \tag{4.5}$$

Here, b_n denote the Weibull fatigue life exponent and N^*_0 the characteristic fatigue life of a reference fatigue test specimen of volume V_0 subject to a homogeneous stress cycle of amplitude $\bar{\sigma}_\mathrm{a}$ and stress ratio R.

Equation (4.5) was used in Paper 2 for predicting the fatigue life of the hydro-turbine blade model in Fig. 4.1(a). The weakest-link approach gave the predicted fatigue lives shown in Fig. 4.3. For each specimen (R1 to R4), the fatigue life has been predicted for $P_\mathrm{f} = 10\%$, 50% and 90%. The weakest-link predictions are seen to be in satisfactory agreement with the experimentally observed lives.

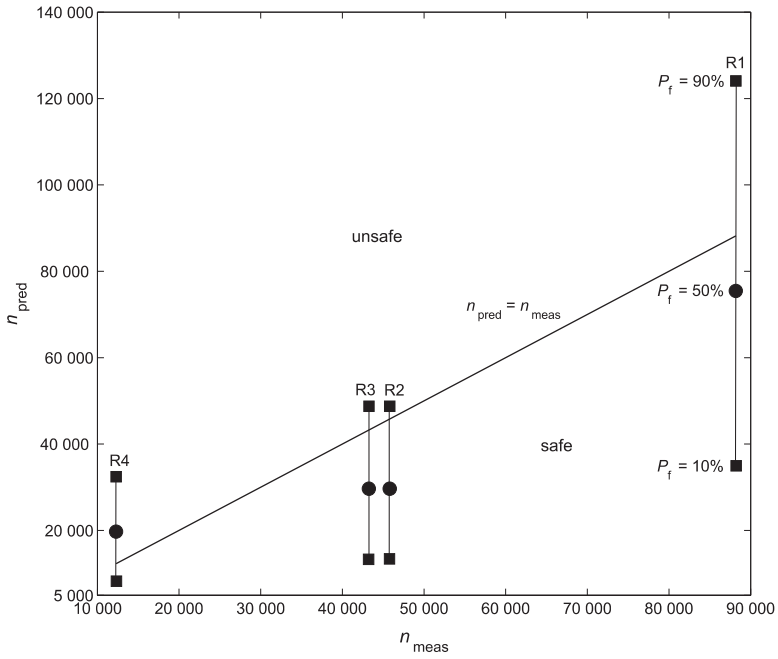

Figure 4.3: Weakest-link based fatigue life predictions of the hydro-turbine blade shown in Fig. 4.1(a). The figure is taken from Paper 2.

4.3 Multiaxial stress criteria

All multiaxial stress criteria aim at translating the local stress state into an equally damaging uniaxial stress state. Some well known multiaxial stress criteria are maximum principal stress, Sines [36], Crossland [37], Dang Van [38], Findley [39], Matake [40] and McDiarmid [41]. These criteria have been implemented in the finite-element post-processor P•FAT. The critical plane based criteria, i.e., Dang Van, Findley and Matake have been implemented by using an adaptive algorithm [42] that gives a strong reduction of calculation times. A broad review of multiaxial stress criteria have been presented in [43, 44].

CHAPTER 5

Explicit Fatigue Assessment Methods

When a commerically available finite element code such as ABAQUS is used for performing a crack growth analysis, the crack is explicitly modelled as an integrated part of the component. For each crack growth increment, the mesh surrounding the crack has to be re-meshed. Re-meshing techniques applied to crack growth problems have been treated in several papers, e.g. [45–47]. Examples of codes that have implemented re-meshing techniques for handling crack growth analysis of 3D components are FRANC3D [48], BEASY [49] (both use the boundary element method) and ADAPCRACK3D [50, 51] (uses the finite element method). In order to reduce the time required for performing a crack growth analysis, the component geometry is often simplified so that a standard handbook solution can be used for performing a fatigue life prediction. Such handbook solutions are available in the programs NASGRO [52] and AFGROW [53]. Another approach is to perform the crack growth analysis by assuming a homogeneous stress field based on the maximum stress acting on the component surface. This maximum stress approach yields acceptable results provided that the stress decreases slowly, i.e., the stress gradient is low, and when the geometrical simplification can be justified. An alternative is to use results from a standard finite element stress analysis and account for a crack by using weight functions [54,55]. This approach has been implemented in the stand-alone finite-element post-processor P•FAT. By 'drawing' the number, size and position of crack-like defects from distribution functions and repating this process for a large number of nominally equal components ('Monte Carlo' simulation), the fatigue life distribution of the component can be obtained by means of fatigue crack growth calculations. With this, one has a post-processing tool that can estimate the probability of component failure.

5.1 Single defect approach

In the single defect module, a single crack-like defect can be inserted into the component at a desired location. It is capable of modeling the growth of an embedded and a surface crack in the operating and residual stress field of a generic component. The crack-like defect is assumed to grow on the plane of maximum principal stress. Weight-functions [56], together with the stress field of the crack-free component, are used to compute the required stress intensity factors. Generally, the direction of maximum principal stress in the uncracked component changes as the crack grows on a specific plane. In the present work, the change of the crack growth direction is neglected. This is a good approximation as long as the crack is small compared with the dimensions of the component, i.e., for a large fraction of the fatigue life.

The crack surface is automatically meshed with plane elements. Subsequently, numerical integration (Gauss quadrature) is performed for determining the stress intensity factor at several locations at the crack front. For each incremental step, this process repeats itself: the crack surface is re-meshed, and updated stress intensity factors for the current crack are obtained. The program also updates the location of the crack front relative to the free surface. Hence, if the crack grows through the component surface, the crack is regarded as a surface crack, see Fig. 5.3. A crack is treated as a corner crack if it starts from or propagates into a right-angled corner. Failure of a component is defined to occur when the crack has reached a predefined size, or if the stress intensity factor K has reached the fracture toughness K_{Ic}. When a surface crack breaks the opposing free surface, it has to be treated as a through-crack. This may be a most relevant situation, e.g., for a crack growing through a thin plate. On the other hand, for initial defects that are much smaller than the thickness of the plate, a through-crack is only present during a small fraction of the component life. Thus, instead of explicitly modelling the through-crack, crack growth is terminated as soon as the surface crack breaks the opposing free surface.

5.1.1 Example

As a practical example of the use of the single defect module, a welded aluminium rectangular hollow section T-joint, see Fig. 5.1(a), has been investigated. The T-joint was tested in four-point bending with a constant stress ratio $R = \sigma_{\min}/\sigma_{\max} = 0.1$, resulting in a constant bending moment throughout the weld region. Details about manufacturing, weld characteristics, test rig arrangement and fatigue test results can be found in Tveiten et al. [57]. A welding simulation has been carried out in Weldsim [58–60] in order to obtain the residual stress field. The operating stress field was found by using ABAQUS [61]. The T-joint was modelled using eight-noded brick elements with reduced integration. For reasons of symmetry, only one quarter of the T-joint had to be considered. The load was applied to the chord through cylindrical rods, see Fig. 5.1(a). A submodel with a highly refined mesh, see Fig. 5.1(b), was used to accurately capture the peak stress and the adjacent stress field. The boundary conditions imposed on the submodel are obtained from the global model. The submodel

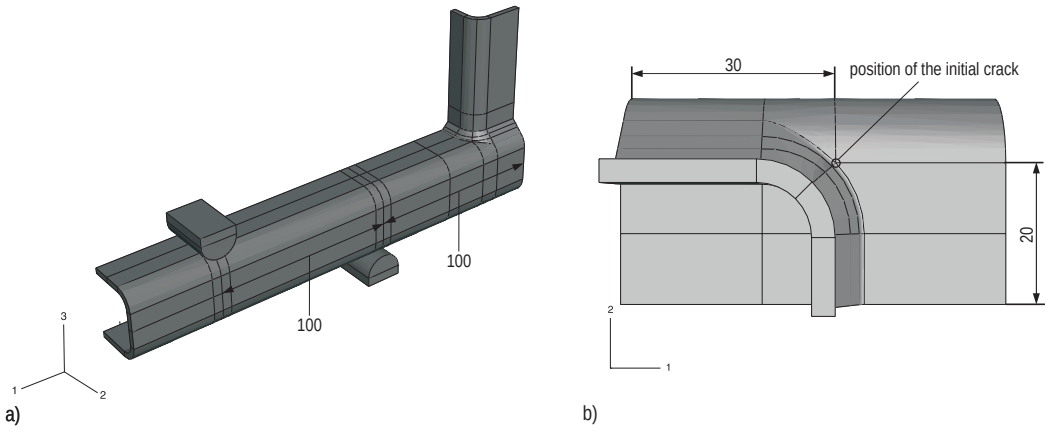

Figure 5.1: T-joint configuration: (a) global model and (b) submodel.

was meshed with twenty-noded brick elements with reduced integration. The weld was modeled with a weld angle of 45° and with a weld toe radius of 1 mm, cf. Tveiten et al. [57]. The operating stress field from the submodel and the residual stress field from the weld simulation are combined in the finite-element post-processor to obtain the spatial distribution of the stress amplitude and the mean stress.

Fatigue crack growth calculations have been performed with a semi-elliptic surface crack of initial depth $a_\mathrm{i} = 50$ μm. The initial aspect ratio has been assumed to be $a/c = 1$. The position of the initial crack is shown in Fig. 5.1(b). The fatigue crack growth analysis was terminated, when the crack had reached a depth of 95% of the wall thickness, i.e., 2.85 mm. The material properties for the aluminium alloy are given in Table 5.1. The predicted fatigue life curve is shown

Table 5.1: Mechanical properties of the 6082-T6 aluminium alloy.

Fatigue limit [62]	$\Delta\sigma_\mathrm{A}(R = 0) = 148$ MPa
Stress intensity threshold [63]	$\Delta K_\mathrm{th}(R = 0.1) = 2.08$ MPa$\sqrt{\mathrm{m}}$
Walker exponent [62]	$\gamma = 0.78$
Crack growth coefficient [62]	$C(R = 0.1) = 6.1 \cdot 10^{-12}$ [MPa,m]
Crack growth exponent [62]	$m = 5.1$

in Fig. 5.2 together with fatigue test results that have been reported in [57]. Even though the steepness of the predicted and the experimental $S - N$ curves are somewhat different, the overall agreement is good. The predicted curve is non-conservative at elevated stresses but approaches the expermental curve as the stress decreases. Eventually, the two curves crosses and the predicted fatigue limit for the T-joint is obtained at approximately 55 MPa. This is clearly a over prediction since some of the data points are below the predicted curve. It is worth mentioning that the fatigue limit of the T-joint is strongly dependent on the intrinsic fatigue limit of the material [$\Delta\sigma = 148$ MPa at $R = 0$]. However, the intrinsic fatigue limit has been calculated based on the ultimate tensile strength

[62], and thus, the fatigue limit of the T-joint is rather uncertain.

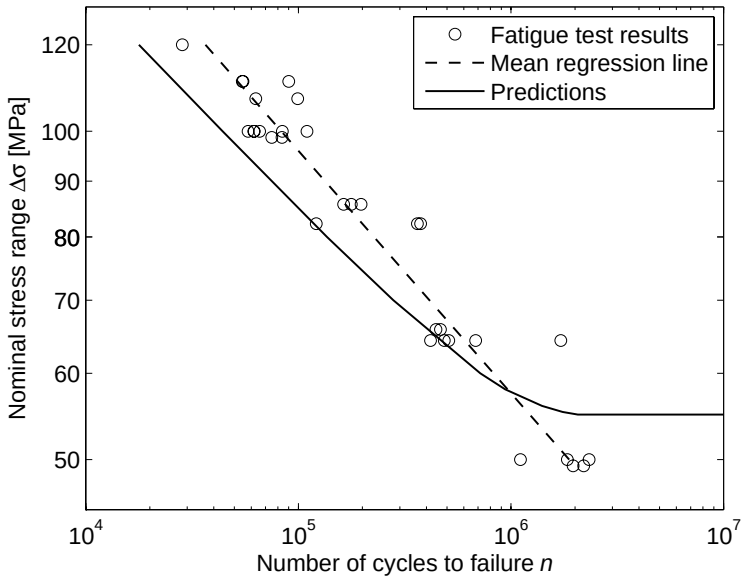

Figure 5.2: Fatigue test results for the considered T-joint configuration [Fig. 5.1] together with the finite-element post-processor based prediction curve.

5.2 Random defect approach

The number of defects in each finite element is obtained by 'drawing' from a Poisson distribution. The location of each defect in an element is found by drawing from an uniform distribution while its size is found from an extreme value distribution. By repeating this process for a large number of nominally equal components (Monte Carlo simulation) and performing crack growth calculations, the fatigue life distribution of the component is obtained.

In the present work, the interaction between single cracks and the subsequent joining of these and the formation of a new, larger crack have been neglected. Thus, only one single, dominating crack is considered at a time. This assumption requires that the number of potentially life-controlling defects is small, a situation that occurs for stress cycles close to the fatigue limit (in the HCF regime) and for components with a low density of 'large' metallurgical defects. Future fatigue testing and simulation of components with known defect distributions should give a better understanding of the influence on fatigue life of the interaction between cracks.

5.3 Weight-factor solutions

The stress field ahead of a crack in a linear elastic body can be characterised by means of the stress intensity factor K. This is a function of the geometry of the component and the crack as well as the stress field. For simple geometries,

K can be obtained from handbook solutions [30] or from asymptotic solutions [Papers 6 and 7]. For more complex geometries, the stress intensity factor can be obtained by using weight functions together with the stress field of the crack-free component. Weight factor solutions for an embedded crack [13], a surface crack [14] and a corner crack [15], as shown in Fig. 5.3, have been implemented in the finite-element post-processor.

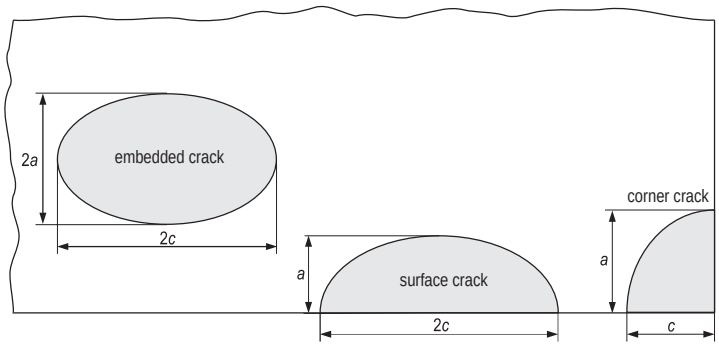

Figure 5.3: Crack configurations implemented in P•FAT. The figure is taken from Paper 3.

The weight function, $g(x', y'; \mathrm{P})$, is defined as the stress intensity factor value at the crack front point P, when a pair of opposite unit opening forces are applied at an arbitrary point P' on the crack surface, cf. Fig. 5.4(a). In the case of a distributed symmetrical loading on the crack surface, the stress intensity factor K is obtained by integrating the product of the weight function $g(x', y'; \mathrm{P})$ and the stress distribution of the crack free solid $\sigma_{\mathrm{a}}(x', y')$ over the crack surface area A_{crack}:

$$K(\mathrm{P}) = \int_{A_{\mathrm{crack}}} \sigma_{\mathrm{a}}(x', y') g(x', y'; \mathrm{P}) \, \mathrm{d}A_{\mathrm{crack}}. \tag{5.1}$$

The relationship between the weight function and the displacement field is given in [55]. The integral in equation (5.1) may be solved by means of Gauss-Legendre quadrature. This procedure subdivides the crack surface into plane elements. A typical finite element mesh for an embedded crack is shown in Fig. 5.4(b).

5.4 Asymptotic solutions

For a surface crack of depth a in the notch stress field, cf. Fig. 5.5(a), the stress intensity solution is asymptotically the same as for a surface crack in a smooth solid, except that the remote stress is being amplified by the stress concentration factor K_{t}. Thus, as $a \to 0$,

$$K = F\sigma_\infty \sqrt{\pi a} = F_0 K_{\mathrm{t}} \sigma_\infty \sqrt{\pi a}, \tag{5.2}$$

where F_0 is the geometry factor for the current surface crack emanating from a smooth surface. When the crack grows beyond the notch stress field, the remote stress field dominates the stress intensity factor, which may now be estimated by

$$K = F_0 \sigma_\infty \sqrt{\pi (a + d)}, \tag{5.3}$$

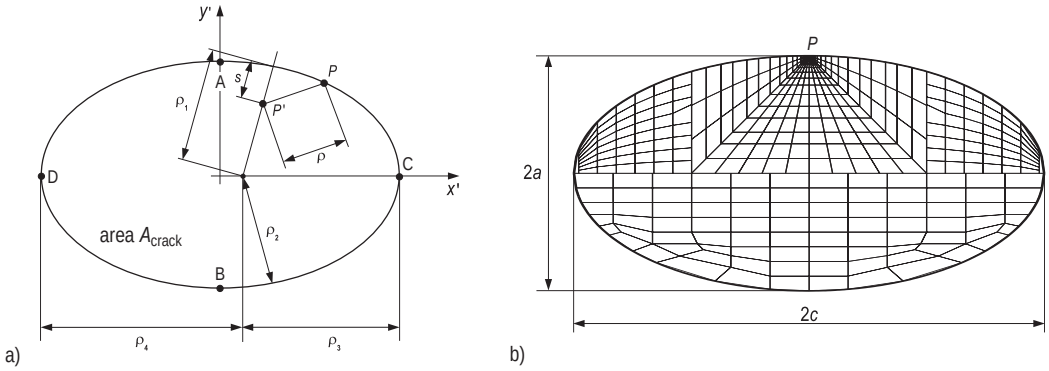

Figure 5.4: (a) Schematic drawing of an embedded crack and definition of parameters for obtaining the stress intensity factor. (b) Typical finite element mesh for an embedded crack. The figure is taken from Paper 3.

where d denotes the notch depth. An equation for K, which asymptotically agrees with the near and remote field estimates is given in Paper 6. The asymptotic expression is given by

$$K = F_0 \sigma_\infty \sqrt{\pi D}, \tag{5.4}$$

where D is an 'equivalent' surface crack depth, which can be estimated by

$$D = a + d\left[1 - \exp\left(-\frac{a}{a^*}\right)\right], \tag{5.5}$$

and

$$a^* = \frac{d}{K_t^2 - 1}. \tag{5.6}$$

The transition crack depth a^* is defined as the crack depth at which the asymptotic equations (5.2) and (5.3) for the stress intensity factors of shallow and deep cracks, respectively, yield equal results.

The weight function implementation of a semi-elliptic surface crack is now compared with the asymptotic solution for the deepest point of the crack front. A semi-elliptic surface crack located at the root of a semi-circular edge notch in a semi-infinite plate subjected to uniaxial tension σ_∞ perpendicular to the symmetry plane of the notch is considered. The cracked configuration is shown in Fig. 5.5(a). The crack is characterised by its depth a and its surface length $2c$, as shown in Fig. 5.5(b).

Fig. 5.5(b) shows the geometry factor F_A for the deepest point, $A(a;0)$, for the aspect ratio $a/c = 1$. As can be seen, the weight function based F_A values are in good agreement with the asymptotic solution.

In Paper 7, the asymptotic method presented in Paper 6 is extended to cover cracked V-notched specimens.

5.5 Non-linear crack mechanics

For the full potential of the finite-element post-processor to be realised, it is important that the single and the random defect modules are extended to cover non-linear material behaviour. Paper 8 is a preliminary work in this direction.

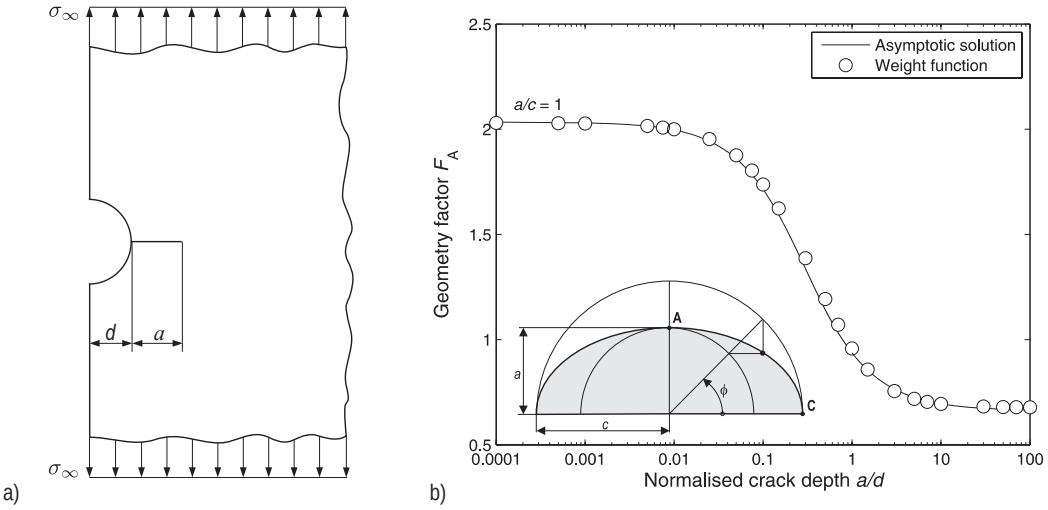

Figure 5.5: (a) Semi-infinite notched plate [$K_t = 3.1$] under uniform remote stress σ_∞. (b) Geometry factors F_A for the deepest point $A(a;0)$ of a semi-elliptic surface crack emanating from the notch root.

Closed-form stress and strain solutions of elastic-plastic cracked solids are rare. By idealizing the material behaviour as non-linear elastic, Rice [64] was able to solve two-dimensional crack problems exhibiting plastic deformation. Rice derived a path-independent contour integral J, which replaces the stress intensity factor under plastic deformation.

In Paper 8, an approximate method for estimating the J integral for shallow cracks has been presented. The proposed equation for estimating J makes use of the linear elastic and the fully plastic solution to interpolate over the entire range from small- to large-scale yielding. The elastic geometry factor is obtained by means of the stress intensity factor. In the fully plastic formulation, the plastic geometry factor is obtained by considering a pure power-hardening solid, which reduces at one limit to an incompressible linear elastic solid, and at the other to a perfectly plastic solid. The solutions are given for three basic configurations: a double-edge cracked plate under tension and bending; a notched plate under tension with a crack at the root of the notch; a single-edge-cracked plate under bending.

CHAPTER 6

Suggestions for further work

There are several items which are left untreated in this thesis. Some suggestions for further work are:

- Extend the weakest-link approach to non-linear material behaviour.
- Develop a database describing the weakest-link parameters for some common manufacturing processes.
- Non-proportional loading.
- Review of previous experimental investigations of the growth of short fatigue cracks under constant and variable amplitude loading. Perform a reassessment of these test data by means of the suggested short crack growth model.
- Sub-mm fatigue-crack growth testing on selected steels (forged, cast, welded) with continuous monitoring (microscopic, potential drop or other techniques); smooth specimens should be used for model development, notched specimens for validation purposes.
- Modeling of fatigue crack growth from defects that cannot be regarded as cracks.
- Develop a database describing the density and size distribution of material defects.
- Extend and improve weight functions for surface cracks.
- Develop a J-integral estimation procedure that is fully compatible with the results from a standard finite element analysis.

CHAPTER 7

Summary of appended papers

Paper 1

Non-local stress approach for fatigue assessment based on weakest-link theory and statistics of extremes

In the present paper a non-local stress approach for fatigue assessment based on weakest-link theory and statistics of extremes is presented. It is a non-local stress approach in the sense that it takes the complete stress field into account rather than just the highest local stress. The statistical distribution of fatigue strength data from smooth standard specimens serves as a starting point for the computation of the probability of fatigue failure of a mechanical component under cyclic loading. The probability of fatigue failure can be obtained by post-processing results from a standard finite element stress analysis. It is shown that the non-local stress approach can be linked to the probability of finding the fatigue critical defect in the most highly stressed volume of the component. A numerical procedure is presented that is fully compatible with the results from a standard finite element stress analysis. It is further shown how the fatigue strength distribution can be transformed into a fatigue life distribution by using Basquin's equation. Finally, the non-local stress approach is used for predicting the fatigue limit of several specimens and predictions are compared with test results.

Paper 2

Probabilistic fatigue assessment of a hydro-turbine blade model

The assessment of fatigue is an important design consideration for reliable operation of hydraulic turbine runners. The complex geometry and loading of the runner makes it difficult to consistently define parameters such as nominal stress

and notch depth. Hence, it is of great practical interest to be able to use standard finite element stress analysis directly for performing fatigue assessment of mechanical components without the need for carrying out a separate notch evaluation. In the present paper, Weibull's weakest-link model has been adopted and has been extended to multiaxial fatigue and confined plasticity. The present method can easily be adapted to the post-processing of finite element stress analysis. The accuracy of the method has been assessed by predicting the fatigue life of a three-dimensional fatigue test specimen simulating the leading-edge transition between the blade and the crown/band of a hydraulic turbine runner.

Paper 3

A post-processor for fatigue crack growth analysis based on a finite element stress field

In this paper the algorithm needed for performing a crack growth analysis of a three-dimensional component by post-processing results from a standard finite element stress analysis is given. Weight functions are used for calculating the stress intensity factor for an embedded crack and a surface crack. Defects are generated in several nominally equal components, and crack growth calculations are carried out by using a short crack model to determine the probability of component fatigue failure. The algorithm has been implemented in a finite-element post-processor.

Paper 4

Simulation of fatigue crack growth in components with random defects

The paper presents a probabilistic method for the simulation of fatigue crack growth from crack-like defects in the combined operating and residual stress field of an arbitrary component. The component geometry and operating stress distribution are taken from a standard finite element stress analysis. Number, size and location of crack-like defects are 'drawn' from probability distributions. The presented fatigue assessment methodology has been implemented in a newly developed finite-element post-processor, P•FAT, and is useful for the reliability assessment of fatigue critical components. General features of the finite element post-processor have been presented. Important features, such as (i) the determination of the life-controlling defect, (ii) growth of short and long cracks, (iii) fatigue strength and fatigue life distribution and (iv) probability of component fatigue failure, have been treated and discussed. Short and long crack growth measurements have been presented and used for verification of the crack growth model presented.

Paper 5

Reanalysis of Frost's classical fatigue tests on self-arresting cracks at notches

In this paper, a short crack growth model is presented and used for predicting the arrest of cracks growing in stress gradient fields. The crack growth model makes use of an effective stress which can be interpreted as the stress that must be applied to the corresponding smooth semi-infinite cracked plate to obtain the same value of the stress intensity factor as for the considered notched configuration. The short crack growth model has been used for predicting the conditions, under which crack initiation, crack arrest and failure are expected to occur. These predictions have been compared with experimentally obtained data for notched specimens of mild steel. The predictions are found to be in good agreement with the experimental data.

Paper 6

The application of asymptotic solutions to a semi-elliptical crack at the root of a notch

This paper presents an approximate method based on asymptotic solutions for estimating the stress intensity factor K for semi-elliptic surface cracks at stress concentrations. The proposed equation for estimating K makes use of the near-notch and remote-notch solution to interpolate over the entire range from shallow to deep cracks. The near-notch solution is obtained by means of the stress concentration factor. For cracks located in the remote stress field, K is obtained by considering the crack to be located in a smooth plate with a crack depth equal to the sum of the notch depth and the actual crack depth. The accuracy of the predictions is assessed using numerical calculations and solutions found in the literature.

Paper 7

Approximate stress intensity factors for cracked V-notched specimens based on asymptotic solutions with application to T-joints

This paper presents an approximate method based on asymptotic solutions for estimating the stress intensity factor K for semi-elliptic surface cracks at stress concentrations. The proposed equations make use of a reference solution to interpolate over the entire range from shallow to deep cracks. The reference solution is obtained by considering the current crack emanating from the associated specimen with a sharp notch. It is shown that the proposed formulae satisfy the shallow and deep crack asymptotes. The asymptotic solutions are applied to a T-joint with a fillet-weld-shaped transition. The accuracy of the predictions is assessed using numerical calculations.

Paper 8

Non-linear analyis of shallow cracks in smooth and notched plates. Part 1: analytical evaluation

This is the first paper of two that deal with the non-linear analysis of shallow cracks. Simple formulae are given for estimating the J integral for a power-hardening elastic-plastic solid. The proposed equation for estimating J makes use of the linear elastic and the fully plastic solution to interpolate over the entire range from small- to large-scale yielding. The elastic geometry factor is obtained by means of the stress intensity factor. In the fully plastic formulation, the plastic geometry factors are obtained by considering a pure power-hardening solid, which reduces at one limit to an incompressible linear elastic solid, and at the other to a perfectly plastic solid. The solutions are given for three basic configurations: a double-edge-cracked plate under tension and bending; a notched plate under tension with a crack at the root of the notch; a single-edge-cracked plate under bending. Both force control and displacement control are considered. The accuracy of the formulae is assessed using the finite calculations in Part 2.

Bibliography

[1] **Wormsen, A.** and **Härkegård, G.** A statistical investigation of fatigue behaviour according to Weibull's weakest-link theory. In F. Nilsson et al., editor, *Proceedings of the* 15^{th} *European Conference on Fracture*, Stockholm, Sweden, 2004. ESIS.

[2] **Wormsen, A.** and **Härkegård, G.** A local approach for cracks in smooth and notched components. In F. Nilsson et al, editor, *Proceedings of the* 15^{th} *European Conference on Fracture*, Stockholm, Sweden, 2004. ESIS.

[3] **Wormsen, A.** and **Härkegård, G.** Non-linear analysis of shallow cracks in smooth and notched plates. Part 2: finite element validation. *Journal of Strain Analysis for Engineering Design*, 40(3):245–254, 2005.

[4] **Welte, T. M.**, **Wormsen, A.**, and **Härkegård, G.** Influence of different operating patterns on the life of Francis turbine runners. In *Proceedings of the Hydrovision*, Portland, USA, 2006.

[5] **Wormsen, A.** and **Härkegård, G.** Weibull fatigue analysis of notched components under constant and variable amplitude loading. In W. S. Johnson et al., editor, *Proceedings of the International Fatigue Congress 2006*, Atlanta, Georgia, USA, May 2006. Elsevier.

[6] **Fjeldstad, A.**, **Härkegård, G.**, and **Wormsen, A.** The stress intensity factor for a crack in a finite notched plate based on asymptotic solutions. Submitted for publication in Engineering Fracture Mechanics, 2007.

[7] **Wormsen, A.**, **Fjeldstad, A.**, and **Härkegård, G.** Elastic-plastic analysis of a crack at the root of a notch based on the asymptotic matching of solutions. Department of Engineering Design and Materials, Norwegian University of Science and Technology, 2007.

[8] **Neuber, H.** *Kerbspannungslehre*. Springer-Verlag, Berlin, second edition, 1958.

[9] **Peterson, R. E.** *Metal Fatigue*, chapter 'Notch Sensitivity', pages 293–306. McGraw-Hill, New York, 1959.

[10] **Breat, J. L.**, **Murdy, F.**, and **Pineau, A.** Short crack propagation and closure effects in A508 steel. *Fatigue of Engineering Materials & Structures*, 6(4):349–358, 1983.

[11] **Mann, T.**, **Härkegård, G.**, and **Stärk, K.** Short fatigue crack growth in aluminium alloy 6082-T6. *International Journal of Fatigue*, doi:10.1016/j.ijfatigue.2007.01.00, 2007.

[12] **Frost, N. E.** A relation between the critical alternating propagation stress and crack length for mild steels. *Proceedings of the Institution of Mechanical Engineers*, 173:811–827, 1959.

[13] **Wang, X.**, **Lambert, S. B.**, and **Glinka, G.** Weight functions for embedded elliptical cracks. *Engineering Fracture Mechanics*, 59(3):381–392, 1998.

[14] **Shen, G.** and **Glinka, G.** Weight functions for a semi-elliptical crack in a finite thickness plate. *Theoretical and Applied Fracture Mechanics*, 15(3):247–255, 1991.

[15] **Zheng, X. J.**, **Glinka, G.**, and **Dubey, R. N.** Stress intensity factors and weight functions for a corner crack in a finite thickness plate. *Engineering Fracture Mechanics*, 54(1):49–61, 1996.

[16] **Kießling, R.** *Non-metallic Inclusions in Steel.* The Iron and Steel Institute, London, 1966.

[17] **Kießling, R.** and **Lange, N.** *Non-metallic Inclusions in Steels.* The Metals Society, London, 2nd edition, 1978.

[18] **Juvonen, P.** *Effect of Non-Metallic Inclusions on Fatigue Properties of Calcium Treated Steels.* PhD thesis, Helsinki University of Technology, Finland, 2004.

[19] **Atkinson, H. V.** and **Shi, G.** Characterization of inclusions in clean steels: a review including the statistics of extreme methods. *Progress in Materials Science*, 48:457–520, 2003.

[20] **Coles, S.** *An introduction to statistical modeling of extreme values.* Springer series in statistics, London, 3rd edition, 2001.

[21] **Shi, G.**, **Atkinson, H. V.**, **Sellars, C. M.**, and **Anderson, C. W.** Application of the generalized Pareto distribution to the estimation of the size of the maximum inclusion in clean steels. *Acta Materialia*, 47(5):1455–1468, 1999.

[22] **Shi, G.**, **Atkinson, H. V.**, **Sellars, C. M.**, and **Anderson, C. W.** Comparison of extreme value statistics methods for predicting maximum inclusion size in clean steel. *Ironmaking and Steelmaking*, 26(4):239–246, 1999.

[23] **Kitagawa, H.** and **Takahashi, S.** Applicability of fracture mechanics to very small cracks or the cracks in the early stage. In *Proceedings of the Second International Conference on the Mechanical Behavior of Materials*, pages 627–631, Boston, Ma., 1976.

[24] **El Haddad, M. H.**, **Topper, T. H.**, and **Smith, K. N.** Prediction of non-propagating cracks. *Engineering Fracture Mechanics*, 11(3):573–584, 1979.

[25] **Härkegård, G.** An effective stress intensity factor and the determination of the notched fatigue limit. In J. Bäcklund, A. F. Blom, and C. J. Beevers, editors, *Fatigue thresholds: fundamentals and engineering applications*, volume II, pages 867–879. Engineering Materials Advisory Services Ltd., 1982.

[26] **Tanaka, K.**, **Nakai, Y.**, and **Yamashita, M.** Fatigue growth threshold of small cracks. *International Journal of Fracture*, 17(5):519–533, 1981.

[27] **Hertzberg, R. W.** *Deformation and Fracture Mechanics of Engineering Materials.* John Wiley & Sons, Inc., 4th edition, 1996.

[28] **Härkegård, G.**, **Denk, J.**, and **Stärk, K.** Growth of naturally initiated fatigue cracks in ferritic gas turbine rotor steels. *International Journal of Fatigue*, 27(6):715–726, 2005.

[29] **Klesnil, M** and **Lukáš, P.** Influence of strength and stress history on growth and stabilisation of fatigue cracks. *Engineering Fracture Mechanics*, 4(1):77–92, 1972.

[30] **Tada, H.**, **Paris, P. C.**, and **Irwin, G. R.** *The stress analysis of cracks handbook.* Professional Engineering Publishing Limited, Bury St. Edmunds and London, 3rd edition, 2000.

[31] **Newman Jr., J. C.** and **Raju, I. S.** An empirical stress-intensity factor equation for the surface crack. *Engineering Fracture Mechanics*, 15(1-2):185–192, 1981.

[32] **Huth, H. J.** *Fatigue design of hydraulic turbine runners.* PhD thesis, Norwegian University of Science and Technology, Trondheim, Norway, 2005.

[33] **Phillips, C. E.** and **Heywood, R. B.** The size effect in fatigue of plain and notched steel specimens under reversed direct stress. *Proceedings of the Institution of Mechanical Engineers*, 165:113–124, 1951.

[34] **Weibull, W.** A statistical theory of the strength of materials. *Ingeniörsvetenskapsakademiens handlingar*, 151:1–45, 1939.

[35] **Weibull, W.** The phenomenon of rupture in solids. *Ingeniörsvetenskapsakademiens handlingar*, 153:1–55, 1939.

[36] **Sines, G.** *Metal fatigue*, chapter 'Behaviour of metals under complex static and alternating stresses', pages 145–169. McGraw-Hill, New York, 1959.

[37] **Crossland, B.** Effect of large hydrostatic pressures on the torsional fatigue strength of an alloy steel. In *Proceedings of International Conference on Fatigue of Metals*, pages 138–149, London, 1956. Institution of Mechanical Engineers.

[38] **Dang Van, K.** Macro-micro approach in high-cycle multiaxial fatigue. In D. L. McDowell and R. Ellis, editors, *Advances in Multiaxial Fatigue*, pages 120–130, Philadelphia, USA, 1993. American Society for Testing and Materials, ASTM STP 1191.

[39] **Findley, W. N.**, **Coleman, J. J.**, and **Hanley, B. C.** Theory for combined bending and torsion fatigue with data for SAE 4340 steel. In *Proceedings of the International Conference on Fatigue of Metals*, pages 150–156, London, 1956. Institute of Mechanical Engineers.

[40] **Matake, T.** An explanation on fatigue limit under combined stress. *Bulletin of the Japan Society of Mechanical Engineers*, 20(141):257–263, 1977.

[41] **McDiarmid, D. L.** A general criterion for high cycle multiaxial fatigue failure. *Fatigue and Fracture of Engineering Materials and Structures*, 14(4):429–453, 1991.

[42] **Weber, B.**, **Kenmeugne, B.**, **Clement, J. C.**, and **Robert, J. L.** Improvements of multiaxial fatigue criteria computation for a strong reduction of calculation duration. *Computational materials science*, 15(4):381–399, 1999.

[43] **Socie, D. F.** and **Marquis, G. B.** *Multiaxial fatigue*. Warrendale, Pa.: Society of Automotive Engineers, 2000.

[44] **Norberg, S**. *Prediction of the Fatigue Limit – Accuracy of Post-Processing Methods*. Licentiate thesis, Royal Institute of Technology, Stockholm, Sweden, 2006.

[45] **Trädegård, A.**, **Nilsson, F.**, and **Östlund, S.** FEM-remeshing technique applied to crack growth problems. *Computer Methods in Applied Mechanics and Engineering*, 160(1-2):115–131, 1998.

[46] **Bouchard, P. O.**, **Bay, F.**, **Chastel, Y.**, and **Tovena, I.** Crack propagation modelling using an advanced remeshing technique. *Computer Methods in Applied Mechanics and Engineering*, 189(3):723–742, 2000.

[47] **Bouchard, P. O.**, **Bay, F.**, and **Chastel, Y.** Numerical modelling of crack propagation: automatic remeshing and comparison of different criteria. *Computer Methods in Applied Mechanics and Engineering*, 192(35-36):3887–3908, 2003.

[48] Cornell Fracture Group. *FRANC3D 2.6. Concepts and user guide*. Cornell University, Ithaca, New York, 2003.

[49] *BEASY User Guide, Computational Mechanics BEASY Ltd., 2001*, (Ashurst Lodge, Ashurst, Southampton, Hampshire, SO40 7AA, UK).

[50] **Schöllmann, M.**, **Fulland, M.**, and **Richard, H. A.** Development of a new software for adaptive crack growth simulations in 3D structures. *Engineering Fracture Mechanics*, 70(2):249–263, 2003.

[51] **Fulland, M.** and **Richard, H. A.** Application of the FE-method to the simulation of fatigue crack growth in real structures. *Steel Research*, 74(9):584–590, 2003.

[52] *NASA: Fatigue Crack Growth Computer Program 'NASGRO', version 3.0, 2000*, (Reference Manual, JSC-22267B, Engineering Directorate, National Aeronautics and Space Administration, Lyndon B. Johnson Space Center, Houston).

[53] *AFGROW Users Guide And Technical Manual. Air Vehicles Directorate, Air Force Laboratory, Wright-Patterson Air Force Base, Ohio.*

[54] **Bueckner, H. F.** A novel principle for the computation of stress intensity factors. *Z. Angewandte Math. Mech.*, 50:529–546, 1970.

[55] **Rice, J. R.** Some remarks on elastic crack-tip stress fields. *International Journal of Solids and Structures*, 8(6):751–758, 1972.

[56] **Fett, T.** and **Munz, D.** *Stress Intensity Factors and Weight Functions*. Advances in Fracture. Computational Mechanics Publications, 1997.

[57] **Tveiten, B. W.**, **Fjeldstad, A.**, **Härkegård, G.**, **Myhr, O. R.**, and **Bjørneklett, B.** Fatigue life enhancement of aluminium joints through mechanical and thermal prestressing. *International Journal of Fatigue*, 28(12):1667–1676, 2006.

[58] **Myhr, O. R.**, **Klokkehaug, S.**, **Fjær, H. G.**, **Grong, Ø.**, and **Kluken, A. O.** Modelling of microstructure evolution, residual stresses and distortions in 6082-T6 aluminium weldments. *Welding Journal*, 77(7):286–292, 1998.

[59] **Myhr, O. R.**, **Grong, Ø.**, **Klokkehaug, S.**, **Fjær, H. G.**, and **Kluken, A. O.** Modelling of the microstructure and strength evolution during ageing and welding of Al-Mg-Si alloys. In *Proceedings of the sixth international seminar on numerical analysis of weldability*, Graz-Seggau, Austria, October 1-3 2001.

[60] **Fjær, H. G.**, **Myhr, O. R.**, **Klokkehaug, S.**, and **Holm, S.** Advances in aluminium weld simulations applying Weldsim. In *11th International Conference on Computer Technology in Welding*, Columbus, Ohio, USA, December 2001.

[61] *Abaqus/standard, User's manual, version 6.6-1, 2006*, (Hibbit, Karlsson and Sorensen, Pawtucket, Rhode Island).

[62] **Mann, T.** *Fatigue assessment methods for welded structures and their application to an aluminium T-joint.* PhD thesis, Norwegian University of Science and Technology, Trondheim, Norway, 2006.

[63] **Borrego, L. P.**, **Ferreira, J. M.**, and **Costa, J. M.** Fatigue crack growth and crack closure in an AlMgSi alloy. *Fatigue & Fracture of Engineering Materials & Structures*, 24(4):255–265, 2001.

[64] **Rice, J. R.** A path independent integral and the approximate analysis of strain concentration by notches and cracks. *Transactions of the American Society of Mechanical Engineers, Journal of Applied Mechanics*, 35(6):379–386, 1968.

Paper 1 is not included due to copyright.

ORAL REFERENCE: FT81

PROBABILISTIC FATIGUE ASSESSMENT OF A HYDRO-TURBINE BLADE MODEL

A. Wormsen[1], G. Härkegård[1] and H. J. Huth[1]
[1]Norwegian University of Science and Technology, Trondheim, Norway.

ABSTRACT

The assessment of fatigue is an important design consideration for reliable operation of hydraulic turbine runners. The complex geometry and loading of the runner makes it difficult to consistently define parameters such as nominal stress and notch depth. Hence, it is of great practical interest to be able to use standard finite element stress analysis directly for performing fatigue assessment of mechanical components without the need for carrying out a separate notch evaluation. In the present paper, Weibull's weakest-link model has been adopted and has been extended to multiaxial fatigue and confined plasticity. The present method can easily be adapted to the post-processing of finite element stress analyses. The accuracy of the method has been assessed by predicting the fatigue life of a three-dimensional fatigue test specimen simulating the leading-edge transition between the blade and the crown/band of a hydraulic turbine runner.

KEYWORDS

Weibull analysis, effective stress amplitude, finite element analysis, fatigue testing, intermediate-cycle fatigue.

INTRODUCTION

One of the most critical issues regarding reliable operation of hydraulic turbine runners is fatigue. It is crucial that a reliable fatigue assessment can be performed at an early stage in the design process, since the integrity of the runner primarily depends on inherent reliability. Further, power plant operators increasingly demand a quantification of the reliability of the runner instead of the safe/unsafe - conclusions of classical deterministic design methods [**1**].

During the last twenty years, computer simulation has become widely used for the design of hydraulic turbine runners and has made it possible to obtain the stress field with sufficient accuracy using the finite element method. The challenge, then, is to use the stresses from the finite element analysis to make a reliable fatigue assessment based on fatigue data from standard test specimens.

In the present work, a probabilistic fatigue evaluation procedure is presented that can be easily adapted to the post-processing of finite element stress analysis. The weakest-link theory due to Weibull [**2, 3**] has been used in conjunction with Sines' effective stress cycle [**4**].

Data from fatigue tests on a hydro-turbine blade model [**5**], see Fig. 1, of a G-X5CrNi 13-4 cast steel will be used to validate the proposed probabilistic fatigue assessment procedure.

CLASSICAL FATIGUE ASSESSMENT METHODS

Fatigue life assessment of a hydraulic turbine runner, taking into account start-stop-cycles and flow-induced vibrations, is generally based on the *local stress approach*. Thus, for a given stress ratio R, a turbine runner, with the same peak stress amplitude $\sigma_{\mathrm{a,max}}$ as a homogeneously stressed test specimen, is assumed to have the same fatigue life n as the test specimen, that is

$$\sigma_{\mathrm{a,max}} = \sigma^{*}_{\mathrm{A0}}\left(R,n\right). \tag{1}$$

The characteristic fatigue strength of the homogeneously stressed test specimen is denoted by σ^{*}_{A0}. Although it lies close at hand to use the local stress approach, this generally gives too conservative results [**6**]. To account for the effect of the notch, Thum and Buchmann [**7**] introduced the fatigue notch factor K_{f}, defined as the ratio of the characteristic fatigue strength of a smooth reference specimen to the nominal fatigue strength of a notched specimen:

$$K_{\mathrm{f}} = \frac{\sigma^{*}_{\mathrm{A0}}\left(R,n\right)}{\sigma_{\mathrm{A,net}}\left(R,n\right)}. \tag{2}$$

A number of empirical approaches to estimate K_{f} has been suggested. A review of these can be found in [**8-10**]. Two of the best known empirical equations for estimating K_{f} are due to Neuber [**11**] and Peterson [**12**]. However, the use of these equations requires that a nominal stress can be defined. For a simple specimen, such as a tension rod with a circumferential notch, this is no problem. For an arbitrary component, however, it is often not obvious or even possible to consistently define a nominal stress. This problem becomes evident, if finite element results are employed. Hence, it is of great practical interest to be able to estimate an effective stress amplitude directly from a finite element analysis (FEA).

MEAN STRESS EFFECT

Hydraulic turbine runners under in-service fatigue loading exhibit a fatigue strength that depends on the mean stress level. A tensile mean stress is usually detrimental and a compressive stress is beneficial. Several empirical models are available for taking the mean stress effect on the fatigue strength into account, e.g. those developed by Gerber, Goodman, Soderberg, Haigh, Heywood and Walker. A historical review of the subject area is given in reference [**13**]. In the present work, the empirical relation due to Walker is adopted [**14**].

For a smooth reference fatigue test specimen subjected to the uniaxial stress amplitude σ_{a} and stress ratio R_0, Walker introduced the 'equivalent' pulsating stress amplitude

$$\sigma_{\mathrm{a,Walker}}\left(R=0\right) = \frac{\sigma_{\mathrm{a}}}{\left(1-R_0\right)^{1-\gamma}}, \tag{3}$$

where γ denotes a material parameter.

Under multiaxial and proportional loading conditions, the stress amplitude σ_{a} can be reduced to an 'equivalent' uniaxial loading by means of Sines' criterion [**4**]. Sines uses the equivalent stress due to von Mises based on the stress component amplitudes, i.e.

$$\sigma_{\mathrm{a}} = \sqrt{\frac{3}{2}\sigma'_{ij,\mathrm{a}}\sigma'_{ij,\mathrm{a}}}, \quad i,j = 1,2,3, \tag{4}$$

where $\sigma'_{ij,\mathrm{a}}$ denotes the deviatoric stress amplitude tensor. For a multiaxially stressed solid with the loading specified by the stress amplitude σ_a and the stress ratio R, the 'equivalent' stress amplitude, which results in the same fatigue life as the actual combination of σ_a and R, becomes

$$\sigma_{\mathrm{a,Walker}}(R_0) = \left(\frac{1-R_0}{1-R}\right)^{1-\gamma} \sigma_\mathrm{a}(R), \tag{5}$$

with the aid of Eqn. (3). It should be noted that when (confined) plastic flow occurs, the stress ratio $R = \sigma_{\min}/\sigma_{\max} = (\sigma_\mathrm{m}-\sigma_\mathrm{a})/(\sigma_\mathrm{m}+\sigma_\mathrm{a})$, is no longer constant in the solid.

Based on multiaxial fatigue tests, Sines [**4**] suggested that the mean stress equivalent to that of a uniaxial tension(-compression) cycle, σ_m, should be equal to the invariant sum of the mean normal stress components, that is

$$\sigma_\mathrm{m} = \sigma_{ii,\mathrm{m}}. \tag{6}$$

When FEA is performed, the Walker corrected stress amplitude in Eqn. (5) can be calculated at any point in a finite element by using the element shape functions.

PROBABILISTIC FATIGUE DESIGN APPROACH

The local stress approach generally yields too conservative results. There are several reasons for this, such as the influence of the size of the component or the effect of a stress gradient. A two-parameter weakest-link model due to Weibull [**2, 3**], on the other hand, reproduces these factors in qualitative agreement with experimental observations. Weibull's model uses fatigue data from standard test specimens and takes the distribution of stress of the actual component into account. The probability of component failure is predicted to increase, as the volume of highly stressed material increases.

Weibull's weakest-link theory presumes that the scatter of fatigue life or fatigue strength depends on the size distribution of the strength-controlling defects (pores, inclusions, etc.). Clearly, the probability of finding a material defect above a certain size increases with the volume of highly stressed material.

Fatigue strength distribution

The probability of fatigue failure in a homogeneously stressed volume V at an amplitude below σ_A and a given stress ratio R and number of cycles n is given by

$$P_\mathrm{f}(\sigma_\mathrm{a}, n, R) = 1 - \exp\left\{-\left(\frac{\sigma_\mathrm{a}}{\sigma^*_{\mathrm{A0}}(n,R)}\right)^{b_\sigma} \frac{V}{V_0}\right\}. \tag{7}$$

b_σ and σ^*_{A0} are generally referred to as the Weibull shape and scale parameters. In this paper, they will be called the Weibull fatigue strength exponent and the characteristic fatigue strength, respectively. The distribution parameters can be determined from a set of fatigue data from standard smooth reference test specimens of volume V_0. When σ^*_{A0} is only known for the stress ratio R_0 and the applied stress ratio differs from this value, Eqn. (5) can be introduced into Eqn. (7). The probability of fatigue failure corrected to the same stress ratio R_0 as that of the reference fatigue specimen can then be expressed as:

$$P_\mathrm{f}(\sigma_{\mathrm{a,Walker}}, n, R_0) = 1 - \exp\left\{-\left(\frac{\sigma_{\mathrm{a,Walker}}}{\sigma^*_{\mathrm{A0}}(n,R_0)}\right)^{b_\sigma} \frac{V}{V_0}\right\}. \tag{8}$$

When the state of stress is inhomogeneous, it is appropriate to divide the component, whose overall volume is V, into a large number of small volume elements, ΔV_i, each with a nearly constant stress, σ_{ai}. Just as a chain is as strong as its weakest-link, the component will survive, only if each volume element survives. The probability of survival of the whole volume is therefore equal to the product of the probabilities of survival of all the volume elements. As the volume of each individual element tends to zero, the sum becomes an integral and the overall probability of failure can be written as

$$P_{\mathrm{f}}\left(\sigma_{\mathrm{a,Walker}}, n, R_0\right) = 1 - \exp\left\{-\int_V \left(\frac{\sigma_{\mathrm{a,Walker}}}{\sigma^*_{\mathrm{A0}}\left(n, R_0\right)}\right)^{b_\sigma} \frac{\mathrm{d}V}{V_0}\right\}. \tag{9}$$

The main advantage of introducing the Walker stress amplitude, $\sigma_{\mathrm{a,Walker}}$, is when (confined) plastic flow occurs upon first loading. During unloading of the body, no significant reverse yielding is assumed to occur. Under these conditions the subsequent cyclic behaviour will be elastic, but with a stress ratio that is no longer constant throughout the body. Hence, $\sigma_{\mathrm{a,Walker}}$ enables one to transform the stress amplitudes into a single stress ratio R_0, that gives the same fatigue strength as any actual combination of σ_{a} and R.

If Eqn. (9) is identified with that of a component having the volume V_0 and being subjected to a constant uniaxial stress amplitude, $\bar{\sigma}_{\mathrm{a}}$,

$$P_{\mathrm{f}}\left(\bar{\sigma}_{\mathrm{a}}, n, R_0\right) = 1 - \exp\left\{-\left(\frac{\bar{\sigma}_{\mathrm{a}}}{\sigma^*_{\mathrm{A0}}\left(n, R_0\right)}\right)^{b_\sigma}\right\}, \tag{10}$$

and the effective stress amplitude becomes

$$\bar{\sigma}_{\mathrm{a}} = \left(\frac{1}{V_0}\int_V \sigma^{b_\sigma}_{\mathrm{a,Walker}}\,\mathrm{d}V\right)^{1/b_\sigma}. \tag{11}$$

Typical values for b_σ lie between 10 and 40 and can be found in reference [**15**]. For components where a stress concentration factor K_{t} can be defined, the effective stress amplitude may be related to the nominal stress amplitude, $\sigma_{\mathrm{a,net}}$, through the linear relationship

$$\bar{\sigma}_{\mathrm{a}} = K_{\mathrm{f}}\sigma_{\mathrm{a,net}}, \tag{12}$$

where K_{f} denotes the fatigue notch factor and is a measure of the effectiveness of the notch in reducing the fatigue strength of a notched component.

Fatigue life distribution

Consider now the fatigue life N as a random variable, evaluated at the effective stress amplitude $\bar{\sigma}_a$ and stress ratio R_0. In the intermediate cycle regime, i.e. where the fatigue life is given by the sloping part of the Wöhler curve, the following relation may be derived

$$N_0^* \bar{\sigma}_a^m = n\sigma_{A0}^{*m} = \text{constant}, \tag{13}$$

where N_0^* and m denotes the characteristic fatigue life and Wöhler exponent, respectively. Introducing Eqn. (13) into Eqn. (10) yields

$$P_f\left(n, \bar{\sigma}_a, R_0\right) = 1 - \exp\left\{-\left(\frac{n}{N_0^*\left(\bar{\sigma}_a, R_0\right)}\right)^{b_\sigma / m}\right\}. \tag{14}$$

HYDRO-TURBINE BLADE MODEL

In order to validate the methodology for the probabilistic fatigue design of hydraulic turbine runners, it was decided to demonstrate its accuracy and reliability in estimating the fatigue life of a hydro-turbine blade model.

Geometry

The turbine blade model, shown in Fig. 1, simulates the leading-edge transition between blade and crown/band of a runner.

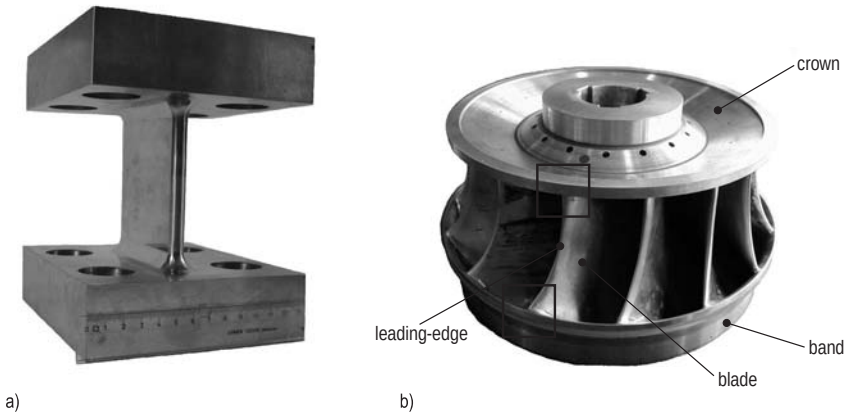

Figure 1: (a) Fatigue test specimen simulating the leading-edge transition zones of (b) the blade of a Francis turbine runner (leading-edge zones are indicated by squares).

A 3D finite element analysis was carried out by modelling an octant of the hydro-turbine blade model. The geometry, displacement constraints and loading conditions (uniaxial tension σ_{net}) are shown in Fig. 2(a), while Fig. 2(b) illustrates a typical finite element mesh employed in the present work. Poisson's ratio was chosen to be $\nu = 0.3$.

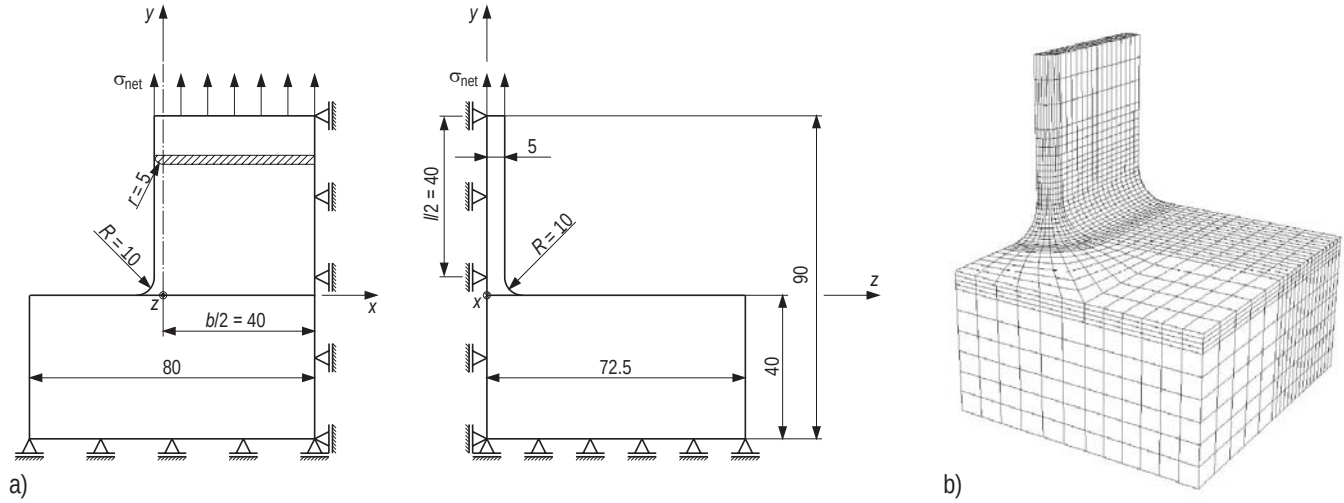

Figure 2: Hydro-turbine blade model; (a) boundary conditions and (b) finite element mesh. The mesh contains 33956 nodes, forming 7286 elements (element type C3D20R in ABAQUS [**16**]).

The blade model is characterised by its height l, its width b, its transition radius R and its edge radius r, as shown in Fig. 2(a). The elastic stress concentration factor, K_t, of the blade model is defined as the ratio between the maximum principal stress, σ_{max}, and the net-section stress, σ_{net}, i.e.

$$K_t = \frac{\sigma_{max}}{\sigma_{net}}. \tag{15}$$

According to FEA, the elastic stress concentration factor $K_t = 1.68$ for the blade model configuration.

Experimental procedure

Four test specimens were manufactured with the dimensions shown in Fig. 3 [**5**]. The specimens were produced from a G-X5CrNi 13-4 casting (200 mm x 300 mm x 1500 mm), a ferritic stainless steel frequently used for cast runners. Each specimen was manually polished with emery cloth. Table 1 gives the chemical composition of the blade steel, Table 2 its mechanical properties.

Table 1: Chemical composition (weight percentage) of the investigated blade steel.

Steel	C	Si	Mn	P	S	Cr	Ni	Mo
G-X5CrNi 13-4	0.040	0.17	0.45	0.032	0.024	12.6	3.59	0.50

Table 2: Properties of the investigated blade steel (at ambient conditions).

Steel	$R_{p0.2}$ [MPa]	R_m [MPa]	E [GPa]	ν	R	f [Hz]
G-X5CrNi 13-4	604	806	160	0.3	0.1	1.5-2.5

Specimens in accordance with Fig. 3 were fixed with eight M30 bolts to a 1000 kN Instron test frame and cycled in pulsating tension (R = 0.1) at 1.5-2.5 Hz [**5**]. Finite element analysis showed that 'ring' material absent in the test specimens due to the presence of Ø33 mm fastener holes has only a minor effect on the stress at the transition [**5**]. The load was chosen so as to yield fatigue lives n between 10^4 and 10^5 cycles. The occurrence of a visible crack defined the life of a specimen.

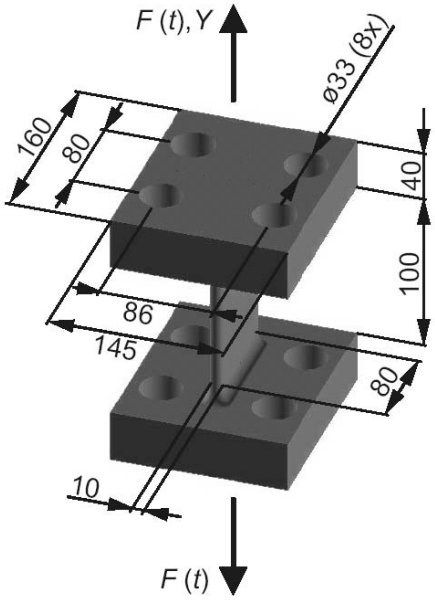

Figure 3: Hydro-turbine blade model; geometry and loading.

Stress redistribution due to confined plasticity occurs upon first loading of the specimen. During unloading no significant reverse yielding occurs. Under these conditions, the subsequent cyclic behaviour will be elastic.

Fatigue test results

Fatigue testing of the blade model revealed low fatigue strength of the cast material. Pores of up to 3 mm in size (minor axis) and of all kind of shapes were distributed throughout the volume, as shown in Fig. 4. These defects turned out to have a more detrimental effect on fatigue life than the geometrical stress concentration. Crack initiation occurred simultaneously at various locations in the 'blade' section. The experimentally observed fatigue lives are listed in Table 3.

Table 3: *S-N* data from experimental fatigue testing and principal results from probabilistic fatigue assessment analyses.

Steel	Specimen no.	R	F_a [kN]	n	$K_f^{\dagger}$	K_t
G-X5CrNi 13-4	R1	0.1	193.4	88 200	1.232	1.68
	R2	0.1	225.9	45 800	1.226	1.68
	R3	0.1	225.9	43 251	1.226	1.68
	R4	0.1	241.7	12 300	1.223	1.68

†Predicted value ($b_\sigma = 15$).

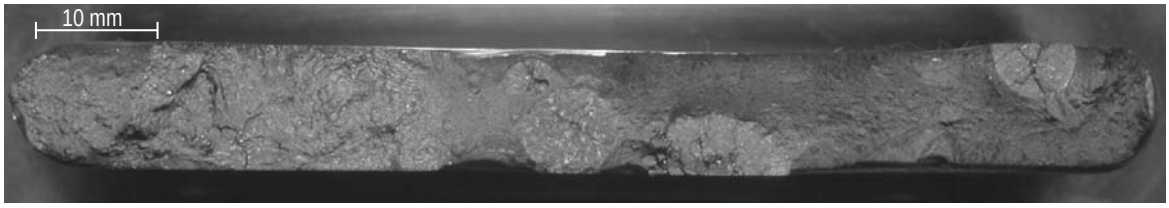

Figure 4: Cracked surface of cast steel G-X5CrNi 13-4 specimen R1 [**5**]**.**

It has been pointed out that the statistical distribution of fatigue life data serves as a starting point for the probabilistic fatigue assessment procedure. Such data were taken from the results reported in references [**17, 18**], which employed smooth cylindrical test specimens, shown in Fig. 5, with a gauge volume $V_0 = 12064$ mm^3. Fatigue testing of these specimens was performed at a frequency of 35 Hz and at stress ratio $R_0 = 0$ under uniaxial loading in a standard laboratory environment. For these specimens, the fatigue life associated with the stress amplitude σ_a and $R_0 = 0$ was given by

$$N_0^* \sigma_a^{6.2} = 1.15 \cdot 10^{20},\ N_0^* < 10^6 \text{ cycles.} \tag{16}$$

From the same investigations, it was found that $b_\sigma \approx 15$.

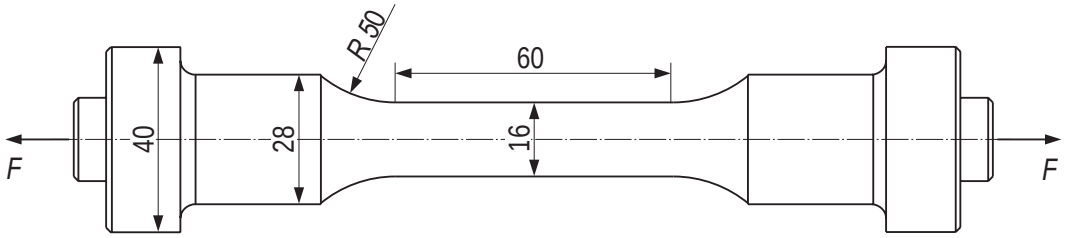

Figure 5: Smooth reference fatigue test specimen.

PROBABILISTIC FATIGUE ASSESSMENT

In the following, the blade specimens (cf. Fig. 3) will be evaluated by means of the probabilistic assessment procedure outlined above.

An elastic-plastic finite element analysis was carried out using the finite element program ABAQUS [**16**]. The material in the FEA was given by the measured stress-strain curve of the considered material. Isotropic hardening and small displacement theory were assumed throughout. The finite element model was first subjected to the maximum load of the cycle. Subsequently, an elastic unloading of the finite element model was performed until the minimum load was reached. From these two stress states, i.e. maximum and minimum loads, the amplitude and mean stresses were computed by means of Sines criterion [**4**]. All stresses were subsequently transformed into an 'equivalent' pulsating stress amplitude $\sigma_{a,Walker}$ ($R_0 = 0$), see Eqn. (5). The Walker exponent was taken as $\gamma = 0.5$, a value representative for a large range of different steels [**6**]. From ABAQUS, stress data were printed out at the nodal points. To be able to compute the effective stress amplitude $\bar{\sigma}_a$ of Eqn. (11), $\sigma_{a,Walker}$ ($R_0 = 0$) can be interpolated through each element utilizing the element shape functions. The integral of Eqn. (11) is in this case evaluated by Gaussian quadrature with 10 x 10 x 10 Gauss points. The effective stress amplitude has been calculated for the specimen shown in Fig. 3, but without fastener holes.

The normalised effective stress amplitude $\bar{\sigma}_a / \sigma_{a,max}$, have been plotted against b_σ in Fig. 6 for specimen R1 (see Table 2). Fig. 6 shows the graph of $\bar{\sigma}_a / \sigma_{a,max}$ against b_σ for two different volume ratios V/V_0. The solid line with a square at each data point is obtained when using the volume of the reference fatigue test specimen in Fig. 5. For a low exponent, i.e. $b_\sigma < 15$, the statistical size effect 'dominates'. As $b_\sigma \to \infty$, the effective stress amplitude asymptotically approaches the maximum stress amplitude $\sigma_{a,max}$ and the two curves coincide. In this case, the Weibull procedure coincides with the local stress approach, and there is no size effect and no influence of the stress gradient on the fatigue life of the component.

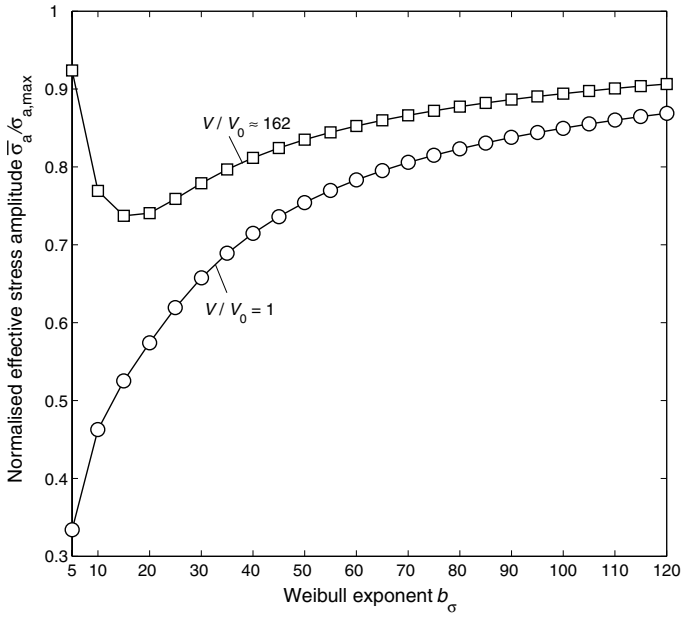

Figure 6: Normalised effective stress amplitude as function of the fatigue strength exponent for specimen R1.

Fig. 7 compares the predicted fatigue lives with those actually measured for the cast steel blade specimens. Fig. 7(a) shows the predicted (n_{pred}) versus the measured fatigue lives (n_{meas}), when the local stress approach is used, see Eqn. (1). The predicted fatigue lives correspond to $P_S = 50\%$, since the median Wöhler curve for the smooth reference fatigue test specimens is used. This method yields conservative life predictions deviating from the observed number of cycles by nearly a factor of 10. The probabilistic fatigue assessment procedure yields the predicted fatigue lives as shown in Fig. 7(b). For each specimen (R1 to R4), the fatigue life has been predicted for P_S = 10%, 50% and 90%. According to Eqn. (14), the fatigue life at a given probability of fatigue failure can be expressed as

$$n = N_0^* \left(\bar{\sigma}_a, R_0\right)\left[-\ln\left(1-P_f\right)\right]^{m/b_\sigma} . \tag{17}$$

The probabilistic predictions are seen to be in satisfactory agreement with the experimentally observed lives.

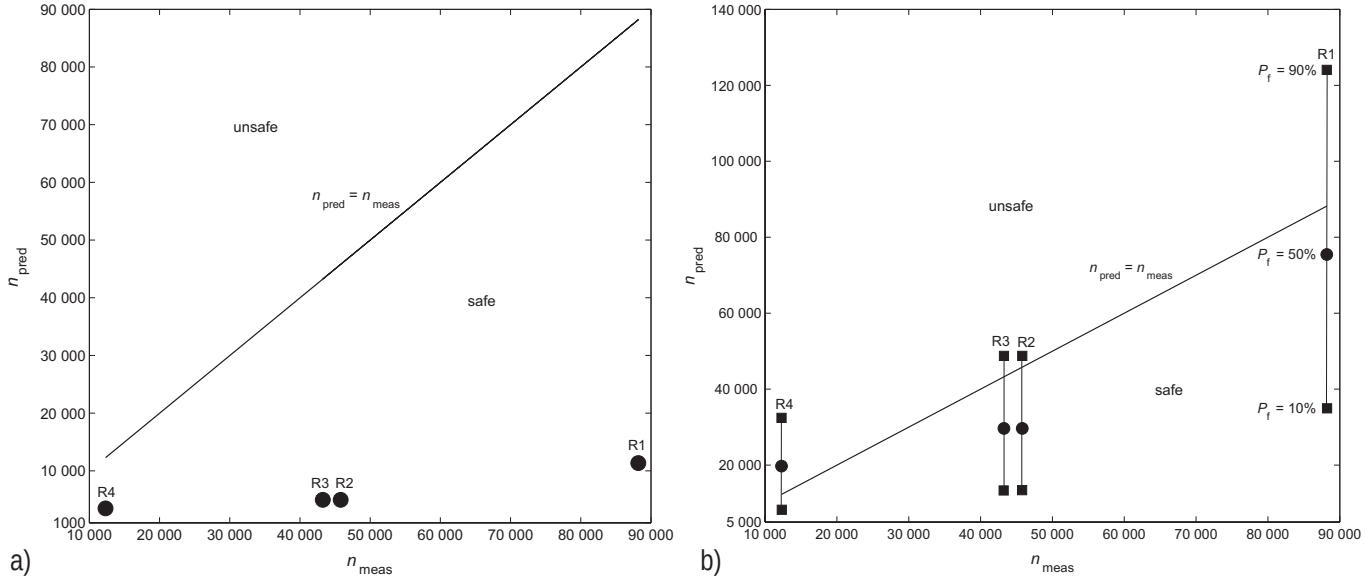

Figure 7: Life predictions by (a) the local stress approach and (b) the probabilistic fatigue assessment procedure (b_σ = 15) for the G-X5CrNi 13-4 cast test specimens (R1 to R4).

CONCLUSIONS

A probabilistic fatigue assessment procedure has been presented, which considers the effect of size, stress gradients and stress redistribution due to confined plasticity upon first loading. The weakest-link theory due to Weibull has been used in conjunction with Sines' effective stress cycle.

Fatigue tests have been performed on a hydro-turbine blade model, manufactured from a G-X5CrNi 13-4 cast steel slab and representing the leading-edge transition between the blade and the band/crown of a Francis turbine runner. The load range was chosen to yield fatigue lives between 10^4 and 10^5 cycles.

Using the local stress approach in the intermediate cycle regime, i.e. where the fatigue life is given by the sloping part of the Wöhler curve, yields life predictions nearly a factor of 10 less than those observed experimentally. The probabilistic predictions were seen to be in satisfactory agreement with the experimentally observed lives.

The probabilistic fatigue assessment procedure should be a useful tool for the quantification of reliability of hydraulic turbine runners, as well as other fatigue loaded components.

ACKNOWLEDGMENTS

The authors gratefully acknowledge the research support for this work provided by GE Energy (Norway) AS.

REFERENCES

1. **Faanes, S.** and **Børresen, B.** (2004). In: *22nd IAHR Symposium on Hydraulic Machinery and Systems, Stockholm*.
2. **Weibull, W.** (1939). In: *Ingeniörsvetenskapskapsakademiens handlingar*, 151:1-45.
3. **Weibull, W.** (1939). In: *Ingeniörsvetenskapskapsakademiens handlingar*, 153:1-55.
4. **Sines, G.** (1959). In: *Metal Fatigue,* pp. 145-169, Sines, G. and Waisman, J. L. (Eds). McGraw-Hill, New York.
5. **Huth, H. J.** (2005). PhD thesis, Norwegian University of Science and Technology, Norway.
6. **Dowling, N. E.** (1999). *Mechanical Behavior of Materials*. Prentice Hall, Inc., London.
7. **Thum, A.** and **Buchmann, W.** (1932). *VDI-Verlag*, Berlin.
8. **Yao, W., Xia, K.,** and **Gu, Y. (**1995) *Int. J. Fatigue.* 17, 245.
9. **Makkonen, M.** (1999). PhD thesis, Lappeenranta University of Technology, Finland.
10. **Ciavarella, M.** and **Meneghetti, G.** (2004) *Int. J. Fatigue.* 26, 289.
11. **Neuber, H.** (1958). *Kerbspannungslehre.* Springer-Verlag, Berlin.
12. **Peterson, R. E.** (1959). In: *Metal Fatigue*, pp. 293-306, Sines, G. and Waisman, J. L. (Eds). McGraw-Hill, New York.
13. **Sendeckyj, G. P.** (2001). *Int. J. Fatigue.* 23, 347.
14. **Walker, K.** (1970). In: *Effects of Environment and Complex Load History on Fatigue Life*, pp. 1-14. ASTM STP 462, Philadelphia.
15. **Wormsen, A.** and **Härkegård, G.** (2004). In: *The 15th European Conference of Fracture,* F. Nilsson et al. (Eds). ESIS, Stockholm.
16. Abaqus/standard, User's manual, version 6.5-1.
17. **Buxbaum, O.** and **Ostermann, H.** (1983). *Ausfallsichere Bemessung von Laufrädern für Wasserkraftmaschinen aus rostfreiem Stahlguss unter Berücksichtigung von Korrosion und Gefügezustand.* Technical report, Fraunhofer Institute for Structural Durability, Darmstadt.
18. **Sonsino, C. M.** and **Diererich, K.** (1990) *Werkst. Korros.* 41, 330.

A post-processor for fatigue crack growth analysis based on a finite element stress field

A. Wormsen*, A. Fjeldstad and G. Härkegård
Norwegian University of Science and Technology, Trondheim, Norway.

Abstract

In this paper the algorithm needed for performing a crack growth analysis of a three-dimensional component by post-processing results from a standard finite element stress analysis is given. Weight functions are used for calculating the stress intensity factor for an embedded crack and a surface crack. Defects are generated in several nominally equal components, and crack growth calculations are carried out by using a short crack model to determine the probability of component fatigue failure. The algorithm has been implemented in a finite-element post-processor.

Keywords: Finite element analysis, fatigue crack growth, weight function, defect size distribution, probability of component fatigue failure.

NOTATION

A	defect size (random variable)
A_{crack}	defect area
a	defect size
a'	intrinsic crack length
a_0	scale parameter in the extreme value distribution
a_0^*	characteristic largest defect size
a_{crit}	critical defect size
a_{f}	final defect size
a_{i}	initial defect size
a_{th}	peak over threshold defect size
C	coefficient in crack growth law
c	half the surface crack length
F	geometry factor
FEA	finite element analysis
$G(a)$	generalised extreme value distribution
g	weight function
$H(a)$	generalised Pareto distribution
$\lvert\mathbf{J}\rvert$	Jacobian determinant
K	stress intensity factor
K_{Ic}	fracture toughness
K_{t}	stress concentration factor $= \sigma_{\max}/S_{\text{net}}$
ΔK_{th}	threshold stress intensity factor range
L	distance from a given point to the free surface
m	exponent in crack growth law
n	number of cycles
$\mathbf{N}$	element shape functions
N_{els}	number of elements
N_{Gauss}	number of Gauss points in one of the coordinate directions
N_{nodes}	number of nodes
$N_{\text{nodes,el}}$	number of nodes per element
$\mathbf{n}_1$	eigenvector associated with the maximum principal stress
$\mathbf{n}_{\text{f}}$	element face normal
P_{s}	probability of survival
R	stress ratio $= \sigma_{\min}/\sigma_{\max}$
$\mathbf{R}$	orthogonal rotation matrix
$\mathbf{S}$	translation vector
S_{net}	net-section stress
$\mathbf{T}$	transformation matrix
V	volume
ΔV	element volume
W_i	weight factor of the i^{th} Gauss point
x, y, z	global coordinate system
x', y', z'	transformed coordinate system
z_1	number of critical defects per unit volume
$\Delta\sigma$	stress range $= \sigma_{\max} - \sigma_{\min}$
σ_{a}	(equivalent) stress amplitude
σ_{A}	fatigue limit
σ_{m}	(equivalent) mean stress
$\sigma_{\max}$	maximum stress
$\sigma_{\min}$	minimum stress
σ_{n}	stress normal to the crack plane
σ_{ij}	operating stress tensor
σ_{ij}^0	residual stress tensor
ξ, η, ζ	non-dimensional parent element coordinates
ξ'	shape parameter in the extreme value distribution

*Corresponding author: Department of Engineering Design and Materials, Norwegian University of Science and Technology, Richard Birkelandsvei 2B, Trondheim, NO-7491 , Norway; email: anders.wormsen@ntnu.no

1 Introduction

At a time when the industry is continuously challenged to come up with better and less costly products, and this in ever shorter cycles, all product development processes must be improved, including fatigue design. In order to comply with this development, it is the authors' conviction that standard fatigue analysis tools should reflect that fatigue is caused by the (random) growth of fatigue cracks from randomly distributed defects. Unfortunately, this is bound to make the fatigue design process much more complex. Hence, a robust fatigue assessment tool, directly applicable to the results from a standard finite element stress analysis, would be of great importance in the process of developing optimised, safe and reliable structural components.

As shown in Table 1, there is a variety of approaches to the fatigue analysis of a mechanical component, all basically related to fatigue crack propagation. The initiation based approaches use conventional $S-N$-data as a starting point, and the fatigue life, N, is usually defined as the number of load cycles required for a macroscopic crack to develop. The propagation based approaches consider the actual growth of a crack from an initial (defect) size a_{i} to a final size a_{f}.

Standard methods for fatigue life predictions are deterministic by nature, i.e., material properties including defect size are considered as predetermined quantities. Two of the most widespread deterministic fatigue assessment methods are:

- '*Local stress approach*' – Life prediction based on the equivalence between the most highly stressed point of a component and a standard smooth fatigue specimen under the same stress.

- '*Single defect approach*' – Life prediction based on the growth of a single 'worst-case' crack-like defect at the location of maximum stress.

The probabilistic approaches, on the other hand, assume material properties to be randomly distributed:

- '*Weakest-link approach*' – Assumes the probability of survival of a component to be the product of the probabilities of survival of the (small) elements into which the component has been divided for purposes of analysis. The probability of survival of an element is a function of the stress cycle, the characteristic fatigue strength and the size of the element.

- '*Random defect approach*' – The model is based on a finite element stress analysis and assumptions on the defect distribution as well as a theory for the growth of short cracks. Each finite element is associated with one or more defects by 'drawing' from a Poisson distribution. The initial posistion of a defect is obtained from a uniform distribution while its size is obtained from an extreme value distribution. The defects are considered to be crack-like, and the number of cycles required for each defect to become critical is determined. By carrying out a large number of such simulations, the fatigue life distribution of the component is obtained.

When a commerically available finite element code such as ABAQUS is used for performing a crack growth analysis, the crack is explicitly modelled as an integrated part of the component. For each crack growth increment, the mesh surrounding the crack has to be remeshed. Re-meshing techniques applied to crack growth problems have been treated in several papers, e.g. [**1**–**3**]. Examples of codes that have implemented re-meshing techniques for handling crack growth analysis of 3D components are FRANC3D [**4**], BEASY [**5**] (both use the boundary element method) and ADAPCRACK3D [**6,7**] (uses the finite element method). In order to reduce the time required for performing a crack growth analysis, the component geometry is often simplified so that a standard handbook solution can be used for performing a fatigue life prediction. Such handbook solutions are available in the programs NASGRO [**8**] and AFGROW [**9**]. Another approach is to perform the crack growth analysis by assuming a homogeneous stress field based on the maximum stress acting on the component surface. This maximum stress approach yields acceptable results provided that the stress decreases slowly, i.e., the stress gradient is low, and when the geometrical simplification can be justified. An alternative is to use results from a standard finite element stress analysis and account for a crack by using weight functions [**10, 11**]. This approach has been implemented in the stand-alone finite-element post-processor P•FAT. By 'drawing' the number, size and position of crack-like defects from distribution functions and repating this process for a large number of nominally equal components ('Monte Carlo' simulation), the fatigue life distribution of the component could be obtained. With this, one has a post-processing tool that can estimate the probability of component failure by means of fatigue crack growth calculations. The application of this feature should be of considerable interest in assessing the influence of defects on the reliability of cast components.

The finite-element post-processor also supports the local stress approach and the weakest-link approach [**12**–**14**]. The post-processor can perform fatigue crack growth calculations of embedded cracks and surface cracks, see Fig. 1. The code strictly handles only homogeneous mechanical properties. Piecewise homogeneous 'quality zones' may be taken into account in the process of generating defects, i.e., number, position and size. In addition, the proposed method is presently restricted to proportional loading.

Table 1: Different approaches to fatigue analysis, all related to fatigue crack growth.

Approaches to fatigue analysis	Deterministic	Probabilistic
Initiation based	Local Stress	Weakest Link
Propagation based	Single Defect	Random Defect

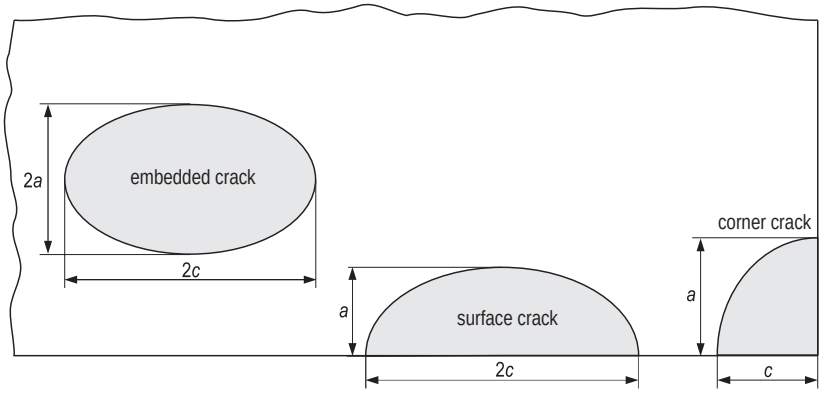

Figure 1: Crack configurations implemented in the finite-element post-processor.

The paper is organised as follows. In Section 2, the principal features of the finite-element post-processor are given. Section 3 addresses the basic numerical codes needed, and in Section 4 it is shown how crack-like defects are propagated. Section 5 describes how defects are generated, and in Section 6 a flow-chart of the random defect module is given. Finally, some conclusions are drawn in Section 7.

2 Principal features of P•FAT

P•FAT is designed as a stand-alone finite-element post-processor with the component geometry and stresses given by a standard finite element program. Data needed for the computation are nodal coordinates, element topology and stresses. In addition to operating stresses, process-related residual stresses can be taken into account. Such residual stresses may be imported directly from, e.g., casting or welding simulations. The surface elements are found automatically and are used for defining the geometry of the component.

In the propagation based approaches, the initial crack-like defect is regarded as an embedded crack, or as a surface crack, depending on the location of the crack front relative to the free surface. A crack is treated as a corner crack, if it starts from or propagates into a right-angled corner.

Failure of a component occurs, when the crack has reached a predefined size, or the stress intensity factor K has reached the fracture toughness K_{Ic}. When a surface crack breaks the opposing free surface, it has to be treated as a through-crack. This may be a most relevant situation, e.g., for a crack growing through a thin plate. On the other hand, for initial defects that are much smaller than the thickness of the plate, a through-crack is only present during a small fraction of the component life. Thus, instead of explicitly modelling the through-crack, crack growth is terminated as soon as the surface crack breaks the opposing free surface.

P•FAT is compatible with standard finite element codes such as ABAQUS, ANSYS and NASTRAN. It is written in standard FORTRAN and can be operated under Windows and UNIX/LINUX.

3 Post-processing of finite element stress analysis

3.1 Multiaxial stress criterion

The fatigue crack growth is assumed to be controlled by the normal stress cycle on the plane perpendicular to the direction of the maximum principal stress at the crack origin. Thus, the stress amplitude, σ_{a}, at an arbitrary point on the crack plane is calculated according to

$$\sigma_{\mathrm{a}} = \sigma_{\mathrm{n,a}} = n_{1i}\sigma_{ij,\mathrm{a}}n_{1j},\ i,j = 1,2,3, \qquad (1)$$

and the mean stress, σ_{m}, by

$$\sigma_{\mathrm{m}} = \sigma_{\mathrm{n,m}} = n_{1i}(\sigma_{ij,\mathrm{m}} + \sigma^{0}_{ij})n_{1j}. \qquad (2)$$

$\mathbf{n}_1$ is the unit eigenvector of the maximum principal operating stress, and σ_{ij}^0 denotes the residual stress tensor.

Generally, the direction of maximum principal stress in the uncracked component changes as the crack grows on a specific plane. In the present work, the change of the crack growth direction is neglected. Generally, this can be justified as long as the crack is small compared with the dimension of the component, i.e., for a large fraction of the fatigue life.

3.2 Numerical formulation

Consider now a defect located in an arbitrary elastic body subject to the combined operating and residual stress field $\sigma_{ij}(\mathbf{x})$. The origin of the crack-like defect is given by the reference point $\mathbf{x}_0 = [x_0, y_0, z_0]^{\mathrm{T}}$. A local coordinate system, $\mathbf{x}'$, is attached to the crack origin, $\mathbf{x}_0$, as shown in Fig. 2. The local coordinate system is defined by means of the transformation matrix

$$\mathbf{T} = [\mathbf{R}\ \mathbf{S}] = \begin{bmatrix} R_{11} & R_{12} & R_{13} & x_0 \\ R_{21} & R_{22} & R_{23} & y_0 \\ R_{31} & R_{32} & R_{33} & z_0 \end{bmatrix}, \qquad (3)$$

where $\mathbf{R}$ is a 3×3 orthogonal matrix, known as the rotation matrix, defining the orientation of the local coordinate system. $\mathbf{S}$ is a 3×1 translation vector defining the origin of the coordinate system. Vectors given in the local coordinate system are marked with a prime ($'$). The rotation matrix is given by the vectors $\mathbf{n}_2$, $\mathbf{n}_3$, and $\mathbf{n}_1$, respectively, as

$$\mathbf{R} = [\mathbf{n}_2\ \mathbf{n}_3\ \mathbf{n}_1], \qquad (4)$$

where $\mathbf{n}_1$ is perpendicular to the crack surface and is equal to the eigenvector associated with the maximum principal stress. The $\mathbf{n}_3$ vector is determined as the vector that gives the shortest length, L, between a free surface point and the crack origin, see Fig. 2. $\mathbf{n}_2$ is perpendicular to $\mathbf{n}_3$ and $\mathbf{n}_1$. Since $\mathbf{R}$ is an orthogonal matrix, i.e., $\mathbf{R}^{-1} = \mathbf{R}^{\mathrm{T}}$, the transformation from global to local coordinates, is given by

$$\mathbf{x}' = \mathbf{R}^{\mathrm{T}}\mathbf{x} - \mathbf{R}^{\mathrm{T}}\mathbf{S}. \qquad (5)$$

To obtain the stress intensity factor, K, the crack surface is automatically meshed with plane isoparametric elements in the post-processor. The stress amplitude normal to the crack plane, σ_{a}, can be found when the corresponding parent global element coordinates, $\boldsymbol{\xi} = [\xi, \eta, \zeta]^{\mathrm{T}}$, and the element number in the un-cracked component is known. The latter is found by first performing a transformation from $\boldsymbol{\xi}'$ to $\mathbf{x}'$. $\boldsymbol{\xi}'$ is the parent element coordinates for the crack elements. With an isoparametric description of the crack geometry, the transformation is given by

$$\mathbf{x}' = \mathbf{N}(\boldsymbol{\xi}')\mathbf{x}'_{\mathrm{nodes}}, \qquad (6)$$

where $\mathbf{N}$ is the element shape function matrix and $\mathbf{x}'_{\mathrm{nodes}}$ is the local coordinates of the nodes in the crack element mesh. The corresponding global point $\mathbf{x}$ is found according to

$$\mathbf{x} = \mathbf{R}\mathbf{x}' + \mathbf{S}. \qquad (7)$$

The point $\mathbf{x}$ is within an element if the following condition is satisfied for all element faces

$$\mathbf{n}_{\mathrm{f}} \cdot \mathbf{v} \geq 0,\ \mathbf{v} = \mathbf{x}_{\mathrm{s}} - \mathbf{x}, \qquad (8)$$

where $\mathbf{n}_{\mathrm{f}}$ denotes the surface normal at the point $\mathbf{x}_{\mathrm{s}}$, see Fig. 3.

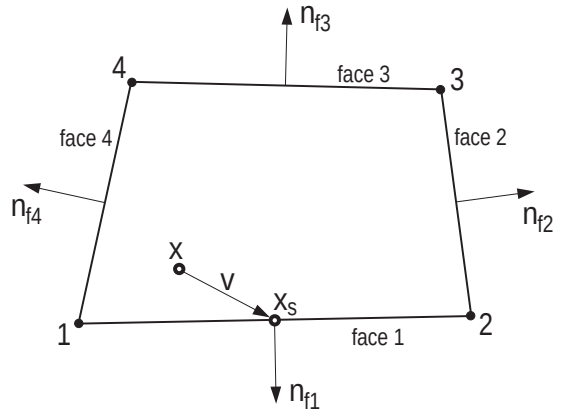

Figure 3: A point $\mathbf{x}$ within an element and definition of the element face normal $\mathbf{n}_{\mathrm{f}}$ (a plane four-noded element is used for illustration).

The parent global element coordinates, $\boldsymbol{\xi}$, are obtained by using a Newton-Kantorovich iteration algorithm. This algorithm computes a solution of

$$\mathbf{f}(\boldsymbol{\xi}) = \mathbf{x} - \mathbf{N}\mathbf{x}_{\mathrm{nodes}} = \mathbf{0}, \qquad (9)$$

given an initial approximation $\boldsymbol{\xi}^{(0)}$ (starting value of the iteration). It is appropriate to use $\boldsymbol{\xi}^{(0)} = \mathbf{0}$ as a starting value, i.e., the center of the element. For the initial guess, one has the Taylor series with remainder in the form

$$\mathbf{f}(\boldsymbol{\xi}) = \mathbf{f}(\boldsymbol{\xi}^{(0)}) + \mathbf{f}'(\boldsymbol{\xi}^{(0)})(\boldsymbol{\xi} - \boldsymbol{\xi}^{(0)}) + \mathbf{R}(\boldsymbol{\xi}). \qquad (10)$$

If one omits the remainder term $\mathbf{R}(\boldsymbol{\xi})$, then

$$\mathbf{f}(\boldsymbol{\xi}^{(0)}) + \mathbf{f}'(\boldsymbol{\xi}^{(0)})(\boldsymbol{\xi} - \boldsymbol{\xi}^{(0)}) = \mathbf{0}. \qquad (11)$$

Hence, one could form the iterative sequence of approximations as

$$\boldsymbol{\xi}^{(k+1)} = \boldsymbol{\xi}^{(k)} - \mathbf{f}'^{(k)}(\boldsymbol{\xi}^{(k)})^{-1}\mathbf{f}(\boldsymbol{\xi}^{(k)}),\ k = 0, 1, \ldots, \qquad (12)$$

where

$$f'_{ij} = -\left(\frac{\partial \mathbf{N}}{\partial \boldsymbol{\xi}_j}\right)\mathbf{x}_{\mathrm{nodes},i},\ i, j = 1, 2, 3. \qquad (13)$$

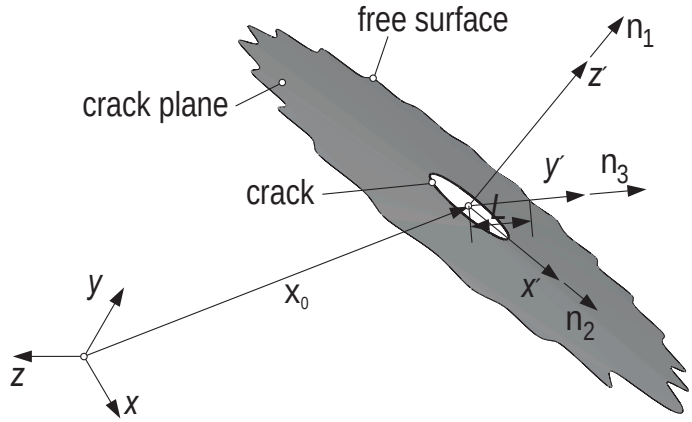

Figure 2: Definition of the crack plane and the local coordinate system $\mathbf{x}'$.

The iteration is continued until the condition

$$|\boldsymbol{\xi}^{(k+1)} - \boldsymbol{\xi}^{(k)}| \leq \epsilon, \tag{14}$$

is satisfied with the desired accuracy ϵ.

The stress amplitude normal to the crack plane, σ_{a}, at a given position $\mathbf{x}$, can then be found as **[15]**

$$\sigma_{\mathrm{a}} = \sum_{i=1}^{N_{\mathrm{nodes,el}}} N_i(\boldsymbol{\xi})\sigma_{\mathrm{a}i}, \tag{15}$$

where the index i ranges over the number of nodes in the element and N_i is the i^{th} element of the element shape function.

Since the influence of a free surface is included in the calculation of the stress intensity factor K, the surface elements of the component must be identified. A free element surface is characterised by a unique combination of face nodes.

When the component surface is identified the distance, L, from the point $\mathbf{x}$ to the free surface in a direction $\mathbf{e}$ (unit vector) can be calculated, cf. Fig. 4. However, before L can be found the element surface which $\mathbf{e}$ passes through must be identified. The vector $\mathbf{e}$ passes through a free element surface, if and only if,

$$\mathbf{n}_{\mathrm{sf}} \cdot \mathbf{e} \leq 0, \tag{16}$$

for all spanned faces, see Fig. 4. Here, $\mathbf{n}_{\mathrm{sf}}$ is the spanned face normal as shown in Fig. 4. The distance, L, between $\mathbf{x}$ and an unknown point $\mathbf{x}_{\mathrm{s}}$ [see Fig. 4] located on the element surface is found according to

$$L = \frac{(\mathbf{x}_{\mathrm{node}} - \mathbf{x}) \cdot \mathbf{n}_{\mathrm{f}}}{\mathbf{e} \cdot \mathbf{n}_{\mathrm{f}}} = \frac{|\mathbf{x}_{\mathrm{node}} - \mathbf{x}| \cos\alpha}{\cos\theta}. \tag{17}$$

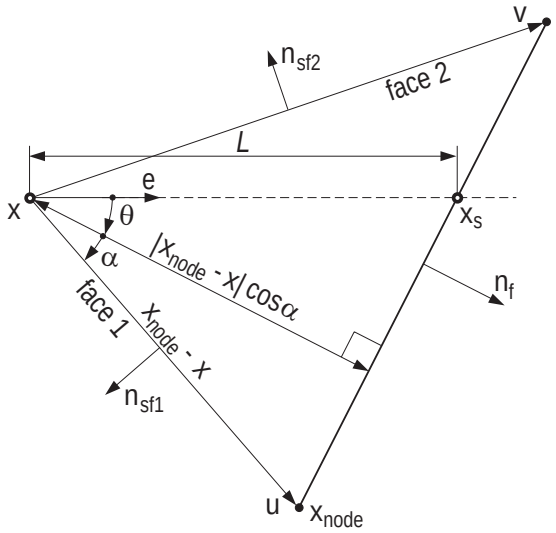

Figure 4: Graphical illustration of the distance L between the point $\mathbf{x}$ and a free element face with face normal $\mathbf{n}_{\mathrm{f}}$.

4 Crack growth approach

In the propagation based modules, the fatigue life is obtained by summing up the number of cycles necessary to propagate an initial crack-like defect to a user defined

critical state. For the fatigue life to be properly calculated, the crack growth law should take the behaviour of short cracks into account [**16, 17**]. In the next Subsection, the crack growth law is presented, followed by a short description of the crack growth increment procedure. Finally, it is shown how the stress intensity factor, K, is calculated using the stress field from the un-cracked component.

4.1 Crack growth law

El Haddad et al. [**18**] defined the 'effective' crack length as the sum of the actual crack length and an intrinsic crack length. By using this effective crack length in conjunction with the fatigue crack growth law by Klesnil and Lukáš [**19**], Fjeldstad et al. [**20**] derived the following equation for the growth rate of short fatigue cracks:

$$\frac{\mathrm{d}a}{\mathrm{d}n} = C\Delta K_{\mathrm{th}}^{m}\left[\left\{\left(\frac{\Delta\sigma}{\Delta\sigma_{\mathrm{A}}}\right)^{2}+\left(\frac{\Delta K}{\Delta K_{\mathrm{th}}}\right)^{2}\right\}^{\frac{m}{2}}-1\right]. \tag{18}$$

In equation (18), $\Delta\sigma_{\mathrm{A}}$ is the fatigue limit of a smooth, polished fatigue specimen without (major) defects, $\Delta\sigma$ is the stress range normal to the crack plane and ΔK_{th} is the threshold stress intensity range.

The constant C of the crack growth law, the fatigue limit and the threshold stress intensity range can all be transformed to the present R-ratio by using Walker's equation [**21**] as shown in [**22**]. The exponent m of the crack growth law generally varies only weakly with R [**22**] and can be assumed to be constant.

4.2 Determination of crack growth increments

By rearranging equation (18), the fatigue life, n, is obtained by means of numerical integration with an adaptive crack increment control. The maximum allowable crack increment is controlled in such a way that the aspect ratio a/c cannot change more than, say, 2% for each incremental step. The increment is denoted by $\delta(\mathrm{A})$ and represents the growth of the point A on the crack front (see Figs. 5(a) and 8(b)). By using $\delta(\mathrm{A})$ as a starting point, the incremental growth, $\delta(\mathrm{P})$, for an arbirary point P along the crack front is estimated according to

$$\delta(\mathrm{P}) = \delta(\mathrm{A})\left(\frac{\Delta K(\mathrm{P})}{\Delta K(\mathrm{A})}\right)^{m}. \tag{19}$$

4.3 Stress intensity factor

The prediction of crack behaviour has always been a challenge for researchers, and crack propagation represents a real concern among engineers. In linear elastic crack mechanics, the stress intensity factor, K, is the main parameter to seek. In this Subsection, a method for numerical determination of stress intensity factors in three-dimensional geometries will be given and verified. The method is based on the theory of weight functions, which computes the required stress intensity factor based on the stress field of the crack-free component. The use of weight functions in crack mechanics was first proposed by Bueckner [**10**] and subsequently generalised by Rice [**11**]. The reader is referred to the above references for a detailed discussion on the theoretical aspects of the method.

Consider now a two-dimensional crack located in an arbitrary elastic body subjected to the combined operating and residual stress field $\sigma_{ij}(\mathbf{x})$. The crack is assumed to grow in a direction perpendicular to the direction of the maximum principal stress determined at the crack origin $\mathbf{x}_0$, cf. Fig. 2. A local coordinate system $\mathbf{x}'$ is introduced at $\mathbf{x}_0$, see Fig. 2. The transformation from global to local coordinates is given by equation (5). The weight function, $g(x', y'; \mathrm{P})$, is defined as the stress intensity factor value at the crack front point P, when a pair of symmetrical unit opening forces are applied at an arbitrary point P′ on the crack surface, cf. Fig. 5(a). In the case of a distributed symmetrical loading on the crack surface, the stress intensity factor K is obtained by integrating the product of the weight function $g(x', y'; \mathrm{P})$ and the stress distribution of the crack free solid $\sigma_{\mathrm{a}}(x', y')$ over the crack surface area A_{crack}:

$$K(\mathrm{P}) = \int_{A_{\mathrm{crack}}} \sigma_{\mathrm{a}}(x', y')g(x', y'; \mathrm{P})\,\mathrm{d}A_{\mathrm{crack}}. \tag{20}$$

The relationship between the weight function and the displacement field is given in [**11**].

The integral in equation (20) can be solved numerically for instance by Gauss-Legendre quadrature. This procedure subdivides the crack surface into N_{els} plane elements with N_{nodes} nodes. By virtue of the property of definite integrals, the stress intensity factor is obtained by performing a summation over all elements on the crack surface:

$$K \approx \sum_{k=1}^{N_{\mathrm{els}}}\Big(\sum_{i=1}^{N_{\mathrm{Gauss}}}\sum_{j=1}^{N_{\mathrm{Gauss}}}\sigma_{\mathrm{a}}(\xi_i', \eta_j')g(\xi_i', \eta_j'; P')\times |\mathbf{J}(\xi_i', \eta_{\mathbf{j}}')|\, W_i\, W_j\Big). \tag{21}$$

Here, $|\mathbf{J}|$ is the determinant of the Jacobian maxtrix and (ξ', η') the corresponding non-dimensional parent crack element coordinates at the Gauss points. W_i is the weight factor of the i^{th} Gauss point and N_{Gauss} is the number of Gauss points in each coordinate direction.

4.3.1 *Embedded crack*

For an infinite body with an embedded crack under distributed loading perpendicular to the plane of the crack,

the weight function is given by [**23**]

$$g(x', y'; P') = \frac{\sqrt{2s}}{\pi^{3/2}\rho^2}\sqrt{1 - \frac{s}{8\rho_1} - \frac{s}{8\rho_2} - \frac{s}{8\rho_3} - \frac{s}{8\rho_4}}, \tag{22}$$

where s is the shortest distance between the point P′ and the crack front, and ρ is the distance between P and P′, see Fig. 5(a). ρ_1 to ρ_4 are parameters depending on the shape of the crack [**23**].

To obtain the stress intensity factor, the crack surface is meshed with plane elements as shown in Fig. 5(b). K is calculated numerically by using equation (21). The mesh density and size are adjusted according to the local value of the weight function. Since the weight function becomes singular when P′ approaches P, a fine mesh is used around P. Fig. 5(b) illustrates a typical finite element mesh used. In order to obtain a proper description of the growth of an embedded crack, K is calculated at four locations, i.e., points A, B, C and D [see Fig. 5(a)], at the crack front.

The K solution proposed by Wang et al. [**23**] holds for an embedded elliptical crack located in an infinite body. In order to take into account the free surface effect on K, an empirical 'stress intensity magnification factor' proposed by Fett and Mattheck [**24**] is used. The magnification factor is multiplied with the weight function based K solution. The stress intensity magnification factor depends on the distance, L, from the crack center to the free surface and the aspect ratio a/c, cf. Fig. 6.

In Fig. 6(a), geometry factors F [see equation (24)] at four locations on the crack front of an embedded crack have been plotted against the aspect ratio, a/c. The crack is located in an infinite body and the crack surface is subjected to the stress field

$$\sigma_{\mathrm{a}}(y') = \sigma_0 \left(\frac{y'}{a}\right)^i. \tag{23}$$

The geometry factor F is defined as

$$F = \frac{K}{\sigma_0\sqrt{\pi a}}. \tag{24}$$

The solid and dotted lines are obtained by using the weight function given in equation (22). Along with these solutions, analytical results presented by Green and Sneddon [**25**] ($i = 0$) and Shah and Kobayashi [**26**]($i = 1, 2$) are shown as single points. As can be seen, the weight function based F values are in good overall agreement with the analytical predictions, with a maximum deviation of less than 4%. Fig. 6(b) shows the geometry factor at the same four locations, but now plotted against a/L. The weight function based F values, shown as solid lines, are obtained for a crack with aspect ratio $a/c = 0.5$ and subjected to a uniform stress field, i.e., $i = 0$. Results presented by Noguchi et al. [**27**] are shown as squares. For $a/L = 0$, the geometry factor solution corresponds to an embedded crack located in an infinite body. As a/L increases, the influence of the free surface leads to higher F values. The weight function based F values are in good agreement with the results presented by Noguchi et al., with a maximum deviation of less than 4% when $a/L \leq 0.9$.

When the embedded elliptical crack shown in Fig. 7 reaches the free surface, there follows a relatively rapid crack extension through the cusp-shaped ligaments on each side of the point of break-through [**28**]. After this transitory phase, the depth of the surface crack $\approx 2a$, and the curvature at the deepest point of the crack is nearly the same as that of the embedded crack. If the shape of the surface crack is to remain semi-elliptic, its semi-width $\approx \sqrt{2}c$, i.e., it is about 40% wider than the crack before break-through. However, in order to compensate for the 'missing' cycles of the transitory phase, the 'effective' semi-elliptic surface crack is assumed to be somewhat smaller and to have the same area as the embedded crack, as shown in Fig. 7.

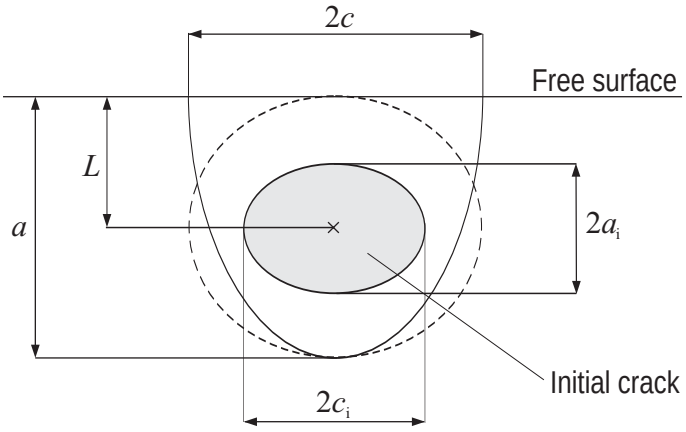

Figure 7: Sketch of a near surface crack and how it is assumed to unfold to a surface crack.

4.3.2 *Surface crack*

For a semi-elliptical surface crack growing in an arbitrary component, the crack will in many cases propagate along an uneven surface. Hence, the local coordinate system of the crack must be updated for each crack growth increment. The initial coordinate system is denoted by $\mathbf{x}'_{\mathrm{s}}$, see Fig. 8(a). The semi-elliptical crack is growing perpendicularly to the maximum principal stress. The updated coordinate system is denoted by $\mathbf{x}''_{\mathrm{s}}$, as shown in Fig. 8(a). The updated coordinate system is determined by the two points where the crack front and the free surface intersect. The updated coordinate system is rotated until the x''_{s}-axis is parallel with the line between the two surface points, see Fig. 8(a). These are found by stepwise moving along the crack front until the points are found to be outside the

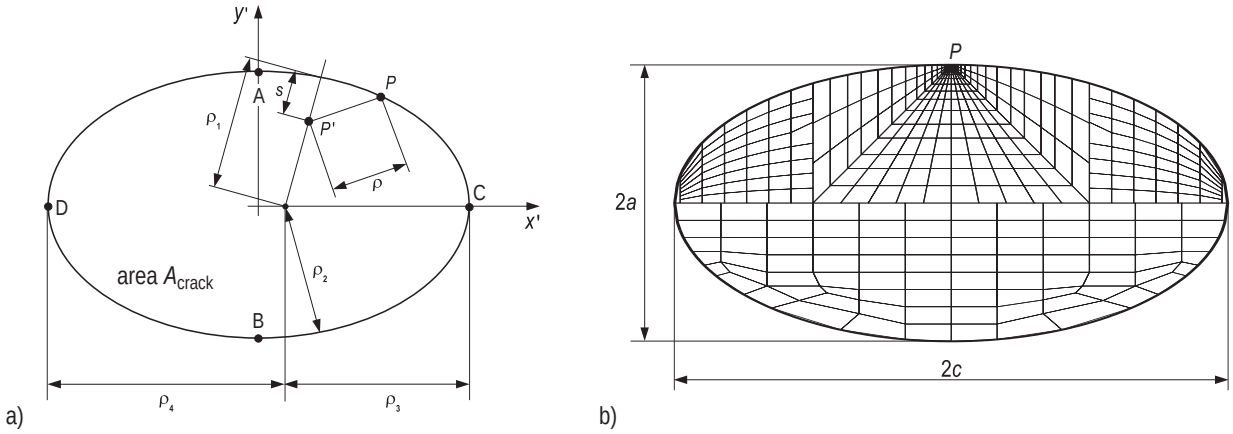

Figure 5: (a) Schematic drawing of an embedded elliptical crack and definition of parameters for obtaining the stress intensity factor. (b) Typical finite element mesh used for an embedded elliptical crack.

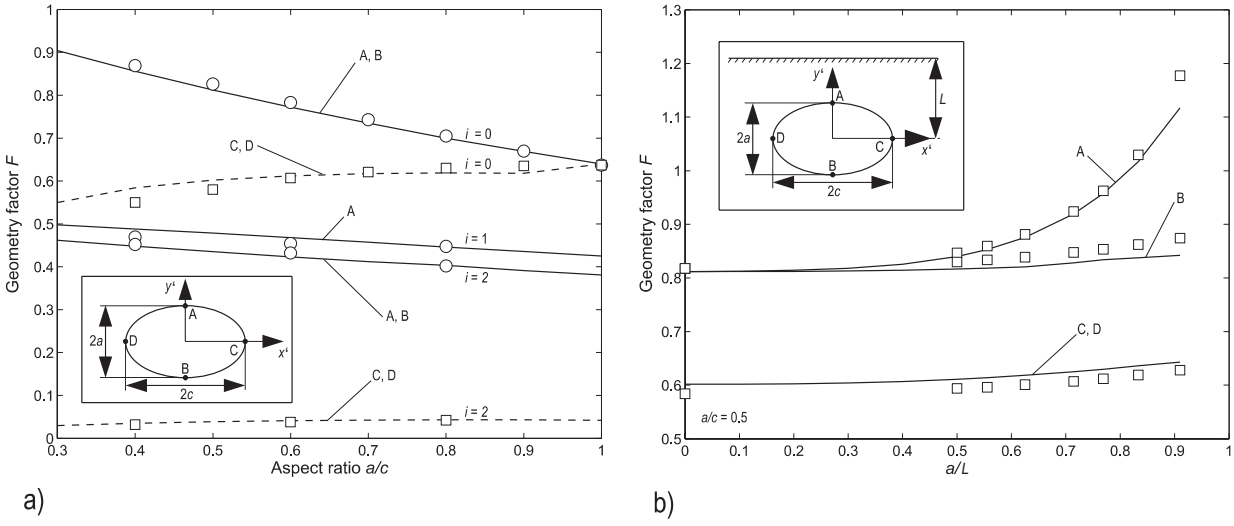

Figure 6: Geometry factors for an embedded crack (a) in an infinite body and (b) in a semi-infinite body. In (b) the aspect ratio $a/c = 0.5$.

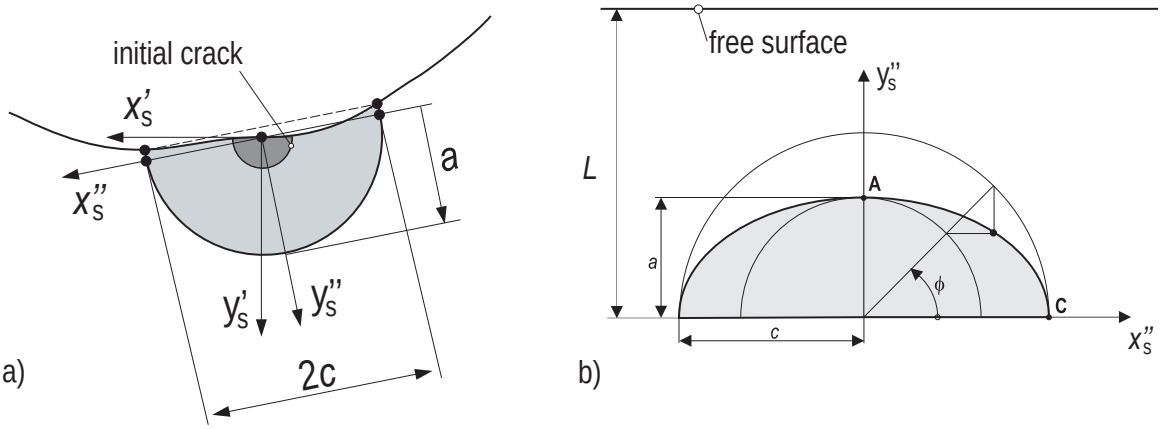

Figure 8: (a) Definition of the crack coordinate system and (b) a two dimensional view of a semi-elliptical crack.

component geometry, followed by an iterative process in order to determine the points more accurately.

For an arbitrary body with a semi-elliptic surface crack of depth a and aspect ratio a/c (cf. Fig. 8(b)) under a loading, σ_{a}, perpendicular to the crack surface, the weight function at the deepest point of the crack front $\mathrm{A}(a;0)$ is given by

$$g_{\mathrm{A}}(y_{\mathrm{s}}'';a/c) = \frac{2\left(1+f_{\mathrm{A}}(y_{\mathrm{s}}'',a/c,a/L)\right)}{\sqrt{2\pi(a-y_{\mathrm{s}}'')}}. \qquad (25)$$

The function $f_{\mathrm{A}}(y_{\mathrm{s}}'',a/c,a/L)$ is given in [**29**]. Similarly, at the intersection between the crack front and the free surface, $\mathrm{C}(0;c)$, the weight function is given by [**29**]

$$g_{\mathrm{C}}(y_{\mathrm{s}}'';a/c) = \frac{2\left(1+f_{\mathrm{C}}(y_{\mathrm{s}}'',a/c,a/L)\right)}{\sqrt{\pi y_{\mathrm{s}}''}}. \qquad (26)$$

The above weight function for the surface point C was established by Shen and Glinka [**29**] from a near surface point by means of the finite element method. The reason for this is that the stress singularity at the surface point is different from $1/\sqrt{r}$ and that the conventional stress intensity factor, therefore, does not apply at C. There is, however, only a small region in the vicinity of C, where the stress singularity is different from $1/\sqrt{r}$.

As can be seen from equations (25) and (26), the underlying weight function only considers the stress gradient in the depth direction of the crack. To obtain the stress intensity factor, K, the line from the crack origin to the deepest point of the crack is meshed with two noded line elements. The element length is progressively decreased towards the point where the weight function becomes singular. The numerical integration is performed according to equation (21).

Fig. 9(a) shows the geometry factor F_{A} for the deepest point, $\mathrm{A}(a;0)$ (cf. Fig. 8(b)), versus a/L when the crack surface is subjected to four different stress fields, see equation (23). The solid lines are obtained by using the weight function of equation (25). Along with weight function based F_{A} values, finite element results presented by Nilsson [**30**] are shown. As can be seen, the weight function based F_{A} values are in good overall agreement with the results presented by Nilsson, with a maximum difference of less than 4%. In Fig. 9(b), the corresponding geometry factors, F_{C}, for the crack surface point $\mathrm{C}(0;c)$ are shown. Also for the crack surface point, the agreement is found to be good.

5 Defect generation

Scatter plays an eminent role in the prediction of the fatigue life of a component. There are several possible sources for the scatter. It may be due to the random character of the loading. It may also be due to inaccuracies in how the loading is applied. Deviations from the nominal dimensions of the component cause scatter in the stresses. Lacking repeatability in the manufacturing conditions leads to variability of chemical composition, microstructure and mechanical properties. This includes fatigue limit and the crack growth rate of the material. Last, but not least, metal alloys contain metallurgical defects such as non-metallic inclusions and pores. Fatigue cracks are prone to initiate and grow from such defects. The present Section presents a methodology for generating the number, position and size of defects within a component.

5.1 Number and position of defects

There are two different approaches based on the statistics of extremes for estimating the size of the largest defect in a large volume of material. The first approach, called the *block maximum* method, uses the generalised extreme value distribution [**31**]. In this method, a polished cross-section is divided into k equally sized areas of size A_0 that are inspected for defects using optical microscopy [**32**]. Hence, the observation set consists of k measurements of maximum defect sizes, $a_{\mathrm{max1}},\ldots,a_{\mathrm{max}}$. The corresponding sizes in a volume V_0 can be estimated by using a stereological approximation as shown in [**33, 34**]. The expected number of defects per unit volume of the material is denoted by z_0. In the second approach, all defects with sizes above a certain (high) threshold, a_{th}, are considered. The differences between the defect sizes and the threshold, i.e., $a_i - a_{\mathrm{th}}$, are fitted to a generalised Pareto distribution [**31**]. This approach is therefore often called the *peak over threshold* method. The expected number of defects with sizes greater than a_{th} is denoted by $z_0(a_{\mathrm{th}})$.

The number of defects in a finite element of volume ΔV is obtained by 'drawing' from a Poisson distribution, i.e.,

$$\Pr(I=i) = \frac{[z_0\Delta V]^i}{i!}\exp[-z_0\Delta V],\ i\in\{0,1,2,\ldots\} \qquad (27)$$

where, I is the random number of defects. The element volume is calculated as

$$\Delta V = \sum_{i=1}^{N_{\mathrm{Gauss}}}\sum_{j=1}^{N_{\mathrm{Gauss}}}\sum_{k=1}^{N_{\mathrm{Gauss}}} |\mathbf{J}(\xi_i,\eta_j,\zeta_k)|\, W_i\, W_j\, W_k. \qquad (28)$$

It should be noted that the intrinsic property of a Poisson process is that the occurrence of a defect at a location $\mathbf{x}\in V$ neither encourages, nor inhibits, the occurrence of other defects in a neighborhood of $\mathbf{x}$, or in any other location, and that defects in separate volumes are mutually independent [**34**]. This assumption requires that the number of potentially life-controlling defects is small, a situation that occurs for stress cycles close to the fatigue limit (in the HCF regime) and for components with a low density of 'large' metallurgical defects.

When assigning the defect location, the parent element domain $\boldsymbol{\xi}$ is used. The location of a defect within

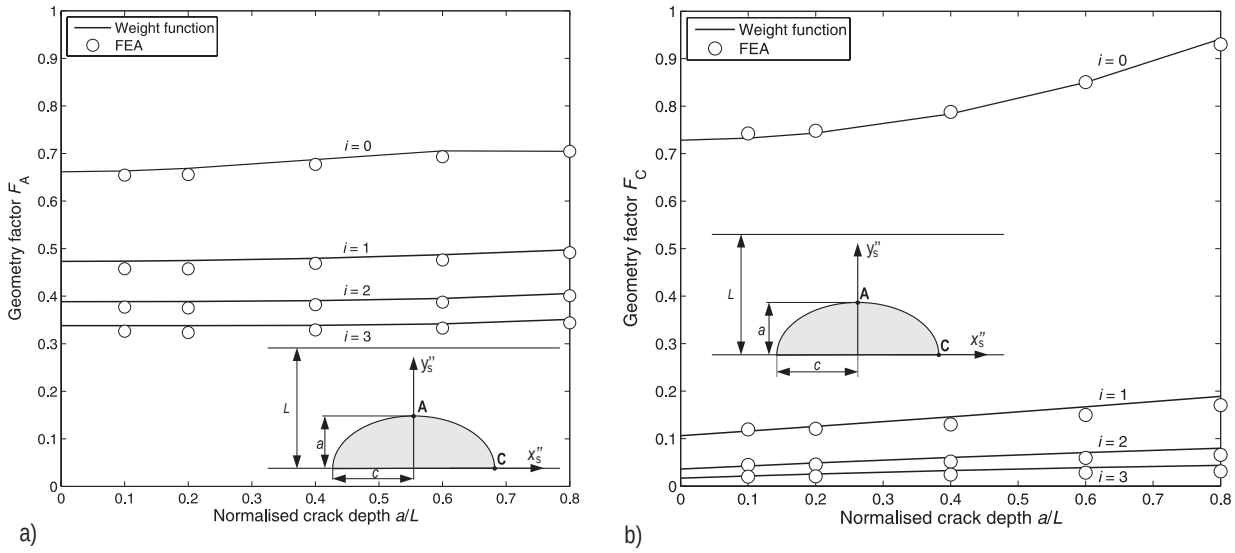

Figure 9: Geometry factors (a) F_{A} for the deepest point $\mathrm{A}(a;0)$ and (b) F_{C} for the surface point $\mathrm{C}(0;c)$ of a semi-elliptical crack with aspect ratio $a/c = 1$.

an element is obtained according to

$$\begin{bmatrix} \xi \\ \eta \\ \zeta \end{bmatrix} = 2 \begin{bmatrix} U_1(0,1) \\ U_2(0,1) \\ U_3(0,1) \end{bmatrix} - 1, \tag{29}$$

where U is a uniform random number between 0 and 1. Fig. 10 shows the position of randomly generated defects within a cube of volume 1000 mm^3.

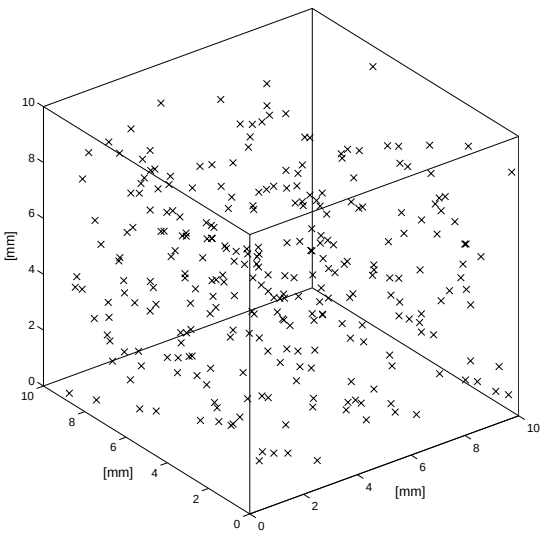

Figure 10: Example of generated number and position of defects within a 1000 mm^3 cube.

5.2 Defect size distributions

According to the generalised extreme value (GEV) distribution the probability that a defect of size $A_{\max} \leq a_{\max}$ is located within an element of volume ΔV is given by

$$\begin{aligned} G(a_{\max}) &= \Pr[A_{\max} \leq a_{\max}] \\ &= \exp\left\{ -\left[1 + \xi'\left(\frac{a_{\max} - a_0^*}{a_0}\right)\right]^{-1/\xi'} \frac{\Delta V}{V_0} \right\}, \end{aligned} \tag{30}$$

where $a_0 > 0$ denotes the scale parameter, a_0^* the location parameter and ξ' the shape parameter. The probability that a defect of size $A_{\max} \leq a_0^*$ is located within the control region V_0 equals $\exp(-1) \approx 36.8\%$. The location parameter, a_0^*, is therefore often called the characteristic largest defect size in volume V_0 [**34**]. The GEV distribution combines the Gumbel (Type I, $\xi' = 0$), Fréchet (Type II, $\xi' > 0$) and the reversed Weibull (Type III, $\xi' < 0$) distributions into a single distribution.

The Gumbel, Fréchet and reversed Weibull distributions have distinctly different forms of tail behaviour. When $\xi' < 0$, i.e., for the reversed Weibull distribution, the upper limit $a_{\max+} = a_0^* - a_0/\xi'$. Thus, the probability of finding defects $\geq a_{\max+}$ is zero. The Gumbel ($\xi' = 0$) and Fréchet ($\xi' > 0$) distributions have no upper limit.

When the peak over threshold method is used, all defects larger than a sufficiently high threshold a_{th} are measured either from a single inspection region or from k sub-regions. The observation set then consists of i measurements, $a_1, \ldots, a_i$. A generalised Pareto distri-

bution with distribution function [**31**]

$$H(a) = \Pr[A \leq a | A > a_{\text{th}}] = 1 - \left[1 + \xi' \left(\frac{a - a_{\text{th}}}{\tilde{a}_0}\right)\right]^{-1/\xi'}, \tag{31}$$

is fitted to the values $a_i - a_{\text{th}}$. The scale parameter $\tilde{a}_o$ is given by

$$\tilde{a}_0 = a_0 + \xi'(a_{\text{th}} - a_0^*), \tag{32}$$

where a_0, a_0^* and ξ' are equal to those in equation (30). The range of $a - a_{\text{th}}$ is $0 < a - a_{\text{th}} < \infty$ if $\xi' \geq 0$ and $0 < a - a_{\text{th}} < -\tilde{a}_0/\xi'$ if $\xi' < 0$. The generalised Pareto distribution was applied to defects in clean steels for the first time in [**35, 36**].

The generated sample of defect sizes is converted into crack dimensions by first assuming that all generated defects are embedded circular cracks of radius c. If the drawn defect cuts the free surface of the component, the 'effective' surface crack is assumed to be semi-elliptic of width $2c$ and a depth a equal to the depth below the surface of the drawn defect.

5.3 Defect criterion and probability of fatigue failure

The Kitagawa-Takahashi diagram [**37**] clearly shows that the fatigue strength decrease with increasing crack size. In addition, there exists a critical crack size, a_{crit}, below which cracks are non-damaging. In the present work, the Kitagawa-Takahashi diagram [**37**] is used for finding out whether a crack is potentially damaging or not.

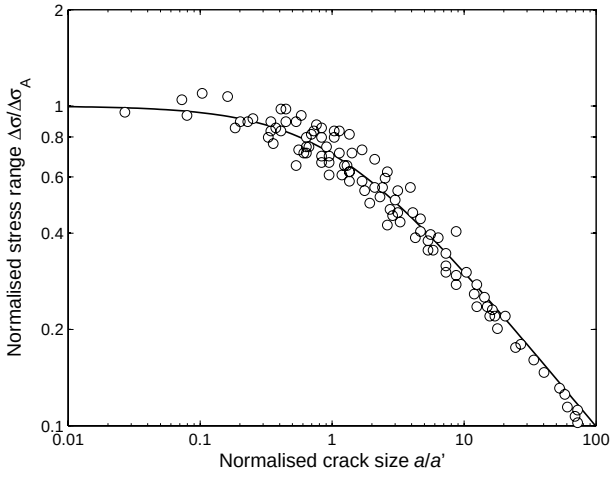

Figure 11: Kitagawa-Takahasi diagram with experimental data for both ferrous and nonferrous alloys gathered by Tanaka et al. [**38**] and Hertzberg [**39**].

Consider now a small, homogeneously stressed volume element ΔV subjected to an equivalent stress amplitude σ_{a}. The smallest crack initiating failure in ΔV is denoted by a_{crit} and can be estimated according to [**37**]

$$a_{\text{crit}} = a' \left[\left(\frac{\Delta\sigma_{\text{A}}}{\Delta\sigma}\right)^2 - 1\right], \tag{33}$$

where the 'intrinsic' crack length is given by

$$a' = \left(\frac{\Delta K_{\text{th}} \Delta\sigma}{\Delta K \Delta\sigma_{\text{A}}}\right)^2 a. \tag{34}$$

Cracks with sizes less than a_{crit} are removed from the component. The expected number of remaning cracks per unit volume is denoted by z_1. The critical crack density, z_1, is defined as the expected number of cracks per unit volume of the material that yields a fatigue strength (random variable) $\sigma_{\text{A}} \leq \sigma_{\text{a}}$.

6 Flow-chart of the random defect module

In this Section a flow-chart of the random defect module is presented. The flow-chart is shown in Fig. 12. The flow-chart can be divided into three main parts: (i) input, (ii) defect generation and (iii) crack growth.

In the input part of the flow-chart, data needed for the computation are given. In the defect generation part, the number, size and position of the defects are generated. The number of critical defects, z_1, are subsequently determined by using a Kitagawa-Takahashi diagram, see Subsection 5.3.

In the crack growth part, all generated defects are initially embedded circular cracks of radius c. For defects cutting the free surface of the component, the 'effective' surface crack is assumed to be semi-elliptic of length $2c$ and a depth a, equal to the depth below the surface of the drawn defect. The location of the crack front relative to the free surface is determined for each crack growth increment. This enables one to determine when an embedded crack starts to grow as a surface crack and when a surface crack breaks the opposing free surface. Failure of a component occurs, when the crack has reached a predefined size a_{f}, or the stress intensity factor K has reached the fracture toughness K_{Ic}. The fatigue life of a single component is determined as the smallest computed life for all crack-like defects.

7 Conclusions

P•FAT is designed as a stand-alone finite-element post-processor with the component geometry and stresses given by a standard finite element program. Data needed for the computation are nodal coordinates, element topology and stresses. The surface elements are found automatically and are used for defining the geometry of the component.

The life-controlling defect is determined by means of the stress field and the initial crack growth rate. The

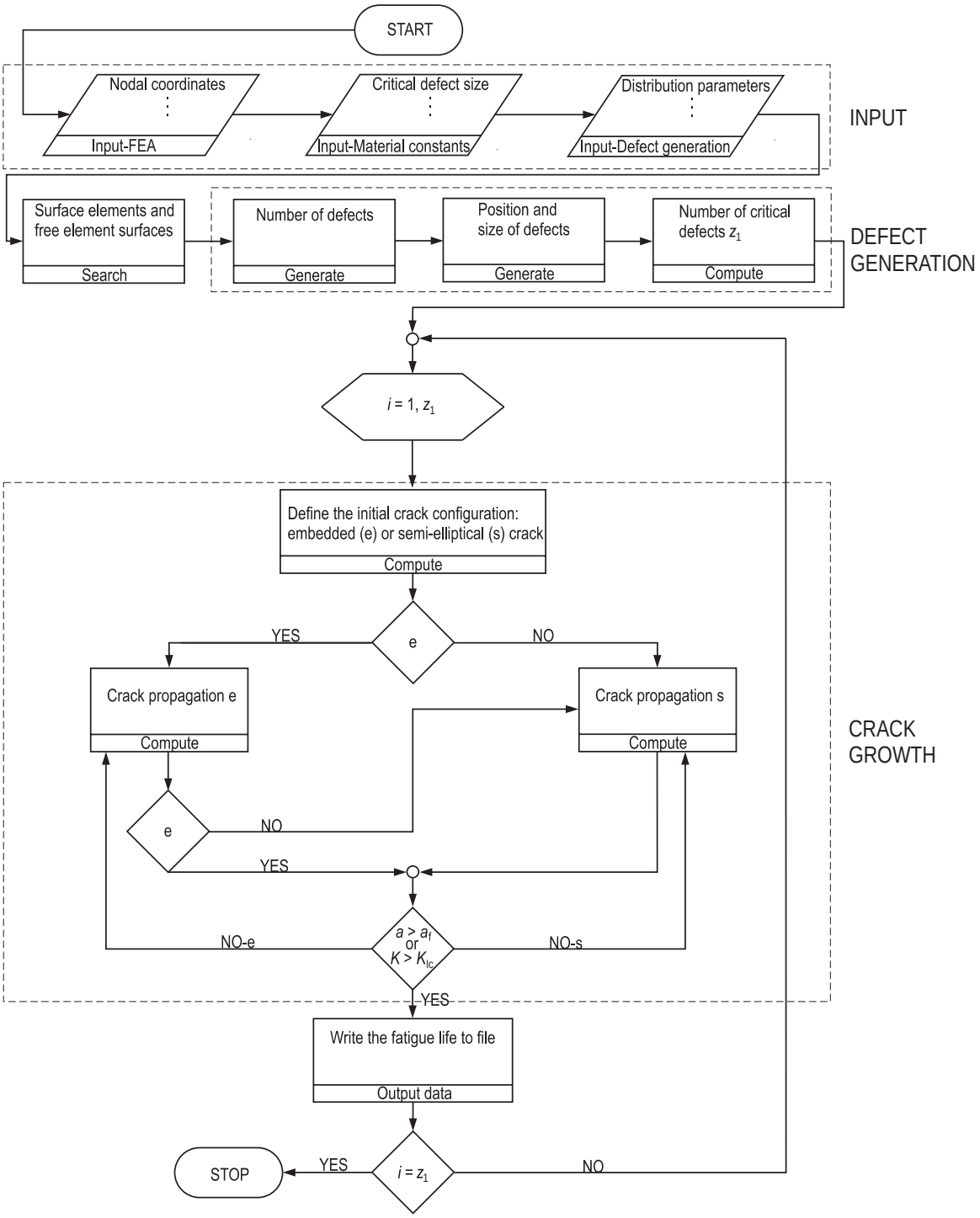

Figure 12: Flow-chart of the procedure for calculating the fatigue life of a single component.

number of defects in each finite element is obtained by 'drawing' from a Poisson distribution. The location of each defect in an element is found by drawing from a uniform distribution. The defect size is obtained by drawing from an extreme value distribution.

The life-controlling defect is then regarded as an embedded crack or as a surface crack. Fatigue life prediction is carried out using a short crack growth model. The defects are considered to be crack-like and to grow on the plane of maximum principal stress. Weight functions, together with the stress field of the crack-free component, are used to compute the required stress intensity factors. The crack surface is automatically meshed with plane elements with subsequent numerical integration (Gauss quadrature) for determining the stress intensity factor at several locations at the crack front. For each incremental step, this process repeats itself: the crack surface is re-meshed, and updated stress intensity factors for the current crack are obtained. The program also updates the location of the crack front relative to the free surfaces. Hence, if the crack grows through the component surface, the crack is regarded as a surface crack.

By repeating this process for a large number of nominally equal components (Monte Carlo simulation), the fatigue life distribution of the component is obtained. Thus, the designer will be able to estimate the probability of component fatigue failure.

Acknowledgments

The authors gratefully acknowledge the research support for this work provided by GE Energy (Norway) AS, the Research Council of Norway and the industrial participants within the NorLight project. The authors would like to express their gratitude to K. Holthe, O. I. Sivertsen, E. Berg and B. Skallerud for assistance and helpful discussions during the work presented herein.

References

[1] **Trädegård, A.**, **Nilsson, F.**, and **Östlund, S.** FEM-remeshing technique applied to crack growth problems. *Computer Methods in Applied Mechanics and Engineering*, 160(1-2):115–131, 1998.

[2] **Bouchard, P. O.**, **Bay, F.**, **Chastel, Y.**, and **Tovena, I.** Crack propagation modelling using an advanced remeshing technique. *Computer Methods in Applied Mechanics and Engineering*, 189(3):723–742, 2000.

[3] **Bouchard, P. O.**, **Bay, F.**, and **Chastel, Y.** Numerical modelling of crack propagation: automatic remeshing and comparison of different criteria. *Computer Methods in Applied Mechanics and Engineering*, 192(35-36):3887–3908, 2003.

[4] Cornell Fracture Group. *FRANC3D 2.6. Concepts and user guide.* Cornell University, Ithaca, New York, 2003.

[5] *BEASY User Guide, Computational Mechanics BEASY Ltd., 2001*, (Ashurst Lodge, Ashurst, Southampton, Hampshire, SO40 7AA, UK).

[6] **Schöllmann, M.**, **Fulland, M.**, and **Richard, H. A.** Development of a new software for adaptive crack growth simulations in 3D structures. *Engineering Fracture Mechanics*, 70(2):249–263, 2003.

[7] **Fulland, M.** and **Richard, H. A.** Application of the FE-method to the simulation of fatigue crack growth in real structures. *Steel Research*, 74(9):584–590, 2003.

[8] *NASA: Fatigue Crack Growth Computer Program 'NASGRO', version 3.0, 2000*, (Reference Manual, JSC-22267B, Engineering Directorate, National Aeronautics and Space Administration, Lyndon B. Johnson Space Center, Houston).

[9] *AFGROW Users Guide And Technical Manual. Air Vehicles Directorate, Air Force Laboratory, Wright-Patterson Air Force Base, Ohio.*

[10] **Bueckner, H. F.** A novel principle for the computation of stress intensity factors. *Z. Angewandte Math. Mech.*, 50:529–546, 1970.

[11] **Rice, J. R.** Some remarks on elastic crack-tip stress fields. *International Journal of Solids and Structures*, 8(6):751–758, 1972.

[12] **Wormsen, A.**, **Sjödin, B.**, **Härkegård, G.**, and **Fjeldstad, A.** Non-local stress approach for fatigue assessment based on weakest-link theory and statistics of extremes. Accepted for publication in Fatigue & Fracture of Engineering Materials & Structures, August 2007.

[13] **Wormsen, A.**, **Härkegård, G.**, and **Huth, H. J.** Probabilistic fatigue assessment of a hydroturbine blade model. In W. S. Johnson et al., editor, *Proceedings of the International Fatigue Congress 2006*, Atlanta, Georgia, USA, May 2006. Elsevier.

[14] **Wormsen, A.** and **Härkegård, G.** Weibull fatigue analysis of notched components under constant and variable amplitude loading. In W. S. Johnson et al., editor, *Proceedings of the International Fatigue Congress 2006*, Atlanta, Georgia, USA, May 2006. Elsevier.

[15] **Cook, R. D.**, **Malkus, D. S.**, **Plesha, M. E.**, and **Witt, R. J.** *Concepts and applications of finite element analysis.* John Wiley and Sons, Inc., 4th edition, 2002.

[16] **Miller, K. J.** The behaviour of short fatigue cracks and their initiation. Part 1 – A review of two recent books. *Fatigue of Engineering Materials*, 10(2):75–91, 1987.

[17] **Miller, K. J.** The behaviour of short fatigue cracks and their initiation. Part 2 – A general summary. *Fatigue of Engineering Materials*, 10(2):93–113, 1987.

[18] **El Haddad, M. H.**, **Smith, K. N.**, and **Topper, T. H.** Fatigue crack propagation of short cracks. *Journal of Engineering Materials Technology*, 101(1):42–46, 1979.

[19] **Klesnil, M** and **Lukáš, P.** Influence of strength and stress history on growth and stabilisation of fatigue cracks. *Engineering Fracture Mechanics*, 4(1):77–92, 1972.

[20] **Fjeldstad, A.**, **Wormsen, A.**, and **Härkegård, G.** Simulation of fatigue crack growth in components with random defects. *Engineering Fracture Mechanics*, doi:10.1016/j.engfracmech.2007.04.006, 2007.

[21] **Walker, K.** The effect of stress ratio during crack propagation and fatigue for 2024-T3 and 7075-T6 aluminum. In *Effects of Environment and Complex Load History on Fatigue Life*, pages 1–14. ASTM STP 462, Philadelphia, 1970.

[22] **Mann, T.** *Fatigue assessment methods for welded structures and their application to an aluminium T-joint.* PhD thesis, Norwegian University of Science and Technology, Trondheim, Norway, 2006.

[23] **Wang, X.**, **Lambert, S. B.**, and **Glinka, G.** Weight functions for embedded elliptical cracks. *Engineering Fracture Mechanics*, 59(3):381–392, 1998.

[24] **Fett, T.** and **Mattheck**. Stress intensity factors of embedded elliptical cracks for weight function applications. *International Journal of Fracture*, 40(1):R13–R18, 1989.

[25] **Green, A. E.** and **Sneddon, I. N.** The distribution of stress in the neighborhood of a flat elliptical crack in an elastic body. Cambridge Philosophical Society, 1950.

[26] **Shah, R. C.** and **Kobayashi, A. S.** Stress intensity factor for an elliptical crack under arbitrary normal loading. *Engineering Fracture Mechanics*, 3(1):71–93, 1971.

[27] **Noguchi, H.**, **Smith, R. A.**, **Carruthers, J. J.**, and **Gilchrist, M. D.** Stress intensity factors of embedded elliptical cracks and an assessment of the ASME XI defect recharacterisation criteria. *International Journal of Pressure Vessels & Piping*, 70(1):69–76, 1997.

[28] **Dai, D. N.**, **Nowell, D.**, and **Hills, D. A.** Eigenstrain methods in 3-D crack problems; an alternative integration procedure. *Journal of Mechanics and Physics of Solids and Structures*, 41(6):1003–1017, 1993.

[29] **Shen, G.** and **Glinka, G.** Weight functions for a semi-elliptical crack in a finite thickness plate. *Theoretical and Applied Fracture Mechanics*, 15(3):247–255, 1991.

[30] **Nilsson, L.** Stress intensity factors for semi-elliptical surface cracks in plates subjected to a complex stress field. SAQ/FoU-Report 98/10, SAQ KONTROLL AB, Stockholm, Sweden, 1998.

[31] **Coles, S.** *An introduction to statistical modeling of extreme values.* Springer series in statistics, London, 3rd edition, 2001.

[32] **Atkinson, H. V.** and **Shi, G.** Characterization of inclusions in clean steels: a review including the statistics of extreme methods. *Progress in Materials Science*, 48:457–520, 2003.

[33] **Anderson, C. W.** and **Coles, S. G.** The largest inclusions in a piece of steel. *Extremes*, 5:237–252, 2002.

[34] **Anderson, C. W.**, **de Maré, J.**, and **Rootzén, H.** Methods for estimating the sizes of large inclusions in clean steels. *Acta Materialia*, 53(8):2295–2304, 2005.

[35] **Shi, G.**, **Atkinson, H. V.**, **Sellars, C. M.**, and **Anderson, C. W.** Application of the generalized Pareto distribution to the estimation of the size of the maximum inclusion in clean steels. *Acta Materialia*, 47(5):1455–1468, 1999.

[36] **Shi, G.**, **Atkinson, H. V.**, **Sellars, C. M.**, and **Anderson, C. W.** Comparison of extreme value statistics methods for predicting maximum inclusion size in clean steel. *Ironmaking and Steelmaking*, 26(4):239–246, 1999.

[37] **Kitagawa, H.** and **Takahashi, S.** Applicability of fracture mechanics to very small cracks or the cracks in the early stage. In *Proceedings of the Second International Conference on the Mechanical Behavior of Materials*, pages 627–631, Boston, Ma., 1976.

[38] **Tanaka, K.**, **Nakai, Y.**, and **Yamashita, M.** Fatigue growth threshold of small cracks. *International Journal of Fracture*, 17(5):519–533, 1981.

[39] **Hertzberg, R. W.** *Deformation and Fracture Mechanics of Engineering Materials.* John Wiley & Sons, Inc., 4th edition, 1996.

Available online at www.sciencedirect.com
ScienceDirect
Engineering Fracture Mechanics xxx (2007) xxx–xxx
Engineering Fracture Mechanics
www.elsevier.com/locate/engfracmech

Simulation of fatigue crack growth in components with random defects

A. Fjeldstad *, A. Wormsen, G. Härkegård

Norwegian University of Science and Technology, Richard Birkelandsvei 2B, NO-7491 Trondheim, Norway

Received 18 December 2006; received in revised form 22 March 2007; accepted 3 April 2007

Abstract

The paper presents a probabilistic method for the simulation of fatigue crack growth from crack-like defects in the combined operating and residual stress fields of an arbitrary component. The component geometry and stress distribution are taken from a standard finite element stress analysis. Number, size and location of crack-like defects are 'drawn' from probability distributions. The presented fatigue assessment methodology has been implemented in a newly developed finite-element post-processor, P • FAT, and is useful for the reliability assessment of fatigue critical components. General features of the finite element post-processor have been presented. Important features, such as (i) the determination of the life-controlling defect, (ii) growth of short and long cracks, (iii) fatigue strength and fatigue life distribution and (iv) probability of component fatigue failure, have been treated and discussed. Short and long crack growth measurements have been presented and used for verification of the crack growth model presented.

Keywords: Fatigue; Crack growth; Short crack; Probability of failure; Defect size distribution; Finite-element post-processor

1. Introduction

In terms of fatigue design, it is of ultimate importance that computer simulations undergoes the same improvements regarding accuracy and speed as all the other steps in a product development process. It is the authors' conviction that a standard fatigue analysis tool should reflect that fatigue is a probabilistic phenomenon caused by the (random) growth of small fatigue cracks from randomly distributed defects. Unfortunately, this is bound to make the fatigue design process much more complex. Hence, a robust fatigue assessment tool, directly applicable to the results from a standard finite element stress analysis, would be of great importance in the process of developing optimised, safe and reliable structural components.

* Corresponding author. Present address: Department of Engineering Design and Materials, Norwegian University of Science and Technology, Richard Birkelandsvei 2B, NO-7491 Trondheim, Norway.
E-mail address: Arne.Fjeldstad@ntnu.no (A. Fjeldstad).

0013-7944/$ - see front matter © 2007 Elsevier Ltd. All rights reserved.
doi:10.1016/j.engfracmech.2007.04.006

Nomenclature

A	defect size (random variable)
a	defect size
a'	intrinsic crack length
a_0	scale parameter in the extreme value distribution
a_0^*	characteristic largest defect size
a_{crit}	critical defect size
a_{th}	peak over threshold defect size
c	half the surface crack length
C	coefficient in crack growth law
d	notch depth
F	geometry factor
$G(a)$	generalised extreme value distribution
$H(a)$	generalised Pareto distribution
ΔK	stress intensity range
ΔK^*	stress intensity range associated with $R = 0$
ΔK_{eq}	equivalent stress intensity range
K_{Ic}	mode I fracture toughness
K_{t}	stress concentration factor $= \sigma_{\max}/S$
ΔK_{th}	threshold stress intensity range
m	exponent in crack growth law
N	fatigue life (random variable)
n	number of cycles
$\mathbf{n}_1$	unit eigenvector of the maximum principal stress
P_{f}	probability of failure
P_{s}	probability of survival $= 1 - P_{\text{f}}$
R	stress ratio
S	remote stress
S_{net}	net-section stress
t	thickness of plane specimen
V	volume
V_0	reference volume
w	width of plane specimen
z_1	critical defect density
γ	Walker exponent
ξ'	shape parameter in the extreme value distribution
ρ	notch radius
σ_1	maximum principal stress
σ_{a}	stress amplitude $= \Delta\sigma/2$
σ_{m}	mean stress
σ_{A}	fatigue strength (random variable)
σ_{A0}^*	characteristic fatigue strength
σ_{ij}	operating stress tensor
σ_{ij}^0	residual stress tensor

To comply with thise needs, a probabilistic fatigue assessment tool has been developed that is capable of predicting the fatigue life of a component. The prediction is based on the fatigue properties of the material and their scatter, and on the operating stresses from a finite element analysis of the component. The post-

Please cite this article in press as: Fjeldstad A et al., Simulation of fatigue crack growth in components with ..., Eng Fract Mech (2007), doi:10.1016/j.engfracmech.2007.04.006

processing of the stresses includes residual stresses, which may be imported directly from casting or welding simulations.

Scatter plays an eminent role in the prediction of the fatigue life of a component. There are several possible sources for the scatter. It may be due to the random character of the loading. It may also be due to inaccuracies in how the loading is applied. Deviations from the nominal dimensions of the component cause scatter in the stresses. Lacking repeatability in the manufacturing conditions leads to variability of chemical composition, microstructure and mechanical properties. This includes fatigue limit and the crack growth rate of the material. Last, but not least, metal alloys contain metallurgical defects such as non-metallic inclusions and pores. Fatigue cracks are prone to initiate and grow from such defects. The present work describes a methodology for simulating the scatter of the fatigue life based on the statistical distributions of defect density and defect size. Material parameters of the crack growth law may also be treated as random variables [1].

2. Finite-element post-processor

P • FAT is designed as a stand-alone, finite-element post-processor with the component geometry and stresses given by a standard finite element program. Data needed for the computation are nodal coordinates, element topology and stresses. It has been developed to perform predictions of crack growth in arbitrary three-dimensional components. It supports the simulation of both a single crack-like defect that can be inserted into the component at a desired location (*single defect module*) and randomly inserted crack-like defects (*random defect module*). The finite element post-processor uses a short crack model to determine the crack growth rate, see Section 3.1. The reader is referred to Ref. [1] for the numerical aspects of the crack-growth modules.

The number of defects in each finite element is obtained by 'drawing' from a Poisson distribution. The location of each defect in an element is obtained from a uniform distribution, and the defect size is obtained by 'drawing' from an extreme value distribution. The defects are considered to be crack-like, and the number of cycles required for a given defect to become critical is determined.

The crack-like defects are assumed to grow on the plane of maximum principal stress. Weight-functions [2], together with the stress field of the crack-free component, are used to compute the required stress intensity factors. Generally, the direction of maximum principal stress in the uncracked component changes as the crack grows on a specific plane. In the present work, the change of the crack growth direction is neglected. Generally, this is a good approximation as long as the crack is small compared with the dimensions of the component, i.e., for a large fraction of the fatigue life.

The crack surface is automatically meshed with plane elements. Subsequently, numerical integration (Gauss quadrature) is performed for determining the stress intensity factor at several locations at the crack front. For each incremental step, this process repeats itself: the crack surface is re-meshed, and updated stress intensity factors for the current crack are obtained. The program also updates the location of the crack front relative to the free surfaces. Hence, if the crack grows through the component surface, the crack is regarded as a surface crack or a corner crack, see Fig. 1. Failure of a component occurs when the crack has reached a predefined size, or if the stress intensity factor K has reached the fracture toughness K_{Ic}.

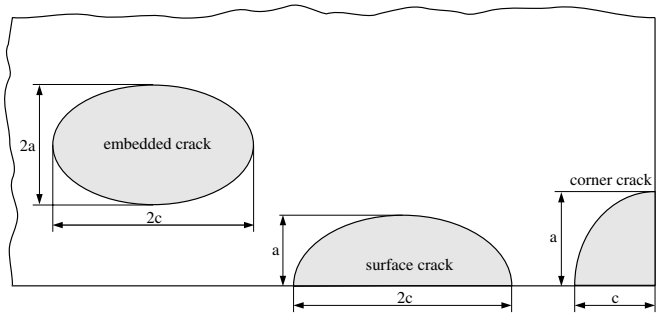

Fig. 1. Crack configurations implemented in the finite-element post-processor.

Please cite this article in press as: Fjeldstad A et al., Simulation of fatigue crack growth in components with ..., Eng Fract Mech (2007), doi:10.1016/j.engfracmech.2007.04.006

In the present investigation, the interaction between single cracks and the subsequent joining of these and the formation of a new, larger crack have been neglected. Thus, only one single, dominating crack is considered at a time. This assumption requires that the number of potentially life-controlling defects is small, a situation that occurs for stress cycles close to the fatigue limit (in the HCF regime) and for components with a low density of 'large' metallurgical defects. Future fatigue testing and simulation of components with known defect distributions should give a better understanding of the influence on fatigue life of the interaction between cracks.

By repeating the foregoing analysis for a large number of nominally equal components (Monte Carlo simulation), the fatigue life distribution of the component is obtained. Thus, the designer will be able to find the probability of fatigue failure.

The main steps for obtaining the fatigue life distribution of a component can be summarised as follows:

1. Develop a 3D FE model and perform a stress analysis of a component using a standard finite element program, such as ABAQUS, ANSYS, or NASTRAN.
2. The number, size and location of crack-like defects in each finite element are 'drawn' from probability distributions.
3. Calculate the maximum principal stress for all defects.
4. Perform fatigue crack growth calculations.
5. Repeat steps 2–4 for a large number of nominally equal components to obtain the fatigue life distribution of the component.

3. Crack growth law

The stress field ahead of a crack in a linear elastic body can be characterised by means of the stress intensity factor K. This is a function of the geometry of the component and the crack [cf. Fig. 1] as well as the stress field. For simple geometries, K can be obtained from handbook solutions [3] or asymptotic solutions [4,5]. For more complex geometries, the stress intensity factor can be obtained by using weight functions together with the stress field of the crack-free component. Weight factor solutions for an embedded crack [6], a surface crack [7] and a corner crack [8], as shown in Fig. 1, have been implemented. The current crack configuration is automatically identified. The initial crack is assumed to grow on the plane of maximum principal stress [1].

The stress amplitude, σ_a, at an arbitrary point on the crack plane, is given by

$$\sigma_a = n_{1i}\sigma_{ij,a}n_{1j}, \quad i,j = 1,2,3. \tag{1}$$

and the mean stress, σ_m, by

$$\sigma_m = n_{1i}(\sigma_{ij,m} + \sigma^0_{ij})n_{1j}. \tag{2}$$

$\mathbf{n}_1$ is the unit eigenvector of the maximum principal stress, and σ^0_{ij} denotes the residual stress tensor.

The use of stress intensity factors was extended to fatigue problems by Paris and Erdogan [9], who suggested a power-law relationship between the crack growth rate da/dn and the stress intensity range ΔK, viz.,

$$\frac{da}{dn} = C\Delta K^m, \tag{3}$$

where C and m are material parameters. Klesnil and Lukáš [10] extended Paris' law into the near threshold region by including the threshold stress intensity range, ΔK_{th}:

$$\frac{da}{dn} = C(\Delta K^m - \Delta K^m_{th}). \tag{4}$$

3.1. An equivalent stress intensity range for short cracks

The fatigue tests by Kitagawa and Takahashi [11] clearly show that the fatigue limit of a cracked solid can be determined by means of the threshold of the stress intensity range for long cracks only. For short cracks,

Please cite this article in press as: Fjeldstad A et al., Simulation of fatigue crack growth in components with ..., Eng Fract Mech (2007), doi:10.1016/j.engfracmech.2007.04.006

however, the fatigue limit asymptotically approaches the ordinary fatigue limit as determined by means of a smooth specimen. Both the long and the short crack fatigue limits are satisfied by an equation initially given by El Haddad et al. [12] for $F = 1$, and generalised by Härkegård [13] to an arbitrary geometry factor, F, viz.

$$\Delta\sigma = \frac{\Delta K_{\mathrm{th}}}{F\sqrt{\pi(a+a')}} = \frac{\Delta\sigma_{\mathrm{A}}}{\sqrt{1+a/a'}}. \tag{5}$$

The characteristic crack length, a', which signifies the transition between short cracks, $a < a'$, and long cracks, $a > a'$, is defined by

$$a' = \frac{1}{\pi}\left(\frac{\Delta K_{\mathrm{th}}}{F\Delta\sigma_{\mathrm{A}}}\right)^2. \tag{6}$$

By replacing the geometry factor F, a' can be written as

$$a' = \left(\frac{\Delta K_{\mathrm{th}}\Delta\sigma}{\Delta K\Delta\sigma_{\mathrm{A}}}\right)^2 a. \tag{7}$$

One may interpret a' as an 'intrinsic' crack length, which should be added to the length of the real crack to yield an 'effective' crack length. Fig. 2a shows a Kitagawa–Takahashi diagram with experimental data for both ferrous and nonferrous alloys gathered by Tanaka et al. [14] and Hertzberg [15]. When crack growth behaviour is controlled by linear elastic fracture mechanics, i.e., $a \gg a'$, $\Delta\sigma$ varies as $1/\sqrt{a}$. At the other extreme where $a \ll a'$, the fatigue limit asymptotically approaches the fatigue limit, $\Delta\sigma_{\mathrm{A}}$, of a smooth, polished fatigue specimen without major defects.

Rewriting Eq. (5) in terms of the stress intensity range yields

$$\Delta K = \frac{\Delta K_{\mathrm{th}}}{\sqrt{1+a'/a}}. \tag{8}$$

In Fig. 2b, Eq. (8) is shown as a solid line together with the data presented in [14,15]. For long cracks, ΔK asymptotically approaches the stress intensity range ΔK_{th}. For short cracks, however, the stress intensity range required for a crack to grow varies as $\sqrt{a}$.

The preceding equations explicitly depend on the intrinsic crack length, a', which, in its turn, depends on the geometry factor, F. The latter will not be constant, if the crack shape changes [16], or the finite dimensions of the solid must be considered. This inconvenience can be avoided by eliminating the crack length, a, between Eqs. (5) and (8). Thus, one obtains

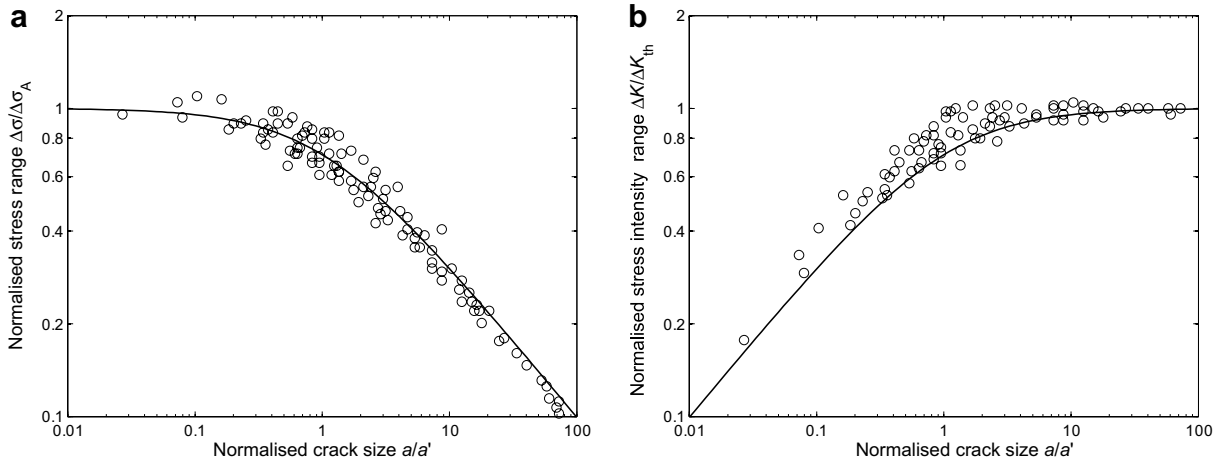

Fig. 2. Normalised threshold behaviour versus normalised crack size. (a) Normalised stress range and (b) normalised stress intensity range. Data points have been gathered by Tanaka et al. [14] and Hertzberg [15].

Please cite this article in press as: Fjeldstad A et al., Simulation of fatigue crack growth in components with ..., Eng Fract Mech (2007), doi:10.1016/j.engfracmech.2007.04.006

$$\left(\frac{\Delta K}{\Delta K_{\mathrm{th}}}\right)^2 + \left(\frac{\Delta \sigma}{\Delta \sigma_{\mathrm{A}}}\right)^2 = 1. \tag{9}$$

This equation was originally used by Härkegård et al. [17] to correlate the stress range, $\Delta\sigma$, and the stress intensity range, ΔK, below which short cracks did not propagate in two ferritic steels. In Fig. 3, the data points of Fig. 2 have been replotted in a diagram with $\Delta\sigma/\Delta\sigma_{\mathrm{A}}$ as the abscissa and $\Delta K/\Delta K_{\mathrm{th}}$ as the ordinate. The seemingly large scatter in Fig. 3 compared with that in Fig. 2a and b can be explained by the change to linear scales from logarithmic scales.

If Eq. (9) is rewritten as

$$\Delta K\left[1 + \left(\frac{\Delta K_{\mathrm{th}}}{\Delta K}\right)^2 \left(\frac{\Delta \sigma}{\Delta \sigma_{\mathrm{A}}}\right)^2\right]^{1/2} = \Delta K_{\mathrm{th}}, \tag{10}$$

the left member may be interpreted as an equivalent stress intensity range for short and long cracks,

$$\Delta K_{\mathrm{eq}} = \Delta K\left[1 + \left(\frac{\Delta K_{\mathrm{th}}}{\Delta K}\right)^2 \left(\frac{\Delta \sigma}{\Delta \sigma_{\mathrm{A}}}\right)^2\right]^{1/2}. \tag{11}$$

By introducing Eq. (7) into the above equation, ΔK_{eq} can be expressed as

$$\Delta K_{\mathrm{eq}} = \Delta K\sqrt{1 + \frac{a'}{a}}. \tag{12}$$

For $a \gg a'$, ΔK_{eq} asymptotically approaches the stress intensity range ΔK.

By introducing Eq. (11) into Eq. (4), the crack growth rate can be expressed as

$$\frac{\mathrm{d}a}{\mathrm{d}n} = C\Delta K_{\mathrm{th}}^m\left[\left\{\left(\frac{\Delta K}{\Delta K_{\mathrm{th}}}\right)^2 + \left(\frac{\Delta \bar{\sigma}}{\Delta \sigma_{\mathrm{A}}}\right)^2\right\}^{m/2} - 1\right]. \tag{13}$$

To determine the 'effective' stress range, $\Delta\bar{\sigma}$, for a surface crack at the root of a notch (Fig. 4, left), the same surface crack in a semi-infinite body is considered (Fig. 4, right). $\Delta\bar{\sigma}$ is now defined as the remote stress range that yields the same ΔK as for the crack at the root of a notch. Hence,

$$\Delta \bar{\sigma} = \frac{\Delta K}{F\sqrt{\pi a}}, \tag{14}$$

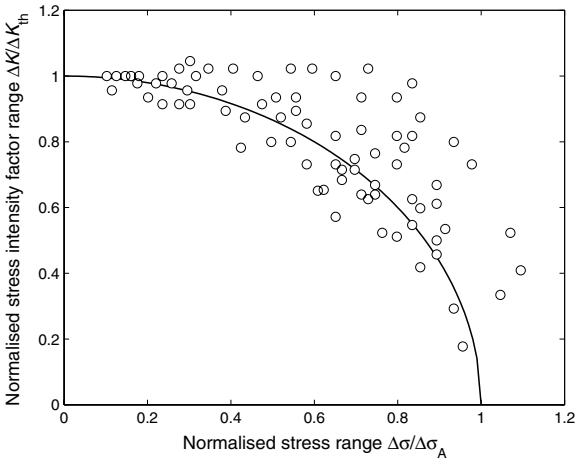

Fig. 3. Relation between the stress range and the stress intensity range required to propagate a crack. Data points have been gathered by Tanaka et al. [14] and Hertzberg [15].

Please cite this article in press as: Fjeldstad A et al., Simulation of fatigue crack growth in components with ..., Eng Fract Mech (2007), doi:10.1016/j.engfracmech.2007.04.006

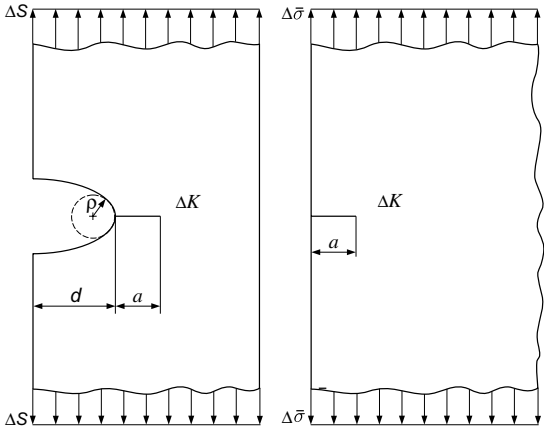

Fig. 4. Definition of the effective stress range $\Delta\bar{\sigma}$. The smooth edge-cracked plate has the same ΔK value as the notched plate when subjected to $\Delta\bar{\sigma}$.

where F is the geometry factor for the current crack in a semi-infinite plate. For an edge through-crack, $F = 1.122$ [3], and for an elliptic surface crack with aspect ratio $a/c = 1$, $F = 0.663$ [18] at the deepest point of the crack front.

For a long crack, i.e., $a \gg a'$, Eq. (13) reduces to the crack growth law proposed by Klesnil and Lukáš [10], see Eq. (4).

3.2. Influence of the load ratio

Several models that address the mean stress dependency of fatigue crack propagation have been presented in the literature. The different mean stress equations are either crack closure based or empirically based.

By plotting da/dn as a function of the equivalent zero-to-tension stress intensity range, and by suitable choice of the exponent γ

$$\Delta K^* = \frac{\Delta K}{(1-R)^{1-\gamma}}, \quad R = \frac{K_{\min}}{K_{\max}}, \tag{15}$$

Walker [19] found that he could make crack growth data for $R \neq 0$ fall into a narrow scatter-band corresponding to $R = 0$. At positive stress ratios, γ, usually takes values between 0.2 and 0.8, where $\gamma = 0.2$ gives a strong and $\gamma = 0.8$ a weak dependency on R. The constant C of the crack growth law, the stress range, the fatigue limit and the threshold stress intensity range can all be transformed to $R = 0$ by using Walker's equation as shown in [20,21]. The exponent m of the crack growth law generally varies only weakly with R [22] and is assumed to be constant in this work.

3.3. Crack growth measurements

Crack growth measurements obtained from the literature [23,24] have been reanalysed in order to verify the crack growth law given by Eq. (13). Both studies consider the growth of short cracks in the near-threshold regime.

Fig. 5 shows crack growth measurements carried out by Breat et al. [23] on A508 steel specimens. The objective of this investigation was to compare the crack growth behaviour of long cracks, initially 13–16 mm, with the behaviour of short cracks, initially 0.3–0.5 mm. The short crack measurements were performed on four point bending specimens. For long crack measurements, compact tension specimens were used. The crack propagation tests were carried out at $R = 0.1$. The specimens with long cracks were subjected to a nominal stress range well below that of specimens with short cracks. In both cases, the crack growth rates were measured

Please cite this article in press as: Fjeldstad A et al., Simulation of fatigue crack growth in components with ..., Eng Fract Mech (2007), doi:10.1016/j.engfracmech.2007.04.006

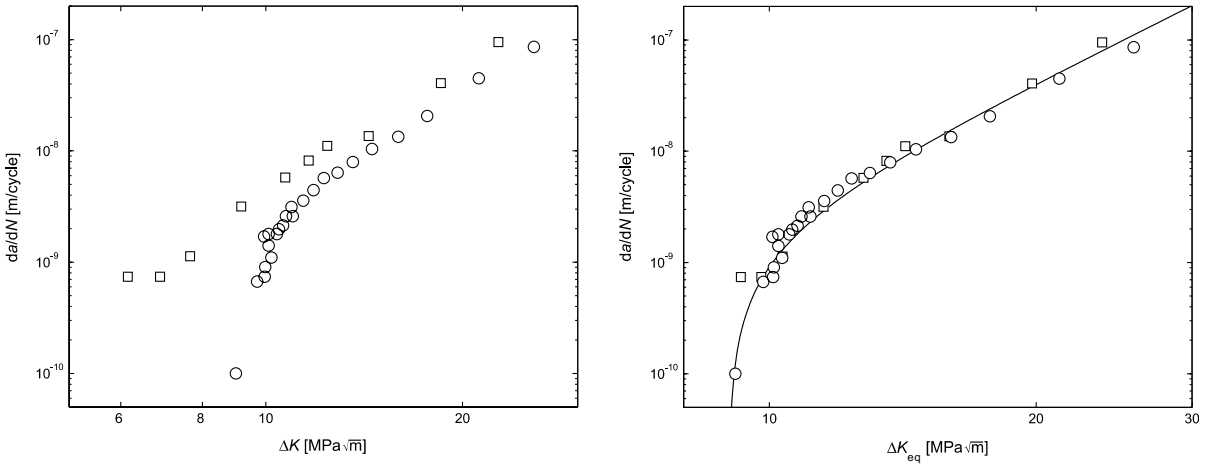

Fig. 5. Crack growth rates in A508 steel [23] as a function of (a) ΔK, and (b) ΔK_{eq}.

for increasing ΔK levels at a constant load level. Fig. 5a clearly shows that short cracks grow at a significantly higher rate than long cracks when rates are compared on the basis of ΔK. Tentative reasons for this state of affairs are:

- A short crack remains open during a larger part of the load cycle than a long crack [25].
- ΔK is no longer characterising the crack tip stress and strain field because the plastic zone is in the order of the crack length [26,27].

In Fig. 5b, the same data have been plotted against the equivalent stress intensity factor ΔK_{eq} [see Eq. (11)]. The short and long crack measurements collapse into one line, which is well described by the solid line, obtained from Eq. (4).

Fig. 6a shows crack growth data for the aluminium alloy 6082-T6. The crack growth measurements have been presented by Mann [24] and were carried out at a stress ratio of $R = 0.1$. According to Borrego et al. [28], the long crack stress intensity threshold of AA6082-T6 is given by $\Delta K_{th}(R = 0.1) = 2.08\ \mathrm{MPa}\sqrt{\mathrm{m}}$. The stress concentration factor at the starter notch was $K_t = 5.7$ [24]. Potential drop measurements were carried out to determine the crack depth, a. The stress intensity factor range, ΔK, was calculated by using an asymptotic

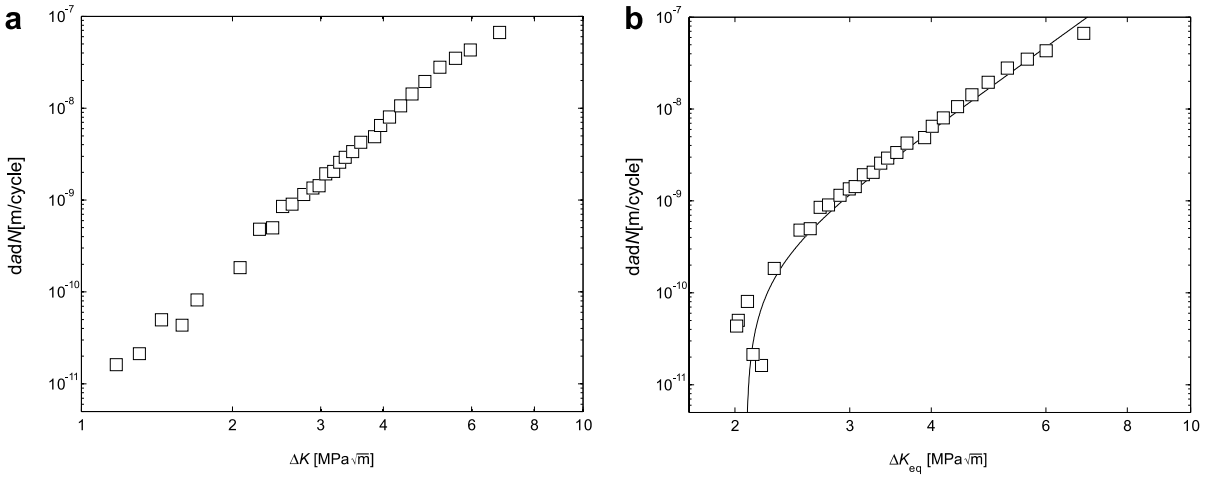

Fig. 6. Crack growth rates in AA6082-T6 [24] as a function of (a) ΔK and (b) ΔK_{eq}.

Please cite this article in press as: Fjeldstad A et al., Simulation of fatigue crack growth in components with ..., Eng Fract Mech (2007), doi:10.1016/j.engfracmech.2007.04.006

solution presented in [4]. The crack growth measurements of the aluminium alloy were carried out by increasing the applied load until a crack had been initiated. The initial crack depth was measured to be approximately 16 μm. Subsequently, the load was reduced stepwise until the crack had reached a depth of approximately 0.5 mm. The load was then kept constant. By applying ΔK_{eq} to the crack growth data in Fig. 6a, one obtains the plot shown in Fig. 6b. The (uncorrected) short crack growth data in the range $\Delta K = 1 - 2$ MPa$\sqrt{\text{m}}$ are seen to be shifted to $\Delta K_{eq} = 2.0 - 2.3$ MPa$\sqrt{\text{m}}$, which is in good agreement with the long crack stress intensity threshold due to Borrego et al. [28].

To judge from the preceding investigations, the crack growth law given by Eq. (13) is a robust and simple crack growth model.

4. Verification of fatigue life predictions

Wormsen et al. [1] showed that the K solutions [6,7] implemented in the finite-element post-processor are in good overall agreement with numerical calculations and solutions found in the literature [29,30]. Based on the conclusions drawn in [1], it is reasonable to assume that the finite-element post-processor yields accurate fatigue life predictions. However, fatigue life predictions may contain errors from other sources than the numerically calculated ΔK values, such as too large crack growth increments when a crack is growing (i) close to a free surface, or (ii) in a gradient stress field.

Life predictions reported in [31,32] have been reanalysed by using Paris' law, see Eq. (3). The mechanical properties presented in Table 1 will be used throughout this Section.

Dai et al. [31] simulated the growth of near-surface cracks located in a semi-infinite body subjected to a remote uniform stress range of $\Delta S = 500$ MPa. The embedded crack grows until it reaches the surface and continues its growth as a surface crack until the fracture toughness, K_{Ic}, is attained. The calculation of K is based on the eigenstrain procedure [33]. This allows the crack to evolve freely. Hence, the transition from an embedded crack to a surface crack may be modelled in detail. As described in [1], a simpler approach has been implemented in the finite-element post-processor. The crack unfolds to a surface crack, once the embedded crack has reached the surface, see Fig. 7. Presented in Table 2 are fatigue life predictions from Dai et al. [31] along with results from the finite-element post-processor. The predicted fatigue lives are consistently on the safe side of those reported in [31], with an observed maximum difference of less than 12%. The predicted number of cycles until breakthrough are in good overall agreement. Thus, the deviation between the

Table 1
Mechanical properties of the investigated steel

Fracture toughness	$K_{Ic} = 150$ MPa$\sqrt{\text{m}}$
Coefficient in Paris' law	$C = 1.0 \cdot 10^{-11}$ [MPa, m]
Exponent in Paris' law	$m = 3$

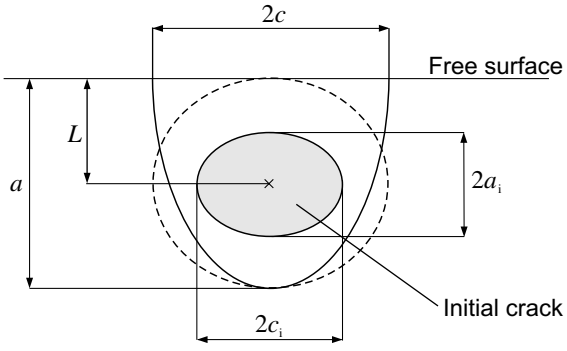

Fig. 7. Sketch of a near surface crack and how it unfolds to a surface crack.

Please cite this article in press as: Fjeldstad A et al., Simulation of fatigue crack growth in components with ..., Eng Fract Mech (2007), doi:10.1016/j.engfracmech.2007.04.006

Table 2
Fatigue life predictions presented by Dai et al. [31] and obtained by using P • FAT

Initial crack geometry [mm][a]			Cycles until breakthrough, n_1		Cycles after breakthrough, n_2		Total cycles until failure, $n_f = n_1 + n_2$	
a_i	c_i	L	Dai et al.	P • FAT	Dai et al.	P • FAT	Dai et al.	P • FAT
1	1	2	8867	8931	14034	11257	22901	20188
1	2	2	3801	4653	12363	11227	16164	15880
2	2	4	3283	3327	8136	6950	11419	10277

[a] See Fig. 7.

two lifetimes can be attributed to the surface crack growth. The difference in the predicted number of cycles after breakthrough is mainly due to the assumption that the embedded crack spontaneously unfolds to a surface crack, cf. Fig. 7.

Fjeldstad et al. [32] simulated the influence of a gradient stress field on the fatigue life using the asymptotic solution by Wormsen et al. [4]. A surface crack located at the root of a semi-circular edge notch ($d = \rho = 20$ mm) in a semi-infinite plate subjected to uniaxial tension $\Delta S = 100$ MPa perpendicular to the symmetry plane of the notch was considered. The cracked configuration is shown in Fig. 8a. The initial crack is characterised by its depth a_i and its surface length $2c_i$, cf. Fig. 8b. According to finite element analysis, the stress concentration factor $K_t = 3.1$ for the notched configuration. In Table 3, results obtained from the finite-element post-processor are presented along with results based on the work in [32]. Again, lifetime predictions from the finite-element post-processor are conservative, with a maximum difference of less than 20%. The difference in fatigue life is here mainly due to the different methods for obtaining ΔK. It is found that the crack aspect ratio a/c in the present analysis is generally beneath that of the analysis described in [32]. A smaller aspect ratio leads to a higher K, which results in a more rapid crack growth, and thus, a shorter fatigue life. Finding the cause of the slightly different behaviour is however outside the scope of this paper.

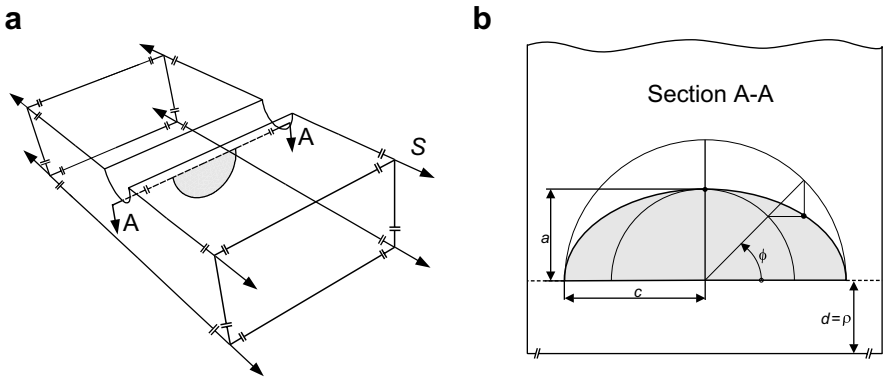

Fig. 8. Schematic drawings of a surface crack emanating from a notch with root radius $\rho = 20$ mm: (a) three-dimensional view and (b) two-dimensional view of the cracked section A–A.

Table 3
Fatigue life predictions of the component shown in Fig. 8 based on Fjeldstad et al. [32] and obtained by the finite-element post-processor

a_i [mm]	a_f [mm]	Fatigue life	
		Fjeldstad et al.	P • FAT
0.2	200	506780	412963
0.2	20	330260	295800
0.02	20	885150	854129

Here, $a_i/c_i = 1$ has been used.

Please cite this article in press as: Fjeldstad A et al., Simulation of fatigue crack growth in components with ..., Eng Fract Mech (2007), doi:10.1016/j.engfracmech.2007.04.006

5. Defects

The fatigue lifetime depends on material defects, e.g., porosity and non-metallic inclusions, which form as a natural part of the manufacturing processes. The volume fraction of inclusions depends directly on the oxygen and sulphur content of the steel.

Due to the small volume of steel that can be examined by conventional inspection methods, the number and size of defects in a large volume have to be estimated by statistical analysis. A description of the different inspection methods, such as non-destructive testing (e.g. ultrasonic, radiographic, eddy-current) and optical microscopy, are given in Ref. [34]. Ultrasonic inspection is nowadays used for the inspection of defects, whose size is greater than approximately 200 μm. The major advantage of this method is that a rather 'large' volume can be inspected. However, in most cases the initial defect size at the failure site is below the detection limit of the ultrasonic inspection method. By using techniques based on surface analysis and optical microscopy, one could detect defects as small as, typically 3 μm. The drawback of this method is that only a small area can be inspected, typically 1 mm^2–15 mm^2. To obtain a sufficient accuracy in the extrapolation from a small area to a large area, the number and size of defects should be counted and measured in several separate control regions.

In the following, methods for the prediction of the size of fatigue critical defects based on the statistics of extremes will be presented.

5.1. Defect distributions

The reliability and performance of metallic components are greatly affected by the size of defects contained in the most highly stressed volume. With improvements in steel-making, the amount and size of defects are being progressively reduced. The likely size of the largest defect within a cast of steel is an important indicator of the quality of the cast. It is of interest both to the manufacturer, for reasons of process control, and to the user, who may wish to use the information on defects to undertake defect-tolerant design and safety assessment of components. Because defects are small and are mostly inside the material, they are difficult to detect and measure. Observations using automated optical microscopy can, however, be made on polished plane regions (control areas), and the maximum defect size in a real component must be obtained by prediction based on some statistical analysis. There are two different approaches based on the statistics of extremes for estimating the sizes of large defects in a large volume from those of a small volume. The first approach, called the *block maximum* method, is based on the generalised extreme value distribution [35]. In this method, only the size of the largest defect in each of the k control areas is measured. The second approach is the *peak over threshold* method. Here, all defects with sizes above a certain high threshold are considered. The overshoot of the defect size above the threshold is fitted to a generalised Pareto distribution [35]. Both methods allow the data on defect sizes in the small control regions to be used for prediction of the maximum defect size in a large volume of steel. And they avoid difficulties in measuring small defects, particularly from a resolution point of view.

5.1.1. Block maximum method

For the block maximum method, the total inspection area is divided into k equally sized, polished control areas, each of size A_0. The three-dimensional size distribution of defects can be estimated from the two-dimensional size distribution by using a stereological approximation as shown in [36,37]. Hence, in the following a control region of volume V_0 is considered. For each of the k control regions, all the defects above the detection limit would need to be measured, to decide which is the largest, i.e., $a_{\max} = \max\{a_1, \ldots, a_i\}$. The result of the block maximum method is a set of k observations of maximum defect sizes, $a_{\max 1}, \ldots, a_{\max k}$. The generalised extreme value (GEV) distribution is fitted to these data. The GEV distribution for a controll region of volume, V_0, is given by

$$G(a_{\max}) = \Pr[A_{\max} \leqslant a_{\max}] = \exp\left\{-\left[1 + \xi'\left(\frac{a_{\max} - a_0^*}{a_0}\right)\right]^{-1/\xi'}\right\}, \tag{16}$$

Please cite this article in press as: Fjeldstad A et al., Simulation of fatigue crack growth in components with ..., Eng Fract Mech (2007), doi:10.1016/j.engfracmech.2007.04.006

where $a_0 > 0$ denotes the scale parameter, a_0^* the location parameter and ξ' the shape parameter. The location parameter, a_0^*, is the $\exp(-1) \approx 36.8\%$ quantile of the generalised extreme value distribution and is often called the characteristic largest defect size in volume V_0. The GEV distribution combines the Gumbel (Type I, $\xi' = 0$), Fréchet (Type II, $\xi' > 0$) and the reversed Weibull (Type III, $\xi' < 0$) distributions into a single distribution. The remarkable feature of the generalised extreme value distribution is that Eq. (16) is the only possible limit for the distribution of the maximum defect size [35].

The Gumbel, Fréchet and reversed Weibull, have distinctly different forms of tail behaviour. When $\xi' < 0$, i.e., for the reversed Weibull distribution, its upper end-point $a_{\max+} = a_0^* - a_0/\xi'$. Thus, the probability of finding defects $\geqslant a_{\max+}$ is zero. The Gumbel ($\xi' = 0$) and Fréchet ($\xi' > 0$) distributions are unlimited upwards.

Consider a homogeneously stressed volume, V_0, subjected to an (equivalent) stress amplitude σ_a. The smallest defect initiating failure in V_0 is denoted by a_{crit}. For long fatigue lives close to the fatigue limit, a_{crit} can be estimated by means of the Kitagawa-Takahashi model [11], cf. Eq. (5), as

$$a_{crit} = a' \left[\left(\frac{\sigma_A}{\sigma_a} \right)^2 - 1 \right], \tag{17}$$

where the intrinsic crack length, a', is given by Eq. (6). If the largest defect within V_0 exceeds a_{crit}, then V_0 will fail. This is the same as stating that the applied stress σ_a is above the fatigue limit (random variable), σ_A, for the volume element V_0. Hence,

$$\Pr[A_{\max} \geqslant a_{crit}] = 1 - G(a_{crit}) = \Pr[\sigma_a \geqslant \sigma_A]. \tag{18}$$

In Fig. 9, a Kitagawa–Takahashi diagram is shown together with a probability density curve of the maximum defect size. The critical defect density, z_1, is defined as the expected number of defects per unit volume of the material that yields a fatigue limit (random variable) $\sigma_A \leqslant \sigma_a$. The shaded area in Fig. 9 is equal to the probability that at least one defect has a size greater than a_{crit}. The probability of failure under homogeneous stress is given by

$$P_{f,V_0} = \Pr[A_{\max} \geqslant a_{crit}] = \Pr[\sigma_a \geqslant \sigma_A] = z_1 V_0. \tag{19}$$

From Fig. 9 it can be seen that the expected number of critical defects decreases with decreasing stress level. Clearly, this has a large effect on the probability of failure. A similar shift could arise from uncertainty in the Kitagawa–Takahashi model. Also a small reduction in maximum defect size by increasing the steel cleanliness,

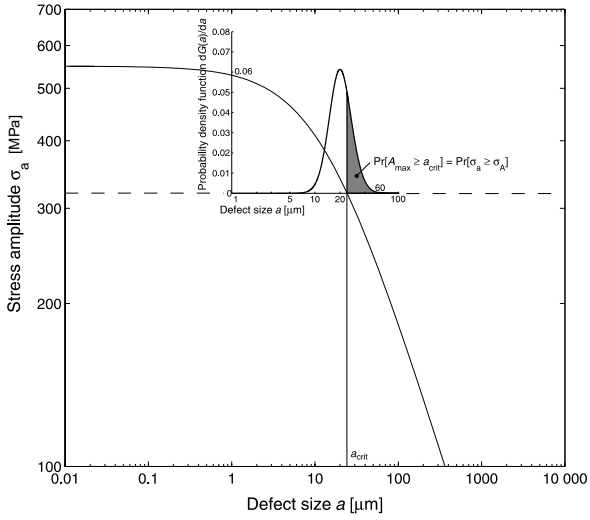

Fig. 9. Illustration of the block maximum method for estimating the fatigue failure probability of a homogeneously stressed volume due to the interaction between the defect size distribution and the applied loading.

Please cite this article in press as: Fjeldstad A et al., Simulation of fatigue crack growth in components with ..., Eng Fract Mech (2007), doi:10.1016/j.engfracmech.2007.04.006

which shifts the density curve to the left, has a similar, large effect. According to Eqs. (19) and (16), the probability of survival, $P_{s,V_0} = 1 - P_{f,V_0}$, is given by

$$P_{s,V_0} = 1 - z_1 V_0 = \Pr[A_{\max} \leqslant a_{\text{crit}}] = \exp\left\{-\left[1 + \xi'\left(\frac{a_{\text{crit}} - a_0^*}{a_0}\right)\right]^{-1/\xi'}\right\}. \tag{20}$$

For an arbitrary volume, V, under homogeneous stress, the probability of survival of the whole volume is equal to the product of the probabilities of survival of all the volume elements. Since, the number of volume elements is V/V_0, one obtains

$$P_{s,V} = P_{s,V_0}^{V/V_0} = \exp\left\{-\left[1 + \xi'\left(\frac{a_{\text{crit}} - a_0^*}{a_0}\right)\right]^{-1/\xi'} \frac{V}{V_0}\right\}. \tag{21}$$

Fig. 10 shows the probability of survival versus the applied stress assuming the maximum defect size to be Gumbel distributed. A homogeneously stressed bearing steel [38] with an intrinsic fatigue limit $\sigma_A = 550$ MPa and $a' = 9.5$ μm is considered. From the figure, it is seen that Eq. (21) takes the size of the specimen into account.

When the state of stress is inhomogeneous, it is appropriate to divide the component, whose overall volume is V, into a large number of small volume elements, ΔV_i, each with a nearly constant (equivalent) stress amplitude, σ_{ai}. Under inhomogeneous stress, a_{crit} will depend on the location $\mathbf{x} = [x, y, z]^T$ of the volume element. Thus, the probability of survival of the i^{th} element is given by

$$P_{s,\Delta V_i} = \exp\left\{-\left[1 + \xi'\left(\frac{a_{\text{crit}}(\mathbf{x}) - a_0^*}{a_0}\right)\right]^{-1/\xi'} \frac{\Delta V_i}{V_0}\right\}. \tag{22}$$

Again, the probability of survival of the component equals the product of the probabilities of survival of all the volume elements, i.e.,

$$P_{s,V} = \exp\left\{-\sum_{i=1}^{V/\Delta V}\left[1 + \xi'\left(\frac{a_{\text{crit}}(\mathbf{x}) - a_0^*}{a_0}\right)\right]^{-1/\xi'} \frac{\Delta V_i}{V_0}\right\}. \tag{23}$$

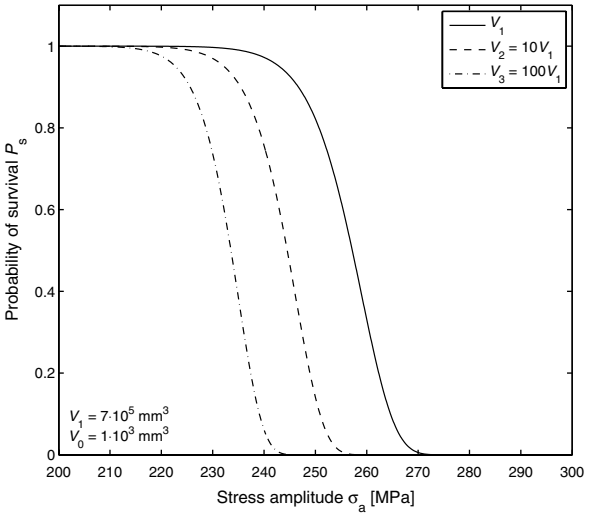

Fig. 10. Probability of survival for a smooth uniaxial loaded specimen versus the applied stress assuming the maximum defect size to be Gumbel distributed ($\xi' = 0$, $a_0^* = 20$ μm and $a_0 = 2$ μm).

Please cite this article in press as: Fjeldstad A et al., Simulation of fatigue crack growth in components with ..., Eng Fract Mech (2007), doi:10.1016/j.engfracmech.2007.04.006

As the volume of each individual element tends to zero, the overall probability of survival becomes

$$P_{s,V} = \exp\left\{-\int_V \left[1+\xi'\left(\frac{a_{crit}(\mathbf{x})-a_0^*}{a_0}\right)\right]^{-1/\xi'} \frac{dV}{V_0}\right\}. \tag{24}$$

This equation can either be solved by means of numerical integration or by 'drawing' defect sizes from the generalised extreme value distribution [see Eq. (16)].

5.1.2. Peak over threshold method

For the block maximum method, all the defects above the detection limit would need to be measured to decide which is the largest. The rest of the data are then discarded. This can be a wasteful process that sets aside valuable data. In contrast, for the peak over threshold method, *all* defects above a certain size are measured, giving more data to the parameter estimation of the defect size distribution. The peak over threshold method was applied to defects in clean steels for the first time by Shi et al. [39,40].

For the peak over threshold method, either a single inspection volume or k sub-volumes are chosen for counting and measuring defects larger than a sufficiently high threshold a_{th}. The result is a set of i observations, $a_1, \ldots, a_i$. The statistical analysis is made on the excesses of these sizes over the threshold, that is on the values $a_i - a_{th}$. A generalised Pareto distribution is given by [35]

$$H(a) = \Pr[A \leqslant a | A > a_{th}] = 1 - \left[1+\xi'\left(\frac{a-a_{th}}{\tilde{a}_0}\right)\right]^{-1/\xi'}, \tag{25}$$

is fitted to these excesses. The scale parameter $\tilde{a}_o$ is given by [35]

$$\tilde{a}_0 = a_0 + \xi'(a_{th} - a_0^*), \tag{26}$$

where a_0, a_0^* and ξ' coincide with the parameters of the associated generalised extreme value distribution for block maxima, see Eq. (16). The range of $a - a_{th}$ is $0 < a - a_{th} < \infty$ if $\xi' \geqslant 0$ and $0 < a - a_{th} < -\tilde{a}_0/\xi'$ if $\xi' < 0$. When $\xi' = 0$, the maximum defect size follows a Gumbel distribution [37]. For $\xi' > 0$, the maximum defect size follows a Fréchet distribution and for $\xi' < 0$, a reversed Weibull distribution [37].

The expected number of defects with sizes greater than a_{th} in the inspection volume V_0 is assumed to be Poisson distributed with mean $z_0(a_{th})V_0$, where $z_0(a_{th})$ is the expected number of defects of size greater than a_{th} per unit volume. The expected number of critical defects in V_0 is Poisson distributed with mean [37]

$$z_1 V_0 = z_0(a_{th}) V_0 \Pr[A \geqslant a_{crit} | A > a_{th}]. \tag{27}$$

The homogeneously stressed volume, V_0, will survive only if all defects have a size smaller than a_{crit}, i.e., $z_1 V_0 = 0$. Hence, from the Poisson distribution,

$$P_{s,V_0} = \Pr[A \leqslant a_{crit}] = \Pr[z_1 V_0 = 0] = \exp\{-z_0(a_{th}) V_0 \Pr[A \geqslant a_{crit} | A > a_{th}]\}, \tag{28}$$

and from Eq. (25), one obtains

$$P_{s,V_0} = \exp\left\{-z_0(a_{th}) V_0 \left[1+\xi'\left(\frac{a_{crit}-a_{th}}{\tilde{a}_0}\right)\right]^{-1/\xi'}\right\}. \tag{29}$$

If $z_0(a_{th}) = 1/V_0$ and $a_{th} = a_0^*$, the above equation becomes identical to Eq. (20). It is this fact that connects the peak over threshold method and the block maximum method.

6. A simplified procedure for determining the life-controlling defect

When performing a Monte Carlo simulation for obtaining the fatigue life distribution of a component, one must generally perform a crack growth analysis of all defects located in each one of the nominally equal components. Since a fatigue crack growth calculation is a computer intensive task, it would be of interest to see whether it is possible to directly identify the life-controlling defect from the stress field and the initial crack growth rate. If this is possible, one could greatly reduce the simulation time. A crude simplified defect selection procedure has been implemented in the finite-element post-processor. This procedure is presented below.

Please cite this article in press as: Fjeldstad A et al., Simulation of fatigue crack growth in components with ..., Eng Fract Mech (2007), doi:10.1016/j.engfracmech.2007.04.006

Non-propagating defects are removed from the component by means of the Kitagawa–Takahashi diagram [11]. The remaining defects are sorted based on their initial crack growth rate. In order to determine the life-controlling defect, the stress field in the proximity of the defect must be taken into account. This is done by using a crude correction of the initial crack growth rate with respect to the stress gradient acting on the crack surface. The method is described in Ref. [32]. Here, the fatigue life of cracked specimens subjected to a gradient stress field is compared with the fatigue life of cracked specimens subjected to a homogeneous stress field.

To see how well the defect selection procedure works, a double-edge-notched-tension plate subjected to a nominal stress range $\Delta S = 450$ MPa at $R = 0$ has been considered. The investigated configuration is shown in Figs. 11a and 12. The largest notch is semi-circular with a radius $\rho = 20$ mm and a stress concentration factor $K_t = 3.5$. The smallest notch is U-shaped with a radius $\rho = 2$ mm and depth $d = 7$ mm. The stress concentration factor for the U-shaped notch is $K_t = 4.8$. The notched configuration is an interesting example due to the two different notch geometries which both suit as potential locations for the life controlling defect. The material parameters used are given in Table 4.

Fig. 11a shows the locations of the potential life-controlling defects contained in one component. The number of critical defects is clearly highest in the proximity of the semi-circular notch, while only a few defects are located near the U-notch. This occurs since the semi-circular notch has a larger highly stressed volume than the U-notch. In order to validate the defect selection procedure, crack growth calculations have been performed for all the defects shown in Fig. 11a. Fig. 11b shows the a priori ranking of the fatigue critical defects due to the selection procedure against the a posteriori ranking obtained by means of crack growth calculations. The figure clearly shows that the defect selection procedure manages to identify the life controlling defect, i.e., the defect that gives the shortest life. However, one can not rule out the possibility that a somewhat less severe defect will be chosen occasionally.

Table 4
Material parameters for a high strength steel [38]

Coefficient in crack growth law	$C(R=0) = 2.08 \cdot 10^{-14}$ [MPa, m]
Exponent in crack growth law	$m = 4.8$
Threshold stress intensity factor range	$\Delta K_{th}(R=0) = 4.4$ MPa$\sqrt{\text{m}}$
Fatigue limit	$\sigma_A(R=0) = 550$ MPa

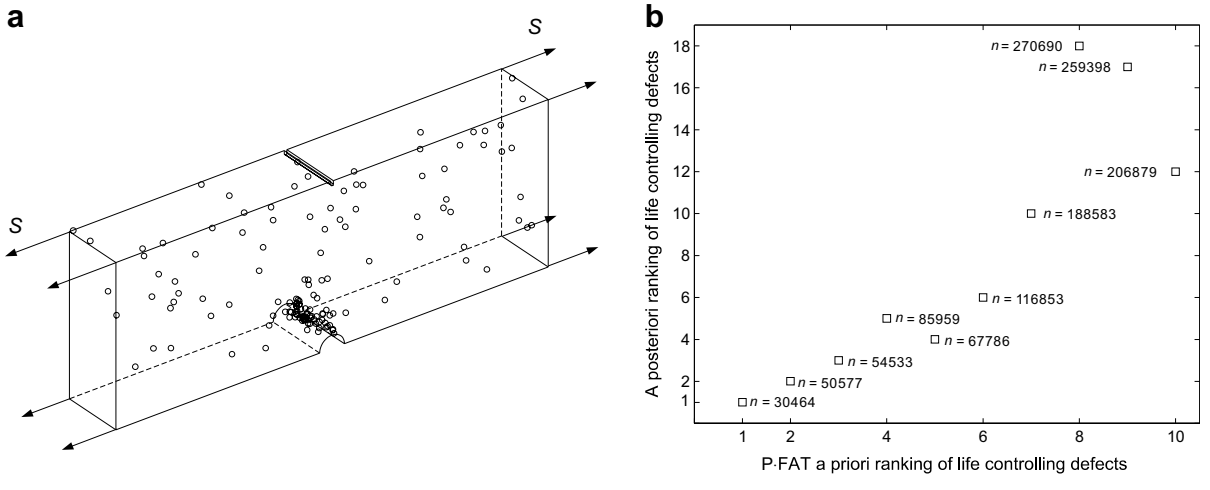

Fig. 11. (a) Potential life-controlling defects in one component, and (b) the a posteriori ranking of the life-controlling defects versus the a priori ranking from P • FAT.

Please cite this article in press as: Fjeldstad A et al., Simulation of fatigue crack growth in components with ..., Eng Fract Mech (2007), doi:10.1016/j.engfracmech.2007.04.006

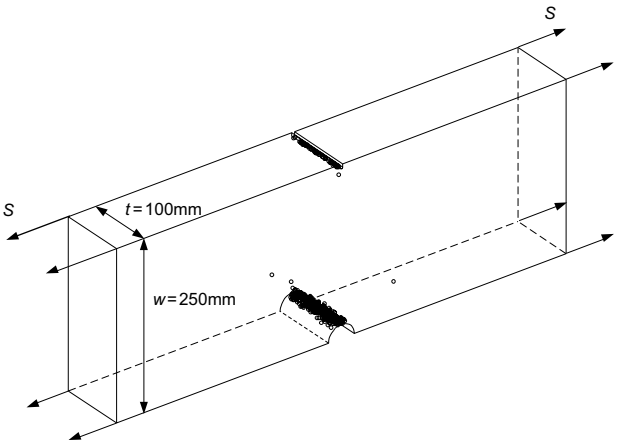

Fig. 12. Example of generated life-controlling defects of 500 components.

Fig. 12 shows the location of the life-controlling defect in 500 components. As can be seen, most of these defects are located in the highly stressed volume of the semi-circular notch, while only a few are located near the more highly stressed U-notch.

7. Simulations

7.1. Geometry

Two different configurations have been investigated: (a) a smooth tension plate and (b) a double-edge-notched tension plate. Both configurations have the volume $V = 6.9 \cdot 10^6\,\mathrm{mm}^3$ and are subjected to the net-section stress amplitude, $S_{a,net} = 320$ MPa at $R = 0$. The specific numerical data employed in the present calculations are given in Table 4.

The first configuration is a smooth plate of width w, height h and thickness t, as shown in Fig. 13a. The double-edge-notched tension plate is shown in Fig. 13b. The notch is semicircular with radius $\rho = w/7$. According to FEA, the elastic stress concentration factor $K_t = \sigma_{1,max}/S = 3.1$ for the notched plate.

One thousand simulations have been carried out for each of the configurations under the assumption that the defect size is Gumbel or Fréchet distributed. The number of crack-like defects in each finite element is 'drawn' from a Poisson distribution. The initial defect locations are given by a uniform distribution [1].

7.2. Results

The different ways of modelling the defect size distributions are separately used to estimate the fatigue limit distribution and the fatigue life distribution of the two investigated configurations. In Table 5, the distribution parameters are presented along with mean and standard deviation values of the size of the life-controlling defect, fatigue limit and fatigue life. Beretta and Murakami [41] found that the distribution functions of inher-

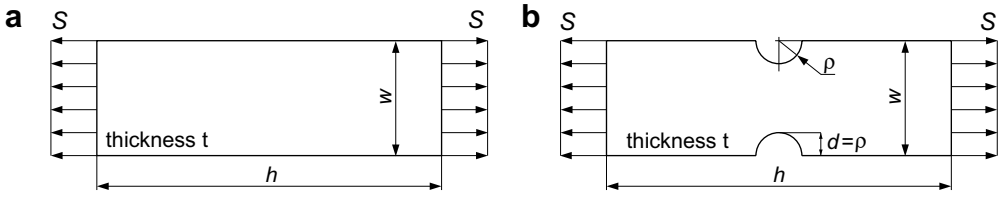

Fig. 13. Specimens considered. (a) A smooth tension plate and (b) a double-edge-notched tension plate.

Please cite this article in press as: Fjeldstad A et al., Simulation of fatigue crack growth in components with ..., Eng Fract Mech (2007), doi:10.1016/j.engfracmech.2007.04.006

Table 5
Mean values and standard deviations of the simulated life-controlling defect size, fatigue limit and fatigue life

Distribution	Parameters			Defect size [μm]		Fatigue limit [MPa]		Fatigue life [k cycles]	
$A_{max}\sim$	a_0^* [μm]	a_0 [μm]	ξ'	Smooth mean (std.[a])	Notched mean (std.[a])	Smooth mean (std.[a])	Notched mean (std.[a])	Smooth mean (std.[a])	Notched mean (std.[a])
Gumbel	20	2	0	38.9 (2.6)	23.0 (3.1)	244 (6.3)	148 (8.0)	110 (11)	4.9 (1.4)
Fréchet	20	0	11.4	46.2 (5.6)	23.2 (3.9)	228 (11)	148 (8.1)	86 (13)	4.9 (1.5)

[a] std: Standard deviation.

ent material inhomogeneities (graphite flakes or nodules, inclusions) have a shape ratio, a_0/a_0^*, typically less than 0.5. Under the assumption that the defect size is Gumbel distributed, a shape ratio $a_0/a_0^* = 0.1$ has been used in the simulations, cf. Table 5.

Size distributions for the life-controlling defects are shown in Fig. 14. Fig. 14a shows the defects size distribution under the assumption that the defect size follows a Gumbel distribution and Fig. 14b shows the associated plot when the defects are 'drawn' from a Fréchet distribution. The mean value and the standard deviation of the life-controlling defect size are given in Table 5. As can be seen, the life-controlling defect in the smooth plate is larger under a Fréchet assumption than under a Gumbel assumption. This occurs since the Fréchet distribution has a heavier upper tail than the Gumbel distribution. Furthermore, the size of the life-controlling defect is much smaller in the notched configuration compared to the smooth plate due to the smaller highly stressed volume. From Fig. 14 and Table 5, it can be seen that the type of the defect distribution has nearly no influence on the size of the life-controlling defect in the notched plate.

The size distributions of the life-controlling defect shown in Fig. 14 have been converted into fatigue limit distributions by using the Kitagawa–Takahashi diagram. The resulting fatigue limit data have been plotted in a Weibull probability chart in Fig. 15. The dashed lines are drawn by using a three-parameter Weibull distribution. The three-parameter (cumulative) Weibull distribution is given by

$$\Pr[\sigma_A \leqslant \sigma_a] = 1 - \exp\left[-\left(\frac{\sigma_a - \sigma_{A0}^*}{\sigma_0}\right)^{b_\sigma}\right], \tag{30}$$

where σ_0 denotes the scale parameter, σ_{A0}^* the location parameter and b_σ the shape parameter. The parameters are given in Table 6 and have been estimated using the maximum likelihood method [35]. Since the simulated data follow the dashed lines rather well, it can be accepted that the fatigue limit for both configurations and defect size distributions are well described by the Weibull distribution. From Fig. 15 and Table 5 it can be seen

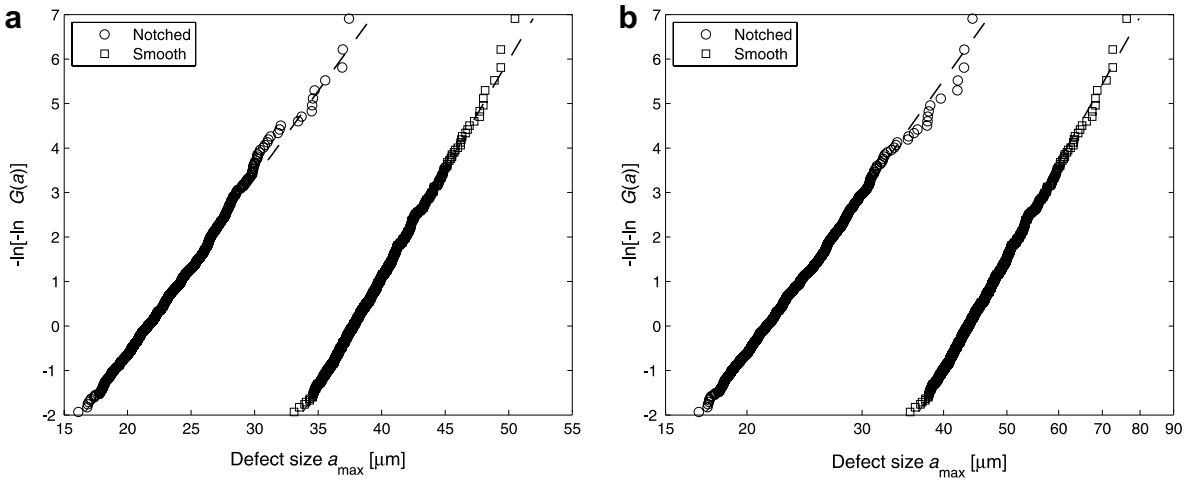

Fig. 14. Simulated life-controlling defect sizes in the two investigated configurations [see Fig. 13] under the assumption that the defect size follows (a) a Gumbel distribution and (b) a Fréchet distribution.

Please cite this article in press as: Fjeldstad A et al., Simulation of fatigue crack growth in components with ..., Eng Fract Mech (2007), doi:10.1016/j.engfracmech.2007.04.006

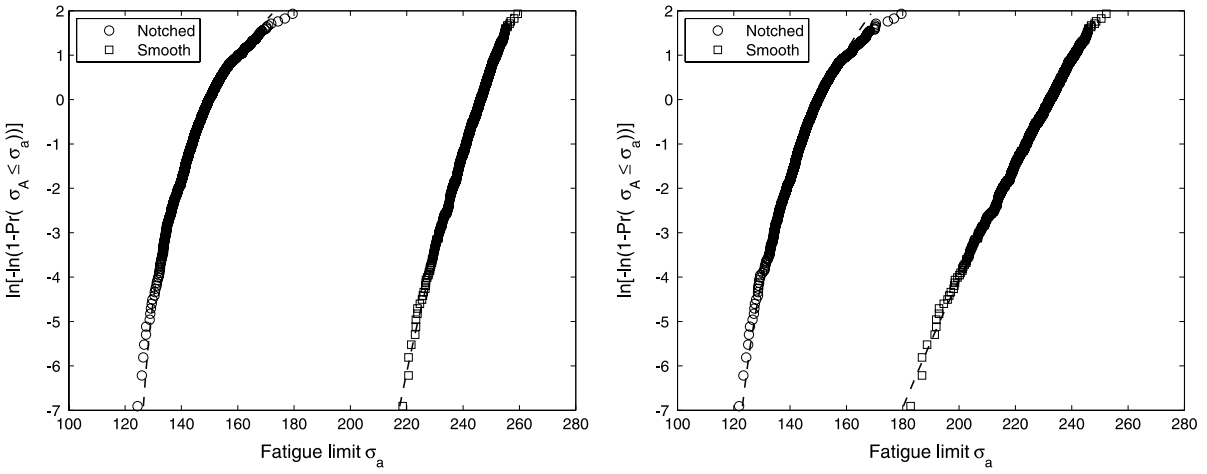

Fig. 15. Fatigue limit distribution for the two investigated configurations [see Fig. 13] under the assumption that the defect size follows (a) a Gumbel distribution and (b) a Fréchet distribution.

Table 6
Weibull distribution parameters of the simulated fatigue limit [Fig. 15] and fatigue life [Fig. 16]

Distribution $A_{max} \sim$		Parameters			Fatigue limit			Fatigue life		
		a_0^* [μm]	a_0 [μm]	ξ'	σ_{A0}^* [MPa]	σ_0 [MPa]	b_σ	n_0^*	n_0	b_n
Gumbel	Smooth	20	2	0	42	204	38.6	588330	551945	5.3
	Notched	20	2	0	123	27	3.3	10018	43429	2.9
Fréchet	Smooth	20	0	11.4	39	194	22.5	244470	664680	5.3
	Notched	20	0	11.4	120	31	3.7	10208	43539	2.8

that the fatigue limit distribution for the notched plate is nearly unaffected by the type of the defect size distribution, as could be expected from Fig. 14.

Fig. 16 shows the fatigue life distribution for the two investigated configurations for $S_{a,net} = 320$ MPa. The simulated data are again plotted in a Weibull probability chart. The dashed lines are drawn by using the three-parameter Weibull distribution:

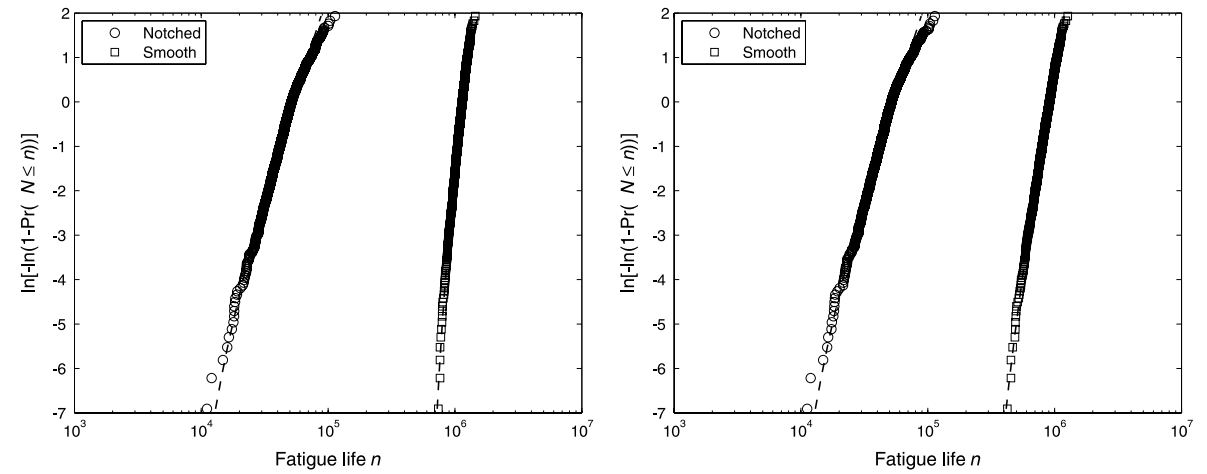

Fig. 16. Fatigue life distribution for the two investigated configurations [see Fig. 13] under the assumption that the defect size follows (a) a Gumbel distribution and (b) a Fréchet distribution.

Please cite this article in press as: Fjeldstad A et al., Simulation of fatigue crack growth in components with ..., Eng Fract Mech (2007), doi:10.1016/j.engfracmech.2007.04.006

$$\Pr[N \leqslant n] = 1 - \exp\left[-\left(\frac{n - n_0^*}{n_0}\right)^{b_n}\right]. \tag{31}$$

Here, n_0 denotes the scale parameter, n_0^* the location parameter and b_n the shape parameter. The parameters are given in Table 6. It can be seen from Fig. 16 that the simulated data are well described by the Weibull distribution. Fig. 16 and Table 6 show that the fatigue life for the notched plate is nearly unaffected by the choice of the defect size distribution.

8. Conclusions

The probability of component fatigue failure can be estimated from an extreme value distribution for large defects and the stress distribution within the component. The fatigue life distribution of a component is obtained by performing crack growth simulations for a large number of randomly distributed defects. The simulations are carried out by using a proposed short crack growth model. An analysis of short and long crack data demonstrated that the short crack model describes the crack growth data very well. Fatigue life predictions have been compared with predictions presented by Dai et al. [31] and Fjeldstad et al. [32]. The fatigue life predictions have been found to be in good agreement with the latter investigations. Further, it has been shown that the presented procedure takes into account the influence of the stress distribution as well as the size of a component on the probability of component fatigue failure. The method can also estimate the reduction in the probability of fatigue failure due to improvements in steel cleanliness and by careful component design.

Simulations of two configurations have been performed. Their fatigue limit and fatigue life distributions have separately been obtained, and found to be well described by a three-parameter Weibull distribution. For the notched configuration, it was found that the fatigue limit and fatigue life were nearly unaffected by the choice of the defect size distribution.

Acknowledgements

The authors gratefully acknowledge the research support for this work provided by The Research Council of Norway and the industrial participants within the NorLight project, and by GE Energy (Norway) AS.

References

[1] Wormsen A, Fjeldstad A, Härkegård G. 2006. A post-processor for fatigue crack growth analysis based a finite element stress field. Comput Method Appl Mech Engng., submitted for publication.
[2] Fett T, Munz D. Stress intensity factors and weight functions. International series on advances in fracture. Southampton: Computational Mechanics Publications; 1997.
[3] Tada H, Paris PC, Irwin GR. The stress analysis of cracks handbook. 3rd ed. Bury St. Edmunds and London: Professional Engineering Publishing Limited; 2000.
[4] Wormsen A, Fjeldstad A, Härkegård G. The application of asymptotic solutions to a semi-elliptical crack at the root of a notch. Engng Fract Mech 2006;73(13):1899–912.
[5] Fjeldstad A, Härkegård G, Wormsen A. Approximate stress intensity factors for cracked V-notched specimens based on asymptotic solutions with application to T-joints. Engng Fract Mech, accepted for publication.
[6] Wang X, Lambert SB, Glinka G. Approximate weight functions for embedded elliptical cracks. Engng Fract Mech 1998;59(3):381–92.
[7] Shen G, Glinka G. Weight functions for a surface semi-elliptical crack in a finite thickness plate. Theor Appl Fract Mec 1991;15(3):247–55.
[8] Zheng XJ, Glinka G, Dubey RN. Stress intensity factors and weight functions for a corner crack in a finite thickness plate. Engng Fract Mech 1996;54(1):49–61.
[9] Paris PC, Erdogan F. A critical analysis of crack propagation laws. J Basic Engng 1963;85:528–34.
[10] Klesnil M, Lukáš P. Influence of strength and stress history on growth and stabilisation of fatigue cracks. Engng Fract Mech 1972;4(1):77–92.
[11] Kitagawa H, Takahashi S. Applicability of fracture mechanics to very small cracks or the cracks in early stage. In: Proceedings of the second international conference on the mechanical behaviour of materials. Boston, Ma: 1976, p. 627–31.
[12] El Haddad MH, Topper TH, Smith KN. Prediction of non-propagating cracks. Engng Fract Mech 1979;11(3):573–84.

Please cite this article in press as: Fjeldstad A et al., Simulation of fatigue crack growth in components with ..., Eng Fract Mech (2007), doi:10.1016/j.engfracmech.2007.04.006

[13] Härkegård G. An effective stress intensity factor and the determination of the notched fatigue limit. In: Bäcklund J, Blom AF, Beevers CJ, editors. Fatigue thresholds: fundamentals and engineering applications, vol. 2. Engineering Materials Advisory Services Ltd.; 1982. p. 867–79.
[14] Tanaka K, Nakai Y, Yamashita M. Fatigue growth threshold of small cracks. Int J Fract 1981;17(5):519–33.
[15] Hertzberg RW. Deformation and fracture mechanics of engineering materials. 4th ed. John Wiley & Sons, Inc.; 1996.
[16] Green AE, Sneddon IN. The distribution of stress in the neighborhood of a flat elliptical crack in an elastic solid. Proc. Cambridge Phil. Soc. 1950:46.
[17] Härkegård G, Denk J, Stärk K. Growth of naturally initiated fatigue cracks in ferritic gas turbine rotor steels. Int J Fatigue 2005;27(6):715–26.
[18] Newman Jr JC, Raju IS. An empirical stress-intensity factor equation for the surface crack. Engng Fract Mech 1981;15(1–2):185–92.
[19] Walker K. The effect of stress ratio during crack propagation and fatigue for 2024-T3 and 7075-T6 aluminium. In: Effects of environment and complex load history on fatigue life, ASTM STP 462, Philadelphia, 1970, p. 1–14.
[20] Mann T, Tveiten BW, Härkegård G. Fatigue crack growth analysis of welded aluminium RHS T-joints with manipulated residual stress level. Fatigue Fract Engng Mater Struct 2006;29(2):113–22.
[21] Mann T. The influence of mean stress on fatigue crack propagation in aluminium alloys. Int J Fatigue 2007. doi:10.1016/j.ijfatigue.2006.11.010.
[22] Mann T. Fatigue assessments methods for welded structures and their application to an aluminium T-joint. PhD thesis, NTNU, Trondheim, Norway, 2006.
[23] Breat JL, Murdy F, Pineau A. Short crack propagation and closure effects in A508 steel. Fatigue Engng Mater Struct 1983;6(4):349–58.
[24] Mann T, Härkegård G, Stärk K. Short fatigue crack growth in aluminium alloy 6082-T6. Int J Fatigue 2007. doi:10.1016/j.ijfatigue.2007.01.00.
[25] Suresh S. Fatigue of materials. 2nd ed. Cambridge University Press; 1998.
[26] Miller KJ. The behaviour of short fatigue cracks and their initiation. Part I – A review of two recent books. Fatigue Engng Mater 1987;10(1):75–91.
[27] Miller KJ. The behaviour of short fatigue cracks and their initiation. Part II – A general summary. Fatigue Engng Mater 1987;10(2):93–113.
[28] Borrego LP, Ferreira JM, Costa JM. Fatigue crack growth and crack closure in an AlMgSi alloy. Fatigue Fract Engng Mater Struct 2001;24(4):255–65.
[29] Shah RC, Kobayashi AS. Stress intensity factor for an elliptical crack under arbitrary normal loading. Engng Fract Mech 1971;3(1):71–93.
[30] Nilsson L. Stress intensity factors for semi-elliptical surface cracks in plates subjected to a complex stress field. Technical Report 1401-5331, SAQ Kontroll AB, Stockholm, Sweden, 1998.
[31] Dai DN, Hills DA, Härkegård G, Pross J. Simulation of the growth of near-surface defects. Engng Fract Mech 1998;59(4):415–24.
[32] Fjeldstad A, Härkegård G, Wormsen A. The influence of a stress gradient on the growth of a fatigue crack. In: Johnson WS et al., editors. Proceedings of the international fatigue congress 2006. Atlanta, Georgia, USA.: Elsevier; 2006. May.
[33] Dai DN, Nowell D, Hills DA. Eigenstrain methods in 3-D crack problems; an alternative integration procedure. J Mech Phys Solids Struct 1993;41(6):1003–17.
[34] Atkinson HV, Shi G. Characterization of inclusions in clean steels: a review including the statistics of extreme methods. Prog Mater Sci 2003;48:457–520.
[35] Coles S. An introduction to statistical modeling of extreme values, 3rd ed. Springer Series in Statistics, London, 2001.
[36] Anderson CW, Coles SG. The largest inclusions in a piece of steel. Extremes 2002;5:237–52.
[37] Anderson CW, de Maré J, Rootzén H. Methods for estimating the sizes of large inclusions in clean steels. Acta Mater 2005;53(8):2295–304.
[38] Sakai T, Sato Y, Nagano Y, Takeda M, Oguma N. Effect of stress ratio on long life fatigue behaviour of high carbon chromium bearing steel under axial loading. Int J Fatigue 2006;28(11):1547–54.
[39] Shi G, Atkinson HV, Sellars CM, Anderson CW. Application of the generalized Pareto distribution to the estimation of the size of the maximum inclusion in clean steels. Acta Mater 1999;47(5):1455–68.
[40] Shi G, Atkinson HV, Sellars CM, Anderson CW. Comparison of extreme value statistics methods for predicting maximum inclusion size in clean steel. Ironmak Steelmak 1999;26(4):239–46.
[41] Beretta S, Murakami Y. Statistical analysis of defects for fatigue strength prediction and quality control of materials. Fatigue Fract Engng Mater Struct 1998;21(9):1049–65.

Please cite this article in press as: Fjeldstad A et al., Simulation of fatigue crack growth in components with ..., Eng Fract Mech (2007), doi:10.1016/j.engfracmech.2007.04.006

A reanalysis of Frost's classical fatigue tests on self-arresting cracks at notches

A. Fjeldstad*, A. Wormsen and G. Härkegård.
Norwegian University of Science and Technology, Trondheim, Norway.

Abstract

In this paper, a short crack growth model is presented and used for predicting the arrest of cracks growing in stress gradient fields. The crack growth model makes use of an effective stress which can be interpreted as the stress that must be applied to the corresponding smooth semi-infinite cracked plate to obtain the same value of the stress intensity factor as for the considered notched configuration. The short crack growth model has been used for predicting the conditions, under which crack initiation, crack arrest and failure are expected to occur. These predictions have been compared with experimentally obtained data for notched specimens of mild steel. The predictions are found to be in good agreement with the experimental data.

Keywords: short crack growth model, effective stress, crack arrest.

NOTATION

a	crack depth
a'	crack depth at transition between shallow and deep crack asymptotes
a_0	intrinsic crack depth
C	coefficient of crack growth law
d	notch depth
F_0	geometry factor for a crack emanating from a smooth surface
K	stress intensity factor
$\Delta K_{\rm th}$	threshold stress intensity range
$\Delta K_{\rm eq}$	equivalent stress intensity range
$K_{\rm t}$	gross stress concentration factor $= \sigma_{\max}/\sigma_\infty$
m	exponent of crack growth law
ρ	notch root radius
$\sigma_{\rm A}$	intrinsic fatigue limit
σ_∞	remote gross stress
$\bar{\sigma}$	effective stress

1 Introduction

In the late fifties, Frost [**1**] carried out a celebrated series of fatigue tests on notched specimens of mild steel. He noticed that cracks, which initiated at the root of the notch, either continued to grow to failure or arrested at some depth below the notch. Thus, in agreement with later observations by Kitagawa and Takahashi [**2**] on *smooth* specimens, cracks were consistently observed in specimens, where the notch strss amplitude exceeds the ordinary, 'intrinsic' fatigue limit, $\sigma_{\rm A}$. However, in severely notched specimens, Frost observed that fatigue cracks were arrested and became 'non-propagating', when the applied stress amplitude fell below some critical level. By plotting the fatigue limit of a *smooth* specimen with a (short) surface crack against the depth of the crack, Kitagawa and Takahashi [**2**] found the fatigue limit to be a steadily decreasing function of the depth, with the intrinsic fatigue limit given by the short crack asymptote. The results by Kitagawa and Takahashi are in good qualitative agreement with a fracture mechanics model by El Haddad et al. [**3**] for a through-crack in a homogeneous stress field. According to El Haddad et al., the long crack asymptote is given by the threshold for crack growth, $\Delta K_{\rm th}$.

In an attempt to understand the mechanisms behind Frost's observations, Smith and Miller [**4**]used $\Delta K_{\rm th}$ to predict the critical level, below which a fatigue crack becomes non-propagating. This gave acceptable agreement for relatively deep cracks ($a > 1.3$ mm) investigated by Frost. However, for smaller cracks, with a depth approaching the intrinsic crack depth, the direct use of $\Delta K_{\rm th}$ would overpredict the critical level. Moreover, since fatigue crack *growth* was not modelled by Smith and Miller, they could not explicitly treat the transition from initial crack growth to crack arrest.

In [**5**], the present authors generalised El Haddad's model to cover the case of a crack of arbitrary shape in an inhomogeneous stress field, e.g., a semi-elliptic crack at the root of a notch. In conjunction with the fatigue-crack-growth law by Klesnil and Lukas [**6**], the generalised model was found to agree well with the growth of short (and long) surface cracks observed in a steel and in an aluminium alloy. In the following it will be shown that the short-crack-growth model of [**5**] is able to model the transition from initial crack growth to crack arrest.

*Corresponding author: Department of Engineering Design and Materials, Norwegian University of Science and Technology, Richard Birkelandsvei 2B, Trondheim, NO-7491 , Norway; email: Arne.Fjeldstad@ntnu.no

Predictions of crack initiations and crack arrest will be compared with the results from the classical fatigue tests by Frost [**1**].

2 Modelling the arrest of fatigue cracks

2.1 A model for the growth of short fatigue cracks

The use of stress intensity factors was extended to fatigue problems by Paris and Erdogan [**7**], who suggested a power-law relationship between the crack growth rate $\mathrm{d}a/\mathrm{d}n$ and the stress intensity range ΔK. Klesnil and Lukáš [**6**] suggested the following equation to extend Paris' law into the near-threshold region:

$$\frac{\mathrm{d}a}{\mathrm{d}n} = C(\Delta K^m - \Delta K_{\mathrm{th}}^m). \tag{1}$$

C and m are material parameters, and ΔK_{th} is the threshold stress intensity range. For a crack in a homogeneous, normal stress field, σ, the stress intensity factor may be expressed in terms of the crack depth, a, and the geometry, F_0, as

$$K = F_0 \sigma \sqrt{\pi a}. \tag{2}$$

A compilation of fatigue tests by Kitagawa and Takahashi [**2**] clearly shows that the fatigue limit of a cracked solid can be determined by means of the threshold of the stress intensity range, ΔK_{th}, for long cracks only. Thus, for short cracks, the fatigue limit asymptotically approaches the ordinary fatigue limit, $\Delta\sigma_{\mathrm{A}} = 2\sigma_{\mathrm{A}}$, as determined by means of a smooth specimen. Both the long and the short crack fatigue limits are asymptotically satisfied by an equation proposed by El Haddad et al. [**3**] for $F_0 = 1$, and generalised by Härkegård [**8**] to an arbitrary geometry factor F_0, viz.

$$\Delta\sigma = \frac{\Delta K_{\mathrm{th}}}{F_0\sqrt{\pi(a+a_0)}} = \frac{\Delta\sigma_{\mathrm{A}}}{\sqrt{1+a/a_0}}. \tag{3}$$

The characteristic crack length, a_0, which signifies the transition between short cracks, $a < a_0$, and long cracks, $a > a_0$, is defined by

$$a_0 = \frac{1}{\pi}\left(\frac{\Delta K_{\mathrm{th}}}{F_0\Delta\sigma_{\mathrm{A}}}\right)^2. \tag{4}$$

One may interpret a_0 as an 'intrinsic' crack length, which should be added to the length of the real crack to yield an 'equivalent' crack length.

Based on the observation [**9, 10**] that short cracks grow faster than long cracks at a given stress intensity level, El Haddad et al. [**3**] introduced an equivalent stress intensity range that accounts for the elevated crack growth rate of short cracks, viz.

$$\Delta K_{\mathrm{eq}} = F_0\Delta\sigma\sqrt{\pi(a+a_0)} \tag{5}$$

Strictly speaking, equations (3) and (5) are only valid for a crack growing in a homogeneous stress field. It would therefore be of great interest to extend the theory by El Haddad et al. to handle crack growth in inhomogeneous stress fields. This can be done by replacing the homogeneous stress range $\Delta\sigma$ with an effective stress range, $\Delta\bar{\sigma}$. This is defined as the stress range that must be applied to the corresponding smooth semi-infinite plate to obtain the same stress intensity range as that of the crack at the root of the notch, cf. Fig. 1. The effective stress range is defined as

$$\Delta\bar{\sigma} = \frac{\Delta K}{F_0\sqrt{\pi a}}. \tag{6}$$

For a shallow edge through-crack, $F_0 = 1.122$ [**11**], and for a semi-elliptic surface crack with aspect ratio $a/c = 1$, the geometry factor at the deepest point of the crack front has the value $F_0 = 0.663$ [**12**].

The preceding equations explicitly depend on the characteristic crack length, a_0, which, in its turn, depends on the crack geometry factor, F_0. The latter will not be constant, if the crack shape changes. This inconvenience can be avoided by substituting $F_0^2 a_0$ and $F_0^2 a$ from equations (6) and (4), respectively, into equation (5). After some rearrangement, one obtains

$$\Delta K_{\mathrm{eq}} = \Delta K_{\mathrm{th}}\left[\left(\frac{\Delta K}{\Delta K_{\mathrm{th}}}\right)^2 + \left(\frac{\Delta\bar{\sigma}}{\Delta\sigma_{\mathrm{A}}}\right)^2\right]^{1/2}. \tag{7}$$

By replacing ΔK in equation (1) by the equivalent stress intensity range of equation (7), one obtains a crack-growth law that accounts for the growth of a short crack in an inhomogeneous stress field, viz.

$$\frac{\mathrm{d}a}{\mathrm{d}n} = C\Delta K_{\mathrm{th}}^m\left[\left\{\left(\frac{\Delta K}{\Delta K_{\mathrm{th}}}\right)^2 + \left(\frac{\Delta\bar{\sigma}}{\Delta\sigma_{\mathrm{A}}}\right)^2\right\}^{m/2} - 1\right]. \tag{8}$$

This equation predicts a finite crack-growth rate as soon as $\Delta\bar{\sigma} > \Delta\sigma_{\mathrm{A}}$, even for a crack of vanishing depth. Using equation (8), Fjeldstad et al. [**5**] were able to unify $\mathrm{d}a/\mathrm{d}n$-data for long and short crack in a low-alloy steel [**13**] and in an aluminium alloy [**14**].

2.2 Crack arrest at notches

The stress field decreases rapidly ahead of a notch and may cause a decreasing crack growth rate for a propagating crack. Fig. 2 shows the normalised equivalent stress intensity factor, $\Delta K_{\mathrm{eq}}/\Delta K_{\mathrm{th}}$, against the normalised crack depth, a/d, for a circumferentially notched specimen subject to tension-compression. The effective stress range $\Delta\bar{\sigma}$ has been calculated as [**15**]

$$\Delta\bar{\sigma} = \Delta\sigma_\infty\sqrt{1+\frac{d}{a}\left[1-\exp\left(-\frac{a}{a'}\right)\right]}, \tag{9}$$

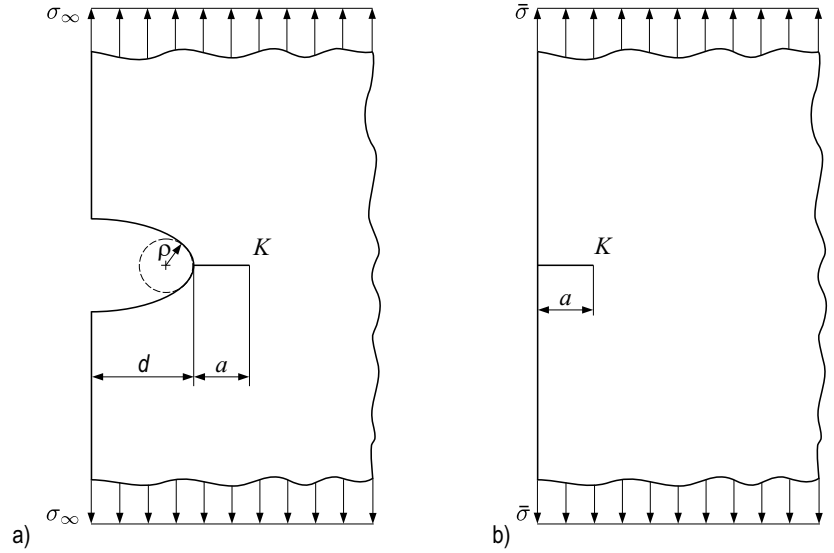

Figure 1: When subjected to the effective stress, $\bar{\sigma}$, the edge-crack of the smooth plate (b) has the same stress intensity factor, K, as that of the crack of the notched plate (a) subjected to the remote stress σ_∞.

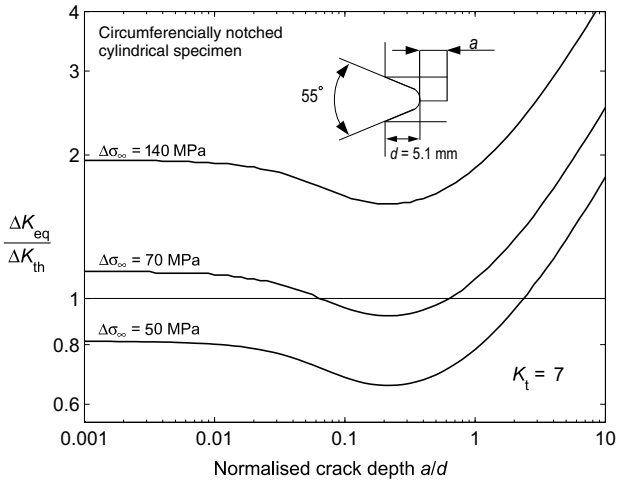

Figure 2: $\Delta K_{\rm eq}/\Delta K_{\rm th}$ versus a/d at three different stress ranges. The curves are obtained by using $\Delta\sigma_{\rm A} = 430$ MPa and $\Delta K_{\rm th} = 13$ MPa$\sqrt{\rm m}$ for $R = -1$.

where the transition crack depth a' is defined by

$$a' = \frac{d}{K_{\rm t}^2 - 1};\ K_{\rm t} = \frac{\sigma_{\max}}{\sigma_\infty}. \tag{10}$$

The stress intensity range, ΔK, is then found by means of equation (6) using $F_0 = 1.122$, i.e., assuming a circumferencial crack of constant depth. In Fig. 2, $\Delta K_{\rm eq}/\Delta K_{\rm th}$ has been presented for three different stress ranges. The upper curve illustrates a situation, where the crack starts to grow from the notch root and continues to grow until final failure. The intermediate curve shows crack initiation and growth, until $\Delta K_{\rm eq}$ falls below $\Delta K_{\rm th}$ and the crack arrests. The lower curve corresponds to a situation, where no crack is initiated.

3 Analysis of Frost's classical fatigue test data

3.1 Comparison of predictions with test data

The existence of crack arrest for short cracks growing from the root of a notch has been experimentally confirmed by Frost [**1**]. The experimental data reported in [**1**] will be compared with predictions from equation (8). The mild steel specimens tested are shown in Fig. 3. The specimen in Fig. 3(a) was subjected to fully reversed tension-compression, while the specimen in Fig. 3(b) was subjected to rotating bending. Both specimens were machined with different notch root radii in order to obtain different $K_{\rm t}$ values. The plain tension-compression fatigue limit of the mild steel was reported to be $\Delta\sigma_{\rm A} = 430$ MPa [**1**]. According to Smith and Miller [**4**], the threshold stress intensity range, $\Delta K_{\rm th}(R = -1)$, for the mild steel considered is 13 MPa$\sqrt{\rm m}$. Based

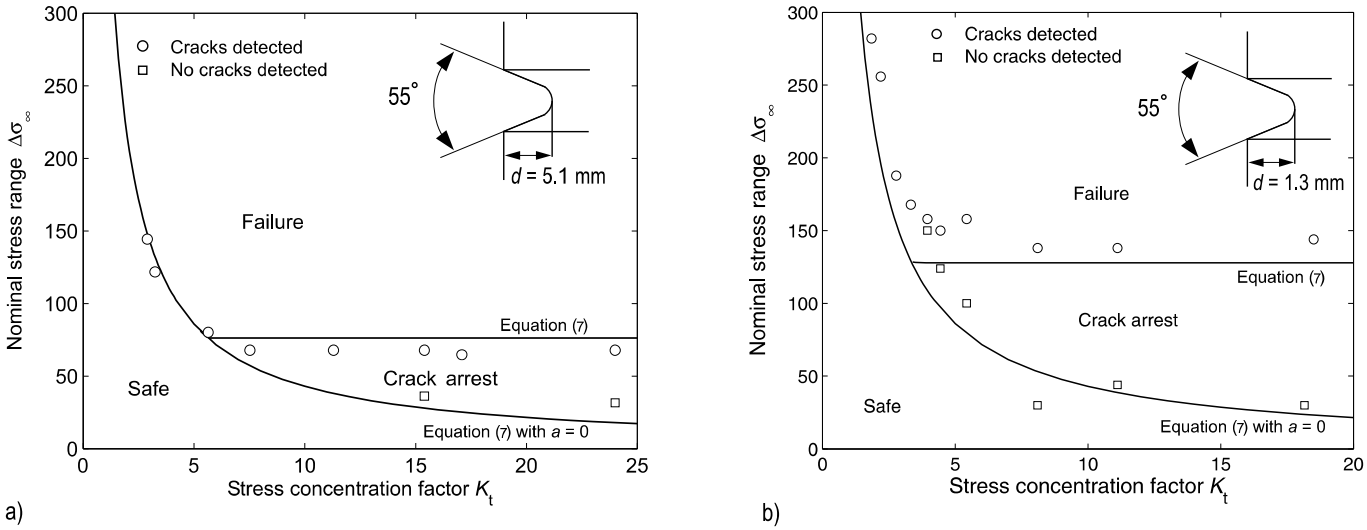

Figure 4: Fatigue regimes in notched components according to the short crack growth model [equation (8)]. The experimental data are from cylindrical specimens of mild steel with notch depth (a) $d = 5.1$ mm [Fig. 3(a)] and (b) $d = 1.3$ mm [Fig. 3(b)] **[1, 16]**.

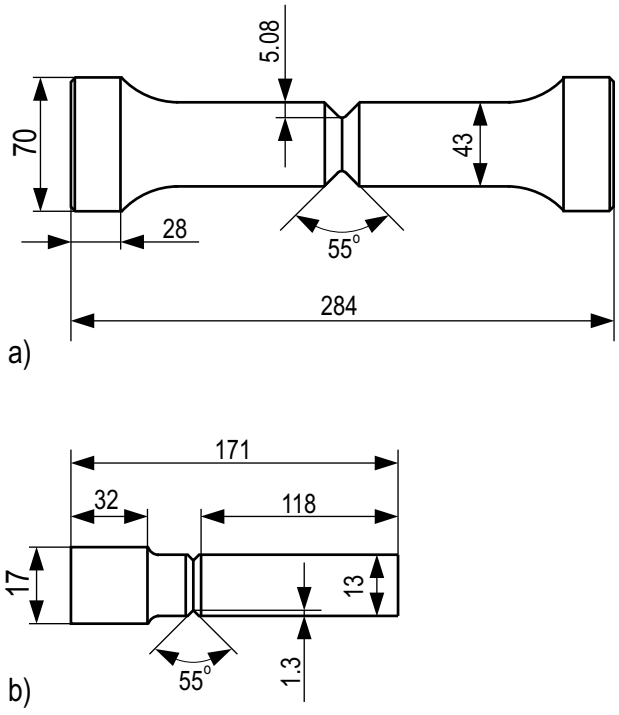

Figure 3: Cylindrical fatigue test specimens subjected to (a) fully reversed tension-compression and (b) rotating bending **[1, 16]**.

on a metallographic examination, Frost **[1]** found that the cracks initiated with an approximately uniform depth around the complete periphery for both types of specimens. Frost's data **[1]** are presented in Fig. 4 together with curves predicted by equation (8). The predictions are carried out by assuming a crack of constant depth around the complete periphery. Fig. 4 is divided into three regions **[4]**: (*i*) one in which no crack will be formed, (*ii*) one in which crack arrest will occur, and (*iii*) one in which a crack will be formed and propagate to failure. As can be seen, the proposed crack growth model agrees very well with the experimental data. Moreover, the crack growth model reveals the change in fatigue limit of notched specimens of the same notch depth d but different notch root radii ρ. Note that the stress level separating the propagation and crack arrest regimes is independent of the stress concentration factor K_t above a certain value of K_t. It is clearly seen that the threshold stress level, at which no crack arrest will occur, is higher for the specimen with notch depth $d = 1.3$ mm than for the specimen with $d = 5.1$ mm.

3.2 Some remarks

The peak stress level needed to form a crack at the root of the notch is low and the degree of notch root plasticity is therefore so small that it could be neglected.

The solid line that defines the boundary between crack arrest and complete failure in Fig. 4 has been obtained by neglecting the effect of notch root plasticity.

The following points summarises the present Section:

- Crack arrest can be predicted by the short crack growth model.

- A crack emanating from the root of a notch, below a certain stress concentration factor, will propagate to failure if the stress range exceeds the fatigue limit.
- Above a certain K_t value the stress level separating the propagation and crack arrest regimes are nearly independent of the stress concentration factor.
- Although no effect of notch plasticity is taken into account in the analysis, the crack growth predictions agrees very well with Frost's experimental data.

4 Conclusions

A short crack growth model has been used to predict the conditions for crack initiation, crack arrest and failure for notched cylindrical specimens of mild steel. The crack growth model uses an effective stress, which is interpreted as the stress that must be applied to the corresponding semi-infinite cracked plate to obtain the same stress intensity factor value as for the notched configuration considered. These analyses show that crack arrest is expected to occur below a certain stress range, which depends on the notch geometry. The predictions are found to be in good agreement with experimental data reported by Frost [**1**].

Acknowledgments

The authors gratefully acknowledge the research support for this work provided by the Research Council of Norway (NFR) and the industrial participants within the NorLight project, and GE Energy (Norway) AS.

References

[1] **Frost, N. E.** A relation between the critical alternating propagation stress and crack length for mild steels. *Proceedings of the Institution of Mechanical Engineers*, 173:811–827, 1959.

[2] **Kitagawa, H.** and **Takahashi, S.** Applicability of fracture mechanics to very small cracks or the cracks in early stage. In *Proceedings of the Second International Conference on the Mechanical Behaviour of Materials*, pages 627–631, Boston, Ma., 1976.

[3] **El Haddad, M. H.**, **Topper, T. H.**, and **Smith, K. N.** Prediction of non-propagating cracks. *Engineering Fracture Mechanics*, 11(3):573–584, 1979.

[4] **Smith, R. A.** and **Miller, K. J.** Prediction of fatigue regimes in notched specimens. *International Journal of Mechanical Sciences*, 20(4):201–206, 1978.

[5] **Fjeldstad, A.**, **Wormsen, A.**, and **Härkegård, G.** Simulation of fatigue crack growth in components with random defects. *Engineering Fracture Mechanics*, doi:10.1016/j.engfracmech.2007.04.006, 2007.

[6] **Klesnil, M.** and **Lukáš, P.** Influence of strength and stress history on growth and stabilisation of fatigue cracks. *Engineering Fracture Mechanics*, 4(1):77–92, 1972.

[7] **Paris, P. C.** and **Erdogan, F.** A critical analysis of crack propagation laws. *Journal of Basic Engineering*, 85:528–534, 1963.

[8] **Härkegård, G.** An effective stress intensity factor and the determination of the notched fatigue limit. In J. Bäcklund, A. F. Blom, and C. J. Beevers, editors, *Fatigue thresholds: fundamentals and engineering applications, volume II*, pages 867–879. Engineering Materials Advisory Services Ltd, 1982.

[9] **Pearson, S.** Initiation of fatigue cracks in comercial aluminium alloys and the subsequent propagation of very short cracks. *Engineering Fracture Mechanics*, 7(2):235–247, 1975.

[10] **Dowling, N. E.** Crack growth during low cycle fatigue of smooth axial specimens. In *ASTM-STP 637*. American Society for Testing and Materials, ASTM, 1978.

[11] **Tada, H.**, **Paris, P. C.**, and **Irwin, G. R.** *The stress analysis of cracks handbook*. Professional Engineering Publishing Limited, Bury St. Edmunds and London, 3rd edition, 2000.

[12] **Newman, Jr. J. C.** and **Raju, I. S.** An empirical stress-intensity factor equation for the surface crack. *Engineering Fracture Mechanics*, 15(1-2):185–192, 1981.

[13] **Breat, J. L.**, **Murdy, F.**, and **Pineau, A.** Short crack propagation and closure effects in A508 steel. *Fatigue of Engineering Materials & Structures*, 6(4):349–358, 1983.

[14] **Mann, T.**, **Härkegård, G.**, and **Stärk, K.** Short fatigue crack growth in aluminium alloy 6082-T6. *International Journal of Fatigue*, doi: 10.1016/j.ijfatigue.2007.01.002, 2007.

[15] **Wormsen, A.**, **Fjeldstad, A.**, and **Härkegård, G.** The application of asymptotic solutions to a semi-elliptical crack at the root of a notch. *Engineering Fracture Mechanics*, 73(13):1899–1912, 2006.

[16] **Frost, N. E.** and **Dugdale, D. S.** Fatigue tests on notched mild steel plates with measurements of fatigue cracks. *Journal of the Mechanics and Physics of Solids*, 5(3):182–188, 1957.

Available online at www.sciencedirect.com
SCIENCE DIRECT®
Engineering Fracture Mechanics 73 (2006) 1899–1912
Engineering Fracture Mechanics
www.elsevier.com/locate/engfracmech

The application of asymptotic solutions to a semi-elliptical crack at the root of a notch

A. Wormsen *, A. Fjeldstad, G. Härkegård

Department of Engineering and Design and Materials, Norwegian University of Science and Technology, Richard Birkelandsevi 2B, NO-7491 Trondheim, Norway

Received 4 June 2005; received in revised form 27 January 2006; accepted 10 February 2006
Available online 18 May 2006

Abstract

This paper presents an approximate method based on asymptotic solutions for estimating the stress intensity factor K for semi-elliptic surface cracks at stress concentrations. The proposed equation for estimating K makes use of the near-notch and remote-notch solution to interpolate over the entire range from shallow to deep cracks. The near-notch solution is obtained by means of the stress concentration factor. For cracks located in the remote stress field, K is obtained by considering the crack to be located in a smooth plate with a crack depth equal to the sum of the notch depth and the actual crack depth. The accuracy of the predictions is assessed using numerical calculations and solutions found in the literature.

Keywords: Stress intensity factor; Geometry factor; Asymptotic solution; Shallow crack; Deep crack; Notch

1. Introduction

For a real component the stress is generally decreasing from a maximum at some critical point at the surface, e.g. in the case of notches or components subjected to bending or torsion. For simplicity and to ensure conservatism, crack growth analyses are often performed assuming a homogeneous stress field based on the maximum stress acting on the surface. This local stress approach yields acceptable results provided that the stress decreases slowly, i.e. the stress gradient is small. However, for steep stress gradients, a crack growth analysis based on the local stress will lead to over-conservative predictions. Since crack growth prediction requires the stress intensity factor K to be known, it is of great practical interest to establish simple formulae for estimating K for a semi-elliptical crack at the root of a notch.

While approximate K estimation procedures are well established for cracks emanating from a smooth surface, the situation is much less satisfactory, when it comes to cracks at the root of a notch. Thus, the present work focuses on through-cracks and semi-elliptical cracks at the root of a surface notch in a semi-infinite plate. Systematic computational efforts over the last 50 years have lead to stress intensity factor solutions for many

* Corresponding author. Tel.: +4773597098.
E-mail address: anders.wormsen@ntnu.no (A. Wormsen).

0013-7944/$ - see front matter
doi:10.1016/j.engfracmech.2006.02.006

Nomenclature

A	deepest point of crack front
a	crack depth
a',a^*	transition crack depth between shallow and deep crack asymptotes
BEA	boundary element analysis
C	intersection between crack front and free surface
c	half the surface crack length
D	equivalent surface crack depth
d	notch depth
E	Young's modulus
E_2	complete elliptic integral of the second kind
F	geometry factor
F_0	geometry factor for a crack emanating from a smooth surface
F_A	geometry factor at point A
F_C	geometry factor at point C
F_∞	reference geometry factor $= F_0\sqrt{1+d/a}$
FEA	finite element analysis
g	Green's function
J	J integral
K	stress intensity factor $= F\sigma_\infty\sqrt{\pi a}$
K_t	stress concentration factor $= \sigma_{max}/\sigma_\infty$
w	width of plane specimen
δ_i	coefficient of ith order term of $\sigma_y(x)$
ν	Poisson's ratio
ξ	dimensionless co-ordinate $= x/a$
ρ	notch root radius
σ_y	normal stress in y-direction
σ_{max}	maximum stress
σ_∞	remote stress
ϕ	angle defining location on semi-elliptical crack front
χ	relative stress gradient

different crack geometries [1], but these are often restricted to a few simple stress fields. For more complex stress fields, only few empirical solutions exist [2–4]. These are mainly given in terms of a set of empirical equations established by means of curve fitting to numerical results.

The objective of the present investigation is to present simplified solutions for the stress intensity factor K for semi-infinite notched plates. These formulae make use of asymptotic solutions to interpolate over the entire range from shallow to deep cracks. Although only semi-infinite notched plates have been considered, these formulae should be equally applicable to other notched components, since the component geometry does not markedly affect the stress intensity values for relatively shallow cracks, provided that the stress field in the vicinity of the crack is the same [4,5]. The present paper shows that asymptotic solutions provide a useful basis for the analysis of cracked notched solids.

2. Linear crack analysis, general equations

For an arbitrary body with a semi-elliptic surface crack of depth a under uniaxial remote tension σ_∞ perpendicular to the plane of the crack, K can be written as

$$K = F\sigma_\infty\sqrt{\pi a}, \tag{1}$$

where F is a dimensionless function of the geometry of the body and the crack. For a crack in the notch stress field, the stress intensity solution is asymptotically the same as for a surface crack in a smooth solid, except that the remote stress is being amplified by the stress concentration factor $K_t = \sigma_{max}/\sigma_\infty$ (see Fig. 1). Thus, as $a \to 0$,

$$K = F\sigma_\infty\sqrt{\pi a} = F_0 K_t \sigma_\infty \sqrt{\pi a}, \tag{2}$$

where F_0 is the geometry factor for the current surface crack emanating from a smooth surface. Well known solutions for a surface crack in a finite plate under tension or bending have been presented by Newman and Raju [6]. For a semi-infinite plate, the geometry factors for tension and bending coincide. For a semi-elliptic surface crack with aspect ratio a/c (cf. Fig. 3(b)), the geometry factor at the deepest point of the crack front A$(a;0)$ can be estimated as

$$F_0(\phi = \pi/2;\, a/c) = F_{A,0} = \frac{1.13 - 0.09\frac{a}{c}}{E_2(a/c)}. \tag{3}$$

Similarly, at the intersection between the crack front and the free surface, C$(0;c)$, the geometry factor can be estimated as

$$F_0(\phi = 0;\, a/c) = F_{C,0} = \frac{1.243 - 0.099\frac{a}{c}}{E_2(a/c)}\sqrt{\frac{a}{c}}. \tag{4}$$

In Eqs. (3) and (4), the aspect ratio, a/c, is limited to the range from 0 to 1, where the complete elliptic integral of the second kind, $E_2(a/c)$, can be approximated by

$$E_2(a/c) \approx \sqrt{1 + 1.464\left(\frac{a}{c}\right)^{1.65}}, \quad 0 \leqslant a/c \leqslant 1. \tag{5}$$

For an edge through-crack, Eq. (3) reduces to

$$F_0 = F_{A,0} = 1.13, \tag{6}$$

in good agreement with the more precise solution $F_0 = 1.122$ [1].

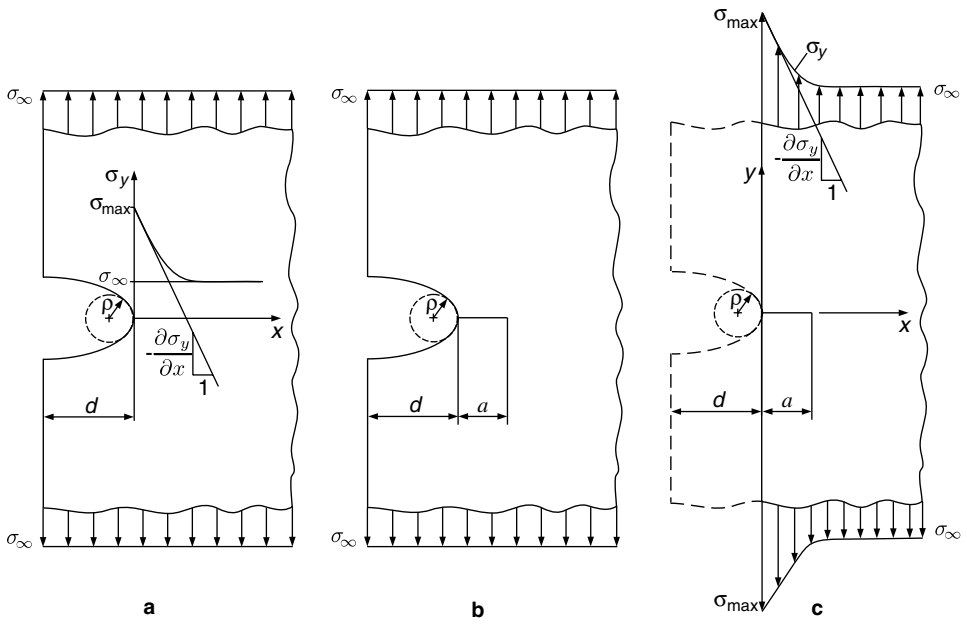

Fig. 1. Semi-infinite notched plate under uniform remote stress σ_∞: (a) stress concentration and stress gradient, (b) through-crack at the root of a surface notch, (c) un-notched cracked plate subjected to the notch stress field $\sigma_y(x)$.

For a crack located in the notch stress field, the asymptotic solution for the geometry factor F becomes

$$F = F_0 K_t. \tag{7}$$

When the crack grows beyond the notch stress field, the remote stress field dominates the stress intensity factor, which may now be estimated by

$$K = F_0 \sigma_\infty \sqrt{\pi(a+d)}, \tag{8}$$

where d denotes the notch depth. Identification with Eq. (1) yields

$$F = F_\infty = F_0 \sqrt{1 + \frac{d}{a}}, \tag{9}$$

where F_∞ denotes a reference geometry factor. When $a/d \gg 1$, F asymptotically approaches the constant value

$$F = F_0. \tag{10}$$

The two preceding asymptotic solutions, i.e. Eqs. (7) and (10), give the upper and lower bound values for the geometry factor F. By using these asymptotic solutions, simple formulae can be established for the geometry factor F of an arbitrarily sized semi-elliptic crack emanating from the root of a notch.

In the next section, geometry factors are presented for through-cracks at the root of a notch. Semi-elliptical cracks will be treated in Section 4.

3. Through-crack at the root of a notch

The configuration considered is a notched semi-infinite plate subjected to a remote stress σ_∞ perpendicular to the symmetry plane of the notch. The notch is characterised by its depth d, its root radius ρ and its elastic stress concentration factor $K_t = \sigma_{max}/\sigma_\infty$. Along with the stress concentration comes a stress field with its largest gradient at the notch root, as illustrated in Fig. 1(a). At the root of the notch, a through-crack of depth a is located as shown in Fig. 1(b). It should be noted that $F_0 = 1.122$ for a through-crack.

3.1. Geometry factors

Several methods are available for determining stress intensity factors [7,8]. In the following, only approximate methods using the 'nominal' stress field equal to the 'local' stress field of the crack-free specimen (in the plane of the subsequent crack) are considered.

3.1.1. Green's function

One of these methods is based on the solution of an edge through-crack of depth a, where the crack surfaces are subjected to a pair of symmetrical point forces, the so-called *Green function*. Once the stress in the plane of the subsequent crack and the appropriate Green function are known, determination of the geometry factor F is reduced to a simple integration procedure.

Consider now an edge through-crack of depth a located in a smooth semi-infinite plate subjected to the notch stress field $\sigma_y(x)$, see Fig. 1(c). The geometry factor F can then be estimated according to

$$F = \frac{1}{\pi} \int_0^1 \frac{\sigma_y(a\xi)}{\sigma_\infty} g(\xi) \mathrm{d}\xi, \tag{11}$$

where $g(\xi)$ is the Green function and $\xi = x/a$. According to Hartranft and Sih [9], the Green function for a crack of depth a subjected to a pair of symmetrical point forces in a semi-infinite plate is given by

$$g(\xi) = \frac{2(1+f(\xi))}{\sqrt{1-\xi^2}}, \tag{12}$$

$$f(\xi) = (1-\xi^2)(0.2945 - 0.3912\xi^2 + 0.7685\xi^4 - 0.9942\xi^6 + 0.5094\xi^8). \tag{13}$$

3.1.2. Stress gradient method

Another method for estimating the F value for a shallow crack at the root of a notch [10,11] is based on work by Benthem and Koiter [12]. For an edge-cracked semi-infinite plate subjected to a linear distribution of stress, one obtains

$$F = F_0(1 + 0.609\chi a). \tag{14}$$

If x denotes the distance below the surface, the relative stress gradient χ is defined as (cf. Fig. 1(c))

$$\chi = \frac{1}{\sigma_{\max}}\left(\frac{\partial\sigma_y(x)}{\partial x}\right)_{x=0}. \tag{15}$$

For a plate of width w subjected to pure bending, the relative stress gradient is given by

$$\chi = -\frac{2}{w}. \tag{16}$$

Eq. (14) may be compared with the geometry factor of a single-edge-cracked plate of width w subjected to bending [1]:

$$F = \frac{\sqrt{\frac{2w}{\pi a}\tan\frac{\pi a}{2w}}}{\cos\frac{\pi a}{2w}}\left[0.923 + 0.199\left(1 - \sin\frac{\pi a}{2w}\right)^3\right]. \tag{17}$$

It turns out that Eq. (14) is accurate for shallow cracks only, and that it should not be extrapolated beyond $a/w = 0.05$.

If a shallow crack at the root of a notch is subjected to the same stress gradient, χ, as the semi-infinite edge-cracked plate loaded by a linear distribution of stress, the geometry factors should be asymptotically equal. Thum et al. [13] found that the relative stress gradient at the root of a semi-elliptic surface notch of root radius ρ could be well approximated by

$$\chi = -\frac{2}{\rho}. \tag{18}$$

Eq. (14) then reduces to

$$F = F_0K_t\left(1 - 1.218\frac{a}{\rho}\right). \tag{19}$$

According to [14], the stress concentration factor for a semi-infinite notched plate subjected to tension can be estimated by

$$K_t = 1 + \left(\frac{0.1}{d/\rho} + \frac{0.13}{(d/\rho)^{1.25}}\right)^{-0.5}. \tag{20}$$

As can be seen from Eqs. (19) and (20), the asymptotic geometry factor, F, for an edge-crack at the root of a notch is only dependent on the ratios a/ρ and d/ρ.

3.1.3. Lukáš and Klesnil's method

For a shallow through-crack at the root of a notch, Lukáš and Klesnil [15] presented a simple formula for the geometry factor, viz.

$$F = \frac{F_0K_t}{\sqrt{1 + 4.5(a/\rho)}}. \tag{21}$$

Again, ρ denotes the notch root radius. As $a/\rho \to 0$, Eq. (21) simplifies to the shallow crack asymptote $F = F_0K_t$. Normalising Eq. (21) with respect to the geometry factor, F_∞, for an edge through-crack in a smooth plate with the total crack depth $a + d$, cf. Eq. (9), yields

$$\frac{F}{F_\infty} = \frac{K_t}{\sqrt{1 + d/a + 4.5(a/\rho) + 4.5(d/\rho)}}. \tag{22}$$

3.2. Geometry factors based on asymptotic solutions

3.2.1. 'Equivalent' surface crack depth

For a through-crack located at the root of a notch, the geometry factor F is bounded by a lower and an upper asymptote, so that $1 \leqslant F/F_0 \leqslant K_t$. Jergéus [16] and Härkegård [17] introduced an equation for F, which asymptotically agrees with the near and remote field estimates. Thus, they suggested that the geometry factor be written as

$$F = F_0\sqrt{\frac{D}{a}}, \tag{23}$$

where D is an 'equivalent' surface crack depth, which can be estimated by

$$D = a + d\left[1 - \exp\left(-\frac{a}{a'}\right)\right], \tag{24}$$

and

$$a' = \frac{d}{K_t^2 - 1}. \tag{25}$$

The transition crack depth a' is defined as the crack depth at which the asymptotic Eqs. (2) and (8) for the stress intensity factors of shallow and deep cracks, respectively, yield equal results.

For a shallow crack, i.e. $a \ll a'$, the equivalent surface crack depth becomes

$$D = K_t^2 a, \tag{26}$$

and, for a deep crack, i.e. $a \gg a'$,

$$D = a + d. \tag{27}$$

Hence, Eq. (23) is in complete agreement with the asymptotic Eqs. (7) and (9).

3.2.2. Normalised geometry factors

For shallow cracks, $a/d \ll 1$, the ratio F/F_∞ is dominated by the stress field from the notch root, and F approaches the shallow crack asymptote, see Eq. (7). For a through-cracked notched plate subjected to uniaxial tension σ_∞ (cf. Fig. 1), the ratio becomes

$$\frac{F}{F_\infty} = \frac{K_t}{\sqrt{1 + \frac{d}{a}}}, \tag{28}$$

which simplifies to

$$\frac{F}{F_\infty} = K_t\sqrt{\frac{a}{d}}, \tag{29}$$

when $a' \ll d$.

For deep cracks, the geometry factor of the cracked notch will approach that of a smooth plate with a crack depth equal to the sum of the notch depth and the actual crack depth.

A simple expression, which asymptotically agrees with the near and remote field estimates is given by

$$\frac{F}{F_\infty} = \sqrt{1 - \exp(-a/a^*)}, \tag{30}$$

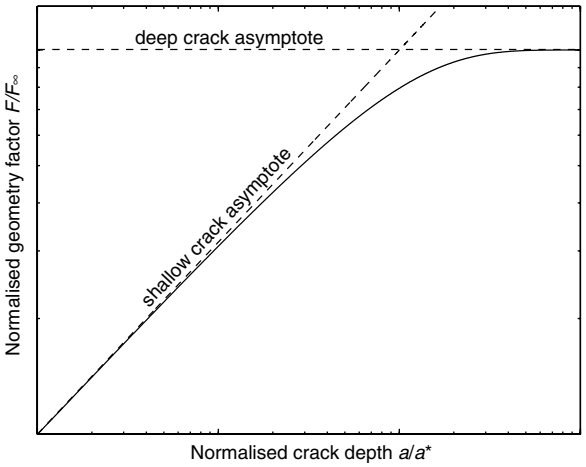

Fig. 2. Principle graph of F/F_∞ against the normalised crack depth a/a^*: logarithmic scales.

where a^* denotes the transition crack depth between the shallow and deep crack asymptotes, defined by the crack depth at which the two asymptotes coincide (cf. Fig. 2). Hence, a^* is determined by setting Eq. (29) equal to unity, which yields

$$a^* = \frac{d}{K_t^2}. \tag{31}$$

It can be shown that Eq. (30) satisfies the asymptotic expressions for shallow and deep cracks. Eq. (30) is depicted in Fig. 2 as a solid line.

4. Semi-elliptic crack at the root of a surface notch

Next, a semi-elliptic crack located at the root of a semi-circular edge notch in a semi-infinite plate subjected to uniaxial tension σ_∞ perpendicular to the symmetry plane of the notch is considered. The cracked configuration is shown in Fig. 3(a). The crack is characterised by its depth a and its surface length $2c$, as shown in Fig. 3(b).

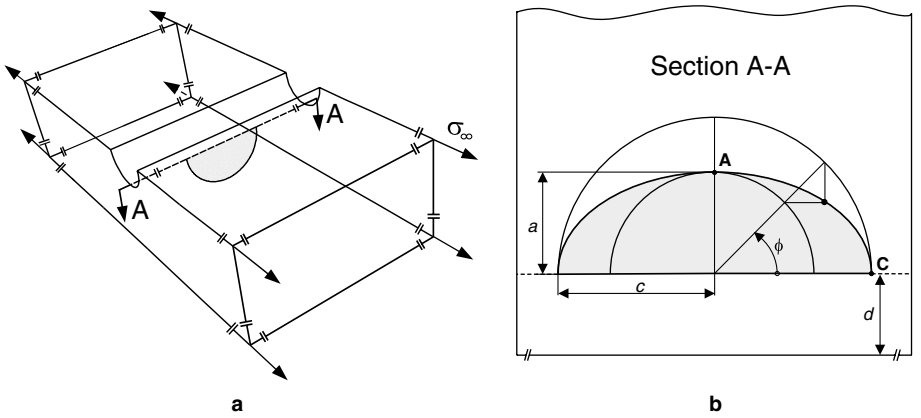

Fig. 3. Schematic drawings of a semi-elliptic crack emanating from the notch root: (a) three-dimensional view and (b) two-dimensional view of the cracked section A–A.

4.1. Geometry factors

4.1.1. Pommier, Sakae and Murakami

Using the body force method [18], Pommier et al. [3] have derived numerical solutions for the geometry factor F of a semi-elliptic surface crack located in a semi-infinite plate subjected to mode I loading. The crack aspect ratio is limited to the interval $0.5 \leqslant a/c \leqslant 2$. Their solution is given by a set of empirical equations, which allow the stress field of the crack-free plate to be fitted to a third-order polynomial.

For the semi-infinite plate, shown in Fig. 1, the normal stress in the y-direction varies with the x-coordinate only. The normal stress $\sigma_y(x)$ is approximated by the third-order polynomial [19]

$$\sigma_y(x) = \sum_{i=0}^{3} \delta_i \cdot (x/d)^i \cdot \sigma_\infty, \tag{32}$$

where δ_i is the coefficient of the ith order term of $\sigma_y(x)$. If Eq. (32) were an exact representation of $\sigma_y(x)$, then $\delta_0 = K_t$.

The empirical equations due to Pommier et al. [3] yield the geometry factor at the deepest point of the crack front A$(a;0)$ (cf. Fig. 3(b))

$$F_A = \sum_{i=0}^{3} \delta_i \cdot (a/d)^i \cdot F_i(\phi = \pi/2;\, a/c), \tag{33}$$

and at the intersection between the crack front and the free surface C$(0;c)$

$$F_C = \sum_{i=0}^{3} \delta_i \cdot (a/d)^i \cdot F_i(\phi = 0;\, a/c). \tag{34}$$

F_i is the geometry factor corresponding to the ith order unit stress field.

4.1.2. Lukáš method for semi-elliptical cracks

Based on work by Grandt and Kullgren [20], Lukáš [21] found that Eq. (21) for a through-crack at the root of a notch could be generalised to a semi-elliptic crack with an arbitrary aspect ratio a/c. It is only necessary to replace F_0 by the geometry factor $F_{A,0}$ for the deepest point of a semi-elliptic crack emanating from a smooth surface and having the same aspect ratio as the crack at the notch root. Thus Lukáš estimated the geometry factor of a semi-elliptic notch crack to be

$$F_A = \frac{F_{A,0} K_t}{\sqrt{1 + 4.5(a/\rho)}}. \tag{35}$$

4.2. Asymptotic solution

Based on work by Jergéus [16] and Härkegård [17], cf. Eq. (23), it is suggested that the geometry factor at the deepest point of the crack front A$(a;0)$ can be written in terms of the crack depth a and the equivalent crack depth D_A as

$$F(\phi = \pi/2;\, a/c) = F_A = F_{A,0}\sqrt{\frac{D_A}{a}}, \tag{36}$$

where $F_{A,0}$ is given by Eq. (3), and $D_A = D$ according to Eq. (24). As for the through-cracked specimens, Eq. (36) asymptotically satisfies the shallow and deep crack estimates $F_{A,0}K_t$ and $F_{A,0}$.

Similar to the deepest point A$(a;0)$, the geometry factor at the surface point C$(0;c)$ is characterised by a shallow and a deep crack asymptote. For shallow cracks, i.e. $a/d \ll 1$, the asymptote is given by

$$F_C = F_{C,0} K_t, \tag{37}$$

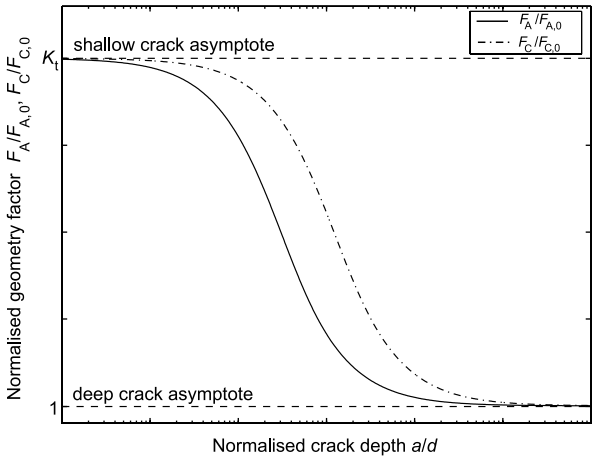

Fig. 4. Principal graph of $F_A/F_{A,0}$ and $F_C/F_{C,0}$ versus the normalised crack depth a/d.

where $F_{C,0}$ is the corresponding geometry factor of a crack in a smooth plate, which can be found by means of Eq. (4). While the surface point C$(0;c)$, regardless of the crack depth, is influenced by the elevated stress at the notch root, it may not be obvious that F_C asymptotically approaches a 'deep crack' solution. However, as the crack grows deeper, a decreasing part of the crack front will be influenced by the notch stress field. The influence decreases until the notch depth becomes insignificant compared with the dimensions of the crack. This can then be regarded as a semi-elliptical surface crack of depth $a+d$ located in a smooth plate. Hence, as the crack grows deeper, the ratio $F_C/F_{C,0}$ asymptotically approaches unity. Based on numerical results, it will be shown in Section 5 that the geometry factor F_C converges more slowly towards its 'deep crack' solution than F_A. Thus, a suitable expression for the equivalent notch depth turns out to be

$$D_C = a + 4d\left[1 - \exp\left(-\frac{a}{4a'}\right)\right]. \tag{38}$$

With this equivalent notch depth, the geometry factor at the surface point can be estimated as

$$F(\phi = 0; a/c) = F_C = F_{C,0}\sqrt{\frac{D_C}{a}}. \tag{39}$$

Fig. 4 shows a principle graph of the normalised geometry factors $F_A/F_{A,0}$ and $F_C/F_{C,0}$ versus the normalised crack depth a/d. As can be seen, both F_A and F_C satisfy the asymptotic solutions for shallow and deep cracks.

5. Numerical analysis

5.1. Through-cracked specimens

5.1.1. Finite element modelling and evaluation procedures

Linear elastic analyses of the finite element models were performed using the finite element program ABAQUS [22]. Fig. 5(a) illustrates a typical finite element mesh employed in the present work. The local mesh in the crack tip region was identical for all models, with 16 elements around the crack tip. Eight-noded isoparametric second-order plane strain elements with reduced integration (2×2 Gauss points; element type CPE8R in ABAQUS [22]) were applied. The finite element models contained 1100–1600 elements. The applied mesh assured sufficient accuracy in all cases investigated. In these analyses, Poisson's ratio was chosen to be $\nu = 0.3$, and small displacement theory was assumed throughout.

5.1.2. Geometry factors

The through-crack configuration considered is shown in Fig. 1. The notch is assumed to be semi-circular, i.e. $d/\rho = 1$. According to Eq. (20), and verified by FEA, the stress concentration factor $K_t = 3.1$ for the

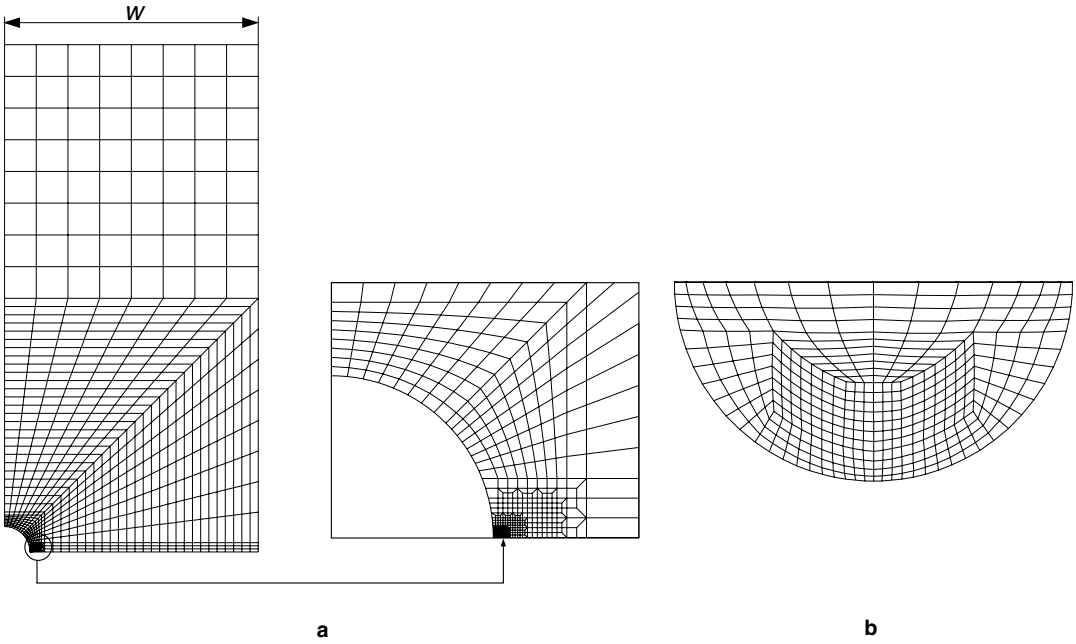

Fig. 5. (a) Finite element mesh for a through-cracked notched specimen ($d/\rho = 1$ and $\rho/w = 0.1$) with a magnified view of the notch root region. The mesh contains 4804 nodes, forming 1527 elements. (b) Boundary element mesh of a semi-circular crack ($a/c = 1$). The mesh contains 403 nodes forming 374 elements.

notched configuration. Subsequently, the different solutions for the geometry factor presented in Section 3 are compared.

Geometry factors, F, have been plotted against the normalised crack depth, a/d, in Fig. 6. Fig. 6 shows the FEA graph of F against a/d together with curves based on asymptotic solutions and Green function. For very shallow cracks, say $a/d < 0.001$, the geometry factor assumes the constant value F_0K_t. As a/d increases, F decreases in a regular fashion. As the crack grows beyond the notch root stress field, the remote stress field

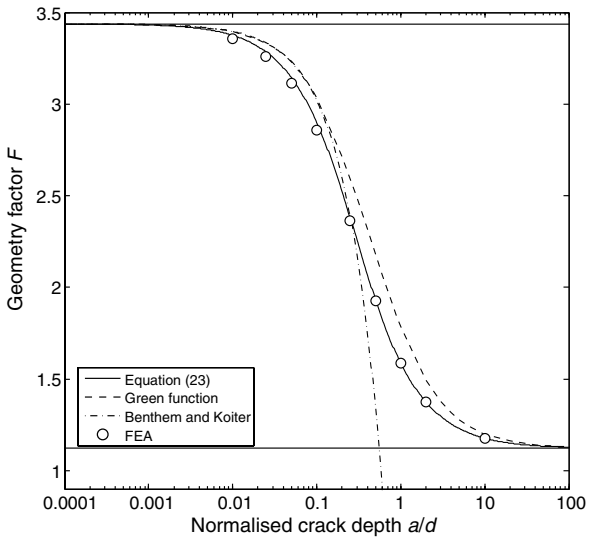

Fig. 6. Geometry factors due to FEA for an edge through-cracked notched plate ($d/\rho = 1$, Fig. 1(b)) with $K_t = 3.1$, together with results obtained from the solutions based on Jergéus and Härkegård, Green's function and Benthem and Koiter.

becomes dominating, and F asymptotically approaches the constant value F_0. The expression for the solid line is given by Eq. (23). As can be seen, the solution is in excellent agreement with the finite element results. The result obtained with Green function is drawn as a dashed curve, the asymptote of which agrees with those predicted by Eq. (23). For intermediate crack depths, the Green function yields values of the geometry factor exceeding those obtained with Eq. (23) by less than 13%.

In Fig. 6, Eq. (19) based on work by Benthem and Koiter [12] is shown as a dash-dotted line. For $a/d < 0.1$, F values generated by the Benthem and Koiter formula are slightly to conservative. For somewhat deeper edge cracks, the Benthem and Koiter values of F fall below the FEA results, since only the tangent of the stress field at the notch root is used. The difference between the FEA results and Eq. (19) is due to the uncertainties related to the determination of the relative stress gradient χ. The χ value from FEA is found to be slightly greater than Eq. (18). Hence, geometry factors from Eq. (19) exceeds those obtained from FEA.

5.1.3. Normalised geometry factors

In Fig. 7 the finite element F values have been normalised with respect to F_∞ for an edge through-crack in a semi-infinite smooth plate with the total crack depth $D = a + d$. The abscissa is the normalised crack depth a/a^*. The solid line is given by Eq. (30). The finite element results have been obtained from three notched plates ($d = 0.1w$) under remote tension with $d/\rho = 0.27$, 0.93 and 1.96. According to Eq. (20), and verified by FEA, the stress concentration factors for these specimens are $K_t = 2$, 3 and 4, respectively. As can be seen from Fig. 7, Eq. (30) is in excellent agreement with the finite element results. For comparison, the results obtained from Eq. (22) according to Lukáš and Klesnil [15] have been depicted as dashed lines in the same figure. For $a/a^* < 1$ the two solutions nearly coincide. For deeper cracks, Eq. (22) gives non-conservative values for the geometry factor. This occurs since Eq. (22) does not fulfil the deep crack asymptotic behaviour.

5.2. Semi-elliptically cracked specimens

5.2.1. Boundary element modelling and evaluation procedures

Fig. 5(b) shows the boundary element mesh of a semi-elliptical crack employed in the present work. The local mesh of the semi-elliptical cracks was similar for all a/c ratios analysed and consisted of 42 elements around the crack front. Four-noded first-order elements were applied.

Elastic analyses of the boundary element models were performed using the boundary element program FRANC3D [23–26]. In this program, the stress intensity factor is evaluated at discrete points at the crack front according to a displacement based method given by Chan et al. [27]. Furthermore, plane strain conditions are assumed all along the crack front.

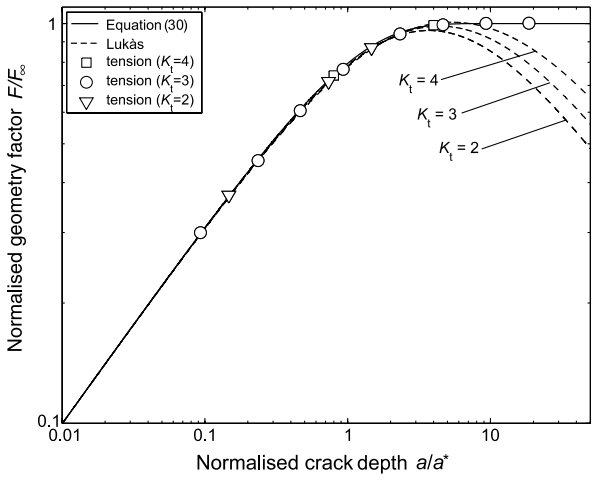

Fig. 7. Geometry factors as functions of the normalised crack depth a/a^* for through-cracked notched plates subjected to remote uniaxial tension (Fig. 1(b)).

5.2.2. Geometry factors

The cracked configuration considered is shown in Fig. 3 and has been analysed under remote uniaxial stress σ_∞. The notch is assumed to be semi-circular, i.e. $d/\rho = 1$. The stress concentration factor $K_t = 3.2$ at the center of the notch. It should be noted that the stress in the three-dimensional case varies from the surface to the center.

In Figs. 8 and 9, the geometry factors F_A and F_C have been plotted against the normalised crack depth a/d. The geometry factors have been obtained by means of the asymptotic solutions for semi-elliptic cracks (Eqs. (36) and (39)), the solution by Pommier et al. [3] and by Lukáš method (Eq. (35)). Along with these solutions, finite element results presented by Lin and Smith [28] and boundary element results are shown.

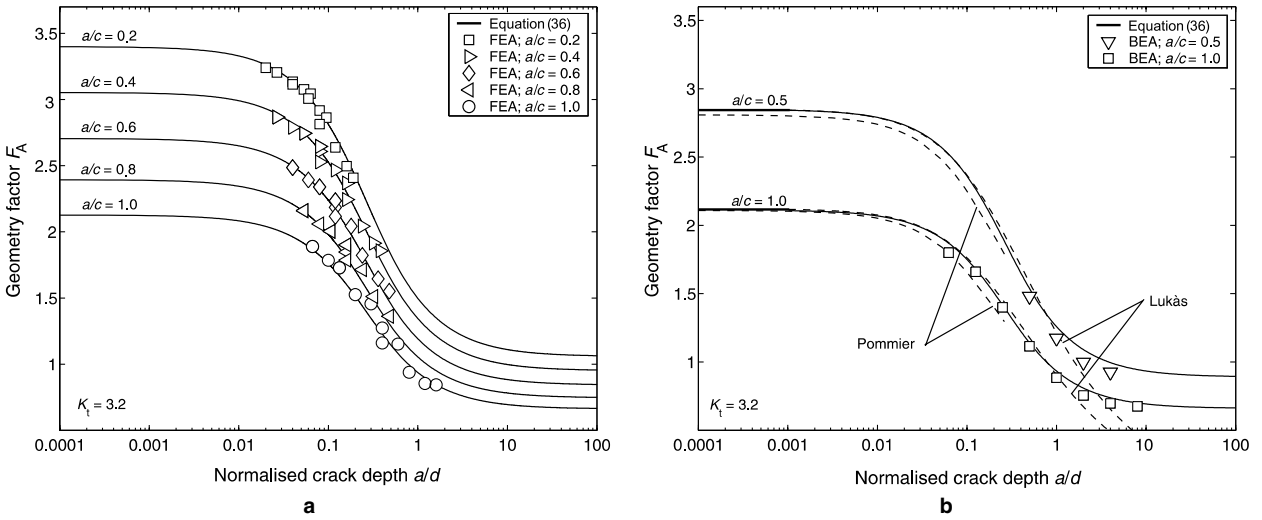

Fig. 8. Geometry factors F_A for the deepest point A$(a;0)$ due to (a) FEA results [28] and (b) BEA results for a semi-elliptically cracked notched plate ($K_t = 3.2$, $d/\rho = 1$) (Fig. 3(a)).

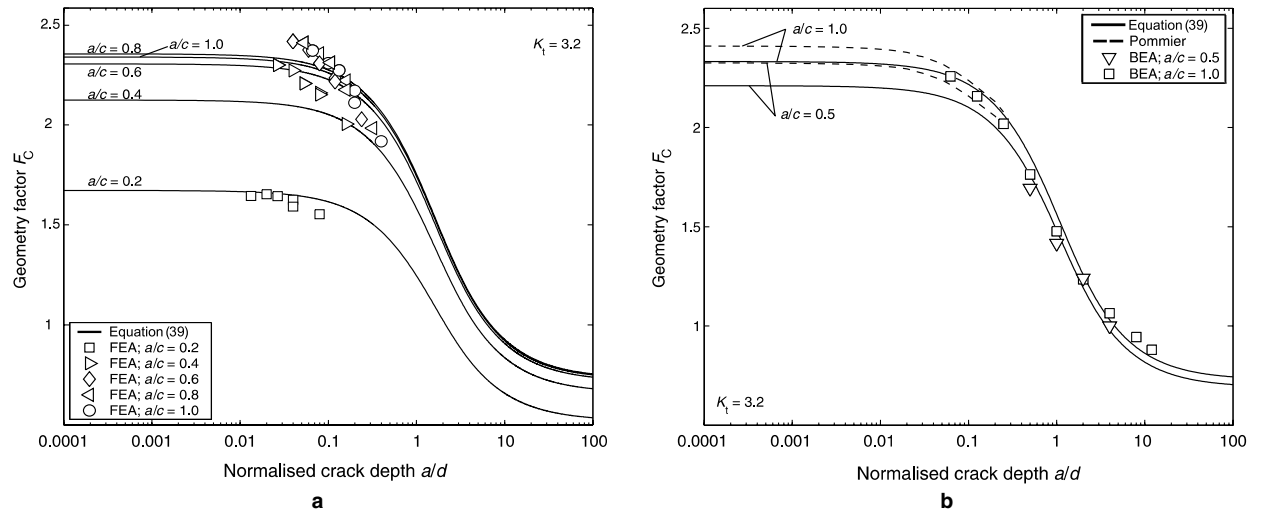

Fig. 9. Geometry factors F_C for the surface point C$(0;c)$ due to (a) FEA [28] and (b) BEA results for a semi-elliptically cracked notched plate ($K_t = 3.2$, $d/\rho = 1$) (Fig. 3(a)).

5.2.3. Geometry factors for the deepest point at the crack front

Fig. 8(a) shows the geometry factor F_A for the deepest point, A$(a;0)$, for the aspect ratios $a/c = 0.2$, 0.4, 0.6, 0.8 and 1.0. The expression for the solid lines is given by Eq. (36). As can be seen, the solution is in good overall agreement with the finite element results presented by Lin and Smith [28].

Fig. 8(b) shows the geometry factors, F_A, generated by means of the asymptotic solutions, Eq. (36), Pommier et al. and Lukáš method for crack aspect ratios $a/c = 0.5$ and 1.0 together with boundary element results. As can be seen, Eq. (36) is in good overall agreement with the boundary element results. For $a/d > 1$, the boundary element results fall slightly below the F_A values from Eq. (36).

For $a/d \leqslant 1$, F_A values generated by Lukáš solution, i.e. Eq. (35), follow the asymptotic solution. For somewhat deeper cracks, Lukáš solution falls below the deep crack asymptote.

The solution due to Pommier et al. is shown in Fig. 8(b) as a dashed curve and is discontinued at $a/d = 0.25$, since this is the maximum range, where the uncracked stress field can be fitted to a third-order polynomial. For $a/c = 0.5$, the F_A values generated from the Pommier solution fall below those of Eq. (36) even for very shallow cracks. This occurs since the $F_{A,0}$ value due to Pommier for $a/c = 0.5$ falls below $F_{A,0}$ due to Newman–Raju. For deeper cracks, values based on Pommier's solution fall slightly below BEA data.

5.2.4. Geometry factors for the crack front surface point

In the previous subsection, results of F_A were presented. This subsection presents geometry factors, F_C, for the crack front surface point C$(0;c)$.

Finite element results in Fig. 9(a) are from Ref. [28]. The solid lines are given by Eq. (39). For shallow cracks, say $a/d < 0.1$, the FEA results exceed the shallow crack asymptote, except for $a/c = 0.2$. FEA results tend to fall below those of Eq. (39), but within acceptable limits.

In Fig. 9(b), geometry factors, F_C, from Eq. (39) and the Pommier et al. solutions are shown for crack aspect ratios $a/c = 0.5$ and 1.0 along with boundary element results. As can be seen, Eq. (39) is in good overall agreement with the boundary element results. For crack depths $a/d < 0.01$ and $a/c = 0.5$ and 1.0, the F_C values generated by the Pommier solution exceed the asymptotic values. This occurs since the Newman–Raju $F_{C,0}$ value is below the corresponding Pommier value.

In the present paper, the proposed asymptotic method has been used in conjunction with Newman and Raju's [6] solution for a surface crack in a finite plate under tension. As can be seen in Fig. 9(b), the Newman–Raju $F_C = K_t F_{C,0}$ value is below the corresponding Pommier value. If the Pommier $F_{C,0}$ value is used, a better agreement is achieved between the present approach and the FE-based results of [28]. In addition, Lin and Smith [28] notes that their F_C values might not be sufficiently accurate for shallow and deep cracks due to the finite element mesh used.

6. Conclusions

Notched specimens with through-cracks or semi-elliptic cracks emanating from the root of the notch have been analysed by means of the finite element and boundary element methods. Simplified solutions for the stress intensity factor K have been presented. These solutions use the stress field ahead of the crack-free notch as the boundary load of an un-notched cracked specimen.

For the through-crack specimens, the solution by Jergéus [16] and Härkegård [17], Eq. (23), is found to be in excellent agreement with the finite element results. The geometry factors generated by means of Green function exceed the FEA values by less than 13%. For $a/d < 0.2$, geometry factors from Eq. (19) slightly exceeds those obtained from FEA.

A simple equation has been proposed for the geometry factor of a through-crack specimen based on a reference solution F_∞. The equation satisfies the shallow and deep crack asymptotes. This solution has been compared with a solution presented by Lukáš and Klesnil [15]. It is found that the two solutions are in good agreement for shallow cracks.

For a semi-elliptic crack at the root of a notch, it has been shown that the geometry factors F_A and F_C are both bounded by a shallow and a deep crack asymptote. The solution by Jergéus and Härkegård for edge through-cracks has been extended to semi-elliptically cracked specimens. Their solution is found to be in good agreement with finite element and boundary element results for both F_A and F_C. For the deepest point A$(a;0)$

of a shallow crack ($a/d \ll 1$) it has been found that the proposed solution is in good agreement with solutions by Pommier et al. [3] and Lukáš [21]. The solution by Pommier et al. for F_C was also found to be in good agreement with the proposed solution for shallow cracks.

Acknowledgments

The authors gratefully acknowledge the research support for this work provided by GE Energy (Norway) AS, the Research Council of Norway – Norges forskningsråd (NFR) and the industrial participants within the NorLight project. The authors also express their gratitude to Dr. Hans-Jörg Huth for the permission to use a computer code for fatigue crack growth based on the work of Pommier et al.

References

[1] Tada H, Paris PC, Irwin GR. The stress analysis of cracks handbook. 3rd ed. Bury St. Edmunds and London: Professional Engineering Publishing Limited; 2000.
[2] Nilsson L. Stress intensity factors for semi-elliptical surface cracks in plates subjected to a complex stress field. SAQ/FoU-Report 98/10, SAQ KONTROLL AB, Stockholm, Sweden, 1998.
[3] Pommier S, Sakae C, Murakami Y. An empirical stress intensity factor set of equations for a semi-elliptical crack in a semi-infinite body subjected to a polynomial stress distribution. Int J Fatigue 1999;21(3):243–51.
[4] Carpinteri A, Brighenti R, Huth HJ, Vantadori S. Fatigue growth of a surface crack in a welded T-joint. Int J Fatigue 2005;27(1):59–69.
[5] Huth HJ. Fatigue design of hydraulic turbine runners. Ph.D. Thesis, Norwegian University of Science and Technology, Trondheim, Norway, 2005.
[6] Newman Jr JC, Raju IS. An empirical stress-intensity factor equation for the surface crack. Engng Fract Mech 1981;15(1–2):185–92.
[7] Rooke DP, Baratta FI, Cartwright DJ. Simple methods of determining stress intensity factors. Engng Fract Mech 1981;14(2): 397–426.
[8] Bloom JM, Van Der Sluys WA. Determination of stress intensity factors for gradient stress field. J Press Ves Technol-Trans ASME 1977;99(3):477–84.
[9] Hartranft RJ, Sih GC. Alternating method applied to edge and surface crack problems. Methods of analysis and solutions of crack problems. Mechanics of fracture. Leyden: Noordhoff; 1973 [chapter 4].
[10] Karlsson A, Bäcklund J. Summary of SIF graphs for cracks emanating from circular holes. Int J Fract 1978;14:585–96.
[11] Schijve J. The stress intensity factor of small cracks at notches. Fatigue Engng Mater Struct 1982;5(1):77–90.
[12] Benthem JP, Koiter WT. Asymptotic approximations to crack problems. Mechanics of fracture, vol. 1. Noordhoff; 1973. p. 137–78.
[13] Thum A, Petersen C, Svenson O. Verformung, Spannung und Kerbwirkung. Eine Einführung. Düsseldorf: VDI-Verlag; 1960.
[14] Beitz W, Grothe K-H, editors. Dubbel – Taschenbuch für den Maschinenbau. 20th ed. Berlin: Springer-Verlag; 2001. p. E103 [chapter E].
[15] Lukáš P, Klesnil M. Fatigue limit of notched bodies. Mater Sci Engng 1978;34(1):61–6.
[16] Jergéus HÅ. A simple formula for the stress intensity factors of cracks in side notches. Int J Fract 1978;14:R113–6.
[17] Härkegård G. An effective stress intensity factor and the determination of the notched fatigue limit. In: Bäcklund J, Blom AF, Beevers CJ, editors. Fatigue thresholds: fundamentals and engineering applications, vol. 2. Engineering Materials Advisory Services Ltd.; 1982. p. 867–79.
[18] Murakami Y. Analysis of stress intensity factors of mode I, II and III for inclined surface cracks of arbitrary shape. Engng Fract Mech 1985;22(1):101–4.
[19] Härkegård G, Huth HJ, Faanes S. FEA-based fatigue assessment methodology for hydraulic turbine runners. In: Strang A, Banks WM, Conroy RD, McColvin GM, Neal JC, Simpson S, editors. Proceedings of the 5th international Charles Parsons turbine conference. London, July 2000, p. 1005–118. IOM Communications Ltd.
[20] Grandt Jr AF, Kullgren TE. Tabulated stress intensity factor solutions for flawed fastener holes. Engng Fract Mech 1983;18(2):435–51.
[21] Lukáš P. Stress intensity factor for small notch-emanated cracks. Engng Fract Mech 1987;26(3):471–3.
[22] Abaqus/standard, User's manual, version 6.4, Hibbit, Karlsson and Sorensen, Pawtucket, Rhode Island, 2003.
[23] Carter BJ, Chen C-S, Ingraffea AR, Wawrzynek PA. A topology based system for simulating 3D crack growth in solid and shell structures. In: Karihaloo BL, Mai YW, Ripley MI, Ritchie RO, editors. Advances in fracture research, ICF5, vol. 4, 1997, p. 1923–34.
[24] Carter BJ, Wawrzynek PA, Ingraffea AR. Automated 3-D crack growth simulation. Int J Numer Meth Engng 2000;47(1):229–53.
[25] Cornell Fracture Group. FRANC3D 2.6. Concepts and user guide. Cornell University, Ithaca, New York, 2003.
[26] Cornell Fracture Group. FRANC3D 2.6. Menu and dialog reference. Cornell University, Ithaca, New York, 2003.
[27] Chan SK, Tuba IS, Wilson WK. On the finite element method in linear fracture mechanics. Engng Fract Mech 1970;2(1):1–17.
[28] Lin XB, Smith RA. Stress intensity factors for semi-elliptical surface cracks in semicircularly notched tension plates. J Strain Anal Engng Des 1997;32(3):229–36.

Available online at www.sciencedirect.com
ScienceDirect
Engineering Fracture Mechanics xxx (2007) xxx–xxx
Engineering Fracture Mechanics
www.elsevier.com/locate/engfracmech

Approximate stress intensity factors for cracked V-notched specimens based on asymptotic solutions with application to T-joints

A. Fjeldstad *, A. Wormsen, G. Härkegård

Department of Engineering Design and Materials, Norwegian University of Science and Technology, Richard Birkelandsvei 2B, Trondheim NO-7491 , Norway

Received 7 September 2006; received in revised form 24 April 2007; accepted 26 April 2007

Abstract

This paper presents an approximate method based on asymptotic solutions for estimating the stress intensity factor K for semi-elliptic surface cracks at stress concentrations. The proposed equations make use of a reference solution to interpolate over the entire range from shallow to deep cracks. The reference solution is obtained by considering the current crack emanating from the associated specimen with a sharp notch. It is shown that the proposed formulae satisfy the shallow and deep crack asymptotes. The asymptotic solutions are applied to a T-joint with a fillet-weld-shaped transition. The accuracy of the predictions is assessed using numerical calculations.

Keywords: Stress intensity factor; Geometry factor; Asymptotic solution; Shallow crack; Deep crack; V-notch; T-joint

1. Introduction

A potential failure mode of welded components is fatigue crack propagation of shallow surface cracks from the weld toe. These cracks, which are roughly semi-elliptic, often grow in stress fields that decrease rapidly, i.e., the stress gradient is high. Hence, a crack growth analysis assuming a homogeneous stress field equal to the maximum stress acting at the surface may lead to overconservative predictions of the lifetime of the component [1]. Since crack growth predictions require the stress intensity factor K to be known, it is of great practical interest to establish simple formulae for estimating K for a semi-elliptical crack at the root of the weld toe.

* Corresponding author.
E-mail address: arne.fjeldstad@ntnu.no (A. Fjeldstad).

0013-7944/$ - see front matter
doi:10.1016/j.engfracmech.2007.04.028

Nomenclature

A	deepest point of crack front
a	crack depth
a^*	transition crack depth between shallow and deep crack asymptotes
C	intersection between crack front and free surface
c	half the surface crack length
d	notch depth
E	Young's modulus
E_2	complete elliptic integral of the second kind
$F(a/c)$	geometry factor for a surface crack
$F_0(a/c)$	geometry factor for a surface crack emanating from a smooth surface
$F_\infty(a/c)$	reference geometry factor for a sharply notched specimen
$F_P(a/c)$	geometry factor for a surface crack in a finite plate
FEA	finite element analysis
g	weight function
K	stress intensity factor $= F\sigma_\infty\sqrt{\pi a}$
K_t	stress concentration factor $= \sigma_{max}/\sigma_\infty$
k_0	parameter of the singular stress field
w_b	semi-width of brace
w_c	width of chord
$\Gamma(v)$	gamma function $= \int_0^\infty \exp(-t)t^{v-1}\,dt$
$\lambda - 1$	exponent of singular stress field
v	Poisson's ratio
ξ	dimensionless co-ordinate $= x/a$
ρ	notch root radius
σ_y	normal stress in y-direction
σ_{max}	maximum stress at crack initiation point
σ_∞	remote stress
ϕ	angle defining location at semi-elliptical crack front
ω	notch opening angle

While K estimation procedures are well established for cracks emanating from a smooth surface, the situation is much less satisfactory, when it comes to cracks at the root of a notch. Wormsen et al. [2] presented an approximate method based on asymptotic solutions for estimating the stress intensity factor K for a semi-elliptical crack at the root of a semi-circular notch. Based on numerical calculations and solutions found in the literature, the accuracy of the approximate method was found to be very good. In the present paper, the asymptotic method presented in [2] is extended to cover cracked V-notched specimens.

During the last few years, empirical stress intensity factors for more complex stress fields have been established. Bowness and Lee [3] presented equations for estimating K for semi-elliptical surface cracks in T-butt joints. The proposed solutions include parameters like crack depth and aspect ratio, attachment footprint and weld angle. Using the body force method [4], Pommier et al. [5] derived a set of emprical equations for estimating the stress intensity factor for a semi-elliptical surface crack located in a semi-infinite plate subjected to mode I loading. Their solution uses the stress field ahead of the crack-free notch as the boundary load on the crack surfaces. The 'notch stress intensity factor' was first introduced by Verreman and Nie [6,7] and further developed by Lazzarin et al. [8–12]. It represents the magnitude of the singular stress field ahead of a V-notch.

The objective of the current investigation is to present simplified solutions for the stress intensity factor K for cracked V-notched specimens. These formulae make use of a reference solution to interpolate over the entire range from shallow to deep cracks. This investigation is restricted to K at the deepest point of the semi-elliptical crack front.

Please cite this article in press as: Fjeldstad A et al., Approximate stress intensity factors for cracked ..., Eng Fract Mech (2007), doi:10.1016/j.engfracmech.2007.04.028

2. V-notches without cracks

The configuration considered is a V-notched plate as shown in Fig. 1. The V-notch is characterised by its depth d, its root radius ρ, its opening angle ω and its elastic stress concentration factor $K_t = \sigma_{max}/\sigma_\infty$. The V-notched plate is loaded by a remote stress σ_∞ perpendicular to the symmetry plane of the notch.

Based on the theory of linear elasticity, Williams [13] was able to show that the asymptotic normal stress in the y-direction, see Fig. 1a, is given by

$$\lim_{x\to 0}\sigma_y(x) = \frac{K}{\sqrt{2\pi x}}, \tag{1}$$

as $\rho/d \to 0$ and $\omega \to 0$.

Williams [13] further demonstrated that singularites less severe than $1/\sqrt{x}$ arise when the notch opens, i.e., $\omega > 0$. In this case, the near-stress-field depends on the notch opening angle ω and may be expressed as [14]

$$\lim_{x\to 0}\sigma_y(x) = \frac{\tilde{K}}{\sqrt{2\pi x^{1-\lambda}}}, \tag{2}$$

where $\tilde{K}$ denotes a generalised stress intensity factor. In the limit when $\omega \to 0$, Eq. (2) reduces to Eq. (1) and $\tilde{K}$ coincides with the standard stress intensity factor K. The eigenvalue λ_i, which determines the order of the stress singularity, is given by

$$\lambda_i \sin 2\alpha + \sin 2\lambda_i\alpha = 0, \quad i = 1, 2, \ldots, \tag{3}$$

where $\alpha = \pi$-$\omega/2$. As ω goes from 0 (cracked body) to π (smooth body), λ varies from 1/2 to 1.

Based on dimensional considerations, it should be possible to rewrite Eq. (2) as [7,15,16]

$$\lim_{x\to 0}\frac{\sigma_y(x)}{\sigma_\infty} = k_0\left(\frac{x}{d}\right)^{\lambda-1}, \tag{4}$$

where k_0 is a dimensionless parameter, which in the case of a semi-infinite cracked V-notched specimen depends only on the opening angle ω.

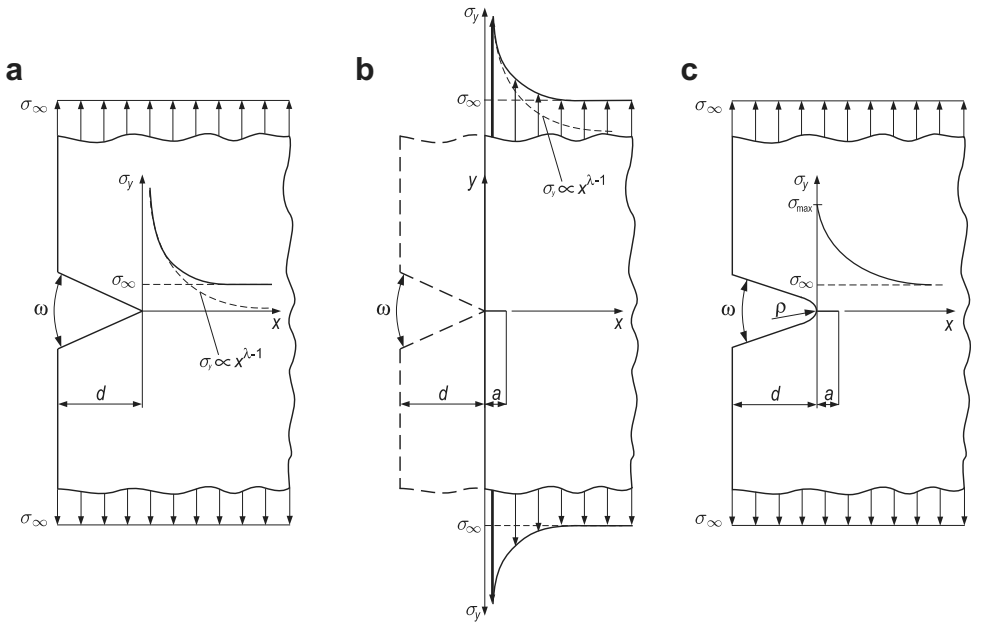

Fig. 1. Semi-infinite V-notched plate under remote uniform stress σ_∞; (a) sharp notch and stress field, (b) unnotched cracked plate subjected to the singular notch stress field $\sigma_y(x)$, (c) through-crack at the root of a blunt notch.

Please cite this article in press as: Fjeldstad A et al., Approximate stress intensity factors for cracked ..., Eng Fract Mech (2007), doi:10.1016/j.engfracmech.2007.04.028

In the following section, stress intensity factors are presented for arbitrarily shaped surface cracks at the root of a notch.

3. V-notches with cracks

As stated in the introduction, cracks frequently initiate at the root of a notch and propagate perpendicularly to the free surface under the influence of a fatigue loading. In order to carry out calculations of fatigue crack growth, it is necessary to know the stress intensity factors for such cracks.

For an arbitrary body with a surface crack of depth a under remote uniaxial tension σ_∞ perpendicular to the plane of the crack, K can be written as

$$K = F(\phi; a/c)\sigma_\infty\sqrt{\pi a}, \tag{5}$$

where $F(\phi;a/c)$ is a dimensionless function of the geometry of the body and the crack. ϕ is an angle defining the location at a semi-elliptical crack front, see Fig. 2. For a surface crack emanating from a smooth surface, i.e., $\omega = \pi$ and $d = 0$, $F(\phi;a/c) = F_0(\phi;a/c)$.

Solutions for a semi-elliptical surface crack in a finite plate under tension and bending have been presented by Newman and Raju [17]. For a semi-elliptic surface crack with aspect ratio a/c, cf. Fig. 2, the geometry factor of the deepest point of the crack front A$(a;0)$ can be estimated as

$$F_0(\phi = \pi/2; a/c) = F_{A,0} = \frac{1.13 - 0.09\frac{a}{c}}{E_2(a/c)}, \tag{6}$$

where the complete elliptic integral of the second kind, $E_2(a/c)$, can be approximated by

$$E_2(a/c) \approx \sqrt{1 + 1.464\left(\frac{a}{c}\right)^{1.65}}, \quad 0 \leqslant a/c \leqslant 1. \tag{7}$$

For an edge through-crack, i.e., $a/c = 0$, Eq. (6) reduces to $F_0 = F_{A,0} = 1.13$, in good agreement with the more precise solution $F_0 = 1.122$ [18]. It should be noted that $F_0 = 1.122$ is used in this paper.

In the following sections, ϕ is set to $\phi = \pi/2$, i.e., the deepest point of the crack front. The geometry factor for an arbitrary surface crack is in the following denoted by $F(a/c)$, while the geometry factors for an edge through-crack and a semi-elliptical crack are denoted by F and F_A, respectively.

3.1. Stress intensity factors for cracks in regular stress fields

For a shallow crack in the notch stress field, the stress intensity solution is asymptotically the same as for a surface crack in a smooth solid, except that the remote stress is being amplified by the stress concentration factor $K_t = \sigma_{max}/\sigma_\infty$, see Fig. 1c. Thus, as $a \to 0$,

$$K = F(a/c)\sigma_\infty\sqrt{\pi a} = F_0(a/c)K_t\sigma_\infty\sqrt{\pi a}. \tag{8}$$

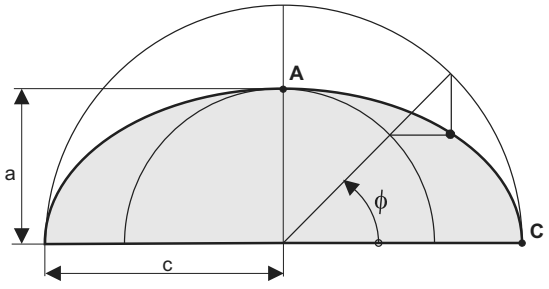

Fig. 2. Two-dimensional view of a semi-elliptical crack.

Please cite this article in press as: Fjeldstad A et al., Approximate stress intensity factors for cracked ..., Eng Fract Mech (2007), doi:10.1016/j.engfracmech.2007.04.028

Neuber [19] found that the stress concentration factor K_t for a semi-infinite V-notched plate under uniform tension is nearly independent of the opening angle ω in the range $0 \leqslant \omega < \pi/2$. This is in agreement of the observation by Nowell et al. [20] that a V-notch with $\omega < \pi/2$ may be regarded as a U-shaped notch with the same depth d and root radius ρ.

When the crack grows beyond the notch stress field, the remote stress field dominates the stress intensity factor, which may be estimated by

$$K = F_0(a/c)\sigma_\infty\sqrt{\pi(a+d)}. \tag{9}$$

Identification with Eq. (5) yields

$$F(a/c) = F_0(a/c)\sqrt{1+\frac{d}{a}}. \tag{10}$$

3.2. Stress intensity factors for cracks in singular stress fields

The overall geometry is now as shown in Fig. 1a, where the notch is considered sharp, i.e., $\rho/d \to 0$, and there is a crack of depth a emanating from the root of the notch. The geometry factor of the sharply V-notched specimen is denoted by F_∞.

Before introducing stress intensity factor solutions for cracks in singular stress fields, it would be convenient to present the weight function method used for deriving a closed form solution of K.

3.2.1. Weight function

When solutions for $F(a/c)$ are not available, the so called weight function may give the geometry factor for an arbitrary crack. A crack of depth a, whose surfaces are subjected to a pair of opposite point forces is considered. Once the stress in the plane of the subsequent crack and the appropriate weight function are known, determination of $F(a/c)$ is reduced to a simple integration procedure.

Consider now a crack of depth a located in a smooth plate subjected to the notch stress field $\sigma_y(x)$, cf. Fig. 1b. The geometry factor F_∞ can then be estimated according to

$$F_\infty(a/c) = \frac{1}{\pi}\int_0^1 \frac{\sigma_y(a\xi)}{\sigma_\infty} g(\xi, a/c)\,\mathrm{d}\xi, \tag{11}$$

where $g(\xi, a/c)$ is the weight function and $\xi = x/a$.

3.2.2. Weight function for edge through-cracks

For a shallow crack, $a/d \ll 1$, Eq. (11) is used as a starting-point. According to Hartranft and Shih [21], the weight function for a crack of depth a, whose surfaces are subjected to a pair of opposite point forces in a semi-infinite plate is given by

$$g(\xi) = \frac{2(1+f(\xi))}{\sqrt{1-\xi^2}}, \tag{12}$$

$$f(\xi) = (1-\xi^2)(0.2945 - 0.3912\xi^2 + 0.7685\xi^4 - 0.9942\xi^6 + 0.5094\xi^8). \tag{13}$$

As was concluded earlier, a sharply notched configuration gives rise to a stress singularity, cf. Eq. (4). This singular term dominates when $a/d \ll 1$, and thus, $\sigma_\infty k_0 (x/d)^{\lambda-1}$ is used as the stress acting on the crack surface. The geometry factor F_∞ is then obtained from Eq. (11) as

$$F_\infty = \frac{2}{\pi}k_0\int_0^1 \frac{1+f(\xi)}{\sqrt{1-\xi^2}}\left(\frac{a\xi}{d}\right)^{\lambda-1}\mathrm{d}\xi. \tag{14}$$

In order to obtain a closed form expression for F_∞, Eq. (14) can be rewritten as

$$F_\infty = \frac{2}{\pi}k_0\tilde{g}_0\int_0^1 \frac{1}{\sqrt{1-\xi^2}}\left(\frac{a\xi}{d}\right)^{\lambda-1}\mathrm{d}\xi, \tag{15}$$

Please cite this article in press as: Fjeldstad A et al., Approximate stress intensity factors for cracked ..., Eng Fract Mech (2007), doi:10.1016/j.engfracmech.2007.04.028

where the factor $1 + f(\xi)$ has been replaced by the constant value $\tilde{g}_0$. The value of $\tilde{g}_0$ will obviously depend on the stress distribution σ_y, which, in the case of a singular stress field, depends on the notch opening angle ω. The constant $\tilde{g}_0$ can be expressed as

$$\tilde{g}_0 = F_0 g_0 = 1.122 g_0. \tag{16}$$

From Table 1 can be seen that g_0 is only weakly dependent on ω, with a maximum difference of less than 5%.

Solving the integral in Eq. (15) and introducing Eq. (16) give

$$F_\infty = F_0 g_0 k_0 l_0 \left(\frac{a}{d}\right)^{\lambda-1}, \tag{17}$$

where

$$l_0 = \frac{1}{\sqrt{\pi}} \frac{\Gamma(\lambda/2)}{\Gamma(\lambda/2 + 1/2)}, \tag{18}$$

and $\Gamma(\cdot)$ denotes the gamma function. Eq. (17) can now be rewritten as

$$F_\infty = F_0 g_0 k_0 l_0 \left(\frac{a}{d}\right)^{\lambda-1} = F_0 F' \left(\frac{a}{d}\right)^{\lambda-1}, \tag{19}$$

where F' is given by

$$F' = g_0 k_0 l_0. \tag{20}$$

3.2.3. Weight function for semi-elliptical cracks

According to Shen and Glinka [23], the weight function for the deepest point of a semi-elliptical surface crack is given by

$$g(\xi) = \frac{2(1 + f(\xi, a/c))}{\sqrt{2(1-\xi)}}, \tag{21}$$

where $f(\xi, a/c)$ can be found in Ref. [23]. By introducing Eq. (21) into Eq. (11), the reference geometry factor, $F_{A,\infty}$, for a semi-elliptical crack located in a singular stress field can be calculated as

$$F_{A,\infty} = \frac{2}{\pi} k_0 \int_0^1 \frac{1 + f(\xi, a/c)}{\sqrt{2(1-\xi)}} \left(\frac{a\xi}{d}\right)^{\lambda-1} \mathrm{d}\xi. \tag{22}$$

As in the previous subsection, the expression given in Eq. (22) can be rewritten in order to simplify the integration procedure.

$$F_{A,\infty} = \frac{2}{\pi} k_0 \tilde{g}_{A,0} \int_0^1 \frac{1}{\sqrt{2(1-\xi)}} \left(\frac{a\xi}{d}\right)^{\lambda-1} \mathrm{d}\xi, \tag{23}$$

Table 1
Values of λ, g_0, k_0, l_0, F' and F'/k_0 for a V-shaped through-cracked notch with $\rho/d = 0$ and $a/d \to 0$

	Notch opening angle ω										
	0°	20°	40°	60°	80°	90°	100°	120°	140°	160°	180°
λ	0.5	0.501	0.504	0.512	0.530	0.544	0.563	0.616	0.697	0.819	1
g_0	1.048	1.048	1.047	1.046	1.044	1.042	1.040	1.034	1.025	1.014	1
k_0	0.572	0.578	0.586	0.611	0.660	0.670	0.744	0.863	1.018	1.148	1
l_0	1.669	1.666	1.659	1.639	1.595	1.563	1.522	1.421	1.295	1.151	1
F'	1	1.009	1.020	1.047	1.098	1.133	1.176	1.268	1.351	1.340	1
F'/k_0	1.749	1.744	1.740	1.714	1.665	1.629	1.582	1.469	1.328	1.167	1

The parameters k_0 and F' are from Ref. [22].

Please cite this article in press as: Fjeldstad A et al., Approximate stress intensity factors for cracked ..., Eng Fract Mech (2007), doi:10.1016/j.engfracmech.2007.04.028

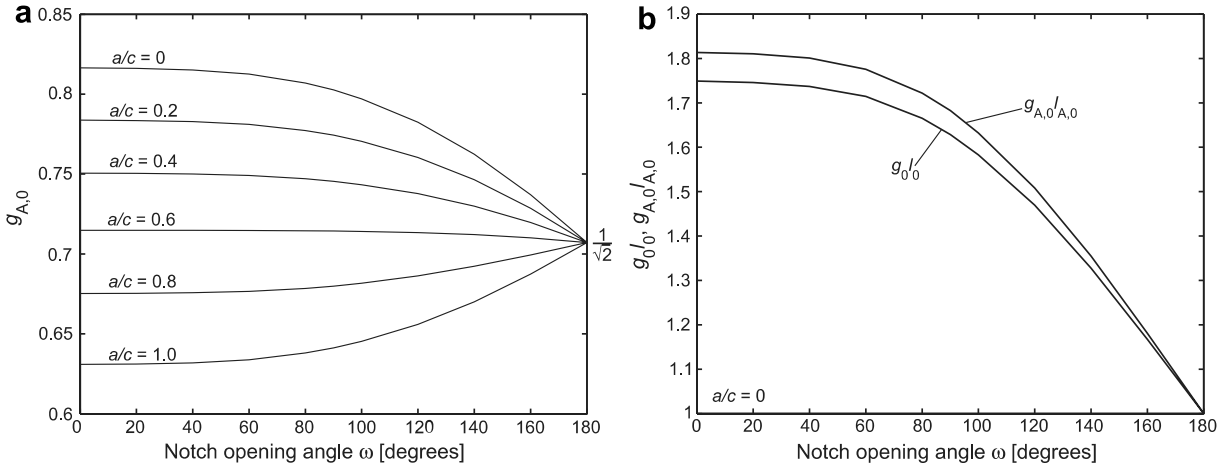

Fig. 3. (a) $g_{A,0}$ as a function of the notch opening angle ω for different values of a/c, (b) $g_0 l_0$ and $g_{A,0} l_{A,0}$ for $a/c = 0$ plotted against the notch opening angle, ω.

where the factor $1 + f(\xi, a/c)$ is replaced by the constant value $\tilde{g}_{A,0}$, which depends on both the opening angle ω and the aspect ratio a/c. $\tilde{g}_{A,0}$ can further be expressed as

$$\tilde{g}_{A,0} = F_{A,0} g_{A,0}. \tag{24}$$

Fig. 3a shows $g_{A,0}$ against ω for different values of a/c.

Solving the integral in Eq. (23) and introducing Eq. (24) give

$$F_{A,\infty} = F_{A,0} g_{A,0} k_0 l_{A,0} \left(\frac{a}{d}\right)^{\lambda-1}, \tag{25}$$

where

$$l_{A,0} = \sqrt{\frac{2}{\pi}} \frac{\Gamma(\lambda)}{\Gamma(\lambda + 1/2)}. \tag{26}$$

Finally, $F_{A,\infty}$ can be presented on the same form as Eq. (19):

$$F_{A,\infty} = F_{A,0} g_{A,0} k_0 l_{A,0} \left(\frac{a}{d}\right)^{\lambda-1} = F_{A,0} F'_A \left(\frac{a}{d}\right)^{\lambda-1}. \tag{27}$$

Fig. 3b shows $g_{A,0} l_{A,0}$ and $g_0 l_0$ versus the opening angle ω. The product $g_{A,0} l_{A,0}$ is obtained using the aspect ratio $a/c = 0$. From the figure it can be seen that the weight function solution for semi-elliptic cracks presented by Shen and Glinka [23] is in good agreement with the edge through-crack solution by Hartranft and Shih [21], with a maximum difference of less than 4%.

4. Geometry factors

4.1. Reference geometry factor $F_\infty(a/c)$

In the present Section, simple expressions for the geometry factors of through-cracks and semi-elliptical cracks emanating from the root of a notch are presented. These expressions have been based on the reference geometry factor $F_\infty(a/c)$ for a sharply cracked V-notched specimen.

In Fig. 4, the geometry factor $F_\infty(a/c)$ has been drawn as a dashed curve. For a shallow crack, i.e., $a/d \to 0$, the singular notch stress field tends to dominate as expressed by Eq. (27). Hence, $F_\infty(a/c)$ asymptotically tends to infinity. As the normalised crack depth a/d increases, $F_\infty(a/c)$ continuously decreases. For sufficiently deep cracks, $F_\infty(a/c)$ asymptotically approaches the geometry factor $F_0(a/c)$ for the current surface crack emanating from a smooth surface.

Please cite this article in press as: Fjeldstad A et al., Approximate stress intensity factors for cracked ..., Eng Fract Mech (2007), doi:10.1016/j.engfracmech.2007.04.028

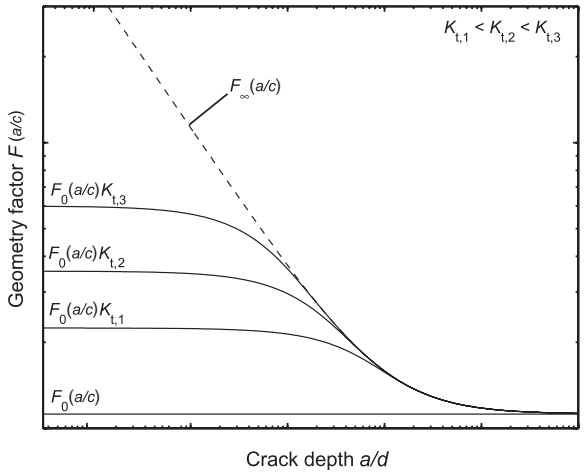

Fig. 4. Principle graphs of geometry factors against the normalised crack depth a/d.

4.2. Geometry factors for cracks in regular stress fields

Geometry factors, $F(a/c)$, have been plotted against the normalised crack depth a/d in Fig. 4 for three notched plates. For shallow cracks, the geometry factor assumes the constant value $F_0(a/c)K_t$. As a increases, $F(a/c)$ continuously decreases and asymptotically approaches $F_\infty(a/c)$. As the crack grows beyond the notch root stress field, the remote stress becomes dominating and both approach the constant value $F_0(a/c)$.

4.3. Normalised geometry factors

Normalising the shallow crack geometry factor solution obtained from Eq. (8) with respect to the geometry factor, $F_\infty(a/c)$, for a surface crack emanating from the root of a sharp notch, i.e., $\rho/d \to 0$, cf. Eq. (27), yields

$$\frac{F(a/c)}{F_\infty(a/c)} = \frac{K_t}{F'(a/c)}\left(\frac{a}{d}\right)^{1-\lambda}. \tag{28}$$

As the crack grows deeper, the above $F_\infty(a/c)$ becomes less sensitive to the singular stress field. Hence, the above fraction asymptotically approaches

$$\frac{F(a/c)}{F_\infty(a/c)} = 1, \tag{29}$$

as shown in Fig. 5a for the notched plate in Fig. 1c. In addition, normalising the crack depth a with respect to a transition crack depth a^* yields a single curve, as shown in Fig. 5b. Wormsen et al. [2] introduced an equation for the normalised geometry factor F/F_∞, which asymptotically agrees with the near and remote field estimates. They suggested that the normalised geometry factor could be written as

$$\frac{F(a/c)}{F_\infty(a/c)} = \left[1 - \exp\left(-\frac{a}{a^*}\right)\right]^{1-\lambda}, \tag{30}$$

where a^* is defined as the crack depth at which the shallow and deep crack asymptotes given by Eqs. (28) and (29), intersect. Hence, a^* is determined by

$$a^* = d\left(\frac{F'(a/c)}{K_t}\right)^{\frac{1}{1-\lambda}}. \tag{31}$$

Please cite this article in press as: Fjeldstad A et al., Approximate stress intensity factors for cracked ..., Eng Fract Mech (2007), doi:10.1016/j.engfracmech.2007.04.028

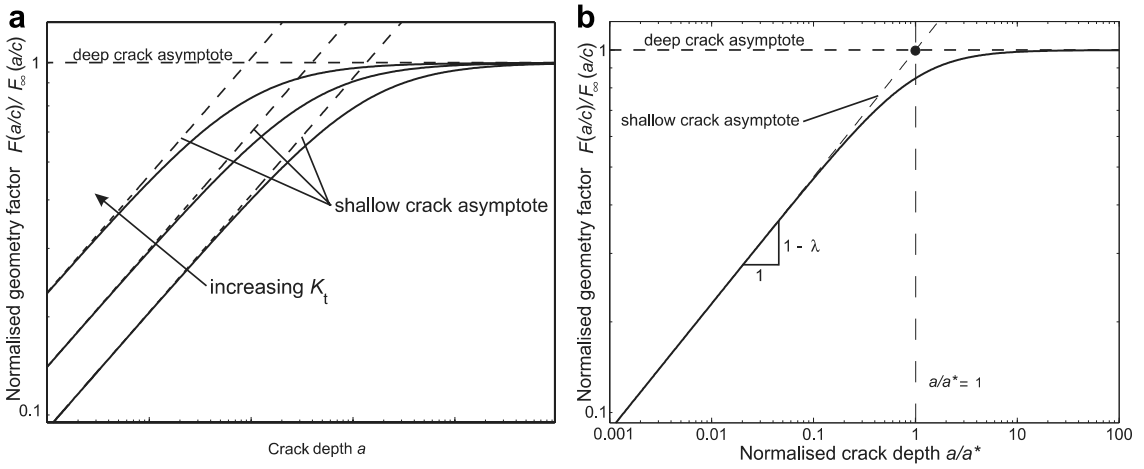

Fig. 5. Principle graphs of normalised geometry factors against (a) the crack depth a, (b) the normalised crack depth a/a^*.

For a notch with $\omega < \pi/2$ and $\rho \ll d$, the stress concentration factor is approximately given by

$$K_t \approx 2\sqrt{\frac{d}{\rho}} \tag{32}$$

With $F' = 1$, see Table 1, the transition crack depth a^* for an edge through-crack becomes

$$a^* \approx \frac{\rho}{4}. \tag{33}$$

An alternative equation that satisfies the shallow and deep crack asymptotes is given by

$$\frac{F(a/c)}{F_\infty(a/c)} = \left[1 + \left(\frac{a^*}{a}\right)^\beta\right]^{\frac{\lambda-1}{\beta}}, \tag{34}$$

where a^* is given by Eq. (31). It has been found that Eq. (34) gives $F(a/c)$ values in somewhat better agreement with numerical values over a wider range of notch opening angles ω and ρ/d values than Eq. (30), provided that the parameter β is chosen properly. With $\beta = 1.35$, Eqs. (30) and (34) differ by less than 3.5%.

5. T-joint configuration

The expressions for the semi-infinite V-notched specimen can be used as a basis for establishing approximate closed form solutions for the geometry factor $F(a/c)$ for finite width T-joints (see Fig. 6). The notch geometry for the T-joints is very similar to the V-notch geometry, both characterised by an opening angle ω and a notch root radius ρ. For both cases, the shallow crack asymptote is given by Eq. (8). However, for the stress raisers shown in Fig. 6, there is no notch depth d that will 'add' to the crack depth, when the crack becomes deeper. Therefore, the deep crack asymptote of the stress intensity factor is given by

$$K = F_0\left(\frac{a}{c}\right)\sigma_\infty\sqrt{\pi a}, \quad a \gg \rho. \tag{35}$$

5.1. Geometry

The accuracy of the formulae presented in Section 4.3 will now be assessed by numerical analyses of a T-joint with a fillet-weld-shaped transition as shown in Fig. 6. The T-joint has a chord width w_c and a brace semi-width $w_b = 3/4w_c$. Its stress concentration factors have been summarised in Table 2. Both edge through-cracked and semi-elliptically cracked specimens will be considered.

The T-joint has a weld-shaped transition as shown in Fig. 6. The transition can be described by a straight line creating a 135° angle with the longitudinal direction of the chord. A circular arc of radius ρ connects the

Please cite this article in press as: Fjeldstad A et al., Approximate stress intensity factors for cracked ..., Eng Fract Mech (2007), doi:10.1016/j.engfracmech.2007.04.028

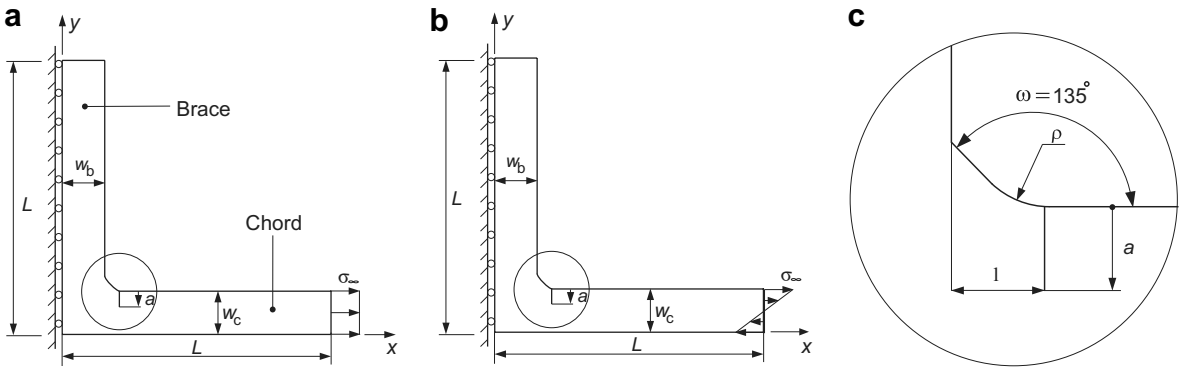

Fig. 6. Boundary conditions applied to the cracked specimens: (a) chord subjected to homogeneous stress, (b) chord subjected to pure bending and, (c) close-up of the notch geometry.

Table 2
Summary of FEA based stress concentration factors for the investigated T-joint

Specimen number	Normalised notch radius ρ/w	Stress concentration factor K_t
1. Fig. 6a	0.0125	2.86
	0.025	2.32
	0.0625	1.84
2. Fig. 6b	0.0125	3.20
	0.025	2.56
	0.0625	1.98

weld and the chord as shown in Fig. 6c. The weld leg length is set to $l = 0.2w_c$. The weld geometry parameters ρ, ω and l are defined according to Tveiten et al. [24]. A surface crack of depth a emanates from the point, where the chord enters the weld toe. The cracked T-joint was subjected to two different loading conditions, namely tension and bending, as shown in Fig. 6a and b, respectively. Symmetry about the vertical centre-line, i.e., $x = 0$, makes it sufficient to model only one half of the T-joint.

6. Geometry factors for T-joint configurations

6.1. Edge through-cracks

In Section 3, simple expressions for the geometry factor, F, for cracks emanating from the root of a V-notch were introduced, which asymptotically agree with the shallow and deep crack asymptotes. These expressions were based on the reference solution F_∞, for a sharply notched specimen, i.e., $\rho/w \to 0$. Next, the expressions for the V-notched plate will be used as a basis for estimating the geometry factor F of a cracked T-joint.

For the V-notched plate in Fig. 1, the geometry factor was given as a function of a/d. However, a characteristic notch depth, d, cannot be defined for a T-joint. Instead, it is suggested that the width, w, of the cracked part of the T-joint to be used as the characteristic length parameter. The geometry factor of the cracked T-joint can then be obtained from Eq. (34), with the transition crack depth given by

$$a^* = w\left(\frac{F'}{K_t}\right)^{\frac{1}{1-\lambda}}. \tag{36}$$

The effect of finite width is taken into account by means of the reference geometry factor F_∞. Hence, for deep cracks, F_∞ asymptotically approaches the geometry factor for the current edge through-crack emanating from the smooth surface of a plate of finite width w. For a single-edge-cracked plate of width w under uniform tension, the geometry factor is given in [18].

Please cite this article in press as: Fjeldstad A et al., Approximate stress intensity factors for cracked ..., Eng Fract Mech (2007), doi:10.1016/j.engfracmech.2007.04.028

6.2. Semi-elliptical cracks

For the semi-elliptically cracked T-joints, the geometry factor F_A for the deepest point at the crack front, A(a; 0), can be estimated by means of Eq. (27), see Fig. 2. As for the edge through-cracked specimens, the effect of finite width is taken into account by means of the reference geometry factor $F_{A,\infty}$. Hence, for deep surface cracks, $F_{A,\infty}$ asymptotically approaches the geometry factor for a surface crack in a finite plate of width w. Solutions for surface cracks in a finite plate under tension and bending have been presented by Newman and Raju [17], see Section 3.

The weight-function can be used to compute the reference geometry factor, F_∞ for a through-crack of arbitrary depth. For a semi-elliptical crack, the weight-function is expected to yield accurate results as long as the crack depth is small compared with the notch radius. When the crack grows and become comparable with the root radius, the use of Eq. (6) is questionable for arbitrary notch angles since the used weight-function, see Eq. (21), is strictly speaking only valid for smooth plates. As a consequence, the accuracy of the K approximation in the intermediate regime can be expected to be higher for through-cracks than for semi-elliptical cracks. To increase the accuracy of $F_{A,\infty}$ one could use finite element results instead of the weight-function method.

7. Numerical analysis

The observation that the geometry factor $F(a/c)$ for various specimens can be estimated by means of Eq. (34), if the geometry factor $F_\infty(a/c)$ is known, is an important aspect of the use of crack mechanics in design. It is therefore of great interest to study the influence on $F(a/c)/F_\infty(a/c)$ of parameters such as crack depth a, aspect ratio a/c, T-joint geometry, and applied loading (actual force or bending moment). The cracked specimens considered are shown in Fig. 6. For each specimen, the geometry factor was evaluated for three ρ/w ratios, cf. Table 2. In the following Subsections, the accuracy of Eq. (34) is assessed by using $\beta = 1.35$.

7.1. Evaluation procedures

Linear elastic plane strain analyses of the edge through-cracked specimens were performed using the finite element program ABAQUS [25]. Eight-noded isoparametric second order plane strain elements with reduced integration were used. Poisson's ratio was chosen to be $v = 0.3$ and small displacement theory was assumed throughout. The geometry factors, F_A, for the semi-elliptically cracked specimens were obtained using a set of empirical equations presented by Pommier et al. [5].

$F(a/c)$ is for both edge through-cracks and semi-elliptical cracks normalised by means of the reference solution $F_\infty(a/c)$. Appendix A describes in detail how $F_\infty(a/c)$ can be obtained.

7.2. Geometry factors

7.2.1. Edge through-cracks

The cracked configurations are shown in Fig. 6. Representative finite element solutions are those of the T-joint with a weld-shaped transition under uniform tension, i.e., the specimen shown in Fig. 6a. Finite element geometry factors, F, have been plotted against the normalised crack depth a/w in Fig. 7a. For shallow cracks, say $a/w < 0.001$, the notch stress field dominates and the geometry factor assumes the constant value F_0K_t, while F_∞ asymptotically tends to infinity. As the crack depth increases, F continuously decreases and asymptotically approaches F_∞. As the crack grows beyond the notch stress field, the remote stress becomes dominating and F and F_∞ asymptotically approach the geometry factor for the current surface crack emanating from a smooth surface in a finite plate.

In Fig. 7b, the finite element F values have been normalised with respect to F_∞. As can be seen, F/F_∞ approaches the deep crack asymptote in a similar fashion for all ρ/w ratios. In fact, by normalising the crack depth a with respect to the transition crack depth a^*, F/F_∞ reduces to a single curve as shown in Fig. 8a. The expression for the solid curve is given by Eq. (34). As can be seen from Fig. 8a, Eq. (34) is in excellent agreement with the finite element results. As shown in Fig. 8b, this is also true for the specimen in Fig. 6b.

Please cite this article in press as: Fjeldstad A et al., Approximate stress intensity factors for cracked ..., Eng Fract Mech (2007), doi:10.1016/j.engfracmech.2007.04.028

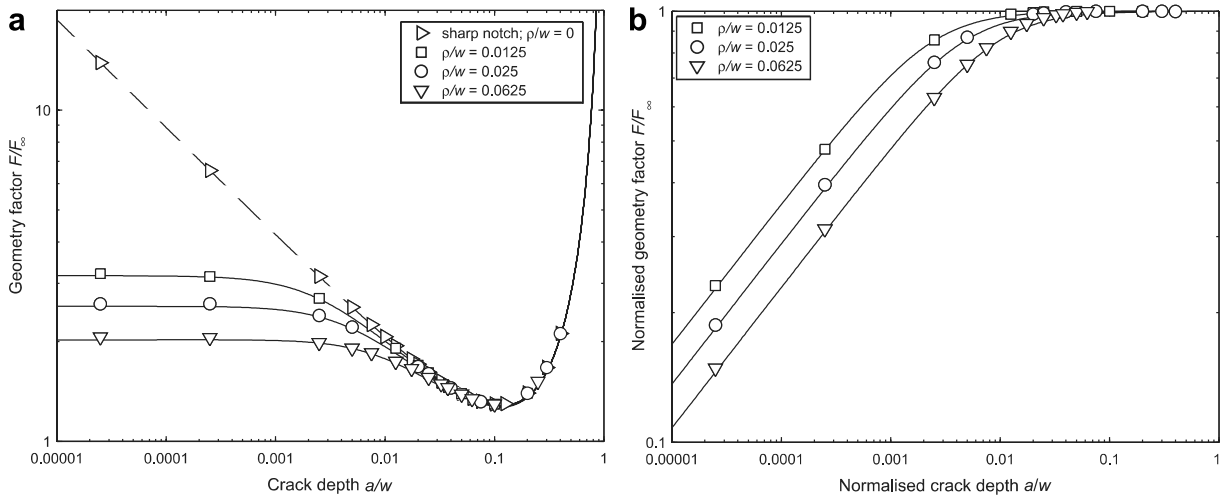

Fig. 7. Geometry factors due to FEA for specimen in Fig. 6a with a through-crack emanating from the chord transition: (a) F and F_∞ against a/w, (b) F/F_∞ against a/w.

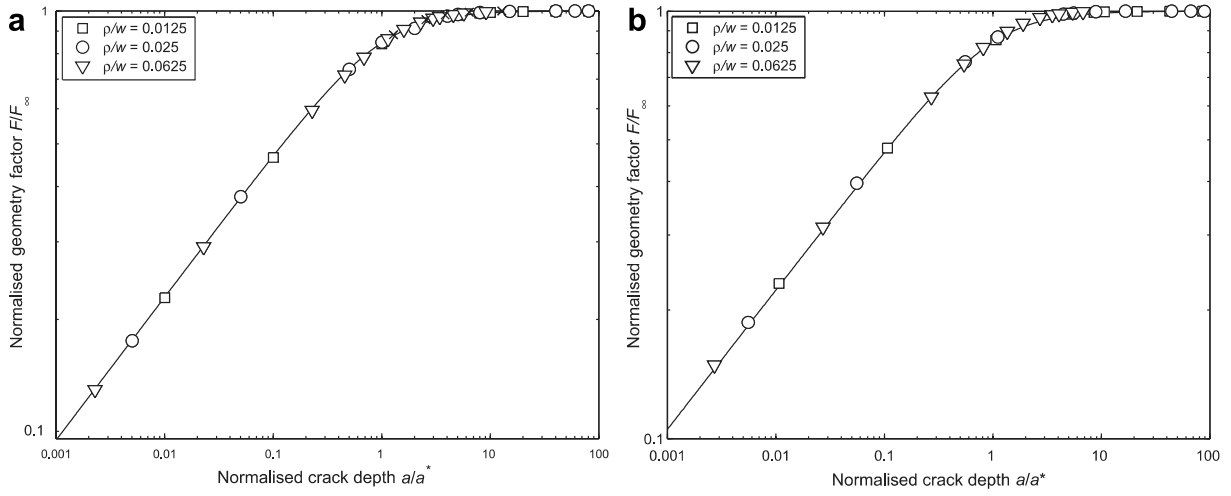

Fig. 8. F/F_∞ finite element results as a function of the normalised crack depth a/a^* for the edge through-cracked (a) specimen in Fig. 6a, (b) specimen in Fig. 6b.

7.2.2. Semi-elliptical cracks

In the previous Subsection, finite element results of F/F_∞ for edge through-cracked specimens were presented. This subsection presents results of $F_A/F_{A,\infty}$, when the crack is semi-elliptic, cf. Fig. 2.

Numerical results in Fig. 9a are for the specimen in Fig 6a with an aspect ratio $a/c = 0.5$ and three (cf. Table 2) different relative notch root radii, ρ/w. Initially, the geometry factor F_A for the deepest point A$(a;0)$ is equal to $F_{A,0}K_t$. For the specimen with a sharp notch, i.e., $\rho/w \to 0$, the geometry factor $F_{A,\infty}$ tends to infinity as $a/w \to 0$, cf. Eq. (27) with d replaced by w. The geometry factor $F_{A,\infty}$ is shown as a dashed line in Fig. 9a. When a/w increases, F_A and $F_{A,\infty}$ continuously decrease.

In Fig. 9b, the geometry factors, F_A, for the specimens with a finite notch root radius, i.e., $\rho/w > 0$, are normalised with respect to the associated factors for a specimen with a sharp notch. Results from analyses carried out on semi-elliptical cracks with aspect ratios $a/c = 0.2$ and 1 are also included. As can be seen, the ratio $F_A/F_{A,\infty}$ asymptotically approaches the deep crack asymptote in a similar fashion for all ρ/w ratios. Hence,

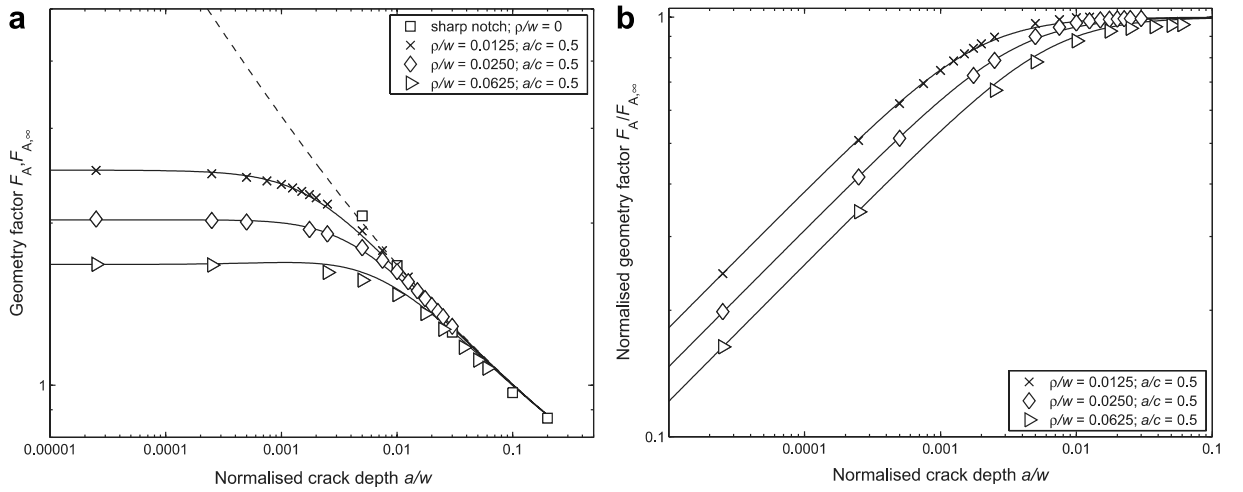

Fig. 9. Geometry factors for the crack front A(a;0) (Fig. 2) for specimen in Fig. 6a: (a) F_A and $F_{A,\infty}$ against a/w, (b) $F_A/F_{A,\infty}$ against a/w.

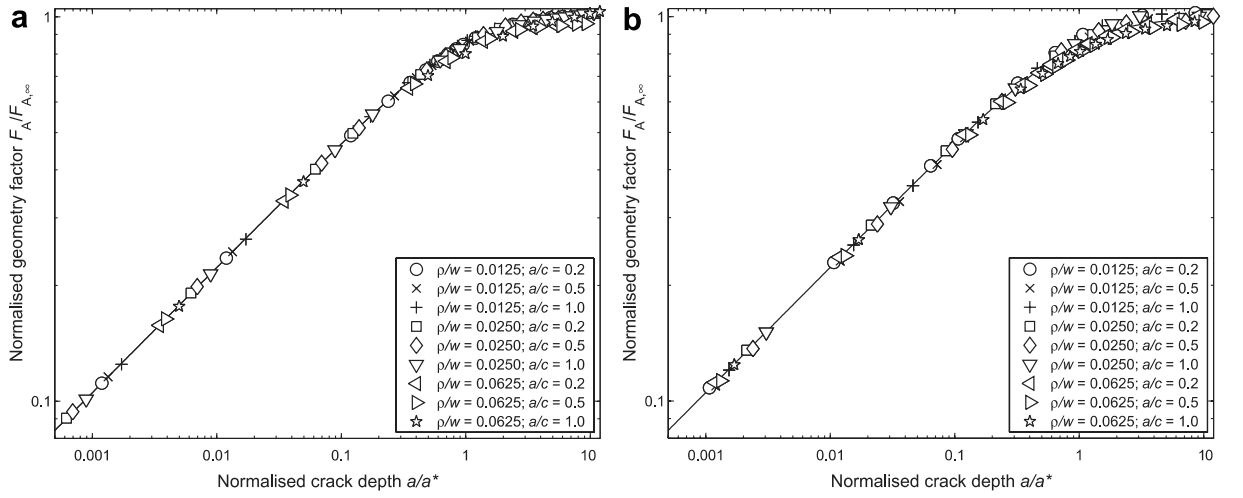

Fig. 10. $F_A/F_{A,\infty}$ results as a function of the normalised crack depth a/a^* for the semi-elliptically cracked (a) specimen in Fig. 6a, (b) specimen in Fig. 6b.

by normalising the crack depth a with respect to the transition crack depth a^*, $F_A/F_{A,\infty}$ reduces to a single curve as shown in Fig. 10a. The expression for the solid curve is given by Eq. (34). As also can be seen from Fig. 10b, Eq. (34) is in excellent agreement with the numerical results.

8. Conclusions

Notched specimens with through-cracks or semi-elliptical cracks emanating from the root of the notch have been investigated. Simplified formulae for obtaining the stress intensity factor K have been presented. The proposed equations for estimating K make use of a reference solution to interpolate over the entire range from shallow to deep cracks. The reference solution is obtained by considering the current crack emanating from the corresponding specimen with a sharp notch. The formulae satisfy the shallow and deep crack asymptotes.

An important aspect of the work has been to apply the solutions to a T-joint configurations. The aim was to calculate K as a function of the normalised crack depth a/w. These results were used to obtain values of the geometry factors $F(a/c)$ and $F_\infty(a/c)$. Once $F_\infty(a/c)$ has been determined, the geometry factor, $F(a/c)$, for spec-

Please cite this article in press as: Fjeldstad A et al., Approximate stress intensity factors for cracked ..., Eng Fract Mech (2007), doi:10.1016/j.engfracmech.2007.04.028

imens with a finite notch root radius, i.e., $\rho/w > 0$, can be estimated using simplified interpolation functions (see Section 4). Moreover, the proposed method and numerical calculations, covering different geometries and applied loading conditions, showed excellent agreement both for edge through-cracks and semi-elliptical cracks.

The procedure for the approximate determination of K should be a useful tool for the life assessment of cracked V-notched specimens and T-joints subject to fatigue loading.

Acknowledgements

The authors gratefully acknowledge the research support for this work provided by The Research Council of Norway and the industrial participants within the NorLight project, and by GE Energy (Norway) AS. The authors also wish to thank Dr. Hans-Jörg Huth for permission to use a fatigue crack growth code with stress intensity factors based on Pommier et al.

Appendix A

Presented in this appendix is a set of formulae for establishing the reference geometry factor $F_\infty(a/c)$. In this work, $F_\infty(a/c)$ is expressed by

$$F_\infty\left(\frac{a}{c},\frac{a}{w}\right) = \left[F'\left(\frac{a}{c}\right)\cdot\left(\frac{a}{w}\right)^{\lambda-1} + f\left(\frac{a}{c},\frac{a}{w}\right)\right]F_P\left(\frac{a}{c},\frac{a}{w}\right), \tag{37}$$

where $F_P(a/c)$ is the geometry factor for the current surface crack emanating from a smooth surface. Fig. 11 shows the geometry factor for a smooth plate, $F_P(a/c)$, along with the reference solution $F_\infty(a/c)$ for a sharp notch ($\rho = 0$) and the geometry factor $F(a/c)$ for a notched specimen with $\rho/w > 0$. The geometry factor for a notched specimen asymptotically approaches $F_P(a/c)$, when the crack has grown beyond the notch root stress field. $F_P(a/c)$ is used in Eq. (37) for describing the deep crack behaviour, since $F_\infty(a/c)/F_P(a/c) = 1$ when $a/w \to 1$. Hence, for deep cracks the following condition applies:

$$\lim_{a/w\to 1} F'\left(\frac{a}{c}\right)\cdot\left(\frac{a}{w}\right)^{\lambda-1} + f\left(\frac{a}{w}\right) = 1. \tag{38}$$

In Eqs. (37) and (38), $F'(a/c)\cdot(a/w)^{\lambda-1}$ accounts for the behaviour of shallow cracks located in singular stress fields, while $f(a/w)$ describes the transition between shallow and deep crack behaviour.

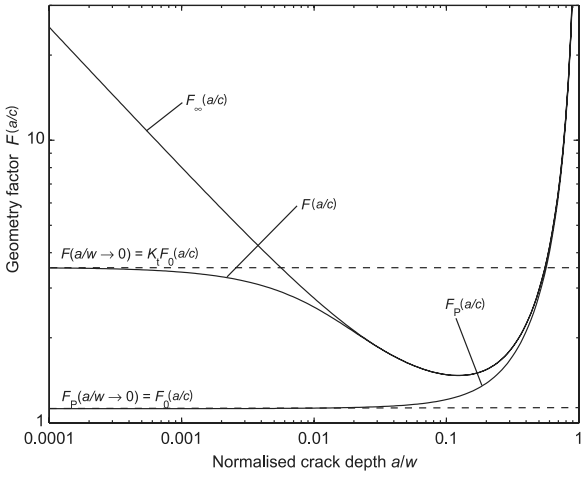

Fig. 11. Principle graphs of the geometry factors for a smooth plate, F_P, sharp-notched plate ($\rho = 0$), F_∞, and a notched plate with a finite notch radius ($\rho/w > 0$), F.

Please cite this article in press as: Fjeldstad A et al., Approximate stress intensity factors for cracked ..., Eng Fract Mech (2007), doi:10.1016/j.engfracmech.2007.04.028

Table 3
Summary of curve fit parameters for F_∞(a/c)

Cracked configuration	a/c	$F'(a/c)$	Regression parameters				$a/w \leqslant$
			b_0	b_1	b_2	b_3	
Fig. 6a[a]	0	0.392	−0.1580	0.4690	0	0	0.9
Fig. 6a[b]	0.2	0.383	−0.4614	0.0356	0.0594	0.0410	0.2
	0.5	0.369	−0.3729	0.0906	0.0560	0.0326	0.2
	1.0	0.340	0.0988	1.4277	1.0177	0.2249	0.2
Fig. 6b[a]	0	0.451	−0.1510	0.8310	0.1590	0.0264	0.9
Fig. 6b[b]	0.2	0.441	−0.4107	0.5193	0.5529	0.1691	0.2
	0.5	0.424	−0.5348	0.1251	0.2237	0.0850	0.2
	1.0	0.391	−1.0548	−0.6227	−0.0543	0.0533	0.2

Here, $\lambda = 0.674$ ($\omega = 135°$) for the configurations considered.
[a] Edge through-crack.
[b] Semi-elliptical crack.

For shallow cracks, $f(a/w)$ approaches zero and $F_P(a/c)$ assumes the constant value $F_0(a/c)$. Hence, Eq. (37) is in total agreement with Eq. (19). Rearranging Eq. (37) gives

$$f\left(\frac{a}{c},\frac{a}{w}\right) = \frac{F_\infty(a/c)}{F_P(a/c)} - F'\left(\frac{a}{c}\right)\cdot\left(\frac{a}{w}\right)^{\lambda-1}. \tag{39}$$

Thus, $f(a/w)$ is bounded between 0 and $1 - F'(a/c)$. Based on numerical results, it is found that $f(a/w)$ can be well approximated by

$$f\left(\frac{a}{w}\right) = 10^{\eta(a/w)}, \tag{40}$$

where the exponent $\eta(a/w)$ is given by the polynomial

$$\eta\left(\frac{a}{w}\right) = b_0 + \sum_{i=1}^{3} b_i\left[\log_{10}\left(\frac{a}{w}\right)\right]^i. \tag{41}$$

The parameters b_i ($i = 0,\ldots,3$) of all specimens considered have been collected in Table 3. The associated values of the factor $F'(a/c)$ of Eq. (39) have also been listed in Table 3. For the through-cracked specimens the parameters have been found by means of the finite element method. The parameters for semi-elliptical cracked specimens have been obtained from a set of empirical equations presented by Bowness and Lee [3].

References

[1] Fjeldstad A, Härkegård G, Wormsen A. The influence of a stress gradient on the growth of a fatigue crack. In: Johnson WS et al., editors. Proceedings of the international fatigue congress 2006, Atlanta, Georgia, USA. Elsevier; 2006.
[2] Wormsen A, Fjeldstad A, Härkegård G. The application of asymptotic solutions to a semi-elliptical crack at the root of a notch. Engng Fract Mech 2006;73(13):1899–912.
[3] Bowness D, Lee MMK. Prediction of weld toe magnification factors for semi-elliptical cracks in T-butt joints. Int J Fatigue 2000;22(5):369–87.
[4] Murakami Y. Analysis of stress intensity factors of mode I, II and III for inclined surface cracks of arbitrary shape. Engng Fract Mech 1985;22(1):101–4.
[5] Pommier S, Sakae C, Murakami Y. An empirical stress intensity factor set of equations for a semi-elliptical crack in a semi-infinite body subjected to a polynomial stress distribution. Int J Fatigue 1999;21(3):243–51.
[6] Nie B, Verreman Y. Rationalization of short crack propagation life at V-notches with the notch stress intensity factor. In: Baïlon JP, Dickson JI, editors. Proceedings of FATIGUE 93. vol. III, 1993. p. 1657–62.
[7] Verreman Y, Nie B. Early development of fatigue cracking at manual fillet welds. Fatigue Fract Engng Mater Struct 1996;19(6):669–81.
[8] Lazzarin P, Tovo R. A unified approach to the evaluation of linear elastic stress fields in the neighborhood of cracks and notches. Int J Fract 1996;78(1):3–19.
[9] Lazzarin P, Tovo R. Notch stress intensity factor approach to the stress analysis of welds. Fatigue Fract Engng Mater Struct 1998;21(9):1089–103.

Please cite this article in press as: Fjeldstad A et al., Approximate stress intensity factors for cracked ..., Eng Fract Mech (2007), doi:10.1016/j.engfracmech.2007.04.028

[10] Lazzarin P, Zambardi R. A finite-volume-energy based approach to predict the static and fatigue behaviour of components with sharp V-shaped notches. Int J Fract 2001;112(3):275–98.
[11] Lazzarin P, Livieri P. Notch stress intensity factors and fatigue strength of aluminium and steel welded joints. Int J Fatigue 2001;23(3):225–32.
[12] Lazzarin P, Lassen T, Livieri P. A notch stress intensity approach to fatigue life predictions of welded joints with different local toe geometry. Fatigue Fract Engng Mater Struct 2003;26(1):49–58.
[13] Williams ML. Stress singularities resulting from various boundary conditions in angular corners of plates in extension. J Appl Mech 1952;24:109–14.
[14] Atzori B, Lazzarin P, Tovo R. Stress distributions for V-shaped notches under tensile and bending loads. Fatigue Fract Engng Mater Struct 1997;20(8):1083–92.
[15] Verreman Y, Baïlon J-P. Fatigue of V-notched members: short crack behaviour and endurance limit. Engng Fract Mech 1987;28(5–6):773–83.
[16] Rooke DP, Baratta FI, Cartwright DJ. Simple methods of determining stress intensity factors. Engng Fract Mech 1981;14(2):397–426.
[17] Newman Jr JC, Raju IS. An empirical stress-intensity factor equation for the surface crack. Engng Fract Mech 1981;15(1–2):185–92.
[18] Tada H, Paris PC, Irwin GR. The stress analysis of cracks handbook. 3rd ed. Bury St. Edmunds and London: Professional Engineering Publishing Limited; 2000.
[19] Neuber H. Kerbspannungslehre. 2nd ed. Berlin: Springer-Verlag; 1958.
[20] Nowell D, Dini D, Duó P. Stress analysis of V-notches with and without cracks, with application to foreign object damage. J Strain Anal Engng Des 2003;38(5):429–41.
[21] Hartranft RJ, Sih GC. Alternating method applied to edge and surface crack problems. Methods of analysis and solutions of crack problems. Mechanics of fracture. Leyden: Nordhoff; 1973 [chapter 4].
[22] Hasebe N, Iida J. A crack originating from a triangular notch on a rim of a semi-infinite plate. Engng Fract Mech 1978;10(4):773–82.
[23] Shen G, Glinka G. Weight functions for a surface semi-elliptical crack in a finite thickness plate. Theor Appl Fract Mech 1991;15(3):247–55.
[24] Tveiten BW, Fjeldstad A, Härkegård G, Myhr OR, Bjørneklett B. Fatigue life enhancement of aluminium joints through mechanical and thermal prestressing. Int J Fatigue 2006;28(12):1667–76.
[25] Abaqus/Standard, User's manual, version 6.4. Hibbit, Karlsson and Sorensen, Pawtucket, Rhode Island, 2003.

Please cite this article in press as: Fjeldstad A et al., Approximate stress intensity factors for cracked ..., Eng Fract Mech (2007), doi:10.1016/j.engfracmech.2007.04.028

Non-linear analysis of shallow cracks in smooth and notched plates. Part 1: analytical evaluation

G Härkegård and **A Wormsen***
Department of Engineering Design and Materials, Norwegian University of Science and Technology, Trondheim, Norway

The manuscript was received on 22 March 2004 and was accepted after revision for publication on 5 October 2004.

DOI: 10.1243/030932405X7845

Abstract: This is the first paper of two that deal with the non-linear analysis of shallow cracks. Simple formulae are given for estimating the J integral for a power-hardening elastic–plastic solid. The proposed equation for estimating J makes use of the linear elastic and the fully plastic solution to interpolate over the entire range from small- to large-scale yielding. The elastic geometry factor is obtained by means of the stress intensity factor. In the fully plastic formulation, the plastic geometry factors are obtained by considering a pure power-hardening solid, which reduces at one limit to an incompressible linear elastic solid, and at the other to a perfectly plastic solid. The solutions are given for three basic configurations: a double-edge-cracked plate under tension and bending; a notched plate under tension with a crack at the root of the notch; a single-edge-cracked plate under bending. Both force control and displacement control are considered. The accuracy of the formulae is assessed using the finite element calculations in Part 2.

Keywords: J integral, geometry factor, constraint factor, force control, displacement control, shallow crack, notch, elastic–plastic, reference stress

1 INTRODUCTION

The non-linear finite element analysis of a mechanical component is a computer-intensive task. Thus, approximate methods for analysing non-linear notched and cracked bodies are of great practical interest.

Neuber's rule [**1**] is one of the best-known models for an approximate calculation of stress and strain at the root of a notch in an elastic–plastic solid. It has been generalized to cover creep, i.e. time-dependent plasticity, by Härkegård and Sørbø [**2**]. Based on finite element analysis, the accuracy of Neuber's rule was studied by Härkegård and Mann [**3**].

In the limiting case, where a sharp notch can be regarded as a crack, the contour integral J has been much used for the prediction of failure in pressure vessels and piping. These are components where the loading can be regarded as force controlled. Another situation occurs when a crack is growing in a component, where the loading is displacement controlled. This is the case for components subject to thermally induced stress. Examples are blades, rotors, and casings in jet engines, gas and steam turbines, as well as other high-temperature components in thermal power plant and process plant. According to Eslami and Shariyat [**4**], the general definition of the primary and secondary stresses can be defined as stresses due to force and displacement control respectively.

While approximate J estimation procedures are well established for long cracks under elastic–plastic conditions [**5**], the situation is less satisfactory for shallow cracks. Thus, the present work is focused on shallow surface cracks, since these are common flaws in many structural components. For a body exhibiting plastic deformation, the applicability of simplified methods to the analysis of cracked components is of great practical interest.

Corresponding author: Department of Engineering Design and Materials, Norwegian University of Science and Technology, Richard Birkelandsvei 2B, Trondheim, NO-7491, Norway. email: anders.wormsen@ntnu.no

The objective of the present paper is to present simplified solutions for the J integral of shallow cracks in smooth and notched specimens. Formulae have been established for several basic configurations. While comprehensive theoretical and experimental investigations have been carried out for a wide range of different components under force control [**6–8**], structural integrity assessment of components under displacement control is still an open issue [**9**]. This paper will treat both force control and displacement control.

2 CONTOUR INTEGRAL J

Closed-form stress and strain solutions of elastic–plastic cracked solids are rare. By idealizing the material behaviour as non-linear elastic, Rice [**10**] was able to solve two-dimensional crack problems exhibiting plastic deformation. Rice derived a path-independent contour integral J, which may be estimated as the sum of an elastic term and a plastic term [**11**]

$$J = \int_{\Gamma} \left(W \, \mathrm{d}x_2 - T_i \frac{\partial u_i}{\partial x_1} \, \mathrm{d}s \right) \approx J^{\mathrm{e}} + J^{\mathrm{p}} \tag{1}$$

The strain energy density W is given by

$$W = \int_0^{\varepsilon_{ij}} \sigma_{ij} \, \mathrm{d}\varepsilon_{ij}, \qquad i,j = 1,2,3 \tag{2}$$

In equation (1) the arc length along the integration contour Γ is denoted by s, and T_i is the traction exerted on the solid bounded by Γ and the crack surfaces. The traction vector T_i can be written as

$$T_i = \sigma_{ij} n_j \tag{3}$$

where n_j is the outward unit normal to Γ.

The elastic component of J is related to the stress intensity factor K as

$$J^{\mathrm{e}} = \frac{K^2}{E'} \tag{4}$$

where $E' = E$ and $E' = E/(1-\nu^2)$ under plane stress and plane strain respectively.

3 NON-LINEAR CRACK ANALYSIS: GENERAL EQUATIONS

3.1 Approximate solutions for the J integral

Based on dimensional considerations, it should be possible to write the path-independent contour integral J for a body with a crack of depth a as

$$J = g \sigma_{\mathrm{e}} \varepsilon_{\mathrm{e}} a \tag{5}$$

where g is a dimensionless function of the specimen geometry and (dimensionless) material parameters. If g is assumed to be a constant for a given geometry, the elastically calculated J becomes

$$J^* = g \sigma_{\mathrm{e}}^* \varepsilon_{\mathrm{e}}^* a \tag{6}$$

and the ratio of the two integrals is

$$\frac{J}{J^*} = \frac{\sigma_{\mathrm{e}} \varepsilon_{\mathrm{e}}}{\sigma_{\mathrm{e}}^* \varepsilon_{\mathrm{e}}^*} \tag{7}$$

where elastically calculated quantities have been denoted by an asterisk.

If this ratio is known, it is possible to predict J by means of a linear elastic analysis. An example of this is given by the R6 procedure [**12**]. Under stress control, which is illustrated in Fig. 1, $\sigma_{\mathrm{e}}^* = \sigma_{\mathrm{e}}$ and

$$\frac{J}{J^*} = \frac{\varepsilon_{\mathrm{e}}}{\varepsilon_{\mathrm{e}}^*} \geqslant 1 \tag{8}$$

i.e. the elastically calculated J^* is on the unsafe side. This situation is reflected in the R6 failure assessment diagram, where $K/K_{\mathrm{c}} = \sqrt{J^*/J_{\mathrm{c}}}$ is given by a decreasing function of the applied stress. If, however, the displacement or strain is controlled (see Fig. 1), $\varepsilon_{\mathrm{e}}^* = \varepsilon_{\mathrm{e}}$ and the ratio becomes

$$\frac{J}{J^*} = \frac{\sigma_{\mathrm{e}}}{\sigma_{\mathrm{e}}^*} \leqslant 1 \tag{9}$$

The elastically calculated J^* now yields a conservative prediction of J. An intermediate situation is given by a shallow crack at the root of a notch. Under small-scale yielding, Neuber's rule [**3**]

$$\sigma_{\mathrm{e}} \varepsilon_{\mathrm{e}} = \sigma_{\mathrm{e}}^* \varepsilon_{\mathrm{e}}^* \tag{10}$$

can be used to predict the actual stress and strain at the notch root from the elastically calculated values.

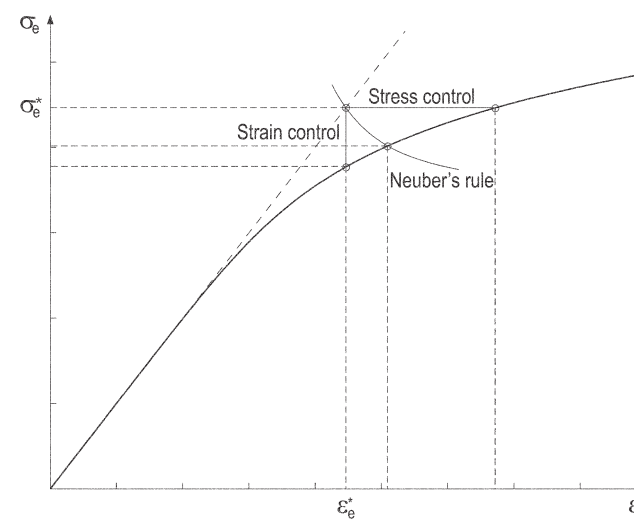

Fig. 1 Graphical interpretation of stress control, strain control and Neuber's rule

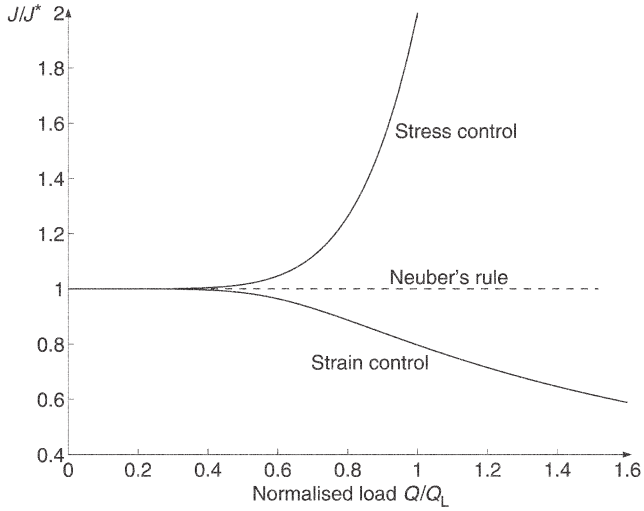

Fig. 2 Principle graphs of J/J^* against normalized load

The associated graphical solution is shown in Fig. 1. In this case

$$\frac{J}{J^*} = 1 \tag{11}$$

For deep cracks, the J solution of the cracked notch will approach that of stress or strain control depending on the prescribed external loading. Principle graphs of J/J^* versus normalized load [see equation (19)] are shown in Fig. 2. The preceding solutions can only give a qualitative idea about the actual J. In fact, the geometry factor g is not a constant (even for a given geometry). Based on work by Webster and Ainsworth [**13**], the J integral of a power-hardening material can be written in terms of the equivalent nominal stress and strain as

$$J = g\left(\frac{a}{w}, n\right)\sigma_{\mathrm{ne}}\varepsilon_{\mathrm{ne}}a \tag{12}$$

Thus, for an elastic–plastic material, which varies from linear elastic behaviour as $\sigma_{\mathrm{ne}} \to 0$ to power-hardening behaviour as $\sigma_{\mathrm{ne}} \to \infty$, it is natural to assume that the J integral can be calculated as the sum of an elastic term and a plastic term according to

$$J = J^{\mathrm{e}} + J^{\mathrm{p}} = g^{\mathrm{e}}\sigma_{\mathrm{ne}}\varepsilon^{\mathrm{e}}_{\mathrm{ne}}a + g^{\mathrm{p}}\sigma_{\mathrm{ne}}\varepsilon^{\mathrm{p}}_{\mathrm{ne}}a \tag{13}$$

The elastically calculated J integral now becomes

$$J^* = g^{\mathrm{e}}\sigma^*_{\mathrm{ne}}\varepsilon^*_{\mathrm{ne}}a \tag{14}$$

Under displacement control, i.e. $\varepsilon_{\mathrm{ne}} = \varepsilon^*_{\mathrm{ne}} = \varepsilon^{\mathrm{e}}_{\mathrm{ne}} + \varepsilon^{\mathrm{p}}_{\mathrm{ne}}$, the ratio J/J^* becomes

$$\frac{J}{J^*} = \frac{g^{\mathrm{p}}}{g^{\mathrm{e}}}\frac{\sigma_{\mathrm{ne}}}{\sigma^*_{\mathrm{ne}}} + \left(1 - \frac{g^{\mathrm{p}}}{g^{\mathrm{e}}}\right)\left(\frac{\sigma_{\mathrm{ne}}}{\sigma^*_{\mathrm{ne}}}\right)^2 \tag{15}$$

while the corresponding expression under force control, i.e. $\sigma_{\mathrm{ne}} = \sigma^*_{\mathrm{ne}}$ and $\varepsilon^{\mathrm{e}}_{\mathrm{ne}} = \varepsilon^*_{\mathrm{ne}}$, yields

$$\frac{J}{J^*} = \frac{g^{\mathrm{p}}}{g^{\mathrm{e}}}\frac{\varepsilon_{\mathrm{ne}}}{\varepsilon^*_{\mathrm{ne}}} + 1 - \frac{g^{\mathrm{p}}}{g^{\mathrm{e}}} \tag{16}$$

Under uniaxial tension, the material is characterized by the Ramberg–Osgood equation

$$\varepsilon_1 = \varepsilon^{\mathrm{e}}_1 + \varepsilon^{\mathrm{p}}_1 = \frac{\sigma_1}{E} + A\sigma^n_1 \tag{17}$$

Under multiaxial stress and proportional loading,

$$\varepsilon_{\mathrm{e}} = \varepsilon^{\mathrm{e}}_{\mathrm{e}} + \varepsilon^{\mathrm{p}}_{\mathrm{e}} = \frac{\sigma_{\mathrm{e}}}{3G} + A\sigma^n_{\mathrm{e}} \tag{18}$$

where the equivalent stress and equivalent strain are denoted by σ_{e} and ε_{e} respectively. Härkegård and Sørbø [**2**] assumed the equivalent nominal stress to be equal to the reference stress [**13**] according to

$$\sigma_{\mathrm{ne}} = \frac{Q}{Q_{\mathrm{L}}}\sigma_{\mathrm{Y}} \tag{19}$$

where Q denotes a generalized load (force P, moment M, pressure p, etc.) and Q_{L} the associated limit load of the component, which is assumed to be perfectly plastic with yield stress σ_{Y} ($Q_{\mathrm{L}} = P_{\mathrm{L}}$ for membrane force, $Q_{\mathrm{L}} = M_{\mathrm{L}}$ for bending, etc.). If u denotes the generalized displacement associated with Q, the limit load is defined by

$$Q_{\mathrm{L}} = \lim_{\mathrm{d}Q/\mathrm{d}u \to 0} Q \tag{20}$$

According to equation (18), the equivalent nominal strain may be expressed as

$$\varepsilon_{\mathrm{ne}} = \varepsilon^{\mathrm{e}}_{\mathrm{ne}} + \varepsilon^{\mathrm{p}}_{\mathrm{ne}} = \frac{\sigma_{\mathrm{ne}}}{3G} + A\sigma^n_{\mathrm{ne}} \tag{21}$$

3.2 Constraint factor

The J integral, as defined by equation (13), requires the determination of an equivalent nominal stress σ_{ne}. The equivalent nominal stress can be calculated from the load and the limit load by means of equation (19). Limit load analysis calculates the maximum load that a given component made of a perfectly plastic solid can sustain. It is further appropriate to present the limit load solution in a non-dimensional form λ by referring it to the limit load of the net cross-sectional area A_{net}. Under uniform tension, the constraint factor λ is defined as

$$\lambda = \frac{P_{\mathrm{L}}}{\sigma_{\mathrm{Y}}A_{\mathrm{net}}} \tag{22}$$

By combining equations (22) and (19), the equivalent nominal stress can be expressed as

$$\sigma_{\mathrm{ne}} = \frac{\sigma_{\mathrm{net}}}{\lambda} \tag{23}$$

where $\sigma_{\mathrm{net}} = P/A_{\mathrm{net}}$ denotes the net section stress.

Under pure bending the constraint factor λ is defined by

$$\lambda = \frac{4M_{\mathrm{L}}}{\sigma_{\mathrm{Y}} l^2 B} \tag{24}$$

where l and B are the ligament width and thickness respectively of the specimen. Closed-form solutions for the constraint factor are available in the literature. Selected solutions are given below for the cracked specimens (see Fig. 1 of Part 2 [**14**]) considered in this work.

3.2.1 Double-edge-cracked tension plate

For double-edge-cracked tension specimens, of width $2w$ and with symmetrically located edge cracks of depth a, Webster and Ainsworth [**13**] stated the following constraint factors

Plane strain

$$\frac{a}{w}\begin{cases} \leqslant 0.884, \\ \geqslant 0.884, \end{cases} \qquad \lambda = \frac{2}{\sqrt{3}}\begin{cases} 1 + \ln\left(\dfrac{1 - a/2w}{1 - a/w}\right) \\ 1 + \dfrac{\pi}{2} \end{cases} \tag{25}$$

Plane stress

$$\frac{a}{w}\begin{cases} \leqslant 0.286, \\ \geqslant 0.286, \end{cases} \qquad \lambda = \begin{cases} 1 + 0.54\dfrac{a}{w} \\ \dfrac{2}{\sqrt{3}} \end{cases} \tag{26}$$

3.2.2 Double-edge-notched tension plate

A pair of symmetrically located edge notches of depth D shown in Fig. 4 in a plate of width $2w$ under simple tension contains a through-thickness crack of length a at the root of each notch. Provided that a is replaced by $D + a$ the constraint factor can be found from equations (25) and (26).

3.2.3 Single-edge-cracked bending plate

For a single-edge-cracked bending specimen with crack depth a and width w, Webster and Ainsworth [**13**] stated the following constraint factors

Plane strain

$$\frac{a}{w}\begin{cases} \leqslant 0.295, \\ \geqslant 0.295, \end{cases} \qquad \lambda = \frac{2}{\sqrt{3}}\begin{cases} 1.26 - 2.72\left(0.31 - \dfrac{a}{w}\right)^2 \\ 1.261 \end{cases} \tag{27}$$

Plane stress

$$\frac{a}{w} \leqslant 0.154, \qquad \lambda = 1.072 \tag{28}$$

3.2.4 Double-edge-cracked bending plate

Based on work by Green [**15**] and Miller [**16**], the constraint factor under plane strain bending can be expressed as

$$\frac{a}{w}\begin{cases} \leqslant 0.336, \\ \geqslant 0.336, \end{cases} \qquad \lambda = \frac{2}{\sqrt{3}}\begin{cases} 1 + 1.13095\dfrac{a}{w} \\ 1.38 \end{cases} \tag{29}$$

The constraint factor under plane stress bending is not known, but must satisfy $1 < \lambda < 2/\sqrt{3}$.

When the constraint factor is known for the considered component, σ_{ne} and $\varepsilon_{\mathrm{ne}}$ can be calculated from equations (19) and (21) respectively. To be able to establish J values according to equation (13) as a function of the applied load requires additional information about the elastic and plastic geometry factors. In the following sections, closed-form solutions are given for g^{e} and g^{p}.

4 DOUBLE-EDGE-CRACKED PLATE UNDER PURE TENSION

A pair of symmetrically located edge cracks of depth a in a plate of width $2w$ under uniaxial tension σ_∞ is considered. The cracked configuration is shown in Fig. 3.

4.1 Elastic geometry factor

The elastic geometry factor g^{e} can be determined by means of the stress intensity factor K. For a crack in a solid under uniaxial tension σ_∞ perpendicular to

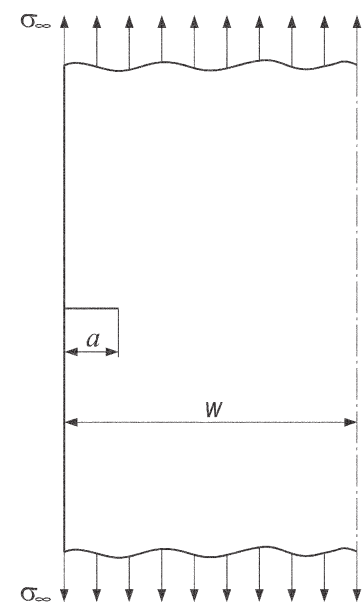

Fig. 3 Double-edge-cracked plate under uniform stress σ_∞

the plane of the crack, K can be estimated by

$$K = f\sigma_\infty\sqrt{\pi a} \tag{30}$$

The stress at infinity, σ_∞, is related to the net section stress σ_{net} through

$$P = \sigma_\infty A_\infty = \sigma_{\text{net}} A_{\text{net}} \tag{31}$$

Introduction of the area ratio $\alpha = A_{\text{net}}/A_\infty$ yields

$$\sigma_\infty = \alpha\sigma_{\text{net}} \tag{32}$$

By combining equations (32) and (23), the stress at infinity can be expressed as $\sigma_\infty = \alpha\lambda\sigma_{\text{ne}}$, and the stress intensity factor as

$$K = f\alpha\lambda\sigma_{\text{ne}}\sqrt{\pi a} \tag{33}$$

According to equations (4) and (13), the elastic component of J is

$$J^{\text{e}} = \frac{K^2}{E'} = g^{\text{e}}\sigma_{\text{ne}}\varepsilon^{\text{e}}_{\text{ne}}a \tag{34}$$

With $\varepsilon^{\text{e}}_{\text{ne}} = \sigma_{\text{ne}}/(3G)$, the elastic geometry factor g^{e} becomes

$$g^{\text{e}} = \frac{3E}{2E'(1+\nu)}(f\alpha\lambda\sqrt{\pi})^2 \tag{35}$$

Under plane strain conditions, equation (35) reduces to

$$g^{\text{e}} = \frac{3(1-\nu)}{2}(f\alpha\lambda\sqrt{\pi})^2 \tag{36}$$

and under plane stress to

$$g^{\text{e}} = \frac{3}{2(1+\nu)}(f\alpha\lambda\sqrt{\pi})^2 \tag{37}$$

4.2 Plastic geometry factor

4.2.1 Edge crack in an infinite plate

Next an infinite solid is considered, i.e. $w \to \infty$, with the equivalent stress and plastic strain related by the power law $\varepsilon^{\text{p}}_{\text{e}} = A\sigma^n_{\text{e}}$. Based on work by He and Hutchinson [**17**, **18**], Webster and Ainsworth [**13**] proposed an approximate solution of the geometric factor g. Under plane strain conditions

$$J = (1.122)^{1+1/n}\pi\sqrt{n}\sigma_{\infty\text{e}}\varepsilon^{\text{p}}_{\infty\text{e}}a = g^{\text{p}}_\infty\sigma_{\infty\text{e}}\varepsilon^{\text{p}}_{\infty\text{e}}a \tag{38}$$

Guided by this solution and finite element results [**14**], a plane stress approximation is given by

$$J = (1.122)^2\pi\sqrt{n}\sigma_{\infty\text{e}}\varepsilon^{\text{p}}_{\infty\text{e}}a = g^{\text{p}}_\infty\sigma_{\infty\text{e}}\varepsilon^{\text{p}}_{\infty\text{e}}a \tag{39}$$

Thus, the geometry factors become

Plane strain

$$g^{\text{p}}_\infty = (1.122)^{1+1/n}\pi\sqrt{n} \tag{40}$$

Plane stress

$$g^{\text{p}}_\infty = (1.122)^2\pi\sqrt{n} \tag{41}$$

For an incompressible linear elastic solid, i.e. $n = 1$, equations (40) and (41) yield

$$g^{\text{p}}_\infty = (1.122)^2\pi \tag{42}$$

With $\nu = \frac{1}{2}$, $f = 1.122$, $\lambda = 2/\sqrt{3}$ (plane strain) or $\lambda = 1$ (plane stress) and $\alpha = 1$, the K-based geometry factor as defined in equation (35) becomes

$$g^{\text{e}}_\infty = (1.122)^2\pi \tag{43}$$

which is in complete agreement with equation (42).

4.2.2 Edge cracks in a finite plate

In section 3.2 it was stated that $\sigma_{\text{ne}} = \sigma_{\text{net}}/\lambda$. The equivalent stress at infinity is given by

$$\sigma_{\infty\text{e}} = \frac{\sigma_\infty}{\lambda_\infty} \tag{44}$$

where λ_∞ is equal to 1 and $2/\sqrt{3}$ under plane stress and plane strain respectively. By combining equations (44), (32), and (23), the equivalent stress at infinity becomes

$$\sigma_{\infty\text{e}} = \alpha\frac{\lambda}{\lambda_\infty}\sigma_{\text{ne}} \tag{45}$$

In a similar manner, the equivalent plastic strain at infinity can be related to the plastic term of the equivalent nominal strain, since $\varepsilon^{\text{p}}_{\infty\text{e}} = A\sigma^n_{\infty\text{e}}$ and $\varepsilon^{\text{p}}_{\text{ne}} = A\sigma^n_{\text{ne}}$, and is given by

$$\varepsilon^{\text{p}}_{\infty\text{e}} = \left(\frac{\sigma_{\infty\text{e}}}{\sigma_{\text{ne}}}\right)^n\varepsilon^{\text{p}}_{\text{ne}} = \left(\alpha\frac{\lambda}{\lambda_\infty}\right)^n\varepsilon^{\text{p}}_{\text{ne}} \tag{46}$$

Introducing equations (45) and (46) into equations (38) and (39) yields

Plane strain

$$J = (1.122)^{1+1/n}\pi\sqrt{n}\left(\alpha\frac{\lambda}{\lambda_\infty}\right)^{n+1}\sigma_{\text{ne}}\varepsilon^{\text{p}}_{\text{ne}}a \tag{47}$$

Plane stress

$$J = (1.122)^2\pi\sqrt{n}\left(\alpha\frac{\lambda}{\lambda_\infty}\right)^{n+1}\sigma_{\text{ne}}\varepsilon^{\text{p}}_{\text{ne}}a \tag{48}$$

It follows from equations (13), (47), and (48) that the fully plastic geometry factor g^{p} can be written

Plane strain

$$g^{\text{p}} = (1.122)^{1+1/n}\pi\sqrt{n}\left(\alpha\frac{\lambda}{\lambda_\infty}\right)^{n+1} \tag{49}$$

Plane stress

$$g^{\text{p}} = (1.122)^2\pi\sqrt{n}\left(\alpha\frac{\lambda}{\lambda_\infty}\right)^{n+1} \tag{50}$$

5 CRACK AT THE ROOT OF A SURFACE NOTCH

The second configuration considered is a notched plate. The notch is characterized by its depth D and its elastic stress concentration factor $K_{tg} = \sigma_1^*/\sigma_\infty$. A through-crack of depth a is located at the root of the notch as shown in Fig. 4. The notched plate is loaded by a remote stress σ_∞ perpendicular to the symmetry plane of the notch.

5.1 Geometry factors

For an edge crack in the near-notch-root stress field, the stress intensity solution is the same as for an edge crack in a smooth solid, except that the remote stress is being amplified by the stress concentration factor K_{tg}; thus

$$K = 1.122 K_{tg} \sigma_\infty \sqrt{\pi a} \tag{51}$$

Thus, according to equation (35), the elastic geometry factor g^e can be expressed as

$$g^e = \frac{3E}{2E'(1+\nu)} (f K_{tg} \alpha \lambda \sqrt{\pi})^2 \tag{52}$$

which is valid as long as the crack is sufficiently small, say $a/D < 0.01$. As the crack grows beyond the notch root stress field, the remote stress field dominates the stress intensity factor, which can be estimated by

$$K = f \sigma_\infty \sqrt{\pi (D + a)} \tag{53}$$

By introducing an equivalent crack length L, Jergéus [**19**] and Härkegård [**20**] obtained an equation for K, which asymptotically agrees with the near and remote field estimates. The expression for L is given by

$$L = a + D\left[1 - \exp\left(-\frac{a}{a^*}\right)\right] \tag{54}$$

where

$$a^* = \frac{D}{(1.122 K_{tg}/f)^2 - 1} \tag{55}$$

The transition crack length a^* is defined as the crack length at which the stress intensity factors of shallow and deep cracks yield equal results; i.e. equations (51) and (53) are equal. Thus, the stress intensity factor can be estimated by

$$K = f \sigma_\infty \sqrt{\pi L} \tag{56}$$

This expression is also found to be in good agreement for intermediate crack depths [**20**]. Expressing the proposed equation for J in terms of the equivalent crack length L makes it possible to calculate g^e from equation (35) and g^p from equations (49) and (50).

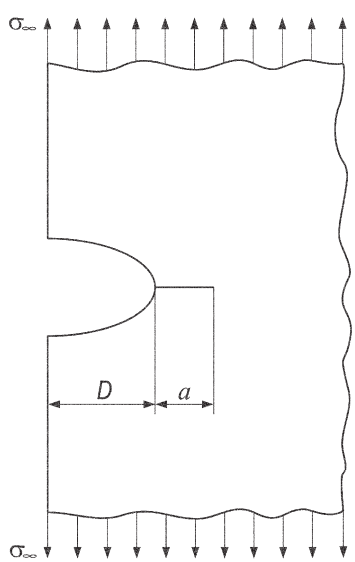

Fig. 4 Through-crack at the root of a surface notch

6 EDGE CRACK IN A PLATE UNDER BENDING

For a machine component, it is commonly found that the stress is decreasing from a maximum at some critical point at the surface. The simplest case corresponds to pure bending, i.e. linearly decreasing stress. It is therefore desirable to establish geometry factors for an edge-cracked plate under plane strain bending. A rectangular plate of width w with an edge crack of depth a is considered.

6.1 Linear elastic geometry factor

The cracked plate carries the moment M. Introducing the limit moment M_L and the associated yield stress σ_Y yields the expression of the equivalent nominal stress as

$$\sigma_{ne} = \frac{M}{M_L} \sigma_Y \tag{57}$$

By combining equations (57) and (24), the equivalent nominal stress can be rewritten as

$$\sigma_{ne} = \frac{4M}{\lambda l^2 B} \tag{58}$$

where the ligament width is given by $l = w - a$. The elastic geometry factor g^e is determined by means of the stress intensity factor K. For an edge-cracked plate subjected to a linearly varying stress perpendicular to the plane of the crack

$$K = f \sigma_{max} \sqrt{\pi a} = f \frac{6M}{w^2 B} \sqrt{\pi a} \tag{59}$$

and thus

$$K = \frac{3}{2} f\lambda \left(\frac{w-a}{w} \right)^2 \sigma_{\mathrm{ne}} \sqrt{\pi a} = \frac{3}{2} f\lambda \alpha^2 \sigma_{\mathrm{ne}} \sqrt{\pi a} \qquad (60)$$

It follows then from equation (34) that

$$g^{\mathrm{e}} = \frac{27E}{8(1+\nu)E'} (f\alpha^2 \lambda \sqrt{\pi})^2 \qquad (61)$$

which under plane strain conditions can be rewritten as

$$g^{\mathrm{e}} = \frac{27(1-\nu)}{8} (f\alpha^2 \lambda \sqrt{\pi})^2 \qquad (62)$$

An expression for the K-based geometry factor f has been given by Tada *et al.* [**21**].

For a pair of symmetrically located edge cracks of depth a in a plate of width $2w$ under pure bending, the elastic geometry factor can also be obtained from equation (61). This can easily be verified from equation (59), provided that w is replaced by $2w$.

6.2 Plastic geometry factor

Once the plastic geometry factor g^{p} is known, the J integral can be found from equation (13), which interpolates over the range from small-scale yielding to large-scale yielding. For an incompressible linear elastic solid, the elastic geometry factor as defined in equation (62) becomes

$$g^{\mathrm{e}} = 1.6875 (f\alpha^2 \lambda \sqrt{\pi})^2 \qquad (63)$$

Guided by this expression, finite element results [**14**], and equation (49), a convenient approximation for the plastic geometry factor for an edge-cracked plate subjected to a linearly varying stress field and plane strain conditions is

$$g^{\mathrm{p}} = 1.6875 (f\alpha^2 \lambda \sqrt{\pi})^2 n^{1/4} \left(\alpha \frac{\lambda}{\lambda_\infty} \right)^{n+1} \qquad (64)$$

7 CONCLUSIONS

An equation for estimating the J integral has been formulated in terms of equivalent nominal stress and strain with the equivalent nominal stress set equal to the reference stress. It is necessary to separate the J integral into an elastic term and a plastic term. The elastic geometry factor was determined by means of the stress intensity factor K. For several basic finite configurations the fully plastic geometry factor was established for specimens with shallow edge cracks, since they are common flaws in many structural components. When the elastic and plastic geometry factors are known, J can be estimated in the range from small-scale yielding to large-scale yielding. It is further pointed out that J is dependent on the type of loading, i.e. displacement or force control. The accuracy of the proposed formulae has been assessed by finite element analysis of some specific configurations in Part 2 [**14**].

REFERENCES

1 **Neuber, H.** Theory of stress concentration for shear-strained prismatical bodies with arbitrary nonlinear stress–strain law. *Trans. ASME, J. Appl. Mechanics*, 1961, **28**, 544–550.

2 **Härkegård, G.** and **Sørbø, S.** Applicability of Neuber's rule to the analysis of stress and strain concentration under creep conditions. *Trans. ASME, J. Engng Mater. Technol.*, 1998, **120**(3), 224–229.

3 **Härkegård, G.** and **Mann, T.** Neuber prediction of elastic–plastic strain concentration in notched tensile specimens under large-scale yielding. *J. Strain Analysis*, 2003, **38**(1), 79–94.

4 **Eslami, M. R.** and **Shariyat, M.** A technique to distinguish the primary and secondary stresses. *Trans. ASME, J. Pressure Vessel Technol.*, 1995, **117**(3), 197–203.

5 **Kumar, V., German, M. D.,** and **Shih, C. F.** An engineering approach for elastic–plastic fracture analysis. EPRI Topical Report NP-1931 Research Project 1237-1, Electric Power Research Institute, Palo Alto, California, 1981.

6 **Harrison, R. P., Loosemore, K.,** and **Milne, I.** Assessment of the integrity of structures containing defects. Technical Report R/H/R6-Rev 2, Central Electricity Generating Board, 1980.

7 **Shih, C. F., Kumar, V.,** and **German, M. D.** Studies on the failure assessment diagram using the estimation method and J-controlled crack growth approach. In *Fracture Resistance Curves and Engineering Applications*, Vol. II, ASTM STP 803 (Eds C. F. Shih and J. P. Gudas), 1983, pp. 239–261 (American Society for Testing and Materials, Philadelphia, Pennsylvania).

8 **Kim, Y. J., Shim, D. J., Choi, J. B.,** and **Kim, Y. J.** Elastic–plastic analyses for surface cracked plates under combined bending and tension. *J. Strain Analysis*, 2002, **37**(1), 33–45.

9 **Hallbäck, N.** and **Nilsson, F.** Fracture assessment for secondary loads. *Fatigue Fracture Engng Mater. Structs*, 1992, **15**(2), 173–185.

10 **Rice, J. R.** A path independent integral and the approximate analysis of strain concentration by notches and cracks. *Trans. ASME, J. Appl. Mechanics*, 1968, **35**(6), 379–386.

11 **Shih, C. F.** and **Hutchinson, J. W.** Fully plastic solutions and large scale yielding estimates for plane stress crack problems. *Trans. ASME, J. Engng Mater. Technol.*, 1976, **98**(4), 289–295.

12 **Milne, I., Ainsworth, R. A., Dowling, A. R.,** and **Stewart, A. T.** Assessment of the integrity of structures containing defects. Technical Report R/H/R6-Rev. 3, Central Electricity Generating Board, 1986.

13 **Webster, G. A.** and **Ainsworth, R. A.** *High Temperature Component Life Assessment*, 1994 (Chapman and Hall, London).

14 Wormsen, A. and **Härkegård, G.** Non-linear analysis of shallow cracks in smooth and notched plates. Part 2: finite element validation. *J. Strain Analysis*, 2005, **40**(3), 245–254.

15 Green, A. P. The plastic yielding of notched bars due to bending. *Q. J. Mechanics Appl. Math.*, 1953, **6**, 223–239.

16 Miller, A. G. Review of limit loads of structures containing defects. *Int. J. Pressure Vessels Piping*, 1988, **32**(1–4), 197–327.

17 He, M. Y. and **Hutchinson, J. W.** The penny-shaped crack and the plane strain crack in an infinite body of power-law material. *Trans. ASME, J. Appl. Mechanics*, 1981, **48**(4), 830–840.

18 He, M. Y. and **Hutchinson, J. W.** Bounds for fully plastic crack problems for infinite bodies. In Second Symposium on *Elastic–plastic Fracture* (Eds C. F. Shih and J. P. Gudas), Vol. I, *Inelastic Crack Analysis*, 1983, ASTM STP 803, I-277–I-290 (American Society for Testing and Materials, Philadelphia, Pennsylvania).

19 Jergéus, H. Å. A simple formula for the stress intensity factors of cracks in side notches. *Int. J. Fracture*, 1978, **14**, R113–R116.

20 Härkegård, G. An effective stress intensity factor and the determination of the notched fatigue limit. In *Fatigue Thresholds: Fundamentals and Engineering Applications*, Vol. II (Eds J. Bäcklund, A. F. Blom, and C. J. Beevers), 1982, pp. 867–879 (Engineering Materials Advisory Services, Warley).

21 Tada, H., Paris, P. C., and **Irwin, G. R.** *The Stress Analysis of Cracks Handbook*, 3rd edition, 2000 (Professional Engineering Publishing Limited, Bury St. Edmunds and London).

APPENDIX

Notation

a	crack depth
a^*	transition crack depth
A	Ramberg–Osgood coefficient
A_{net}	net cross-sectional area
A_∞	gross cross-sectional area
B	thickness of plate
D	notch depth
E	Young's modulus
E'	$= E/(1-\nu^2)$ for plane strain, $= E$ for plane stress
f	K-based geometry factor
g^{e}	elastic geometry factor
g^{p}	plastic geometry factor
G	shear modulus $= E/2(1+\nu)$
J	J integral
J^*	elastically calculated J
J^{e}	elastic component of J
J^{p}	plastic component of J
J_{c}	fracture toughness
K	stress intensity factor
K_{c}	fracture toughness
K_{tg}	elastically calculated stress concentration factor $= \sigma_1^*/\sigma_\infty$
l	semiwidth or width of ligament $= w - a$
L	equivalent surface crack depth
M	bending moment
M_{L}	limit moment of perfectly plastic specimen
n	Ramberg–Osgood stress exponent
n_j	unit normal vector
P	tensile force
P_{L}	limit load of perfectly plastic specimen
Q	generalized load
Q_{L}	generalized limit load of perfectly plastic specimen $= \lim_{\text{d}Q/\text{d}u \to 0} Q$
T_i	traction vector $= \sigma_{ij} n_j$
u	displacement
w	semiwidth or width of plane specimen
W	strain energy density $= \int_0^{\varepsilon_{ij}} \sigma_{ij}\, \text{d}\varepsilon_{ij}$
α	ratio of the net area to the gross cross-sectional area $= A_{\text{net}}/A_\infty$
ε^*	elastically calculated strain
ε^{e}	elastic strain
ε^{p}	plastic strain
ε_{e}	equivalent strain $= \sqrt{\frac{2}{3}\varepsilon'_{ij}\varepsilon'_{ij}} = \sigma_{\text{e}}/(3G) + A\sigma_{\text{e}}^n$
ε_{ne}	equivalent nominal strain $= \sigma_{\text{ne}}/(3G) + A\sigma_{\text{ne}}^n$
ε_{ij}	strain tensor
ε'_{ij}	deviatoric strain tensor
ε_1	uniaxial strain $= \sigma_1/E + A\sigma_1^n$
ε_∞	strain at infinity
λ	constraint factor
λ_∞	constraint factor for an infinite body
ν	Poisson's ratio
ρ	notch tip radius
σ^*	elastically calculated stress
σ_{e}	equivalent stress $= \sqrt{\frac{3}{2}\sigma'_{ij}\sigma'_{ij}}$
σ_{ne}	equivalent nominal stress = reference stress $= (Q/Q_{\text{L}})\sigma_{\text{Y}}$
σ_{ij}	stress tensor
σ'_{ij}	deviatoric stress tensor
σ_{Y}	yield stress of a perfectly plastic solid
σ_1	uniaxial stress
σ_∞	stress at infinity